IMPACT OF ARMATURE REWINDING ON INDUCTION MOTOR EFFICIENCY IN SOUTH AFRICA

Prepared by: Heskin Mkando Mzungu
Department of Electrical Engineering
University of Cape Town

Prepared for: Department of Electrical Engineering
University of Cape Town

Date: 31 August 2009

This thesis is submitted in fulfilment of the requirements for the Masters of Science in Electrical Engineering at the University of Cape Town

Declaration

I, the undersigned, declare that this thesis is my own work. All information that is not of my own has been referenced.

Sign:.....

Acknowledgements

I want to firstly thank God for everything because I am nothing without Him.

I also would like to express my gratitude and appreciation to the following people:

Dr. Azeem Khan (Supervisor)
Dr. Paul Barendse (Co- Supervisor)
Dr. Marubini Manyage

Dr. Ben Sebitosi
Mr. Chris Wozniak

Mr. Richard Okou
Miss. Kgathane Masemola

Prof. Pragasen Pillay

The Advanced Machine and Energy Systems (AMES) research group

The 2007 UCT 1st and 3rd year practical students.

And finally, my many wonderful family and friends for their support and love.

Abstract

The aim of this thesis is to evaluate the impact of armature rewinding on the efficiency of Low Voltage (LV) industrial squirrel cage induction motors in South Africa.

The efficiency of an electric motor is a measure of the effectiveness of the motor to convert electrical power at its terminals to mechanical power at its shaft. Although the definition is seemingly simple and straightforward, the determination of the efficiency of an induction motor is a much-debated topic. Motor manufacturers provide efficiency data obtained through measurement and calculation according to a variety of international standards. Several international standards exist, with each outlining different methods and procedures for the determination of induction motor efficiency. Most notable among the disparities is the treatment of stray losses. For example, the Japanese standard JEC-37 assumes stray losses to be negligible, others such as SANS 34-2 and AS/NZ 1359.5 use a fixed value, while IEEE 112, CSA 390 and IEC 34-2 prefer to make actual measurements. A number of these standards were initially considered. However, after preliminary laboratory-tests were performed, it was observed that the IEEE 112 method B (2004) and IEC 60034-2 segregation method (2007) appeared to be the most consistent and repeatable. The two standards were therefore preferred and subsequently chosen for this project. The South African standard, SANS 34-2, is available but its methods of determining efficiency have been found to be unsupported due to its reference to the IEC 60034-2 (1984) which has been abandoned and replaced. The SANS 34-2 was therefore not used in the testing.

Around the world, motor repairs have always been known to cause efficiency loss and performance deterioration. Rewind studies have been done in the United States, Brazil, Canada, the United Kingdom and elsewhere [32] [37] [59] [63]. The results from most of these studies have however been generally inconsistent with various efficiency loss figures ranging from less than 1% to 6% [32] [37] [59] [63]. It has even been suggested that each rewind would result in a 1% loss for multiple rewinds [37]. With so many inconsistent reports and given that workmanship would vary from

country to country, there was an obvious need for a South African investigation be undertaken to ascertain the real situation in the country.

Three induction motor test-beds were constructed in the Electrical Machines Laboratory at the University of Cape Town (UCT). The test-beds provided flexible ways of supplying, loading and measuring the performance of a range of induction motors. Meticulous attention was paid to all aspects of the test-beds, such as motor mounting, power quality, instrumentation accuracy and calibration. This was to ensure accurate and repeatable results.

New squirrel-cage induction motors ranging from 3kW to 55kW were purchased for testing. This range of motors is the most commonly found in the South African industry. Several tests were performed on each motor to assess the accuracy and repeatability of test results. Statistical analyses were performed on the test results for each motor to obtain a representative average efficiency performance curve for each motor. The motors were then sent for complete armature rewinds and retested according to the aforementioned procedures.

From the results obtained, the impact of rewinds was found to be significant with efficiency drops ranging from 0.1 to 1.86%. The changes in the core and stator losses had the biggest contribution on the change in efficiency. The increase in core losses could be attributed to damage on the core during the winding removal process. Better insertion of the stator winding coils while keeping the same number of effective turns would produce lower stator conductor losses. A change in the efficiency profile was also evident as a result of the changes in the constant and load losses.

In addition to the above tests, the impact of motor rewind procedures was investigated by sending two new identical 3kW motors to be rewound separately by two South African repair companies. The results showed a decrease in efficiency of 0.96% for the larger company and 1.09% for the smaller company at full load. This would appear to suggest that the different techniques and procedures used in different companies affect the losses and efficiency differently.

Table of Contents

List of Figures

List of Tables

Nomenclature

DME:	Department of Minerals and Energy
DSM:	Demand Side Management
ERC:	Energy Research Centre
UCTML:	University of Cape Town's Machine Laboratory
Dyno:	Dynamometers
MUT:	Motor under test
DC :	Direct current
AC :	Alternating current
SANAS :	South Africa National Association of Standards
IEC :	International Electrotechnical Commission
IEEE :	Institute of Electrical and Electronic Engineers
SABS :	South African Beareu of Standard
SANS :	South African National Standard
CSA:	Canadian Standards Association
JEC:	Japanese Electrotechnical Commission
SG:	Strain gauge
THD:	Total harmonic distortion
SLL:	Stray load loss

Chapter 1: INTRODUCTION

1.1. Overview

This chapter gives relevant background into the research and outline the structure of the thesis.

1.2. Background

Eskom generates 95% of South Africa's (SA) electricity and 45% of the electricity used in Africa. It also owns and operates the South African national transmission system [1]. An installed capacity of 43 037MW (with maximum capacity of 38 744MW) is achieved through a generation mix of pumped storage, coal, hydro, nuclear and gas/diesel. The contribution from each source is shown in Table 1-1 with coal being the largest contributor.

Table 1-1: Eskom target generation mix [1]

Eskom Generation mix (% of MW)	
Coal	<70%
Gas/Diesel	Only use for peak supply when needed
Hydro/Nuclear	17% – 28%
Pumped Storage	4% – 10%
Open-cycle gas turbine	Only use for peak supply when needed
Imports	2% – 15%
Renewable energy	>2%

The demand and consumption of electricity per sector in South Africa is shown in Figure 1-1. The industrial sector has the largest consumption and demand of electricity, up to 37.7% consumption and 35.5% demand, followed by residential and then mining.

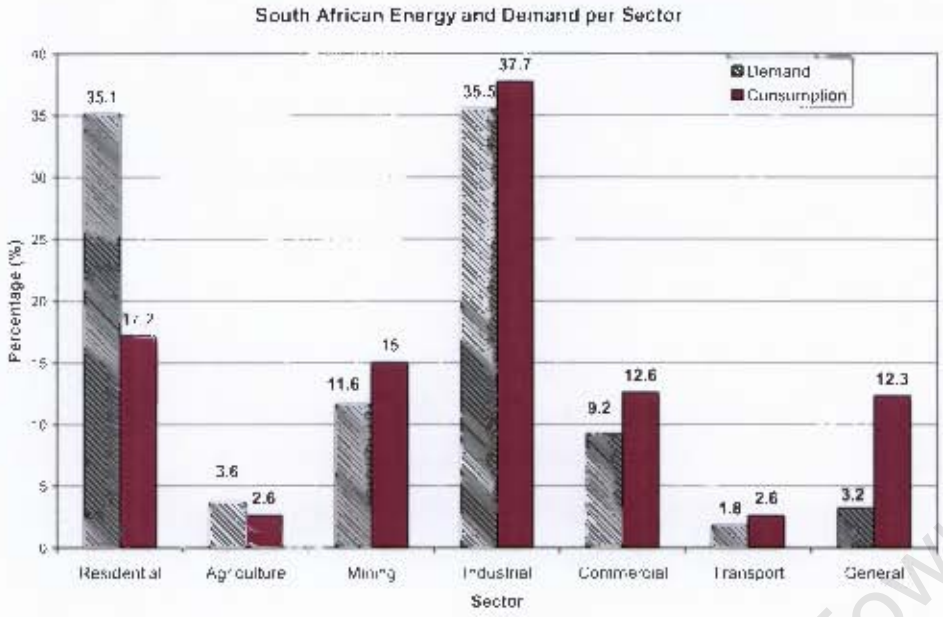

Figure 1-1: Electricity consumption and demand in South Africa (data from 2006) [3]

In 2006, SA experienced an increase in electricity demand, caused by political and economic factors. This resulted in the demand exceeding the supply [2] and subsequent forced outages and interruptions around the country. The problem was also compounded by other factors such as the rising and volatile fuel prices, global warming concerns, and dependence on foreign oil. These problems have highlighted the need for energy efficiency and have accelerated the drive toward energy-efficient, technologies and practices.

The Department of Minerals and Energy (DME) set comprehensive targets for energy efficiency improvements to ease the pressure on Eskom. The target set, by the DME, for 2015 is a total electrical energy reduction of 12% to be achieved as follows: industrial and mining (15%), power generation (15%), commercial and public buildings (15%), the residential sector (10%) and the transport sector (9%) [3].

1.3. Motors and Motorised systems

Motors and motorised systems around the world are estimated to account for 40% of global electric energy consumption [4]. In South Africa, motors account for up to 60% of the total industrial (mining included) energy use and about 57% of the peak

demand generation [4]. According to Eskom Demand Side Management (DSM) [1], an estimated total of 100 000 motors are operating in the Industrial Sector, and consume up to 10 GW of electricity (the equivalent to the power consumption of more than 1,6-million households).

Figure 1-2 shows the distribution of motors according to size. The data was gathered by Eskom DSM in a motor survey conducted in 2007.

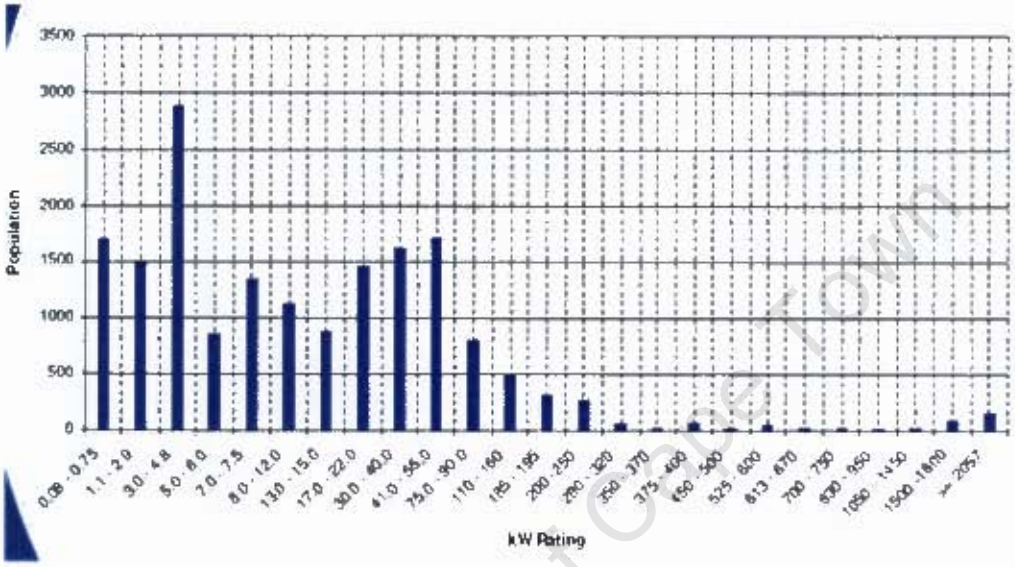

Figure 1-2: Distribution of motors according to size

Data from South Africa's largest motor distributor shows that motors ranging from 0.18 to 90kW are the most common sizes and dominate about 97% of total electric motor market share in South Africa [5]. Table 1-2 shows the estimated demand per motor rating in SA.

Table 1-2: Estimated market demand for electric motors in SA

Motor Rating (kW)	Estimated Market Demand in SA
0.18 - 2.2	40600
3	5200
4	5400
5.5	4800
7.5	6000
9.2	300
11	3700
15	3000
18.5	1500
22	2400
30	1700
37	1300
45	1100
55	1000
75	1100
90	500
110	700
132	300
160	400
185	200
200	200
Total Units	81400

1.3.1. Motor applications

The key industries in which electric motors operate in SA are [5]:

- Petrochemical
- Mining
- Pulp and Paper
- Iron and Steel
- Sugar

The motors perform varying functions ranging from simple conditioning applications to driving the mills that crush millions of tons of coal for power stations. A survey done by the Energy Research Centre (ERC) found that the application of motors is distributed according to Figure 1-3.

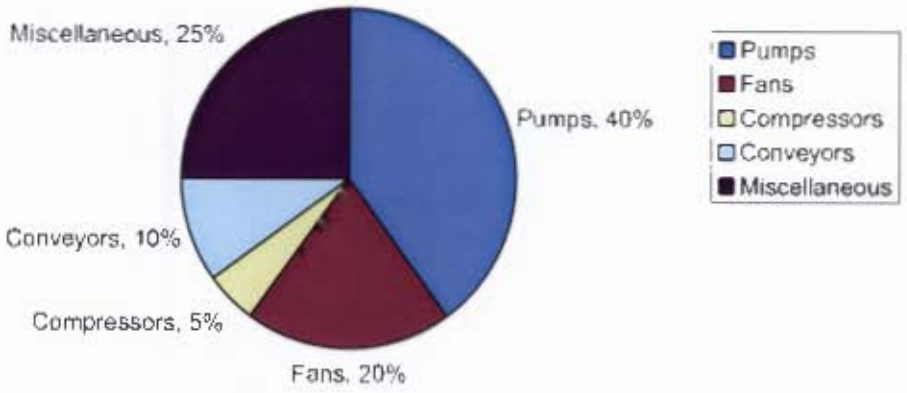

Figure 1-3: Estimated motor applications [5]

1.3.2. Induction Motors

Induction motors (squirrel cage) are the largest single end-use of electricity in industry in South Africa and around the world. This is because induction motors, cross-sectional view shown in Figure 1-4, are simple, versatile and robust machines and are known as the work-horses of 'modern' industry [6] [7]. Squirrel-cage induction motors are electromechanical devices that consist of a cast and balanced rotor and a fixed stator containing conductive windings that when induced produce a magnetic field that spins the rotor.

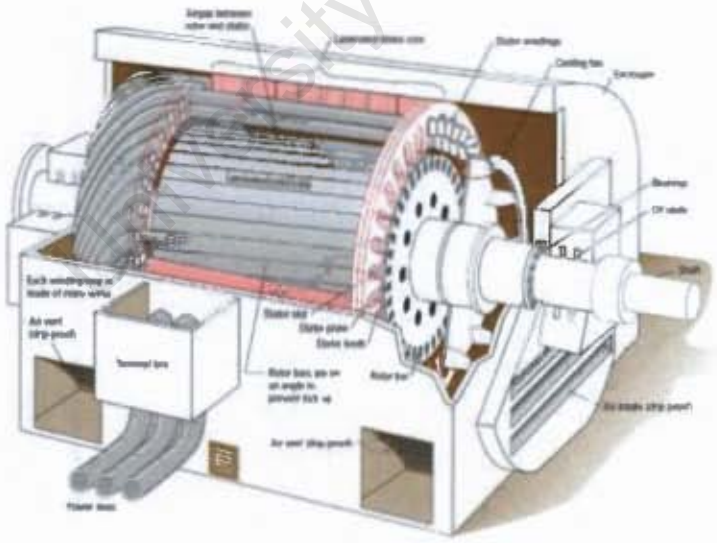

Figure 1-4: Example of an Induction motor

Induction motors therefore have the largest potential for energy saving, with opportunities ranging from the motor user to the utility supplying it with power.

1.3.3. Motor repair industry

Motor repair and rewind in South Africa have been increasing over the past few years. This is a result of increased pressure on industry caused by [8]:

- An increase in the intensity of mining activities, as well as the establishment of new mines in SA. With underground mining being the more common type in South Africa, the depth and size of these mines lead to more use of motors and therefore increase in the need for more motor repair.

- An increase in infrastructure such as roads, railways, the Gautrain project and housing in preparation for the Fifa 2010 soccer World Cup.

- Eskom projects such as the supply capacity expansion (commissioning of mothballed power stations: Camden, Grootvlei and Komati). These projects require the repair of electric motors.

- The sudden increase in industry and urbanisation of countries such as China and India has led to a decrease in the delivery of motors due to the pressure on the world's economy.

In 2005, it was reported that the mining industry in South Africa spent approximately R2-billion on motor repairs [8].

Despite having such a large rewind industry in South Africa, it is not known how various rewinding techniques used by motor repairers affect motor efficiency. This thesis aims to investigate the impact of rewinds on induction motor efficiency.

1.3.4. Impact of rewind and repair on motor induction efficiency

It is widely known internationally that repairs affects induction motor efficiency. A review of research into quantifying this impact on efficiency shows various ranges of efficiency loss.

Ontario Hydro conducted a study in 1991 on electric motor rewinds to determine the effects of rewinds/repairs on electric motor efficiency. Nine 15kW (20Hp) standard efficient motors were damaged then randomly sent to electric motor rewind shops in Canada. The average loss of efficiency was about 1.1%, with the greatest reduction around 3.4%. The efficiency losses were attributed to reduction in conductor cross sectional area, core damage resulting in hot spots, and reduced insulation systems. [59]

A similar study was performed by BC Hydro in 1993 on ten energy efficient motors. The results were different from the study done by the Ontario Hydro. The average loss was 0.5%. The greatest losses were found to be due to increased bearing losses, due to friction, whilst there was little or no increase in core losses observed. The higher friction losses were due to bearing replacement with lower quality bearings [59].

In 1994, J. C. Hirzel of General Electric found efficiency losses ranging from 1.9 to 6%. These results were from four motors ranging from 10 – 200Hp. [62]

The Canadian Electrical Association (CEA) undertook a controlled electric motor repair study in 1995. Several repaired motors were burnt out and underwent the same repair process, including burnouts, dip and bake. Little or no reduction in efficiency was found when the motors went through a controlled repair process. Repeated rewinds (after three rewinds) also showed little to no reduction in efficiency. [59]

In 1998, Dreisilker Electric Motors and the University of Illinois performed a study on the impact of burnout temperatures on electric motors. Temperatures above 320 ℃ were found to cause the stator frames to distort. This was observed on both aluminium and cast iron frames. [59]

In 2003, the Electrical Apparatus Service Association (EASA) and Association of Electrical and Mechanical Trade (AEMT) undertook a larger research project to determine the impact of repair and rewind on induction motor efficiency. The objective was to prepare a 'Good Practice to Maintain Efficiency' document. Twenty-two new motors ranging from 37.5 to 225kW with two smaller motors of 5.5KW were tested before and after rewinding. Motors were tested at the University of Nottingham in the UK. Six motors (75-112kW) averaged losses of 0.4%, ten motors (45-150kW) averaged losses of 0.03% and five motor (75-150kW) averaged increases of 0.5%. The report concludes by stating that motor efficiency can be maintained when 'good' repair practice is followed. [32]

In 2006, Wenping Cao et al performed a comprehensive rewind study involving 23 motors ranging from 5.5 to 225 kW. Cao's results showed that rewinding could impact on motor efficiency and performance. Careful control of the stator winding design while keeping the same number of effective turns will produce a lower stator-conductor loss. This will offset any slight increase in the core, windage, and friction losses. Even repeated rewinds do not cause an appreciable change to the motor efficiency on average [37].

In 2007, Bortoni et al conducted a study in Brazil on a set of eight low-voltage motors with ratings from 2.2 to 11 kW (3 - 15 hp). The study was to determine the influence of rewinding on motor efficiency. The results showed that motor efficiency had a small increase after repair with full-load efficiency increase between - 0.9 and +2.0% respectively. The overall quality of the repair shop was found to have an influence on the impact of the repair on efficiency [63].

Sasol's study into the effects of repairs on motor efficiency found an average drop of 3%. Motors were tested randomly after being repaired [64].

With such diverse conclusions of the effects of repairs on motor efficiency; it is evidently difficult to rely on such results. The rewind procedures followed at a repair shop appears to be the most consistent cause of motor efficiency loss.

1.4. Objectives

The main objectives of this thesis are:

- To build test beds that can be used to accurately and reliably test induction motors ranging from 3 - 55kW in South Africa;

- To analyse the factors that influence induction motor efficiency and

- To examine the effect of rewinding on the efficiency of induction motors by profiling the efficiency loss or gain after rewinding process

1.5. Methodology

The methodology associated with this thesis include:

- Efficiency testing of motors of various kW ratings before rewind to determine the actual efficiency which may differ from the nameplate value;

- Liaise with motor repairers to determine the current rewinding practices that are being employed;

- Performing single armature rewinds on the entire range of motors and

- Retesting the motor efficiency of the rewound motors to determine the impact of the rewinding process or techniques.

1.6. Limitations

- The study is limited to induction motors with squirrel cage rotors because the efficiency standards are based on these motors, and they are most commonly used in South African industries.

- New motors of capacities ranging from 3kW to 55kW have been chosen for the rewind project. Induction motors in this range are popular in South Africa as shown in Figure 1-2. This range also has the greatest potential for energy savings due to their inherently lower efficiencies compared to larger motors.

- The motor repairers used in this thesis are all located in the Western Cape region.

1.7. Structure of thesis

The structure of each chapter begins with a brief overview followed by a literature review of the particular topic (in most chapters) and then the results are presented.

Chapter 2 describes the methodology followed in the construction of the test beds and motor testing.

Chapter 3 presents details of the data analysis that was used in all recorded data

Chapter 4 presents literature and results on motor efficiency and the determination of motor efficiency according to international standards.

Chapter 5 outlines the repair and rewind procedures and how these could impact on motor efficiency. A review of the rewind procedures of two South African repair companies is presented.

Chapter 6 presents the analyses of the results from the repair and rewind testing discussed in chapter 5.

Chapter 7 discusses motor economics scenarios.

Chapter 8 presents the conclusions and recommendations.

1.8. Contributions

- Mzungu, H.M.; Manyage, M.J.; Khan, M.A.; Barendse, P.; Mthombeni, T.L.; Pillay,P., ***'Application of induction machine efficiency testing standards in South Africa',*** Electric Machines and Drives Conference, 2009. IEMDC '09. IEEE International, 3-6 May 2009 Page(s):1455 – 1462

- Prof. P. Pillay, Dr. M. Manyage, Dr. A Khan, Dr. P. Barendse and Mr. M. Mzungu, '***Induction Motor Efficiency and Rewind Study'***, Eskom Demand Side Management Research Report

- H. M. Mzungu, P. Barendse, M. A. Khan and M. Manyage, ***'Determination of Effects on Induction Motor Efficiency,*** ICUE Conference', May 2008

- M.A. Khan, D. Pati and H.M. Mzungu, '***Comparison of a 3kw Standard and High Efficiency Induction Motor',*** Vector Journal, June 2008

- Mzungu, H.M.; Sebitosi, A.B.; Khan, M.A.;. ***'Comparison of Standards for Determining Losses and Efficiency of Three-Phase Induction Motors'***, Power Engineering Society Conference and Exposition in Africa, 2007. PowerAfrica '07. IEEE16-20 July 2007 Page(s):1 - 6

- H. M. Mzungu, A. B. Sebitosi, M. A. Khan, ***'Comparison of Standards for Determining Losses and Efficiency of Three-Phase Induction Motors'***, Vector Journal, July 2007

Chapter 2: TEST BED DEVELOPMENT

2.1. Overview

This chapter describes the methodology that was followed through the entire project. Each section presents a detail process from the motor selection to the construction of test beds and finally, the treatment of the collected data.

2.2. Motor selection

Motors ranging from 3-55kW were selected for the rewind project. This range has the largest motor population and demand of motors in South Africa as shown in Figure 1-2 in Chapter 1. The criteria set for the motors were:

- Standard efficiency motors, 4 Pole, 1500rpm, IP 55 protection
- Foot mounted with standard frames sizes, 50Hz, 380V Delta connection
- Duty cycle: S1, Insulation class F

Table 2-1 shows the actual WEG motor sizes and the ratings for each tested motor. Detailed catalogues for each motor are found in Appendix A.

Table 2-1: Selected motors for project

Motor size (kW)	Speed (rpm)	Current (A)	PF (p.u.)	Frame
3	1390	6.63	0.84	100L
7.5	1450	12.1	0.87	132M
11	1455	22.9	0.83	160M
15	1455	30	0.85	160L
22	1465	42.6	0.85	180L
37	1480	69.1	0.88	225S/M
45	1475	83.2	0.88	225S/M
55	1475	99.4	0.9	250S/M

2.3. Laboratory capabilities

All testing were performed at the University of Cape Town's Machine Laboratory (UCTML). Three test beds were constructed with great emphasis placed on precision

and accuracy in order to ensure reliable results with high repeatability (see Section 2.5).

The UCTML is unique in that it has a flexible distribution system and can provide both AC and DC supplies. The lab is rated at 500kVA and has a 500kVA substation supplied with 11kV. The 11kV supply is stepped down to 500V through a three-phase transformer. The lab contains two 500V, 250kW 4-quadrant DC drives connected to two separate 250kW, 980rpm DC motors; a 6.6kV, 520kW, 57A 980RPM alternator, a 75kW AC variable speed drive, 3 and 12kW DC motor capable of running up to 200% of full-load rated conditions; and three 16kW 400V 40A DC drives.

2.4. Dynamometer System

Efficiency testing requires loading of the test motors and the measurement of both input and output power [10] [11] [12]. Electrical input can be easily measured with a power analyzer. Mechanical power on the other hand requires the measurement of both the shaft speed and torque as shown in Equation 2.1 [13].

$$Power = Speed \times Torque \tag{2.1}$$

Dynamometer (dyno) systems are instruments used to place a controlled mechanical load on devices such as motors. The test system allows for the measurement of torque and rotational speed, which are used to calculate the output power exerted by motors (or engine or other rotating prime mover). Dynamometers *"are to motors and motor drives as oscilloscopes are to electronics – a basic test instrument"* [13].

There are different types of dynamometer systems that are used in motor testing. These are:

- Prony dyno
- Eddy current brake
- Water brake dyno
- Electric motor/generator dyno

2.4.1. Electric motor/generator dyno

The **electric motor/generator type dyno system** is the most widely used loading technique and was therefore used on all three test beds with DC generators to dissipate power. The 3kW and 15kW test beds used the cradled type dyno (see sections 2.3.3 and 2.3.4) and the 250kW test bed used the absorption dyno (see section 2.3.5). Table 2-2 shows ratings of the DC generators for the three test beds.

Table 2-2: Test bed power ratings

Test Bed	DC Motor type	DC Dynamometer Rating	Induction Motors tested
3kW	Separately Excited	3kW	3kW
15kW	Separately Excited	12kW	7.5, 11, 15kW
250kW	Separately Excited	250kW	22, 37, 45, 55kW

An electric motor/generator dyno system is a specialised dynamometer type that operates with an adjustable-speed drive. The dyno can be either an AC or DC machine operating as a generator. The dyno is driven by the test motor and converts the mechanical energy into electrical energy [14].

Loading of the test motor can be achieved through armature current control of the DC generator (Equation 2.2). This can be explained by looking at the separately excited DC motor circuit in generating mode as shown in Figure 2-1 [15]. The field is excited separately by a DC current and its rotor is driven by the test motor at shaft speed ω_m.

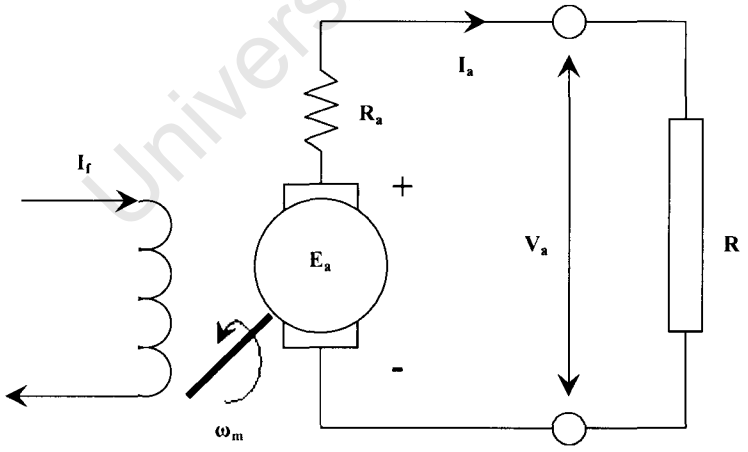

Figure 2-1: Schematic of Generator Set

The torque developed by the armature of the DC motor is a function of the flux and armature current as shown in Equation 2.2 [15]. Torque can be controlled by adjusting the armature current or the field flux.

$$T = K_a \Phi I_a \tag{2.2}$$

Where,

T = developed torque

F = field flux

I_a = armature current

K_a = machine constant

The induced armature voltage back emf (E_a) is a product of the flux and shaft speed. (or the product of the armature current and the sum of the armature and external resistance). Equation 2.3 [15] shows this relationship.

$$E_a = K_a \Phi \omega_m = I_a (R_a + R) \tag{2.3}$$

Where,

E_a = generated DC voltage

R_a – armature resistance

R = external resistance

ω_m = shaft speed

By rearranging Equations 2.2 and 2.3, it can be seen that the torque can be controlled by adjusting either the flux, the external resistance (R) or the current.

$$T = \frac{I_a^2 (R_a + R)}{\omega_m} \tag{2.4}$$

Current control is normally used due to the wide control range. This control is achieved through converters such as four-quadrant DC drives with regenerative braking controls.

2.5. Construction of the test beds

According to Wallace et al [9], the elements for a highly functional and efficient testing laboratory and the production of both accurate and reliable results are:

- Industrial relevant power rating capability;
- Wide range of service voltages, with ability to simulate under-, over- and unbalanced voltages;
- Wide range of machine speeds;
- Mounting of a wide range of machine frame sizes;
- Ability to test both motors and generators;
- Ability to test power electronic converters;
- Ability to make accurate measurements

These elements were closely applied during the construction of the test beds.

2.5.1. 3kW test bed

The 3kW test bed was designed to accommodate motors ranging from 3kW and below. It was constructed on a flat solid base with tracks. Figure 2-2 shows the complete test bed.

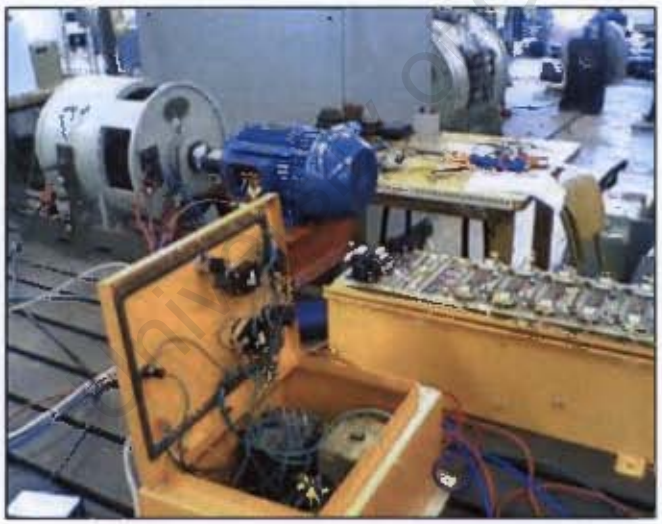

Figure 2-2: 3kW test bed

The DC generator used as a dynamometer is rated at 3kW. This machine is cradled on a double bearing gimble structure and could be loaded to 200% of its rating. Figure 2-

3 shows the cradled dynamometer system. A 50kg load cell is used to measure torque (see Section 2.4.1) and holds the DC motor from rocking.

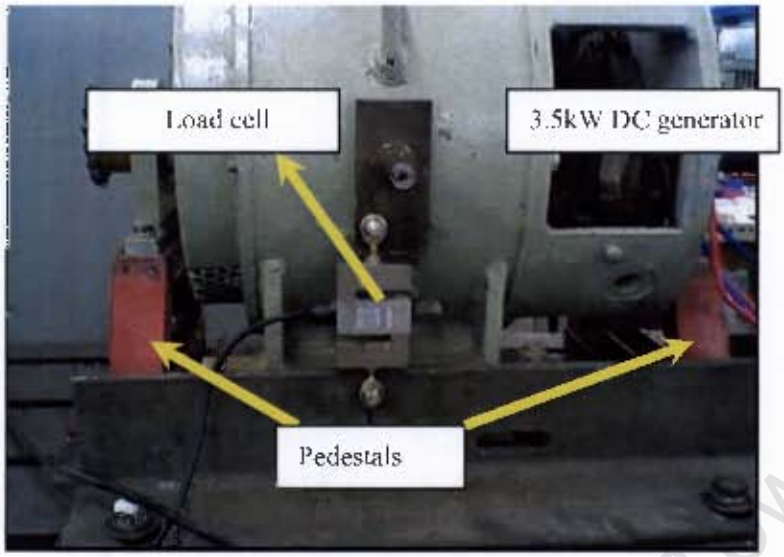

Figure 2-3: Cradled DC dynamometer

2.5.1.1. Motor under test loading

A 16kVA, 380V, 35A, four-quadrant, DC drive, shown in Figure 2-4, was used to control the current of the dyno. A multi-turn potentiometer allowed accurate current control and therefore torque control.

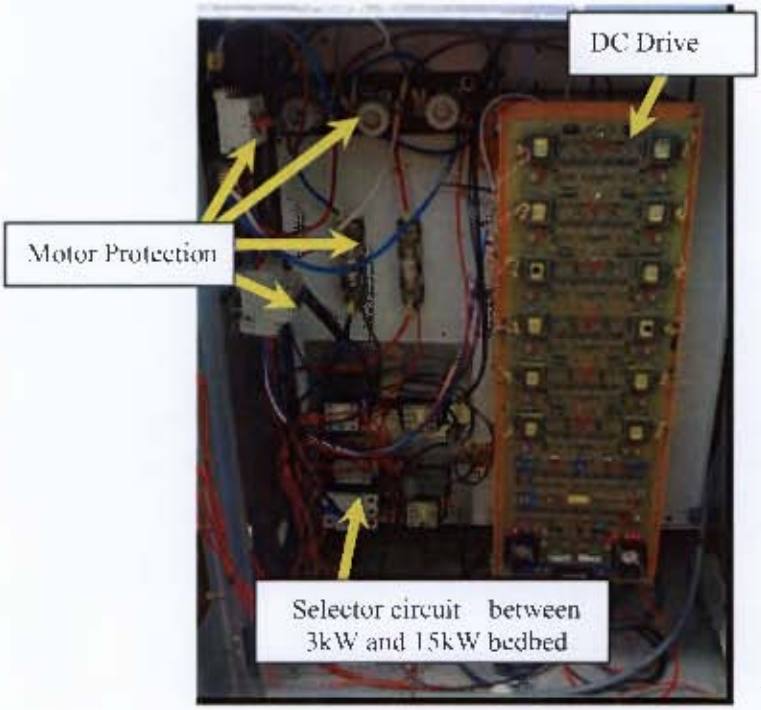

Figure 2-4: 4-Quadrant 16kVA DC Drive

2.5.2. 15kW test bed

The 15kW test bed was designed to accommodate motors from 7.5kW to 15kW. The bed was fitted with a 15kW DC dynamometer that could be loaded to 200% of its rating. Three configurations were attempted:

- Inline torque transducer system with a C-channels base (Figure 2-5),
- Cradled Dyno force system transducer with a C-channels base (Figure 2-6) and
- Cradled Dyno - force system transducer with a solid steel base (Figure 2-7)

2.5.2.1. Inline torque transducer with C-channels

The test bed was designed and constructed to accommodate an inline torque transducer. The motors were mounted on C-channels and the transducer was mounted on two bearing stands as shown in Figure 2-5. This mounting presented a number of challenges. The alignment of the long shaft was difficult and therefore high vibrations were present during testing. The vibrations led to a number of premature failures of

the bearings. The rating to the inline torque transducer is 2000Nm (or 2kNm), which resulted in it being operated at its lowest range resulting to large errors [16]. All the tests performed failed with calculated negative correlation factors (details in Chapter 3).

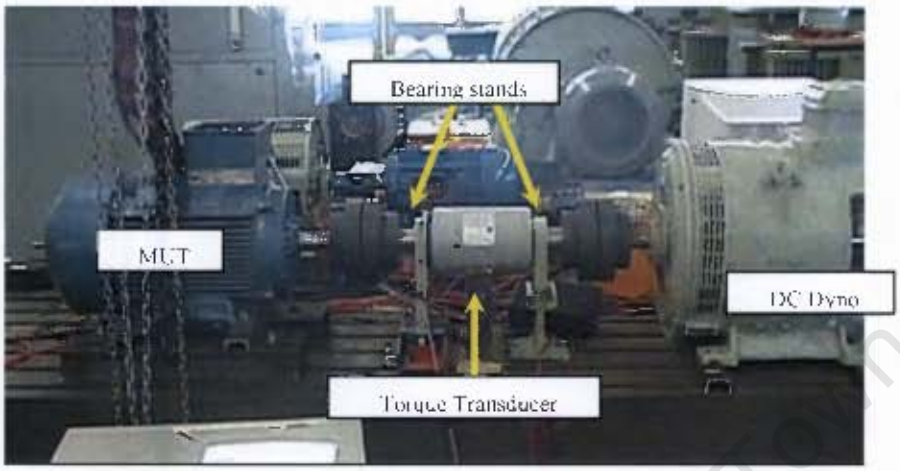

Figure 2-5: 15kW test bed

2.5.2.2. Cradled dyno - force transducer system with C-channels

The MUT and DC dyno were mounted directly with C-channels mountings. The dyno was cradled (see Figure 2-6), similar to the 3kW dyno system, with a 100kg load cell holding the dyno from rocking.

Figure 2-6: 15kW test bed: transducer system with C-channels

It was found that the C-channel type motor mountings distorted when bolts were tightened (Figure 2-7). This distortion led to what is known as 'soft foot' [17]. Motors with soft foot move during operating. This movement results in vibrations, which lead to increased motor losses, and eventually to premature bearing failure.

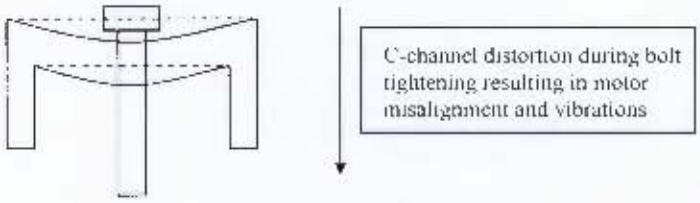

Figure 2-7: C-channels distortion

Various C-channels were used for the different MUT. This meant exhaustive motor overhauls during MUT changeovers. These disadvantages resulted in abandoning the C-channels and redesigning the test bed mountings.

2.5.2.3. Cradled dyno - force transducer system with steel base

Solid still bases were machined for both the MUT and the DC dyno. This can be seen in Figure 2-8 with a mounted 11kW motor. The base was designed to accommodate all tested motors (7.5 - 15kW) without any mounting overhaul.

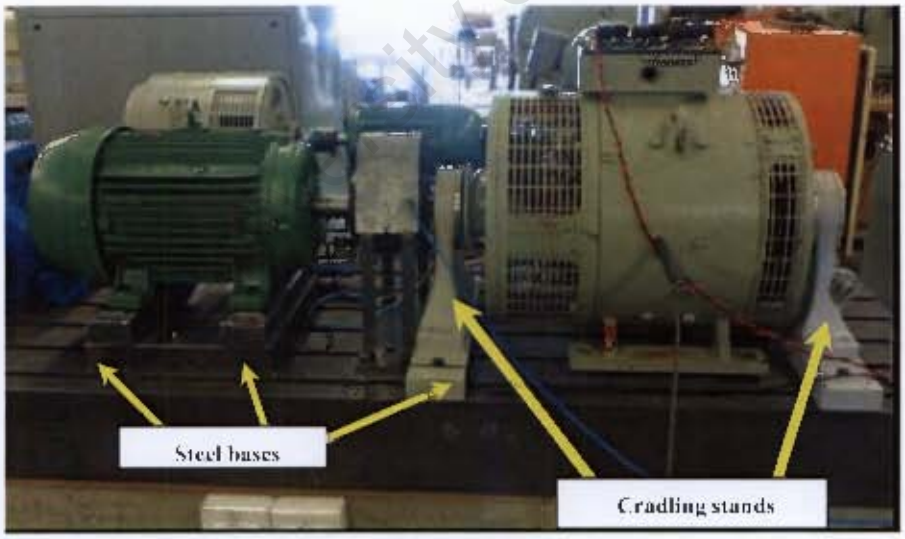

Figure 2-8: 15kW test bed with steel base

Figure 2-9 shows the adjustable base design, which can accommodate all the test motors by shifting the two side steels.

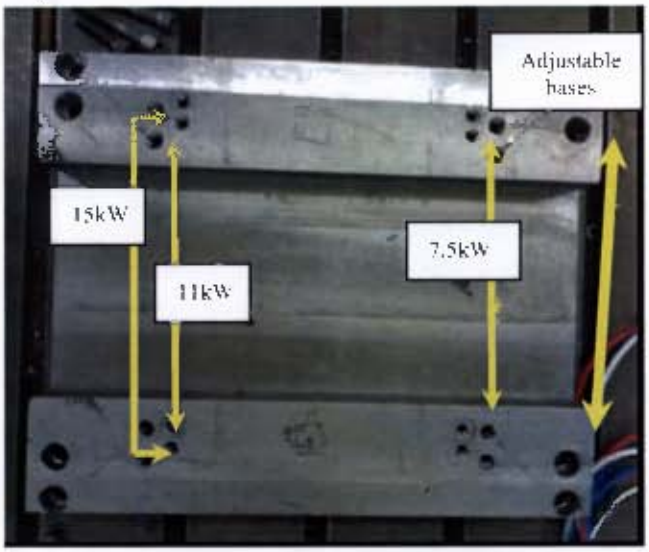

Figure 2-9: Adjustable base design

The base also provided better MUT mounting and this in turn significantly reduced motor vibrations.

2.5.2.4. MUT loading

Loading of the MUT on the 15kW test bed was achieved with a combination of resistor bank and current control of the same DC drive used in the 3kW test bed (Figure 2-10). The resistor banks were used to load the 15kW test motor above rated load, as required by the testing standard. The highest loading achieved on the 15kW motor was 125% of rated load.

Figure 2-10: Resistor banks

2.5.3. 250kW test bed

The 250kW test bed was designed on the UCTML's base plate (Figure 2-11). The base plate is rigid, flat and forms a single plane. The advantage of this is the overall structure remains securely positioned and provides good damping of vibration [17]. The 250kW test bed constructed on this base plate is shown in Figure 2-11. Motors rated from 22kw to 55kW were tested on this test bed.

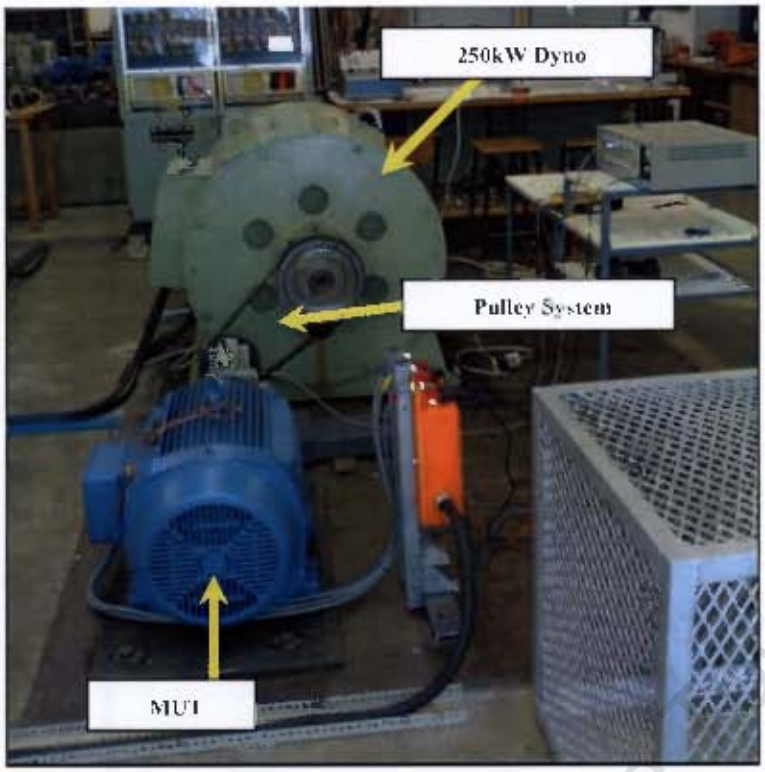

Figure 2-11: 250kW test bed

The 250kW DC dynamometer was mounted on four base plates and the MUT on a flat plate as shown in Figure 2-11. The motors were tightly fastened down using high-tension bolts. The coupling of the dynamometer and the MUT was done through a pulley system. The pulley system converted the 1000 rpm speed rating of the DC dyno to the 1500 rpm speed rating of the test motors.

2.5.3.1. Pulley system

The pulley system was designed for a gear ratio of 2:3 and a maximum power transfer of 90kW. The pulley system brought about a number of advantages in UCTML. It maximized the limited floor space and made the removal and adjustment of the test motors easy.

i) ***Pulley Belts***

Belts, from Gates Synchronous Belts, were used because of the deep tooth and groove contact as shown in Figure 2-12. This deep contact provided superior load-carrying

strength, reduced noise, reduced vibration, and accurate timing and synchronization, with no loss of torque carrying capability [18].

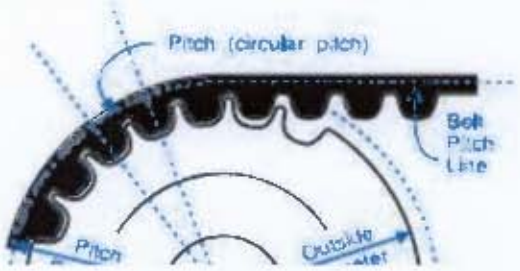

Figure 2-12: Deep tooth and groove contact [19]

ii) *Installation*

When installing a synchronous belt, the right tension is required to achieve optimum performance [19]. If the tension is too low the belt's teeth will jump (also called ratcheting) during high load operating conditions. If the tension is too high the belt's life will be reduced and possible damage could be incurred to bearings, shafts and other drive components. [19]. The recommended installation tension can be estimated in two ways. Calculating the deflecting forces (Equation 2.5) and calculating the recommended belt distance deflection (Equation 2.7) [20]. Figure 2-13 below shows the variables used in Equations 2.5 to 2.7.

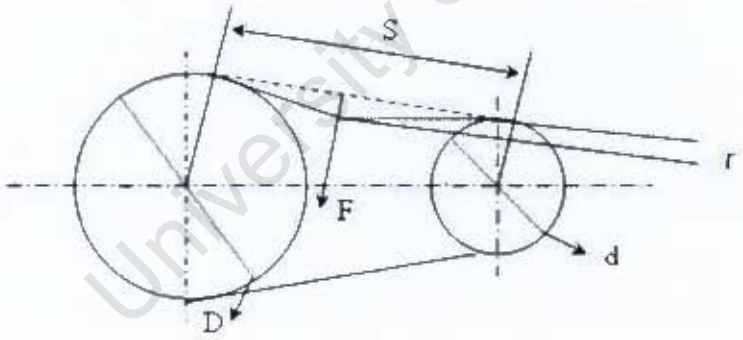

Figure 2-13: Pulley belt variables

Recommended deflecting forces

$$F = \frac{P \times k}{v} \qquad (2.5)$$

Where,

F = deflecting force (N)

P = transmitted power (kW)

k = 60 for maximum installation tension

25 for minimum installation tension

v = belt speed (calculated according to equation 2-6)

$$v = \frac{Pitch \times N \times rpm}{60\ 000} \tag{2.6}$$

Where,

Pitch = see figure 2-13v (mm)

rpm = speed of drive D (see figure 2-13)

N = number of grooves on drive D (see figure 2-13)

Recommended belt deflection

$$r = \frac{S}{50} \tag{2.7}$$

Where,

r = belt deflection (mm)

S = belt span length (mm)

Table 2-8 shows the calculated data for the belt installation.

Table 2-3: Belt Installation data

P(kW)	v (m/s)	Pitch(mm)	N	Deflecting forces (N)		S (mm)	Belt deflection (mm)
				Max	Min		
90	16.45	14	47	328	136	460	9.2

The deflection of the belt (9.2 mm) and maximum forces (328 N) were both used in the belt installation. Figure 2-14 shows the apparatus used to measure the deflection force.

Figure 2-14: Force deflection apparatus

2.5.3.2. Torque transducer mounting

An HBM inline torque transducer was used to measure torque on the 250kW test bed (see Section 2.4.1 for the operation). With a calculated maximum radial force of 5208N on the torque transducer from the pulley, a structure was designed to withstand this force. The transducer structure is shown in Figure 2-15.

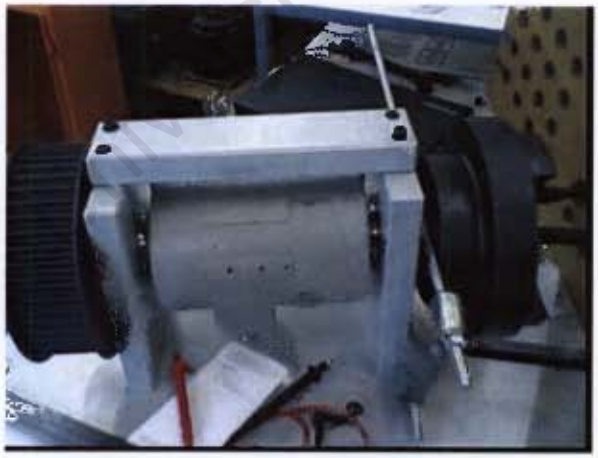

Figure 2-15: HBM inline torque transducer

2.5.3.3. MUT loading

The loading of the MUT on the 250kW test bed is achieved through current control using the 500V, 4-quadrant, DC drive shown in Figure 2-16.

Figure 2-16: 500V 4-quadrant DC drive

2.5.4. Couplings

Fenner taper lock couplings were used on all the motors on the different test beds as shown in Figure 2-17. The couplings come in two parts, the bushing that goes onto the shaft and the coupling that goes over it. The couplings allow quick and easy installation. The straight edge and machined outside offer quick alignment. The rubber, which is wedged between the couplings, accommodates minor misalignment [21].

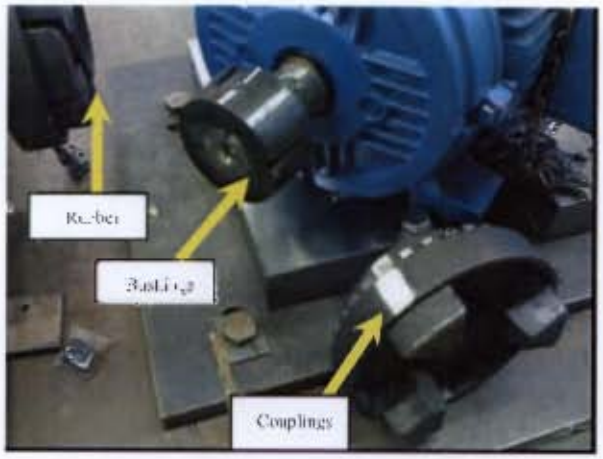

Figure 2-17: Motor couplings

2.5.5. Bearings

Shielded deep-groove ball bearings were used in all the test bed motor mountings as shown in Figure 2-18. These bearings were chosen because they have reduced rotational friction and support both radial and axial loads [21]. Other advantages of the deep-groove bearings are the simple design, long service life and the ease of maintenance.

Figure 2-18: Deep-groove ball bearings

2.6. Instrumentation

Instrumentation plays an important role in determining efficiency accurately and with high repeatability [22]. Efficiency testing requires the following major quantities to be measured accurately: Torque, Speed, Voltage, Current, Power, Temperature and Resistance

Alignment is also another crucial measurement that plays a part in the accuracy and repeatability of the data. The accuracy, calibration and method used for each measurement will be discussed separately.

2.6.1. Torque measurements

Torque is the most crucial mechanical quantity to be measured in a test [16]. The precise measurement of torque is the most demanding aspect to the users of test benches and manufacturers [16]. Torque is used in the determination of the motor output power (Equation 2.1) and has been found to lead to large errors in efficiency determination, if measured incorrectly [22].

Three torque measurement methods were tested and used. These are discussed below.

2.6.1.1. Torque from the output of the DC dynamometer

Rearranging Equation 2.1 shows that torque can be calculated by dividing the output power of the MUT by speed. The output power of the MUT can be calculated by adding the losses of the DC dyno to the DC dyno output power. Figure 2-19 illustrates this procedure. This method was tested on the 3kW test bed using a 3kW motor.

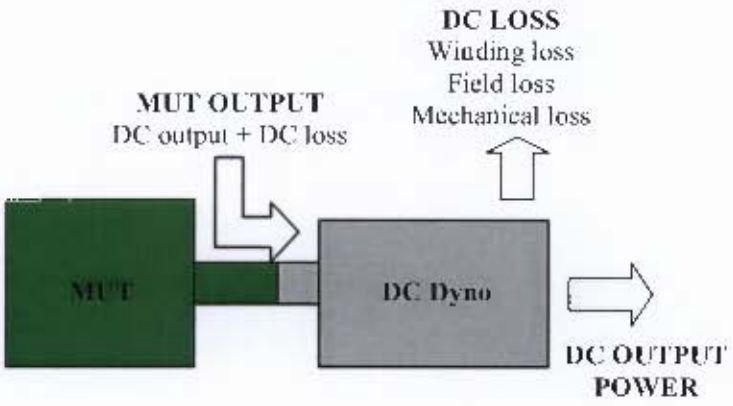

Figure 2-19: Torque determination from DC Dyno loss

The results from this method were compared to the more accurate and well-documented method - measuring reaction torque (see Section 2.4.1.2). The results found are shown in Table 2-4. Large difference in the measured torque was found especially on the lower loading points.

Table 2-4: DC dyno output power method vs reaction torque method

Loading (%)	Reaction Torque (N.m)	DC Dynomometer loss Method (N.m)	Error (%)
100	20.07	19.48	2.92
75	15	14.56	2.91
50	10	7.08	29.23
25	5	2.35	52.99

This method was abandoned due to the large errors that were found to lead to poor determination of efficiency. The cause of the errors is the inaccurate determination of the DC dyno losses. Details of the calculations procedure is found in Appendix B.

2.6.1.2. Reaction torque measurement

Measuring the torque by measuring the reaction force is a commonly used method of torque measurement, especially in engine testing [16]. The principle used is that the torque at the shaft equals the reaction torque of dyno stator. The dyno is free to rotate but is held in position by a load cell. Figure 2-20 shows the 15kW cradled dyno and the load cell.

The force acting on the stator of the dyno is translated to an electric signal by a load cell (or force transducer). The load cell, using strain gauges in a Wheatstone bridge circuit, is rigidly attached to the dyno so that any force on the stator is measured by the transducer. The voltage signal from the transducer is transmitted to a signal amplifier and then to a display. This torque measurement method was used on the 3kW and 15kW test beds.

2.6.1.3. Accuracy and Calibration (change the numbering to next level 2.6.1.2.1)

The disadvantage found in the reaction torque measurement is the need for complex mechanical arrangements. Poor mechanical arrangement leads to vibrations, which lead to 'flickering' of the last digits on the display. The loss of these last digits lowers the torque measurement accuracy [23]. Poor mounting can be detected through calibration.

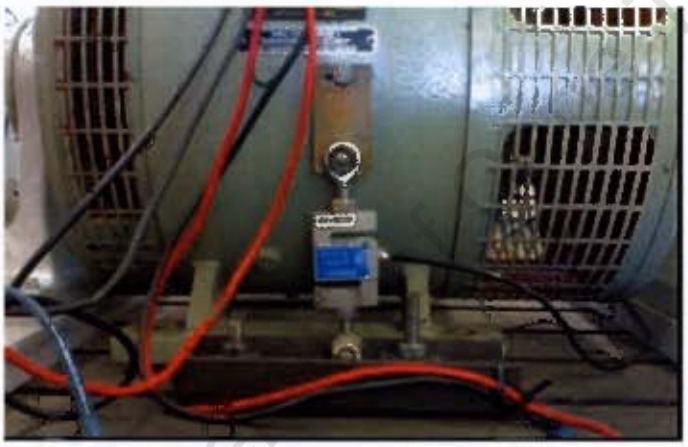

Figure 2-20: Mounted of a 100kg Load cell

Calibration of the load cell on the 3kW and 15kW test beds was done by loading a lever arm with known weights as shown in Figure 2-21 [16]. The weights used were weighed with a calibrated scale. The known applied force (and therefore torque) is used to calibrate the load cell.

Figure 2-21: Torque Calibration

The quality of the load cell and the dyno mounting is reflected in the linearity of the force versus the torque. Figure 2-22 shows the calibration of the load cell on the 15kW test bed. The weights were loaded and unloaded. A minor hysteresis can be seen, which represents the inherent behaviour and hence error of the load cell [24].

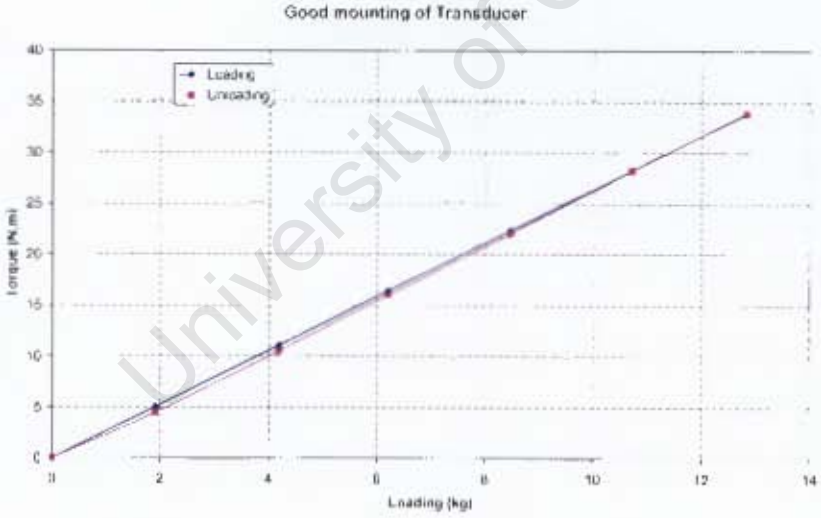

Figure 2-22: Linearity of good, rigid transducer mounting

Poor mounting, as discussed earlier, can be detected during calibration. Figure 2-32 below shows the author's first mounting attempt.

Figure 2-23: Poor mounted of Loadcell

Although the mounting was rigid enough, the lower bar bend during high torque conditions and that results in a curve in the load cell mounting linearity. This is clearly illustrated in Figure 2-24, which leads to significant error in the torque measurement systems.

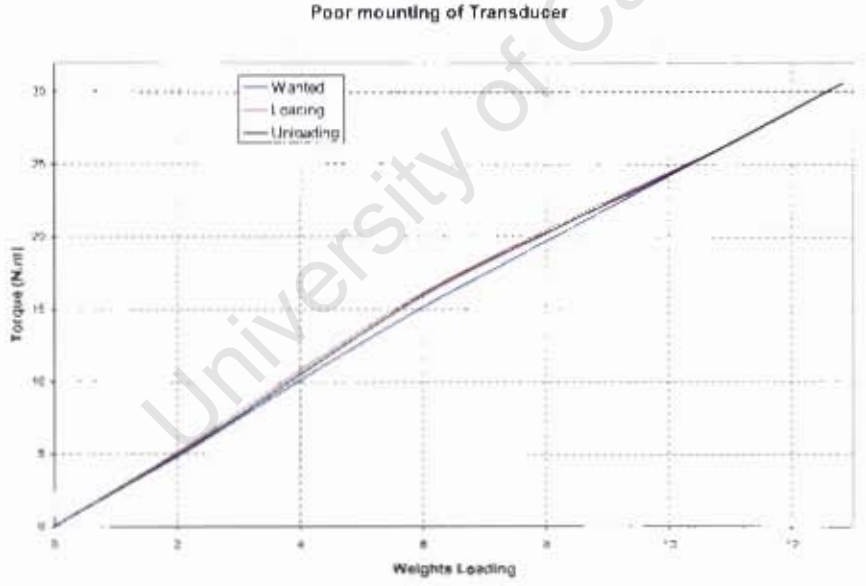

Figure 2-24: Error in linearity due to poor transducer mounting

2.6.1.4. Inline torque measurement (numbering should be 2.6.1.3, update the rest)

Measuring the inline torque requires the measurement of torque on the rotating shafts. This is the most accurate method of measuring torque [16]. A HBM T1 inline transducer rated at 2kN with an output signal of 1.5mV/V was used on the 250kW test bed (Figure 2.5 in Section 2.3.5).

The transducer has a rotor and a stator. The torque signal is produced by the elastic deformation of the rotor. This is done using strain gauges (SGs). SGs measure deformation with a change in resistance proportional to the induced strain [25]. The SGs in the HMB transducer are connected in Wheatstone bridge circuit with temperature compensation SGs. This is shown in Figure 2-25 below.

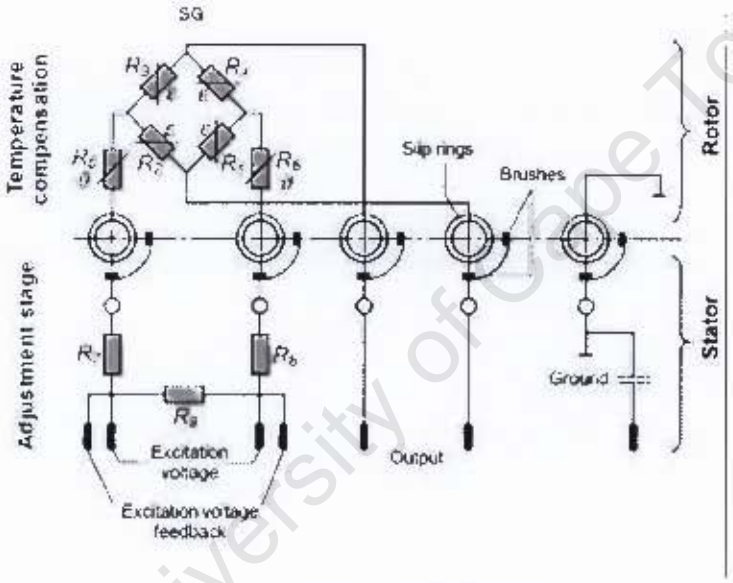

Figure 2-25: Wheatstone bridge circuit [25]

The supply voltage (0.5V - 12V) and measurement signals are transmitted from the rotor to the stator through sliver slip rings and graphite carbon brushes. The brushes are held down by pressure springs. An extra slip ring is included in the HBM transducer to equalize the potential between the rotor and stator. The input resistance is 350 Ohms. [25]

The inline torque transducer operates together with a 5kHz carrier-frequency amplifier [26]. The amplifier satisfies two conditions:

- It amplifies the small signal (7.5 mV at 1.5mV/V with an excitation of 5V) into a suitable signal of ±10V
- It filters brush noise from the signal in order to isolate the component frequency that is physically relevant (5 kHz)

The amplified signal is fed into the power analyzer where averaging and filtering options are available. The operation documents for the T1 are found in the Appendix B.

2.6.1.4.1. Accuracy and Calibration (check numbering)

The transducer has a 0.1% accuracy. Calibration was done using the lever-arm-method [25]. A 2m bar was attached on one end of the torque transducer and blocked on the other side. Weights (weighed by a calibrated scale) were loaded and unloaded to check for linearity. The equation of the calibration line was used to determine the required torque. The calibration setup is shown in Figure 2-26.

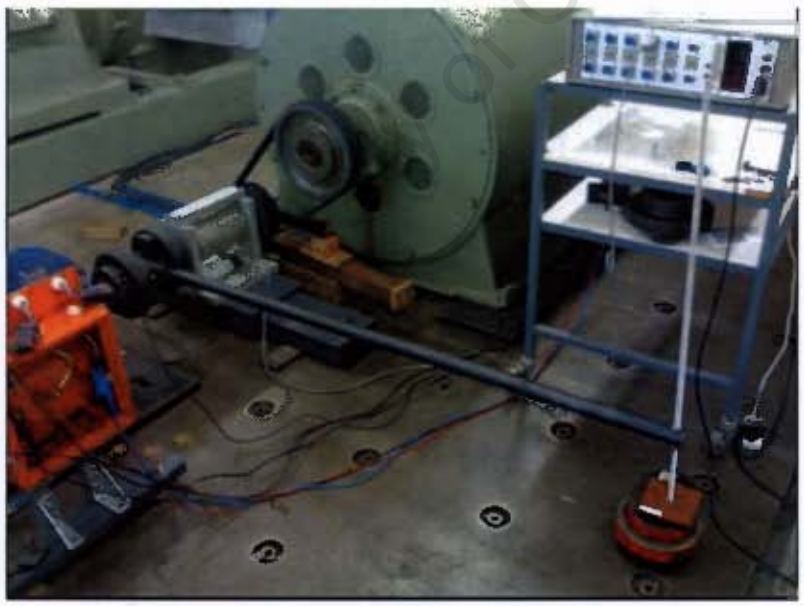

Figure 2-26: Inline Torque calibration using the lever-arm-method

Figure 2-27 shows a graph of the applied force versus the output voltage of the torque transducer. The transducer was zeroed through the amplifier before loading the bar. This compensates for the weight of the bar itself and ensures accuracy of the applied shaft torque. The graph in Figure 2-27 was used to determine the applied shaft torque. Calibration was done frequently before motor testing to check for any drifting caused by temperature.

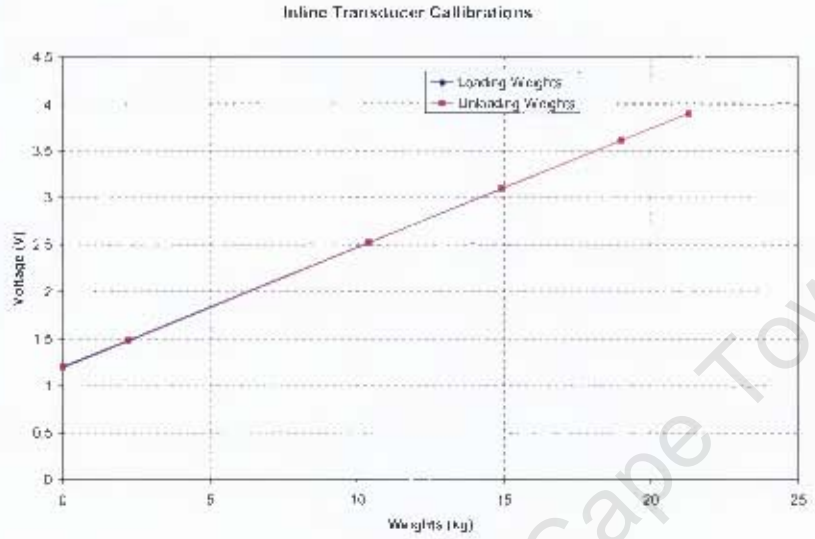

Figure 2-27: Transducer linearity

2.6.2. Voltage, Current, Frequency and Power measurement

The Voltage, Current, Frequency and Power measurements were measured using the WT1600 Yokogawa power analyzer shown in Figure 2-28.

Figure 2-28: WT1600 Yokogawa power analyzer

Current clamps, shown in Figure 2-29, were used for the 250kW test bed. The clamps were used on the 250kW bed because of the high motor current, which exceeded the input current range of the analyzer. The clamps have a ratio of 1000: 1A.

Figure 2-29: Current clamps

2.6.2.1. Accuracy and calibration

The accuracy of the power analyzer for measuring the different elements is shown in Table 2-5 [27].

Table 2-5: Accuracy of Power Analyzer

Measurement element	Accuracy (%)
Power	0.2
Freq	0.1
Current	0.2
Current clamps	0.1
Voltage	0.2

The analyzer was calibrated at a Yokogawa service centre according to the requirements of ISO/IEC 17025:2002. The test laboratories are an accredited laboratory by the SANAS and meet the requirements of the ISO 9001: 2000. The full certificate of calibration can be found in the Appendix B.

2.6.3. Speed measurements

Speed was measured in two ways on the different test beds. The speed on the 3kW was measured using a contact/photo tachometer shown in Figure 2-30. A white strip was attached on the shaft of the motor and this reflected the emitted light.

Figure 2-30: Contact/Photo tachometer

Speed on the 15kW and 250kW bed was measured using a 30 teeth gear with a proximity sensor shown in Figure 2-31. The voltage pulses from the proximity sensor are input to the Yokogawa analyzer (Figure 2-28), where the speed is calculated.

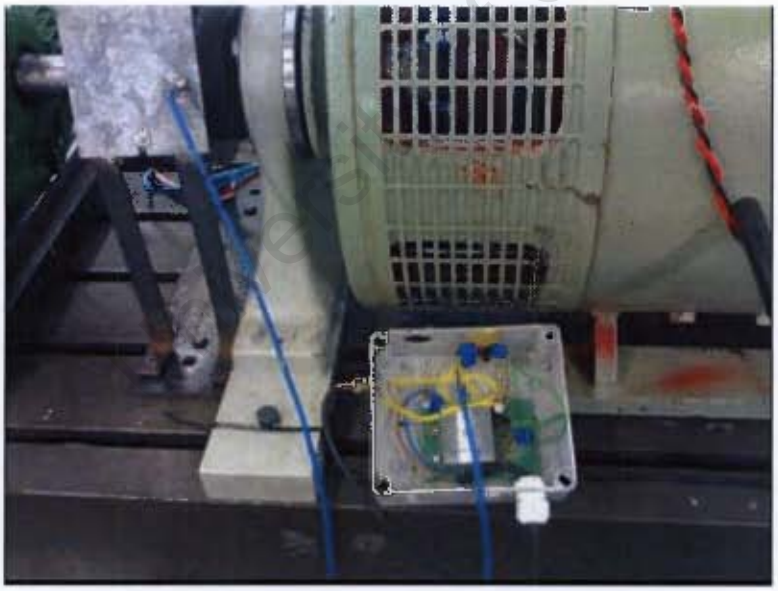

Figure 2-31: 30 teeth gear with a proximity sensor

2.6.3.1. Accuracy and calibration

The accuracy of the contact/photo tachometer (figure 2-30) is 0.05%, which enables speed measurement accuracies up to 1 rpm [28]. The tachometer calibration was done by measuring the speed of a synchronous motor and comparing this to the measured frequency from the calibrated Yokogawa power analyzer.

The accuracy and calibration of the gear and proximity speed sensor was done with a calibrated tachometer. Further accuracy was ensured by sending the speed pulses from the proximity sensor to the Yokogawa analyzer, which has a pulse recorder with an accuracy of 0.2% [27].

2.6.4. Resistance measurement

Winding resistance was measured using a Yokogawa portable Wheatstone Bridge galvanometer shown in Figure 2-32. The galvanometer is used to measure the test motor's winding cold and hot resistance, which are crucial for temperature correction (more details in Chapter 3). The meter uses the Wheatstone bridge principle to measure the unknown winding resistance.

Figure 2-32: Yokogawa galvanometer

The measurement of the winding resistance using the galvanometer at each part-load is not possible. Therefore, the measured resistance at the known temperature is used

to calculate the resistance at any temperature, and hence loading. This is determined by Equation 3-19 in Chapter 3.

2.6.4.1. Accuracy and calibration

The Yokogawa Wheatstone bridge can measure resistances up to three decimal points depending on the multiplier setting. The stated accuracy of the bridge is 0.5% [29]. The accuracy of the calculated resistance at each part-load was determined by comparing actual measured winding resistance, with the motor switched off, to the calculated resistances. Table 2-5 shows comparison of the results obtained from a 3kW motor.

Table 2-6: Accuracy of resistance calculation

Loading (%)	Temp (°C)	Measured resistance (O)	Calculated SANS resistance (O)	Diff (O)	Calculated IEEE/EC resistance (O)	Diff (%)
100	91.21	1.75	1.86	0.11	1.85	0.09
75	79.75	1.71	1.80	0.09	1.78	0.07
50	70.21	1.67	1.74	0.07	1.73	0.05
25	60.62	1.63	1.69	0.06	1.67	0.04

The difference between the measured and calculated resistance ranges from 3% to 5%. The difference can be accounted for by the fact that the motor cools down when power is switched off prior to careful resistance measurement. Furthermore, the difference is also influenced by the point/s at which temperature is measured on the winding. This is discussed in more detail in the next section.

2.6.5. Temperature measurement

Thermocouples were used to measure the winding temperature (see Figure 2-33). Thermocouples are a widely used type of temperature sensor in industry and engineering. Thermocouples operate by converting thermal potential difference into electric potential difference. This is called the Seebeck effect [30]. There are many types of thermocouples (J, K, T, E, N, R, S, and B). The K-type thermocouple is the most commonly used thermocouple type for general purpose. The K-type thermocouple is made up of chromel and alumel metals. Voltage is induced when the two metals are fused or soldered together [21] [30]. (voltage is induced when the sensor is powered, correct?)

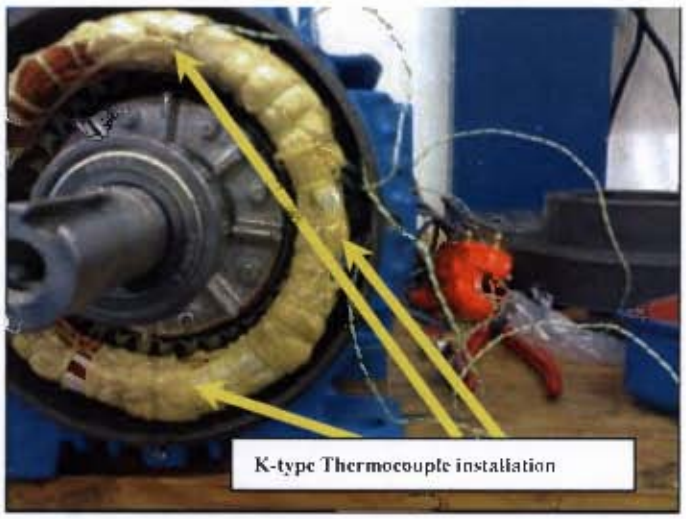

Figure 2-33: Thermocouple installation

Temperature measurement, as discussed in Chapter 3 Section 3.2.4, is used to determine the resistance at each loading point. According to the IEC and IEEE [10] [11], the hottest temperature on the winding is required to be used in the resistance determination. Figure 2-33 shows the position of the thermocouples in the three hottest points in the motor front-end (drive-end) windings. These points were found from measuring the motor front-end windings at 6 different points.

2.6.5.1. Accuracy and calibration

A Pico logger, shown in Figure 2-34, was used to measure and convert the temperature into voltage. The entire temperature system can achieve errors of a maximum of 1°C during testing [30]. This accuracy meets the required accuracy of the standards [12].

Figure 2-34: Pico logger measuring thermocouples

Thermocouples are purchased calibrated, and only loose calibration if impurities and chemicals fuse into the metals [30]. This loss of calibration was tested by comparing the temperature of boiling water measured by a k-type thermocouple to that measured by a thermometer. No difference was found between the two methods, showing good accuracy and calibration.

2.6.6. Alignment

Mounting alignment was measured by using a clock dial. The clock-dial is made up of a dial and a magnetic base. The clock dial measures misalignment with an accuracy of 0.01mm. Two readings are taken at the top and bottom for vertical misalignment, as shown in Figure 2-35, and two readings on the left and right for horizontal misalignment. The direction and distance (?) the dial swings indicates the magnitude and type of misalignment.

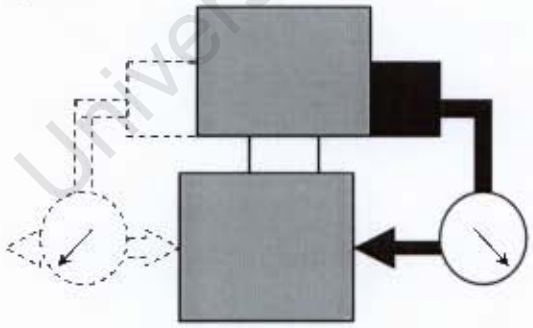

Figure 2-35: Shaft alignment using a clock dial

The dial was also used in aligning the pulley system. The clock dial was adjusted as shown in Figure 2-36. The larger pulley was used as a reference while the smaller one

was adjusted. Any misalignment of the pulley belt can lead to belt wear and eventual tear.

Figure 2-36: Alignment of pulley system using the clock dial

The alignment of motors and the pulley system were aligned to an allowable misalignment of 0.05mm. This misalignment was found to produce low to no vibrations.

2.7. Power Supply

The 380V and 500V AC supply voltages were available in the laboratory,. The 500V supplies the 250kVA DC drives while the 380V is used around the lab to supply different motor sets.

2.7.1. Power quality

The power quality limits required by the standards are shown in Table 2-7. These requirements are far stricter than the utility (i.e. Eskom) power quality national standards [31].

Table 2-7: Standards Power Quality Limits

VOLTAGE	IEEE	IEC	ESKOM
Unbalance	0.50%	0.50%	2%
Frequency	±0.1%	±0.3%	±2%
Total Harmonic Distortion (THD)	5%	negative-sequence component < than 0,5 %	8%

The Eskom supply into the laboratory was found to exceed the required limits. In fact, the power quality varied throughout a day and was very inconsistent (in magnitude and frequency). The THD, voltage unbalance, magnitude and frequency was recorded for the supply over a 24 hours period and are shown in Figures 2-37 to 2-40.

Figure 2-37: Eskom Supply Voltage THD

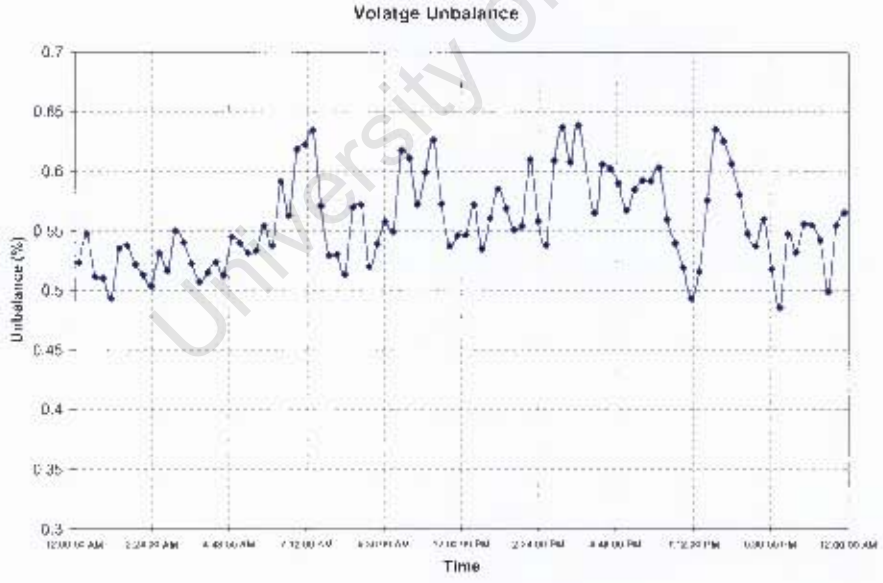

Figure 2-38: Eskom Supply Voltage unbalance

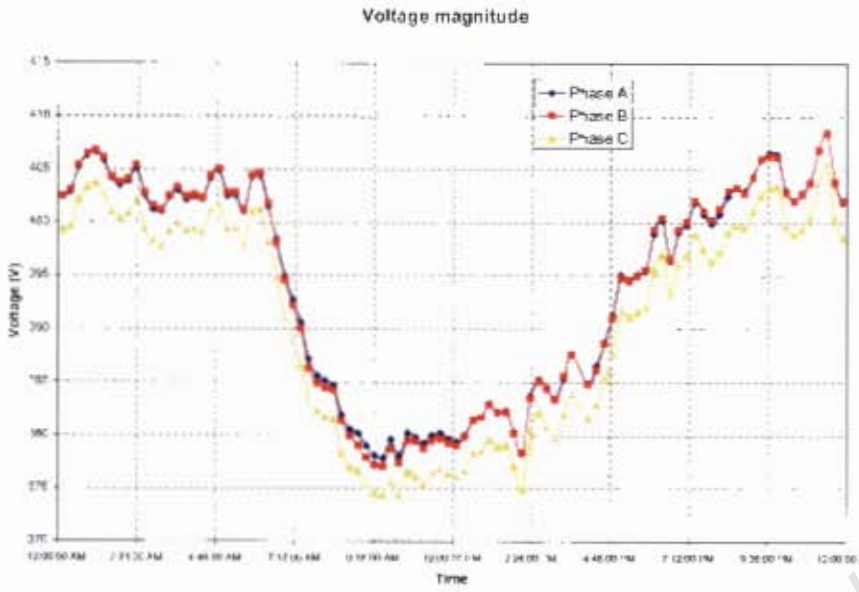

Figure 2-39: Eskom Supply voltage magnitude

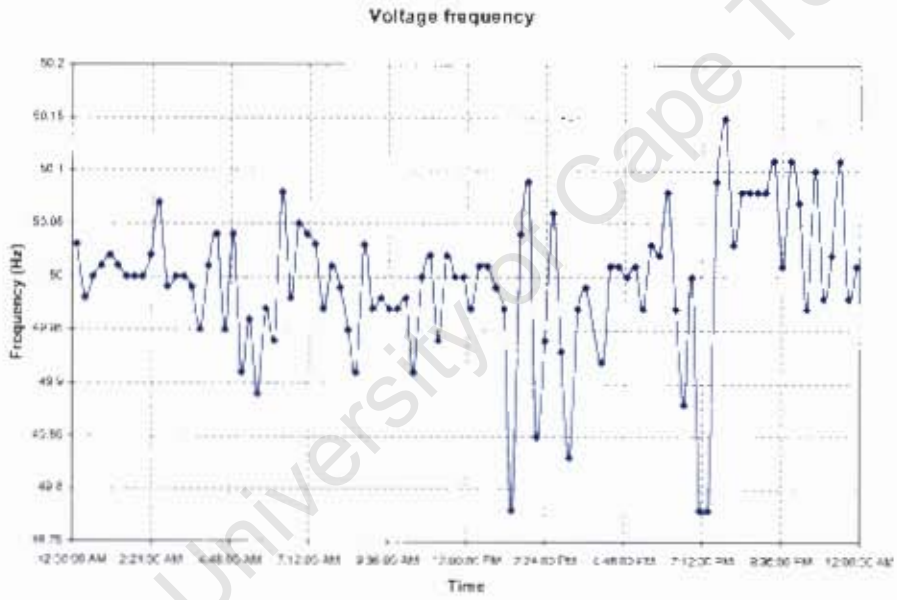

Figure 2-40: Eskom Supply voltage frequency

Tests done using the Eskom supply was found to affect the repeatability of tests. Figure 2-41 shows the result of testing a 15kW motor with the grid supply in the morning and again in the afternoon. A difference in efficiency of up to 1% was found between the tests.

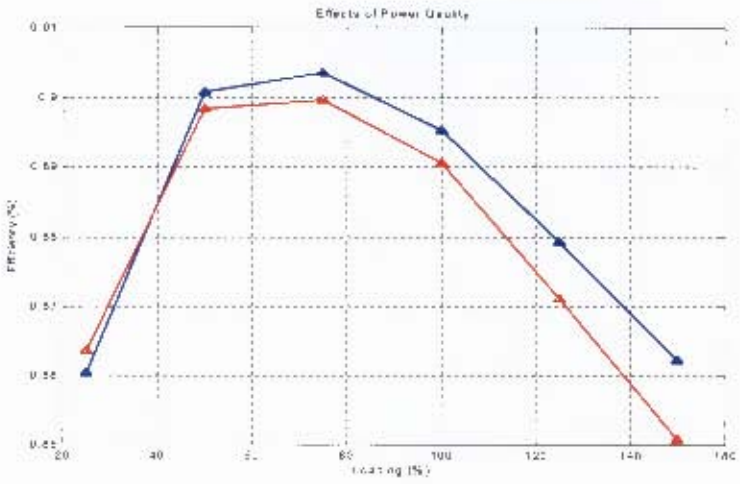

Figure 2-41: Eskom Supply impact on repeatability

The core and stray load loss (SLL) losses of the motor are higher in the afternoon due to the increased voltage THD and unbalance as shown in Figure 2-42. This in turn results in lower efficiency in the afternoon than in the morning. A dedicated laboratory generator supply was therefore chosen as the primary supply for all the motor testing in this project.

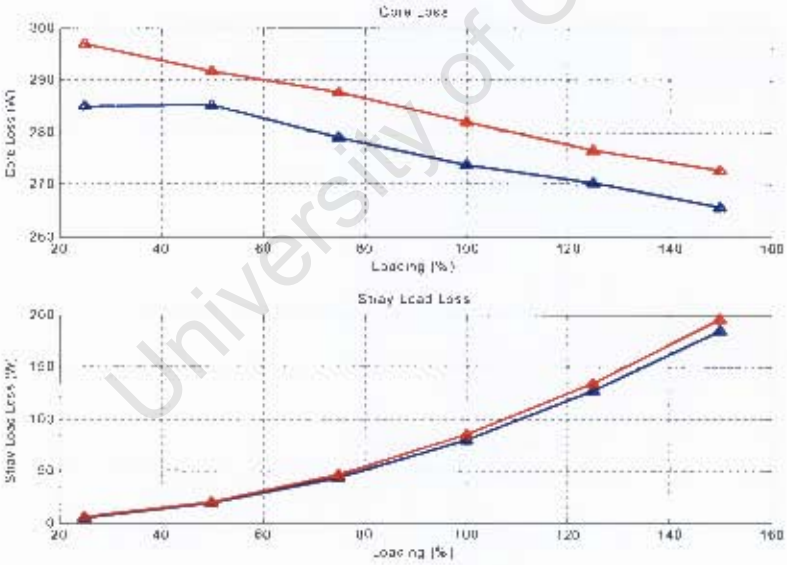

Figure 2-42: Eskom Supply impact on motor losses Morning (red), Afternoon (blue)

2.7.2. Laboratory Generator Supply

The generator set at the UCTML is made up of a 520kVA, 1000rpm, 6.6kV, 6 pole synchronous alternator, which is driven by a 250kW DC motor. The schematic of the generator set is shown in Figure 2-43. The generator produces a good sinusoidal voltage waveform with minimal harmonics. Apart from the excellent supply, the generator has the advantage of producing a wide variable range of voltage up to 6.6kV.

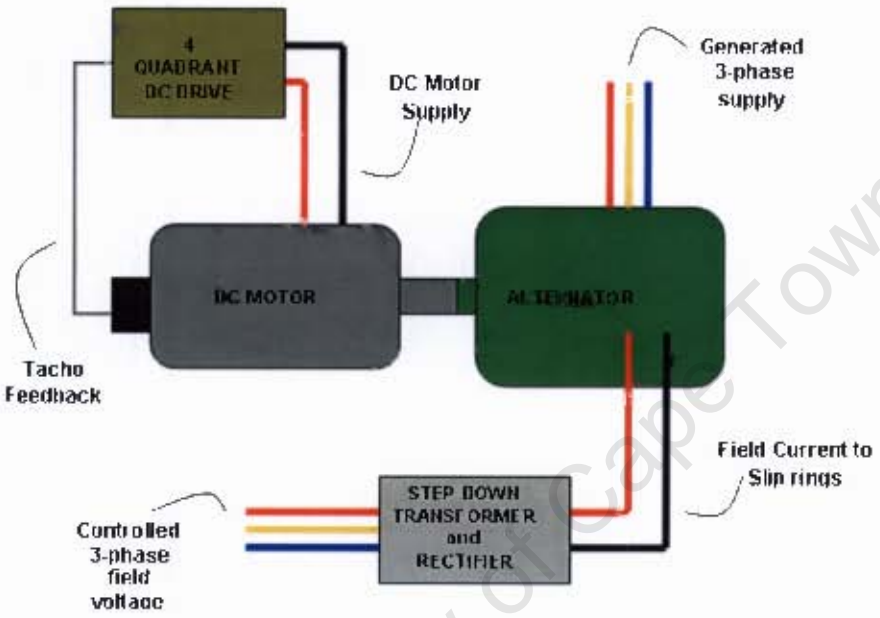

Figure 2-43: Schematic of Generator Set

The generated voltage is controlled by controlling the field current to the alternator's slip rings. This high field current (600A) is produced through a unit made up of a step down transformer and rectifier rated at 10kVA at 500V (see Figure 2-43). The frequency of the generated supply is kept at a constant 50Hz through speed feedback control. The speed from a tachometer is sent to the DC drive, which keeps the speed of the DC motor constant (at 1000rpm).

The generator supply conforms with the PQ specifications set in the IEEE and IEC standards. See Table 2-8 below.

Table 2-8: Generator Power Quality Limits

VOLTAGE	IEEE	IEC	Generator
Unbalance	0.50%	0.50%	0.1%
Frequency	±0.1%	±0.3%	±0.05%
Total Harmonic Distortion (THD)	5%	negative-sequence compotent < than 0.5 %	1%

2.7.3. Power Ratings

The power ratings of each test bed are dependant on the switchgear, the dynamometer system ratings and the type of mounting (see section 2.3). Table 2-9 shows the power ratings of each bed and the power limitation.

Table 2-9: Test bed power ratings

Test Bed	Power ratings	Motors tested	Limitation
3kW	3kW	3kW	Dynamometer system and Switch gear
15kW	15kW	7.5, 11, 15kW	Dynamometer system and Switch gear
250kW	90kW	22, 37, 45, 55kW	Mounting and Switch gear

2.8. Motor operation, safety and maintenance

Induction motor starting current is typically five to eight times the rated current [15]. This is due to low impedance because of a high slip at start-up. This high current results in tripping the motor protection breakers. Different soft starters were therefore employed on different test beds.

2.8.1. Motor starting on 3kW and 15kW test beds

A star- delta starter, shown in Figure 2-44, was built for the 3kW and 15kW test beds. The starter has a timer that automatically switches the supply connection from a star to a delta connection. The delta connection draws square root 3 times more current than star connections [7]. The circuit diagram is found in the Appendix C, Figure C1.

Figure 2-44: Star-delta starter

2.8.2. Motor starting on 250kW test bed

A selector start box, shown in Figure 2-45, with three power supplies was built to start motors in 250kW test bed. The box allowed supplies from a variac supply, generated supply and a variable speed drive supply. Soft starting was possible from all three supplies. Circuit diagrams are found in Appendix C, Figures C2 and C3.

Figure 2-45: 250kW test motor starter

2.8.3. Safety and maintenance

Circuit protection and personal safety are two important concerns that were addressed during the construction of the test beds [17].

Fault protection was achieved by using fuses and circuit breakers. Figure 2-46 shows the protection panel of the 3kW and 15kW test beds, rated at 30A. Figure 2-46 shows the protection for the 250kW test bed, which is rated at 250A. The circuit diagrams are found in Appendix C C5.

Figure 2-46: Protection for the 250kW test beds rated at 250A

Personal safety was ensured by implementing operating procedures (see Appendix C) for all the testing beds. A security gate was used to restrict access to the testing area as shown in Figure 2-47. Furthermore, all moving parts were covered with guards and cages (see Figures 2-8 and 2-11)

Figure 2-47: Test area security gate

Maintenance procedures such as cleaning of the DC dynamometer commutators (shown in Figure 2-48) were done frequently to reduce arcing across the brushes.

Figure 2-48: DC dyno commutator cleaning

Other maintenance procedures included: realignment of motors and pulley systems, mounting bolt tensioning, instrument calibration, equipment temperature monitoring, etc.

2.9. Concluding remarks

The development of the test beds for induction motor testing was presented in this chapter.

Details relating to the construction of the test beds, instrumentation used and the treatment of all collected data were clearly outlined. The test beds were perfected over a period of 1 year. Several improvements were made to the test beds over this period before they were considered to be ready for testing of motors associated with this project.

Chapter 3: DATA ANALYSIS

3.1. Overview

Data analysis involves the collection, modelling and converting of data in an attempt to highlight conclusions and therefore support decision-making [65] [66]. This is achieved using different statistical methods and data analysis techniques.

This chapter presents the statistical methods and data analysis that were applied to all the collected and presented data throughout the thesis.

3.2. MATLAB

MATLAB (**mat**rix **lab**oratory) is a numerical computing environment developed by The MathWorks [81]. MATLAB allows matrix manipulation, plotting of functions and data, implementation of algorithms, creation of user interfaces, and interfacing with programs in other languages in a computer based program. This tool was utilised in all data analysis and calculations done on this thesis. All programs used have been included in Appendix D.

3.3. Repeatability

Although accuracy is important and has been addressed, repeatability is even more crucial in the motor rewind project. Repeatability is defined as the variation in the test results measured with the same method in identical tests, by the same operator, with the same apparatus, in the same laboratory after short intervals of time [67]. Statistically, repeatability is the variation in the standard deviation of repeated tests over a certain period of time. This is known as the repeatability standard deviation (STD) shown in Equation 3.1 [65] [68].

$$\sigma_r = \sqrt{\frac{(x_i - \mu)^2}{N}} \tag{3.1}$$

Where s_r is the repeatability standard deviation (STD)

x_i is the measured variable,

μ is the mean and

N is the number of measured data

The power supply (discussed in Chapter 2), the testing standard used and data collection techniques were found to be the most critical variables, which affect repeatability. These three variables were controlled in the following way:

i) The integrity of the supply was ensured by using a generator. The generated voltage was constant, balanced, perfectly sinusoidal and at 50Hz.

ii) Tests were done according to the procedures in the IEEE 112 and IEC 34-2 standards loss segregation methods. Each motor was run at rated conditions until steady state temperature was reached. The motor was then tested with its windings within 5°C of the steady state temperature.

iii) Motors were tested through five full cycles and then averaged. The variance in the tests for each motor over the five tests is shown in Appendix E and H. The recorded data (current, power, voltage, temperature, etc) during a single test were also averaged over a few data points on the power analyzer.

Table 3-1 shows the repeatability STD for all eight motors. Up to five repeated tests were done on each motor before and after rewinding. Linear regression was used on the test data points (see Section 3.4 below) to calculate the STD for each part-load, using Equation 3.1.

Table 3-1: Repeatability STD for each motor

Loading (%)	3kW	7.5kW	11kW	15kW	22kW	37kW	45kW	55kW
	Repeatability STD							
100	0.14	0.12	0.10	0.11	0.04	0.04	0.03	0.13
75	0.10	0.10	0.10	0.08	0.02	0.02	0.03	0.10
50	0.05	0.07	0.07	0.05	0.01	0.03	0.03	0.06

The overall repeatability per test bed is **0.13%** for the 3kW test bed, **0.12%** for the 15kW bed and **0.09%** for the 250kW test bed.

This repeatability on tests done on the 250kW test bed can be graphically seen from results obtained from the 22kW motor. This is shown in Figures 3-1 and 3-2. The efficiency and losses of the 22kW motor tested over five full test cycles before and after rewind have been ploted. A good repeatability can be observed in Figures 3-1 and 3-2..

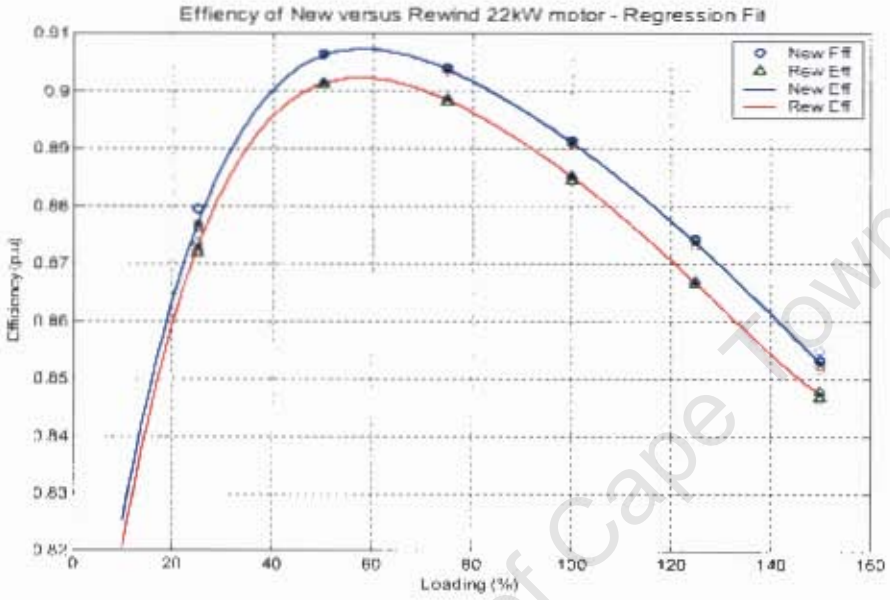

Figure 3-1: Repeatability of the 22kW efficiency over five test cycles

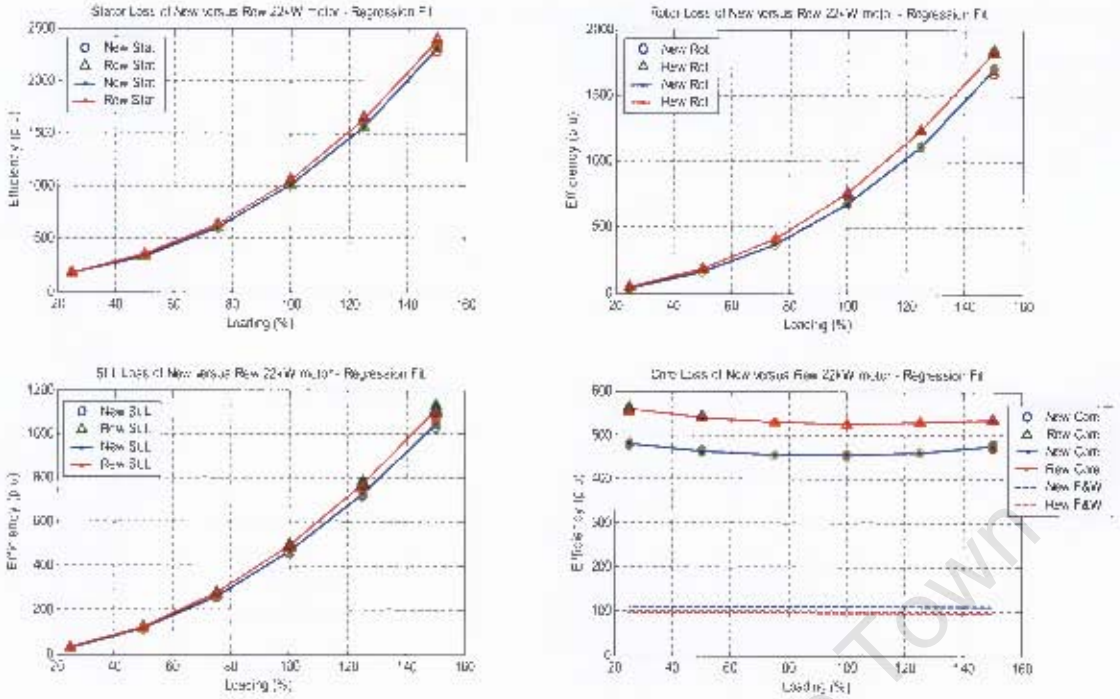

Figure 3-2: Repeatability of the 22kW losses over five test cycles

The repeatability of the losses and efficiency of the motors tested on the other beds are found in Appendix H.

3.4. Regression Analysis

Regression analysis is the modelling of the relationship between one or more independent variables and a dependent variable [65]. The modelling involves least squares functions to obtain a linear regression equation, see Equation 3.2.

$$y = \beta_0 + \beta_1 x + \beta_2 x_1 + ... + \beta_{i-1} x_j + \beta_{i+2} x_{j+1} + \varepsilon \qquad (3.2)$$

Where y is the dependent variable

x_i is the independent variable ($i = 1.....n$)

β_j is the regression coefficient ($j = 1.....m$) and

e is the error term

The raw data is first best-fitted by adjusting the parameters of the model. The regression coefficient or constants are calculated by using the matrix Equation 3.3 shown below [65].

$$(X^T X)\hat{\beta} = X^T y \tag{3.3}$$

Where X^T is the transpose of the vector of independent variables

After formulating the regression model, it is important to check the goodness of fit of the model and the statistical significance of the estimated parameters. The goodness of the fit is checked by the R-squared (or the square of a correlation coefficient) and the analyses of the pattern of residuals. The statistical significance of the model is checked by an F-test of the overall fit. A t-test is then done on the individual parameters.

The goodness or the R-squared of the fit on all the loss and efficiency data had a minimum of 0.95. The F-test on the model estimates were found to be significant.

Examples of best fit curves are illustrated in the 22kW loss and efficiency curves in Figures 3-1 and 3-2.

3.5. Uncertainty or error Measurement

Errors or Uncertainty affect all measurements even when the most carefully designed and executed experiments use 'state of the art' instruments [69] [70]. Uncertainty (or Error) in scientific measurement is made up of three components:

$$\psi = \psi_m + \psi_h + \psi_i \tag{3.4}$$

Where,

ψ = overall error

ψ_m = methodological error

ψ_h =human error

ψ_i = instrumental error

All three components are present in induction motor testing and affect the determination of accurate efficiency [69] [70].

3.5.1.1. Methodological error

The source of methodological errors in efficiency testing relate to the testing standard used [69] [70]. As discussed in Chapter 4, there are several international efficiency testing standards with several methods, using different machine models and assumptions.

The impact of methodological error is discussed in Chapter 4, Section 4.4. The determined efficiencies were different because of the treatment of SLL and the method followed. (The last sentence presents conclusion of the info not discussed yet)

3.5.1.2. Human error

Human errors in efficiency testing are caused by the interpretation and implementation of the different measurement methods provided in the testing standards. These errors arise from an individual's estimation of load conditions, reading of instrumentation, measurement of torque, temperature, resistance, and the sequence of test procedures [69] [70].

The impact of human error can be seen in the 'reproducibility' of the determined motor efficiency [69] [70]. Reproducibility is the variation in the average of the measurements resulting when different operators using the same instrumentation and test beds to take measurements on the same motor. The variation in the tests done by two different operators is shown in Table 3-2.

Table 3-2: Reproducibility of a 7.5kW motor on the 15kW test bed

Loading (%)	Operator 1: Eff (%)	Operator 2: Eff (%)	Variation (STD)
150	81.34	80.66	0.48
125	83.97	83.63	0.24
100	86.09	85.85	0.17
75	87.46	87.32	0.10
50	87.65	87.43	0.15
25	83.83	83.82	0.01

The results in Table 3-2 show better reproducibility at part-loads between 25 - 100% than part-loads above 100%. The difference is attributed to temperature stabilization. At part-loads above 100%, the data is recorded as quickly as possible. The time spent at these higher loads is left to the operator's judgment and therefore different temperatures are measured. Other human errors such as keeping the generator voltage constant (during motor loading), the data averaging setting and data capturing and reading values incorrectly.

3.5.1.3. Instrumentation error

The source of instrumentation error is in the instrument accuracy. Instrumentation error has the largest contribution of the overall error in motor testing. The source of this error in efficiency testing is in the measurement of voltage, current, frequency, power, winding temperature, speed and winding resistance [69] [70]. Errors in these measurements affect the accuracy of determined losses and hence efficiency. In literature, there are a number of instrumentation error evaluation techniques. These are the maximum error estimation (MEE), the worst case estimation (WCE) and the real error estimation (REE) [69] [70].

The REE has been found to be a more realistic estimation of measurement error in motor testing. The reason for this is due to the assumption made in WCE and MEE which states that the instrument's maximum errors occur at the same time. However, the probability of this is highly unlikely [69] [70].

Real Error Estimation (REE)

The motor test system can be represented as a box with a number of inputs and outputs as shown in Figure 3-3.

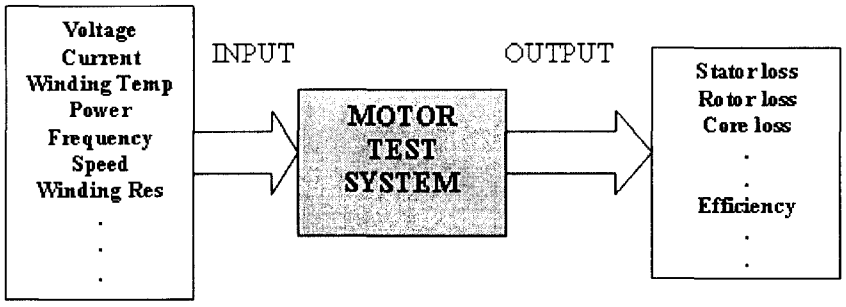

Figure 3-3: Motor testing system [69] [70]

A multi-variable equation as shown in Equation 3.5 [70] represents the *'complex'* and *'non-linear'* nature of a motor testing system [69]. The equation is a transfer function that gives the relationship between the input (accuracy of the instruments) and the output variables (determined motor efficiency and losses).

$$\frac{\Delta y}{y} = \sqrt{\sum_{i=1}^{n}\left(I_{x_i}\frac{\Delta x_i}{x_i}\right)^2 + \frac{1}{y^2}\sum_{j=1}^{m}\left(\frac{\partial f}{\partial z_j}z_j\right)^2} \tag{3.5}$$

Where y is the output,

x_i are the measurement uncertainties (input variables) (where $i = 1,...,n$)

z_i is the additive noise and

I_x is the influence coefficient

Assuming that all the uncertainties are independent and random, changes in the measurement uncertainties (x_i) gives rise to errors in the output. The percentage change of the input over the percentage change of the output is called the influence coefficient (I_x). This is defined by Equation 3.6 [69] [70].

$$I_x = \frac{\Delta y / y}{\Delta x / x_i} = \frac{\partial f}{\partial x_i}\frac{x_i}{y} \tag{3.6}$$

Multiplying this influence coefficient by the measurement uncertainty gives the importance of the input variable and in turn allows easy comparison between the measured parameters [69] [70].

In complex systems such as motor testing systems, the exact terms of the derivatives of Equation 3.6 are not available so therefore small perturbations of the individual variables are injected and the output is measured [69] [70]. Perturbations of 3% were injected into a Matlab motor efficiency determination program. Tables 3-3 and 3-4 show the impact of the perturbation in the 11 and 37kW motors.

Table 3-3: REE, Uncertainty's influence and importance for 11kW efficiency

Variable	Influence Coefficient	WCE (%)	REE (%)	Importance	Accuracy (%)
Torque	0.55665	0.1670	0.0279	1	0.3
Power	0.51650	0.1033	0.0107	2	0.2
Speed	0.99831	0.0499	0.0025	3	0.05
Freq	0.48707	0.0487	0.0024	4	0.1
Temp	0.06276	0.0126	0.0002	5	0.2
Current	0.01423	0.0028	8E-06	6	0.2
Resistance	0.00702	0.0035	1E-05	7	0.5
Voltage	0.00000	0.0000	0.0000	8	0.2
		0.3878	**0.2088**		

Table 3-4: REE, Uncertainty's influence and importance for 37kW efficiency

Variable	Influence Coefficient	WCE (%)	REE (%)	Importance	Accuracy (%)
Torque	0.5471	0.1094	0.012	1	0.2
Power	0.5462	0.1092	0.0119	2	0.2
Speed	1.0525	0.0526	0.0028	3	0.05
Freq	0.5052	0.0505	0.0026	4	0.1
Temp	0.0200	0.0100	0.0001	5	0.2
Current	0.0013	0.0003	7E-08	6	0.2
Resistance	0.0009	0.0005	2E-07	7	0.5
Voltage	0.0000	0.000	0.000	8	0.2
		0.3326	**0.1713**		

The results show the instrumentation errors on the 15kW and 55kW test beds are 0.209% and 0.17% respectively. These are the uncertainty in efficiency testing of the induction motors on the test beds and should be stated and kept in mind with all measured efficiencies.

The importance of the different measurement variables can also be seen in Tables 3-3 and 3-4. The torque, power and speed have high importance rankings and therefore accurate measurement of these variables is crucial to limiting uncertainty. The voltage and resistance on the other hand are not.

3.6. Concluding remarks

This chapter analyses and presents the instrumentation accuracy and errors occurring during efficiency testing. The analysis ensures that conclusions can be made confidently on all presented and discussed data throughout the project.

Chapter 4: INDUCTION MOTOR EFFICIENCY DETERMINATION

4.1. Overview

This chapter presents an in depth discussion on testing of induction motor efficiency.

4.2. Definition of Induction Motor Efficiency

The efficiency of an electric motor is its effectiveness in converting electrical power at its input to mechanical output power at its shaft [15]. The efficiency of an induction motor can be represented as:

$$Efficiency = \frac{P_{output}}{P_{input}} = \frac{mechanical\ \ output\ \ power}{electrical\ \ input\ \ power} \tag{4.1}$$

The input power to an induction motor is electrical power (in Watts), drawn by the motor from the supply. The output power is the fraction of its input power which is converted to mechanical power at its shaft (product of torque and speed).

An ideal motor would have an efficiency of 100%. This is not possible in reality due to losses which occur within the motor and are dissipated in the form of heat. These losses are the difference between the input (electrical) and output (mechanical) power. When considering losses, the efficiency of a motor can also be defined as:

$$Efficiency = \frac{P_{output}}{P_{output} + \sum losses} = \frac{P_{input} - \sum losses}{P_{input}} = 1 - \frac{\sum losses}{P_{input}} \tag{4.2}$$

The input power is equal to the output power plus the losses. Conversely, the output power is equal to the input power minus the losses.

4.2.1. Induction Motor Losses

There are five types of losses which occur in an Induction motor. These losses can be grouped into two categories, load-dependant (or load losses) and load-independent (or

constant losses) losses. The losses vary in magnitude according to both the size and speed of motors. Figure 4-1 shows the common loss proportions in most medium size industrial motors [32].

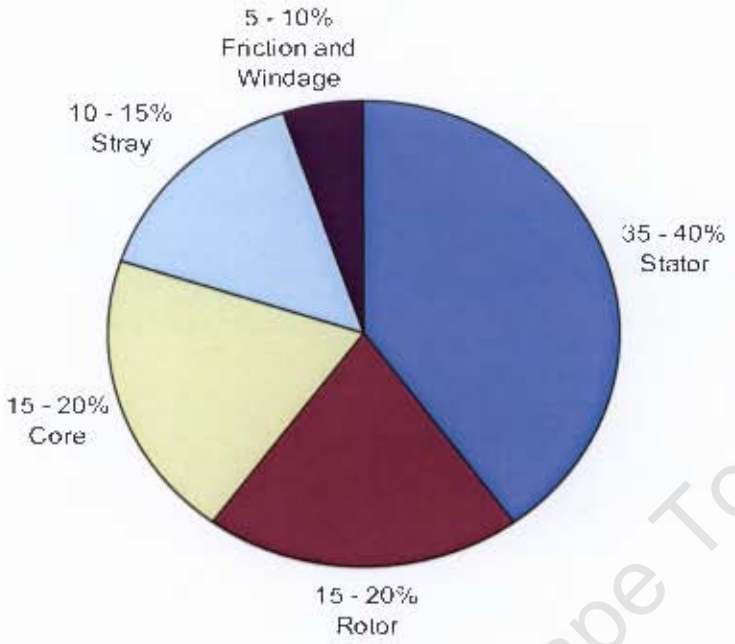

Figure 4-1: Average motor losses in 4-pole induction motors [32]

4.2.1.1. Load-dependant loss

Load-dependant losses vary due to a change in load on the motor and the motor current.

Stator Copper (I^2R) Loss – Power dissipated in the form of heat, due to currents flowing through the internal resistance (skin-effect included) of the stator windings [15].

Rotor Copper (I^2R) Loss Power dissipated in the form of heat, due to currents flowing through to the internal resistance (skin-effect included) of the rotor cage bars [15].

Stray Load Loss (SLL) - non-linear losses that are hard to model and quantify due to their many sources. Some of the causes of SLL have been found to be:

- Space harmonics associated with the stator and rotor and leakage flux associated with the end windings [33]
- Eddy-current losses in stator (primary) or rotor (secondary) winding conductors caused by current dependent flux pulsation [34]
- Flux pulsations in the stator and rotor teeth due to a change in the reluctance of the magnetic path as the rotor passes the stator [35]

4.2.1.2. Load-independent loss

Load-independent losses are 'constant' and are unaffected by the change in load or current.

Stator Core loss - losses resulting from hysteresis (energy used to magnetise core material) and eddy currents (magnetically induced circulating currents in the stator core) in the active iron and other steel parts [34]. Core losses are more apparent at low loadings.

Friction and Windage (or Mechanical) loss - losses caused by friction in the moving parts of an induction motor like the bearings. Energy is also lost in overcoming air movement from the rotor and cooling fan [34].

Figure 4-2 shows the contribution of each loss at different loading points ranging from no-load to 125% of rated load.

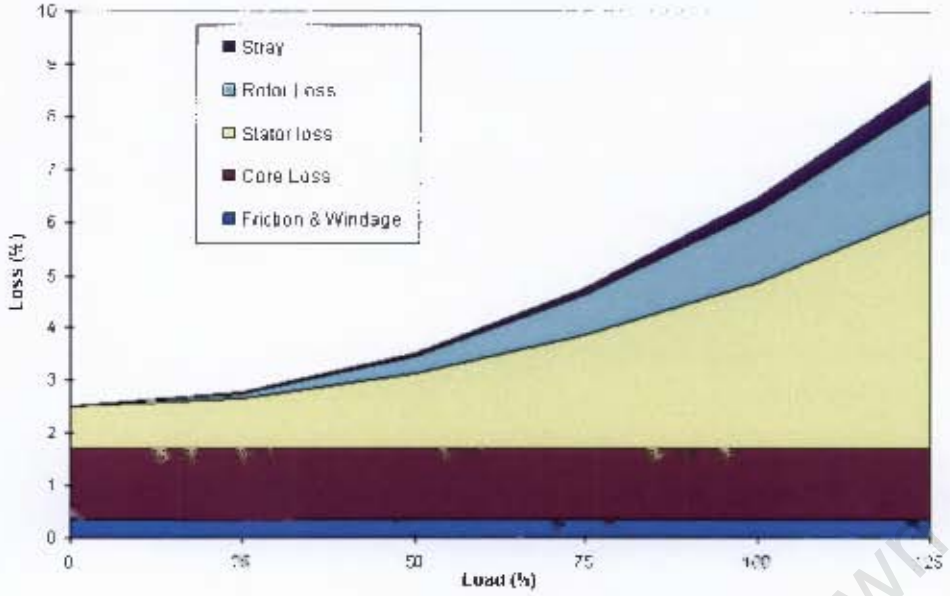

Figure 4-2: Typical loss components of an induction motor plotted against load

4.2.2. Motor Efficiency Profile

Motor efficiency is commonly specified at rated conditions. This is not necessarily relevant in industry where motors operate away from rated conditions and typically at lower efficiencies [36] [37]. According to Emmanuel B. Agamloh [36] and Wenping Cao [37], 29% of all induction motors operating in industry are under-loaded and carry less than 50% of rated load. This practice is intended to allow the motors to accommodate any load fluctuations, overcome voltage dips, increase the potential for future load increases and more importantly allow the motors to operate at higher efficiency [37].

The efficiency profile of a typical motor shown in Figure 4-3 shows that the efficiency increases as the loading on the motor is increased and then starts to decrease as the load increases beyond a certain point. This point is the maximum efficiency point and generally occurs in the region between 50% to 80% load depending on the design on the motor [36] [37].

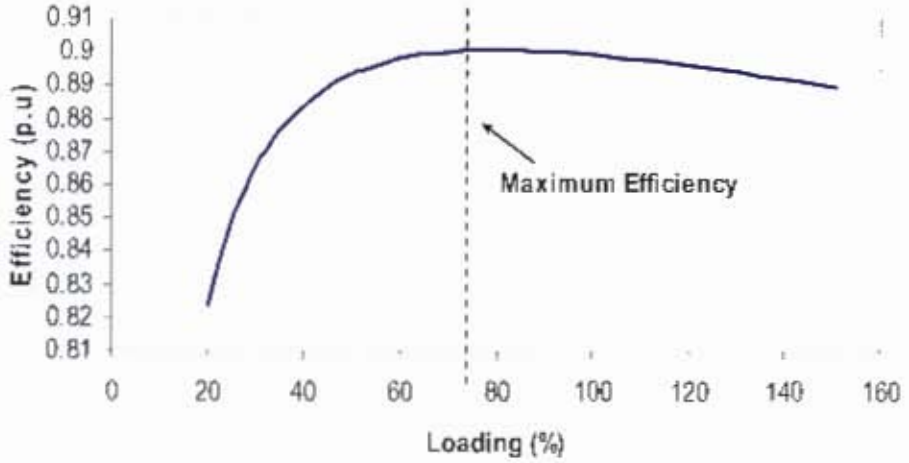

Figure 4-3: Typical efficiency profile of an Induction motor

4.2.2.1. Maximum Efficiency

As discussed previously, the maximum efficiency of a motor usually does not occur at 100% loading (or rated load), but at loads below the rated point. Designers of induction motors vary different design parameters in order to change the relationship between the load-dependant and -independent losses in the motor. The relationship between these two types of losses determines where the peak efficiency for the motor occurs [36]. Figure 4-4 shows that the maximum efficiency point occurs when a motors' load-dependant losses equals its load-independent losses [37].

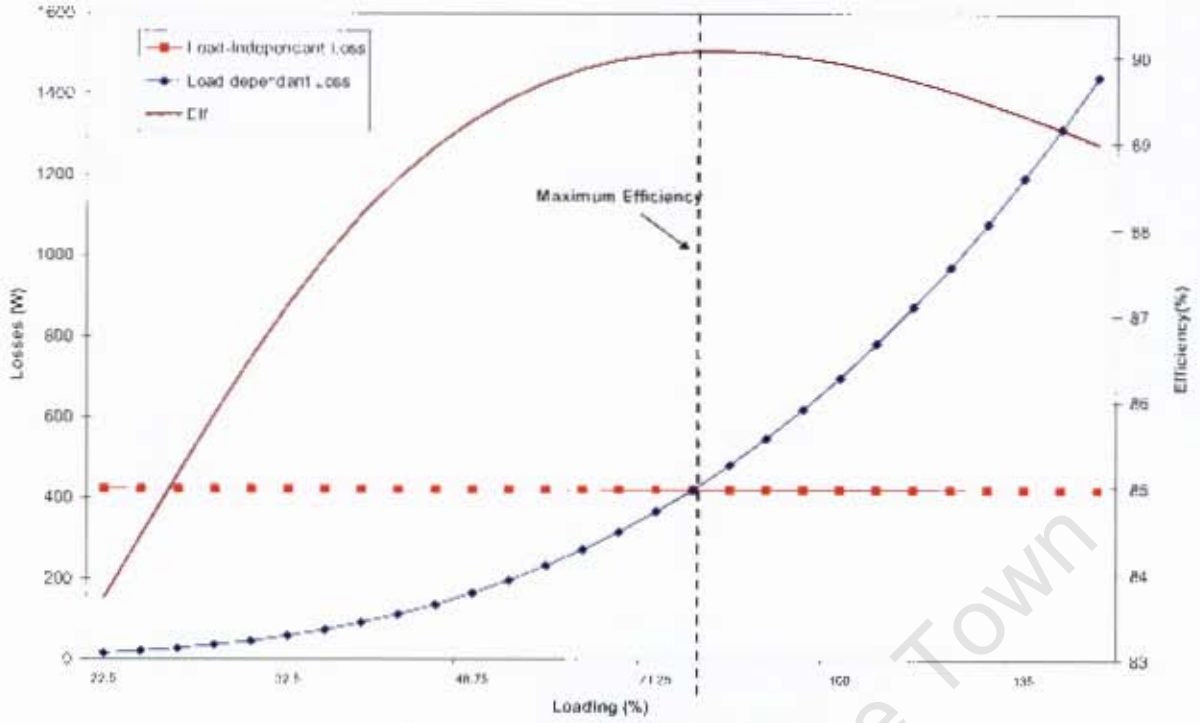

Figure 4-4: Typical efficiency and loss curves of an induction motor

The maximum efficiency point is found between 60% – 75% of rated load. The maximum efficiency load point of any motor can be analytically calculated using Equations 4-3, 4-4 and 4-5 [36].

$$v_L = \frac{p_1(1/\eta_1 - 1) - p_2(1/\eta_2 - 1)}{p_1^2 - p_2^2} \tag{4.3}$$

$$v_o = p_1(1/\eta_1 - 1) - v_L p_1^2 = p_2(1/\eta_2 - 1) - v_L p_2^2 \tag{4.4}$$

$$L^{peak} = \left(\frac{v_o}{v_L}\right)^{\frac{1}{2}} \tag{4.5}$$

Where,

L^{peak} is the peak efficiency peak load point,

p_1 and p_2 are known per unit loading points and

η_1 and η_2 are known efficiency values corresponding to the loading points, p_1 and p_2.

These equations can be used to predict the peak efficiency point of any motor and therefore allow loading the motors efficiently [36].

4.3. Determination of induction motor efficiency

Although the efficiency of an induction motor is simply the ratio of the output mechanical power to the input electrical power (Equation 4.1), the determination of induction motor efficiency is a much-debated topic. An in depth discussion of induction motor efficiency determination is presented in this section.

4.3.1. Motor efficiency test standards

Motor manufacturers provide efficiency data that is obtained through measurements and calculations according to a certain standard [34]. There are a number of international standards that outline the determination of efficiency in different ways. Table 4-1 shows international standards that are in use today.

Table 4-1: International induction motor testing standards

Standard	Description
SANS 60034 Part 2 (SANS 34-2)	'Methods for determining losses and efficiency of rotating electrical machinery from tests (excluding machines for traction vehicles)' - Published in 1996 by the South African Bureau of Standards
IEC 60034 Part 2 (IEC 34-2) 2007	'Standard methods for determining losses and efficiency from tests (excluding machines for traction vehicles)' - Published in 2007 by International Electrotechnical Commission
IEEE 112	"Standard Test Procedure for Polyphase Induction Motors and Generators" - Published in 2004 by International Electrical and Electronic Engineers
JEC-2137	Published by in 2000 by the Japanese Electrotechnical Committee
AS/NZ 1359.5	"Three-phase cage induction motors - High efficiency and minimum energy performance standards requirements" - Published in 2004 by Australia and New Zealand Standards
CSA 390	'Energy Efficiency Test methods for Three-Phase Induction Motors' - Published in 1999 by the Canadian Standards Association

4.3.1.1. Literature on comparison of standards around the world

A great deal of research has gone to identifying the most important standards worldwide. The following conclusions have been made in the literature, after comparing standards:

- Peter Van Roy [38]

  This author concluded that the three most important induction motor testing standards are the American IEEE Standard 112-Method B, the European IEC 60034-2 and the Japanese JEC 37. This due to the different ways that the additional load losses are incorporated.

- Peter Kelly-Detwiler et al (1997) [39]

  This author concluded that the standards that are applied to the majority of motors and are commonly used worldwide are the: the European International Electrotechnical Commission Standard (IEC 34-2), the Japanese Electrotechnical Commission test procedure (JEC 37) and the Institute of Electrical and Electronics Engineering (IEEE) 112.

- B. Renier et al (1999) [33]
  This author concluded that for induction motors there are three important standards. These were the IEEE Standard 112-1996, IEC 34-2 and IEC 34-2A, JEC 37. He also went on to state that several national standards are harmonized to one of these three general standards. Examples are the NEMA MG-1- 1993 standard and the Canadian standard C390 which correspond to the IEEE standard. The major difference between the three standards was in the way in which the values for the stray load losses were obtained at different load levels.

- Austin H. Bonnett (2000) [40]
  This author concluded that no single test method is used throughout the world, but that the most commonly used standards are:
  1) IEEE 112-1996—U.S.;
  2) International Electrotechnical Commission (IEC) IEC 34-2—International;
  3) JEC-37—Japan;
  4) BS-269—Britain;
  5) ANSI C50.20—U.S. (same as IEEE 112);
  6) CSA 390—Canada.

- Aníbal T. de Almeida (2002), [34]
  This author concluded the efficiency data presented on the nameplate of an induction motor, or given by the manufacturer, are measured or calculated according to two main methods i.e. IEEE 112-B and IEC 34-2 (indirect method). He also concluded that the standards use different stray load loss (SLL) evaluation methods.

- Aldo Boglietti et al (2004) [41]
  This author concluded that the most important standards are the IEEE 112-B, IEC 34-2, and JEC 3. The author also concluded, after comparisons based on experimental results, that the stray-load loss measurement is critical for the correct evaluation of induction motor efficiency.

- Most authors agree that the IEEE 112 and IEC 34-2 standards have also been harmonized to many of the existing international standards (See Table 4-2) [10] [11] [42] [43] [44].

Table 4-2: Harmonized standards and available methods

Standard	Available Methods	Harmonized to
AS/NZ	2	IEC 61972 \ IEEE 112
SANS 34-2	3	IEC 34-2
IEC 61972	2	IEEE 112
CSA 390	3	IEEE 112
JEC 37*	3	N/A
IEC 34-2	7	IEC 61972

***Standard was not acquired and therefore information is from literature**

It can be clearly seen that the most important standards around the world are the IEEE 112, the IEC 34-2 and the JEC 37. The SANS 34-2 is added to this list as it is important from a South African perspective.

4.3.2. Comparison of Standards

A detailed comparison was performed between the IEEE 112 (2004), IEC 34-2 (2007), SANS 34-2 (1996) and JEC 37 standards. The determination of SLL is seen as the major difference between the standards. This will therefore be discussed in detail.

4.3.3. Determination of SLL

The major difference between the standards is in the treatment of SLL [34] [41]. The determination of SLL has been discussed in several research papers due to the difficulty to measure and/or calculate the losses analytically. This is a consequence of the complex sources of this loss component (see section 4.1.1). Quantifying SLL accurately is critical for determining the efficiency of induction motors correctly [34].

The methods used in the standards to determine SLL are as follows:

The assignment of SLL: This method is used in the SANS 34-2. The SLL are assigned as 0.5% of rated input power. SLL at other loading points are calculated from the ratio of the load current and the motor rated current.

The method has been found to be unsupported and produces higher efficiencies. A theoretical study of SLL confirms that its magnitude increases as motor size decreases. The assigned SLL of 0.5% of rated power is significantly lower for small motors [45]. Furthermore, Renier et al concluded that the assignment of SLL should be abandoned where possible [33].

The removed rotor and reverse rotation test: As described by the IEEE 112 (method E) and IEC 34-2 (removed rotor and reverse rotation test), the SLL can be determined by measuring the fundamental frequency and the high-frequency components of the inherent SLL. The sum of the two components gives the motor's total SLL. The procedure, which was suggested by Ware [46], involves two tests:

The first test involves removing the rotor and energising the stator with a voltage supply at rated frequency. The fundamental SLL is calculated as the input power minus the stator copper losses, see Equation 4.6.

$$P_{SLL-f} = P_{RR} - P_{Stator} \tag{4.6}$$

Where,

P_{RR} is the input power with the rotor removed

P_{stator} is the copper loss in the stator windings

The second test - to find the high frequency component of the SLL - is obtained by driving the rotor (with an external prime mover) at the synchromous speed in the opposite direction to the airgap field due to stator currents.. The resultant flux will be rotating at twice the speed and therefore the induced currents' frequency will double. This test is called the reverse rotation test. The high frequency component of the SLL is calculated using Equation 4.7.

$$P_{SLL-hf} = (P_m - P_{mec}) - (P_{rr} - P_{rem} - P_{Stator-rr}) \tag{4.7}$$

Where,

P_m and P_{mec} are the mechanical power driving the rotor with and without the voltage applied to the stator respectively,

P_{rr} is the input power with the rotor reverse rotation test,

P_{rem} the input power during the rotor removed test and

$P_{stator\text{-}rr}$ the stator loss for the rotor reverse test.

The total SLL is the sum of the fundamental and high frequency SLL components, see Equation 4.8.

$$P_{SLL} = P_{SLL-f} + P_{SLL-hf} \tag{4.8}$$

This method has been found to be problematic. According to Nailen, this method is seldom performed because of the complex equipment and circuitry needed and the disassembly and reassembly of the test motor. Nailen also explains this direct method is also not widely accepted in Europe and is regarded by some prominent engineers, in the U.K., as "*worthless.*" [45]

The determination of SLL by the E-star method: As defined in the IEC 34-2. The eh-star method is the latest method and has been well received by industry due to its simplicity with no need for dynamometer testing. The disadvantage, though, relates to the extensive post-processing calculations associated with this technique [47]. This method requires operating the tested motor uncoupled and supplying it with an unbalanced supply voltage. The unbalanced supply produces negative sequence current and a reverse rotating flux. High frequency losses associated with this reverse rotating field and the forward rotating rotor can then be calculated. The test circuit is shown in Figure 4-5.

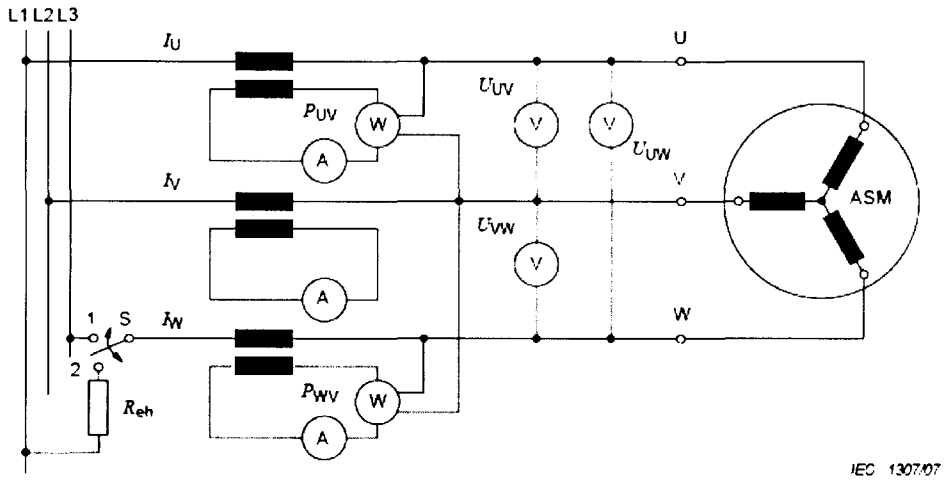

Figure 4-5: Eh-star test circuit [11]

The unbalance is obtained by supplying the star connected stator winding from a single phase voltage source. The negative and positive sequence SLL are determined and summed together to obtain the SLL. This is similar to the previous method of obtaining SLL i.e. the removed rotor and reverse rotation test [47]. The equations relating to the post processing calculations is known to produce similar results to the loss separation method [35] [47].

The determination of SLL through the separation of losses. This is defined in the IEEE 112 method B and IEC 34-2-2 (2007) [10] [11]. This is the most widely used method in the world [34] [37]. The method is done in two stages, a no-load test and a load test.

During the no-load test, the load-independent losses are obtained, i.e. friction and windage (F&W), and core loss. The motor is run uncoupled with a varying voltage supply and the input power is measured. The stator copper losses are calculated at each voltage point using Equation 4.9.

$$P_{NL\_Stator} = 3I_0^2 R_0 \tag{4.9}$$

Where,

I_0 is the measured no-load current and

R_0 is the stator winding resistance per phase.

A constant loss, made up of the F&W (Friction and Windage) and core loss, is calculated by subtracting the no-load stator copper losses from the no-load input power, see Equation 4-10 below.

$$P_{NL\_input} - P_{NL\_Stator} = P_{F\&W} + P_{Core} \tag{4.10}$$

The F&W and core loss are then separated graphically as shown in Figure 4-6. The F&W loss is found by plotting the constant losses against the voltage squared. The assumption made here is that there is no core loss when the applied voltage is zero.

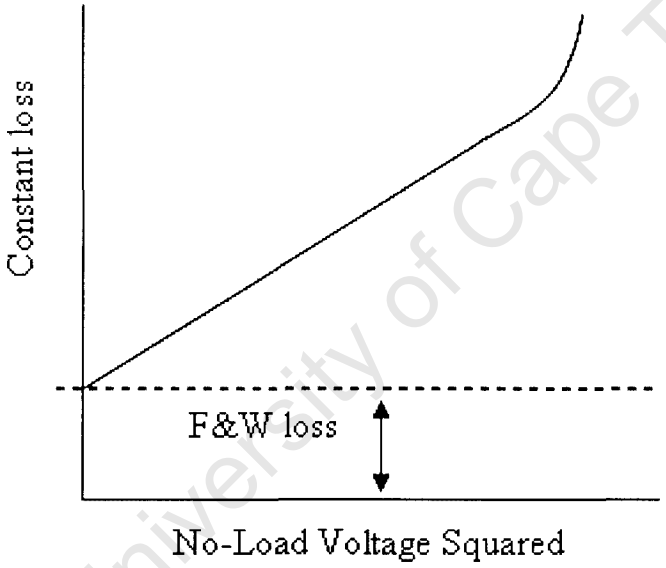

Figure 4-6: F&W and core loss separated graphically

The core loss is determined by subtracting the F&W loss from the constant losses. The core loss at a specific test voltage can be found by plotting the core loss (at each test voltage) versus voltage.

The second stage of the test requires the motor to be coupled to a dynamometer and loaded at number of loading points. The load-dependant losses are obtained through this test. The stator loss at each loading point is calculated using Equation 4.11.

$$P_{L\_Stator} = 3I_L^2 R_s \tag{4.11}$$

The rotor losses are the determined from equation 4.12.

$$P_{L\_Rotor} = (P_{L-input} - P_{core} - P_{L-Stator}) \times s \tag{4.12}$$

The air gap power is the input power minus the core and stator loss, multiplied by the slip (s) at each loading point. The total conventional loss is then subtracted from the total measured loss at each point to get the SLL, Equation 4.13.

$$P_{SLL} = (P_{L-Input} - P_{L-Output}) - P_{L-Stator} - P_{L-Rotor} - P_{Core} - P_{F\&W} \tag{4.13}$$

The calculated 'raw' SLL from Equation 4.13 is then plotted against torque squared (see Figure 4-6) and a best fit curve is estimated.

$$P_{SLL-Raw} = AT^2 + B \tag{4.14}$$

A correlation factor of the best fit curve to the raw SLL data is used to check for the validity of the test results. According to the IEEE and IEC standards, correlation factors equal or above 0.9 and 0.95 respectively, will mean a successful test. The corrected SLL is then calculated using Equation 4.15.

$$P_{SLL-corr} = AT^2 \tag{4.15}$$

The separation of losses method, next to the Eh-star method, has been found to the most accurate test, since it accounts for errors during testing [46] [37].

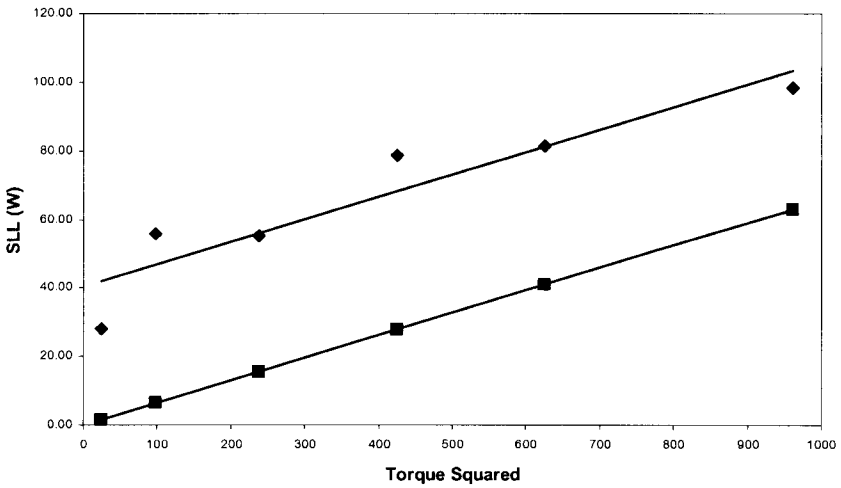

Figure 4-7: SLL correction

The 'raw' SLL from equation 4.13 when plotted against torque squared generally does not result in a straight line as shown in Figure 4-7. This differs from motor design theory where SLLs, in constant voltage motors, are designed to be directly proportional to the torque squared. This is because the mmf of the leakage flux (that is a source of SLL) is directly proportional to the load component of current. Therefore, when plotting SLL against the square of the load current, the result in a straight line through the origin [45]. The separation of losses method forces the 'raw' SLL to a straight line and shifts the line through the origin to obtain the final SLL.

The correlation of the 'raw' SLL data points defines the random error in the calculated SLL. *The lower the correlation fact or the more error prone the test was (?).* Figure 4-8 shows the effect of any random errors on the 'raw' SLL. The errors have a normal distribution with a mean along the best-fit line. The higher the correlation factor, the better the set of collected data.

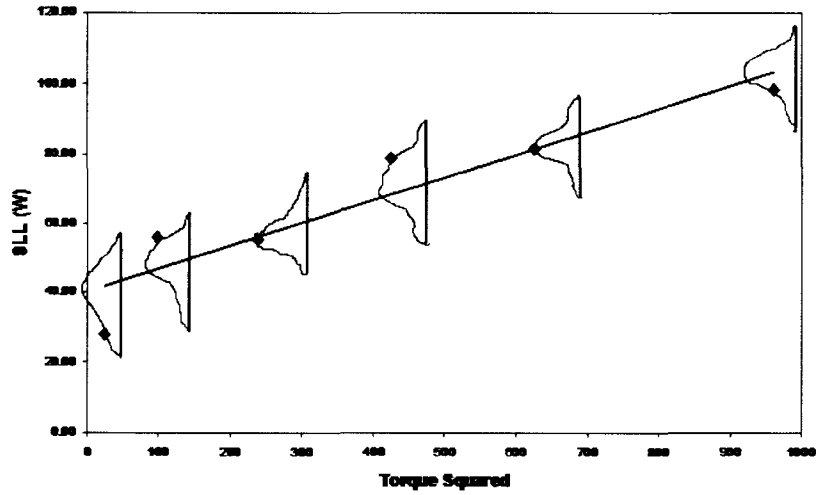

Figure 4-8: Random error in calculated SLL [49]

This statistical method and forcing the data through zero virtually eliminates the most frequent errors in motor testing and in the measurement of mechanical power [49]. This method has also proved to produce tests with high repeatability.

The SLL are ignored all together: The JEC standard ignores SLL completely and makes use of the circle diagram as the principal for calculating efficiency [41]. Due to the difficulty in obtaining the JEC 2137 (published in 2000) and its measurement procedures, the following discussions are summarized from literature.

- Boglietti (2004) [41]

  This author concludes that the JEC 37 less restrictive than the American and European standards. The JEC 37 also neglects stray-load losses and performs no temprature correction of the joule losses. For these reasons, the efficiencies obtained from the JEC 37 are generally higher.

- Nailen, Richard L (2007) [45]

  This author also concludes that by the JEC 37 neglecting the stray load losses, it will result in higher efficiencies than that claimed by the manufacturer who is making use of the IEEE and IEC standards.

4.3.4. General Differences

Apart from SLL determination, there are many other differences between the test standards. These include the test methods, test procedures and the loss calculations. These will be discussed in the next few sections.

4.3.4.1. Test Methods

Table 4-3 shows the number of available methods in each of the standards. The methods follow three basic principles and many of the methods are derivatives of these principles [48].

Table 4-3: Available methods in each of the standards [10] [11] [42]

Test Methods		
IEEE	**IEC**	**SANS**
12 Test Methods	7 Test Methods	3 Test Methods
Method A: Measured input-output < 1 kW (IEEE 112A)	Torque measurement method (IEC 34-2-1)	Direct: Input-output **(SANS 34-2-1)**
Method B: Measured input-output with segregation of losses 1–300 kW (IEEE 112B)	Summation of losses with load test method (IEC 34-2-2)	Summation of losses: The use of the summation of losses used to calculate efficiency. **(SANS 34-2-2)**
Method F: The use of an equivalent circuit is used < 300 kW (IEEE 112F)	Summation of losses without load test method (IEC 34-2-3)	
Method B1, C, E, E1 and F1. These are variations of methods B,F		

The three basic principals are:

- **equivalent circuit** method
- **Pout/Pin or** direct method or
- **summation of losses** indirect method

Each of the three principals has an impact on accuracy, repeatability, cost and ease of testing. A discussion of each of the three principals will attempt to identify best methods to use in testing.

i) *Equivalent circuit method*

Efficiency determination using the equivalent circuit method is defined in methods IEEE 112-F and IEC 34-2-3. The method first requires the determination of the tested motor's equivalent circuit parameters (see figure 4-9). These parameters can be found by performing a locked rotor and no-load test [15]. The equivalent circuits for the 7.5, 11 and 15kW motor were done according to the IEEE and IEC calculation procedure [10] [11].

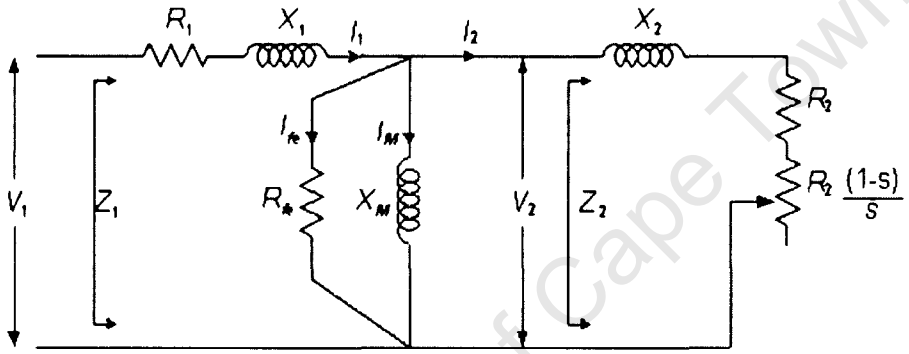

Figure 4-9: Equivalent circuit according to the IEEE [11]

The equivalent circuit method is mostly used in field testing where the tested motor cannot be removed and coupled to a dynamometer. The method is also popular for testing very large motors (up to MW motors) where loading the motors to full rated load is not practical [10] [11].

ii) *Direct or Output/Input method*

Methods IEC 34-2-1, IEEE 112A are direct methods and efficiency is determined by taking the ratio of the measured output mechanical power to the electrical input power. This method of determining efficiency has been found to lead to large errors and have poor repeatability [49]. The reasons for this include:

- The efficiency of an induction motor changes as the bearing grease warms up and begins to flow. The impact of this change in grease on motor efficiency has been found to be very significant and can therefore lead to large discrepancies in induction motor efficiencies [49].

- Due to the output and input values being very large and relatively close in magnitude (differ between 4 to 15%), a slight error in the readings can lead to large errors in the efficiency result. This statement can be illustrated by the following example [50].

Given a 55kW motor with a "true" efficiency of 90% and measuring error (or tolerance) of ±3%. The input and output power recorded data will range from 62.94- 59.28kW and 56.65 - 53.35kW respectively. The efficiency of the 90% efficient motor will therefore have an error ranging from ***84.76 - 95.56 %.***

Table 4-4: Error of output/input

Range due to error		
Input	*Output*	***EFF***
62.94 - 59.28	*56.65 - 53.35*	***84.76 - 95.56***

With a lot of money being spent on motor efficiency decisions based on fractional differences in motors efficiency, determinations of accuracy are very important. The direct (or Pout/Pin) method does not provide dependable and accurate results [48].

- Motors are seen as dynamic systems, so a single efficiency reading can be very misleading. Small but significant fluctuations occur in speed, torque, voltage, current, power, and temperature readings. These are caused by phase belt and slot permeance harmonics and therefore the values are not steady or constant at any one time. Inconsistent input and output powers have been found while testing with the IEEE 112A [49]. Gray et al, found that recorded readings taken at any single point were subject to some test error. This was found no matter how carefully the

instruments are calibrated and how much effort is put into averaging the data. [49].

These errors in efficiency determination are not all addressed in the SANS 34-2-1, IEC 34-2-1 and IEEE 112A methods. The problem of grease is avoided because of the temperature run in the IEEE and IEC. No such precaution is done in the SANS 34-2-1. The temperature correction for the power and slip in IEEE and IEC increases the direct method's repeatability.

iii) ***Indirect or Separation of losses method***

The determination of efficiency through the separation of losses is used in methods IEEE 112B, IEC 34-2-2 and SANS 34-2-2. This method is also known as the *indirect* method.

The separation of losses method is not greatly affected by instrumentation errors as compared to the direct method. The following example will illustrate this [50].

From the previous example in section (i), the same motor is subject to the same error of ±3% of its input measurement and the loss values. Using the following efficiency equation:

$$Efficiency = 1 - \frac{\sum losses}{P_{input}} \quad (4.16)$$

The error in instrumentation will make the losses range from 5.93 to 6.29kW and the input range from 62.94 to 59.28. The calculated efficiency will therefore range from ***89.39 - 90.58.*** *Table 4-5 shows that an error in the loss separation method produces smaller ranges in the efficiency.*

Table 4-5: Errors in loss separation method

		Range	
Input	*Loss*	***EFF (lower input)***	***EFF 2 (higher input)***
62.94 - 59.28	*5.93 - 6.29*	***89.39 - 89.996***	***90.01 - 90.58***

The determination of efficiency through loss separation has been found to be very accurate and widely accepted. Research shows the the following conclusions:

Boglietti et al [11], through testing induction motors, rated at 4, 7.5, 11, and 15 kW, with the old IEC-34-2-2 (1972), JEC 37 and IEEE 112B concluded that the IEEE 112 method B (loss separation) can be considered the most suitable standard for motor efficiency testing.

Gray et al [49], explains that the accuracy of the IEEE 112B makes it the most widely used standard by motor designers. It assists them with new machine designs and helps calibrate and improve their mathematical models. The methods' accurate determination of losses and in particular the SLL makes it the preferred method [49].

Comparison between the standards will now concentrate on the loss segregation methods, i.e. IEEE 112-B, IEC 34-2-2 and SANS 34-2-2.

4.3.4.2. Procedures

The procedures followed by each standard are very different depending on the chosen method under consideration. The procedures followed by the loss segregation method (the most accurate) are slightly different between the standards. Three test procedures are related to this method. The procedures are outlined below.

i) The temperature test (or Heat-run) involves loading the tested motor at the rated conditions (rated load, voltage and frequency) and allowing it to run until the temperature (of the stator windings) does not change by more than 1°C between measurements (every 30 min). The recorded operating temperature together with the ambient temperature are used to determine the specified temperature (equation 4-17) used in temperature correction of power and slip.

$$t_s = t_t + 25°C \tag{4.17}$$

t_s is the specified temperature and t_t is the motor temperature rise which is obtained by subtracting the ambient temp (during the heat-run) from the operating temperature of the motor running at rated load.

The SANS 34-2-2 standard uses temperature rise alone without any correction for ambient conditions. It uses the specified temperature directly.

ii) The variable load test requires the tested motor to be, coupled to a dynamometer and then to be loaded to six-load points ranging from 150% down to 25% of rated load. SANS 34-2-2 does not specify any loading points. The winding temperature before commencement of a test has to be within 10°C or 5 °C of the test temperature (of the heat-run test) according to IEEE 112 B and IEC 34-2-2, respectively. Current, torque, voltage, speed, power and temperature (windings and ambient) are recorded during the test at each load point. The test is performed as quickly as possible to minimize temperature changes in the motor during testing [11].

iii) The No-load test is done with the tested motor uncoupled from the dynamometer. The motor is run with the supply at rated frequency and voltage, for a number of

hours, to stabilise the bearings. The SANS 34-2-2 does not require temperature stabilisation for no-load testing. Once stabilized, the supply voltage is varied from 125% to the point where current begins to increase (due to loss of voltage and increase in slip). Voltage, current, temperature and power are recorded throughout the test.

4.3.4.3. Instrumentation accuracy

The instrumentation requirements of the three standards are shown in Table 4-6. The stringent requirements of the IEEE and IEC allow very accurate efficiencies to be produced [37].

Table 4-6: The instrumentation requirements of the three standards [10] [11] [42]

	IEEE 112 (2004)	IEC (2007)	SANS 34-2
General (%)	0.2	0.2	0.5
Power (W)	±0,2%	±0,2%	±1%
Current (A)	±0,2%	±0,2%	-
Voltage (V)	±0,2%	±0,2%	-
Freq (Hz)	±0,1%	±0,1%	-
Speed (RPM)	±1 RPM	±1 RPM	-
Torque (Nm)	±0,2%	±0,2%	-
Resistance (Ohms)	±0,2%	±0,2%	-
Temperature (°C)	±1 °C	±1 °C	-

4.3.4.4. Loss calculations

The losses are calculated after the testing is completed. The difference in calculation procedure between the standards relate to the determination of core losses and temperature correction.

i) ***Core loss calculation***

The core loss determination in all three standards is as presented in section 4.2.3 and equation 4.12. A plot of the core loss versus no-load test voltage is used to obtain the core loss at exact test voltage. The IEC 34-2-2 takes the resistive voltage drop in the stator winding into account. The recorded input voltage during the load test which is used to determine the core loss, is reduced to a secondary voltage using equation 4.18.

$$V_{sec} = \sqrt{(V_{in} - \left(\frac{\sqrt{3}}{2} IR \sin \varphi\right)^2 + \left(\frac{\sqrt{3}}{2} IR \cos \varphi\right)^2} \qquad \textbf{(4.18)}$$

$$where \quad \cos \varphi = \frac{P_{input}}{\sqrt{3} V_{in} I}, \quad \sin \varphi = \sqrt{1 - \cos^2 \varphi}$$

Where,

V_{in} is the measured voltage during the load test,

I is the current at each loading point,

R is the stator resistance and

P_{input} is the recorded input power at each loading point.

The core losses calculated by the IEC standard will be smaller in magnitude and therefore higher calculated efficiencies would be expected.

ii) ***Temperature correction***

The repeatability and accuracy of determining motor losses has been found to be affected by temperature [41]. This is due to a change in resistance (in stator winding and rotor bars) following a change in motor and ambient temperature.

Equations 4.19 and 4.20 are used for temperature correction of the stator and rotor losses respectively.

$$R_b = \frac{R_a (t_s + k)}{t_t + k} \qquad \textbf{(4.19)}$$

$$s_S = \frac{s_t (t_S + k)}{t_t + k} \qquad \textbf{(4.20)}$$

Where,

R_b is the corrected resistance,

R_a is the measured resistance during the load test,

s_S is the corrected slip to specified temperature,

s_t is the measured slip at load test temperature,

t_s is the specified temperature, t_t is the observed stator temperature and
k is equal to 234.5 for 100% IACS conductivity copper, or 225 for aluminum, based on a volume conductivity of 62% of the rotor or stator material.

The difference in temperature correction between the standards is as follows:

IEEE 112-B (2004) and IEC 34–2 (2007): Stator winding and rotor loss are corrected to a specified temperature, (see equation 4.17). The copper conductivity constant is 234.5.

SANS 34-2 (2007): Stator winding loss is corrected for the temperature rise, whilst slip correction is not specified. The copper conductivity constant is 235.

4.4. Preliminary test results

Preliminary tests were done to compare the different standards. The testing was initially done on a 3kW motor and later extended to the other seven motors of different ratings.. The tests were done in two stages: The comparison of efficiency using different standards and the comparison of efficiency due to different testing methods.

4.4.1. Comparison of test standards

The SANS 34-2, CSA 390, the JEC, the IEEE 112 B and the IEC 34-2 (2007) standards were tested on the eight motors using the loss segregation method. The method is common to all the standards. A comparison of the motor's full-load efficiency can be seen in Table 4-7.

Table 4-7: Comparison of full-load efficiencies of motors as determined by several standards

Motor Size (kW)	IEEE / CSA (%)	IEC (%)	JEC (%)	SANS (%)
3.0	80.5	79.1	80.6	80.7
7.5	86.2	86.5	87.7	87.1
11	85.6	85.8	87.9	86.9
15	87.3	87.6	88.9	88.7
22	88.7	89.2	91.1	90.1
37	90.0	90.0	91.5	91.0
45	90.3	90.6	92.7	92.0
55	90.8	91.1	92.8	92.1

The JEC and SANS standards produce the highest efficiency values while the IEEE, CSA and IEC produce very similar efficiency values. The difference in the standards can be explained by the loss evaluation associated with each standard.

4.4.1.1. SLL

SLL account for between 15 to 20% of total losses and are therefore very significant in efficiency determination. It has been stated that efficiency values determined by neglecting SLL cannot be considers reasonably accurate [45].

The treatment of SLL in the different standards has been discussed earlier in this in this chapter. The JEC ignores SLL, the SANS assigns a value of 0.5% of the input power, the IEEE, IEC and CSA uses the loss separation to calculate SLLs. Figure 4-10 below shows the different values of SLL.

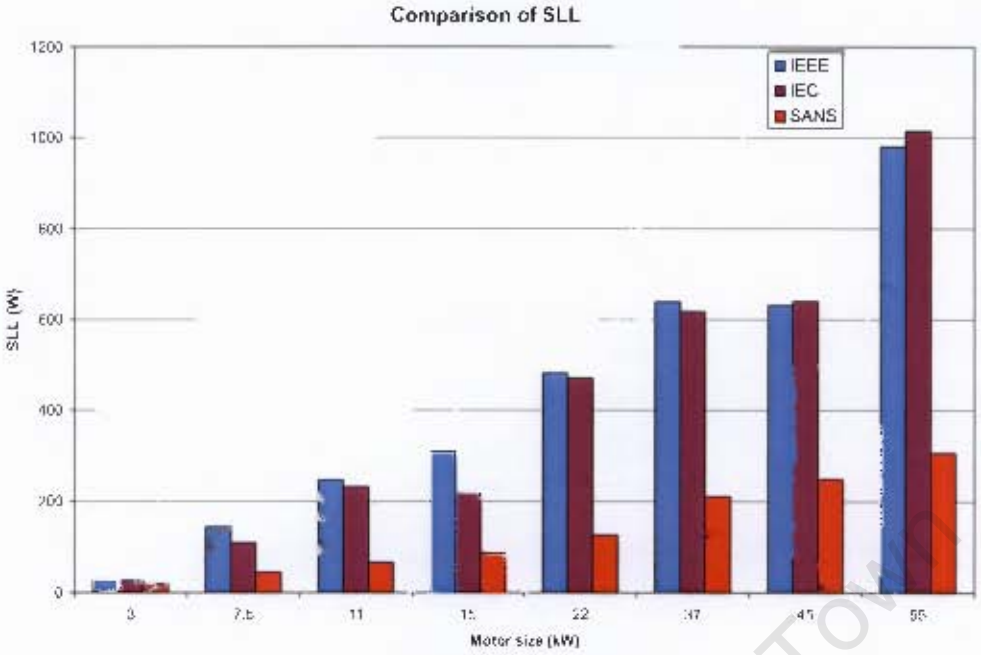

Figure 4-10: Calculated SLL from the IEEE, IEC and JEC

The allocation of SLL used in the SANS standard has been found to be unsupported. Table 4-8 shows SLL as a percentage of measured input power for all motors. It can be seen that the allocated SLL are an underestimate of the SLL determined by other standards. The SLL are small and therefore the calculated efficiencies will be higher.

Table 4-8: SLL as a percentage of input power

Motor size (kW)	Percentage of Input power (%)		
	IEEE	IEC	SANS
3	0.72	0.71	0.5
7.5	1.61	1.22	
11	1.88	1.75	
15	1.79	1.27	
22	1.91	1.86	
37	1.52	1.47	
45	1.27	1.29	
55	1.58	1.64	

4.4.1.2. Core loss

The core loss in the standards is calculated using no-load test results. The IEC 34-2 standards differs from the other standards in that it takes into account the resistive voltage drop in the stator winding. The measured input voltage during the no-load test is reduced to a secondary voltage using the Equation 4.18.The impact of this is that the IEC core loss are smaller in magnitude. Table 4-9 shows the core loss difference between the standards.

Table 4-9: Core loss values of IEEE and IEC

Motor size (kW)	Core loss (W)	
	IEEE /CSA	IEC
3	108.80	79.12
7.5	209.93	171.07
11	375.47	294.70
15	378.19	347.84
22	497.60	453.40
37	653.50	611.41
45	850.75	779.74
55	736.05	625.76

4.4.1.3. Temperature correction

The impact of temperature correction can be seen in the graphs shown in Figures 4-11 and 4-12 (at rated loading). The uncorrected losses are generally lower than the corrected losses. This would result in the higher efficiencies when using the uncorrected losses.

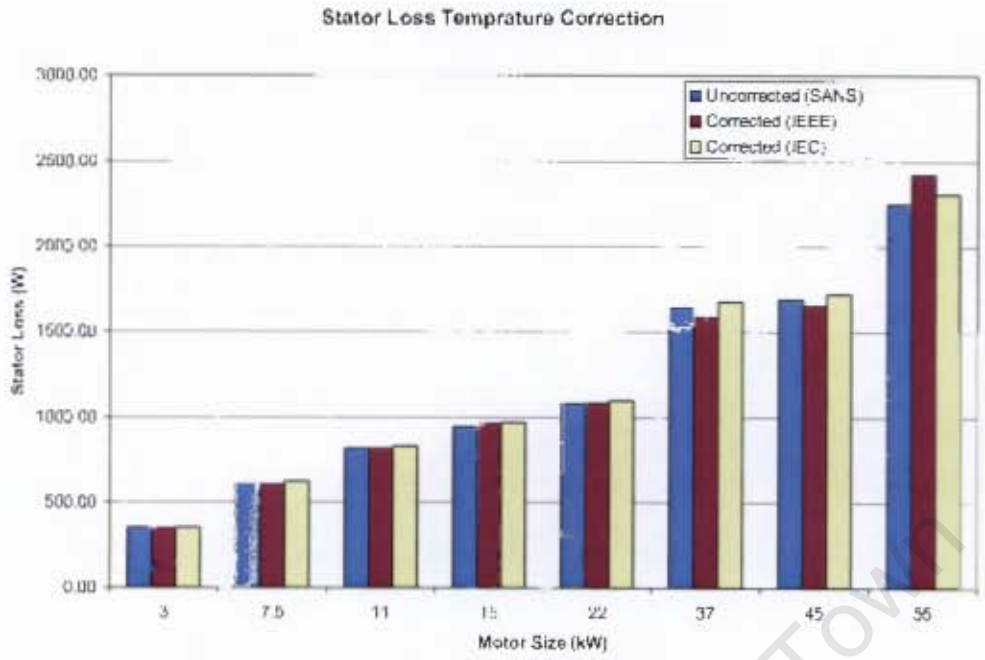

Figure 4-11: Impact of temperature correction on Stator loss

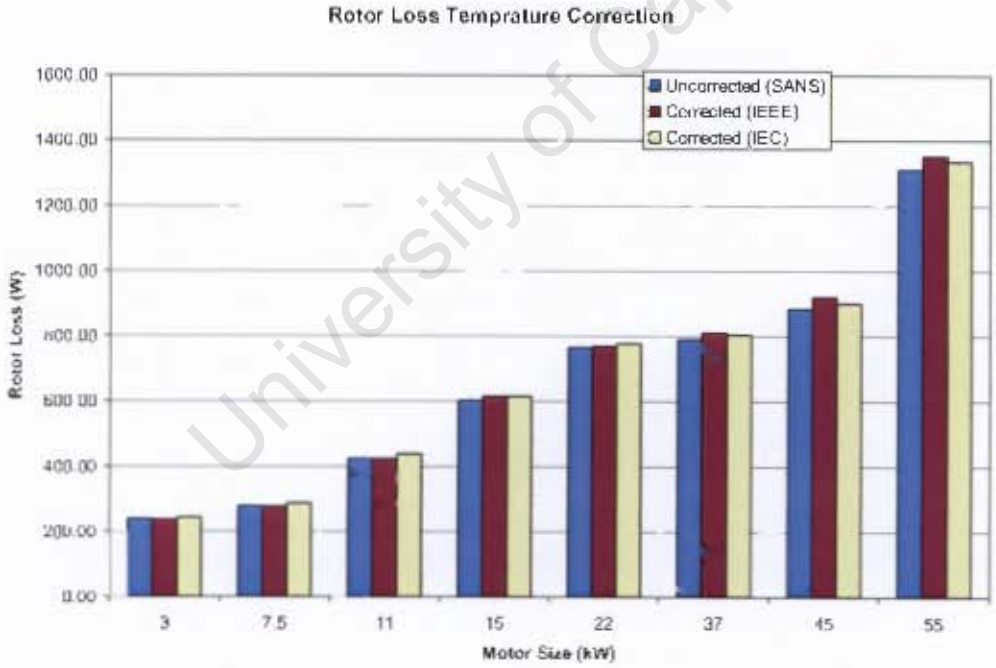

Figure 4-12: Impact of temperature correction on Rotor loss

4.4.2. Comparison of test methods

The second stage compared the impact of using different methods. As discussed in the precious sections, there are several methods associated with each of the standards. The main methods in each standard are based on the equivalent circuit, the loss segregation and direct (Pout/Pin) methods. Comparison of these methods were performed on the 7.5, 11 and 15kW motors. The calculated equivalent circuit parameters according to the IEEE and IEC standards are in Appendix F.

Figures 4-13 to 4-15 show the plots of efficiency curves produced by the different methods used.

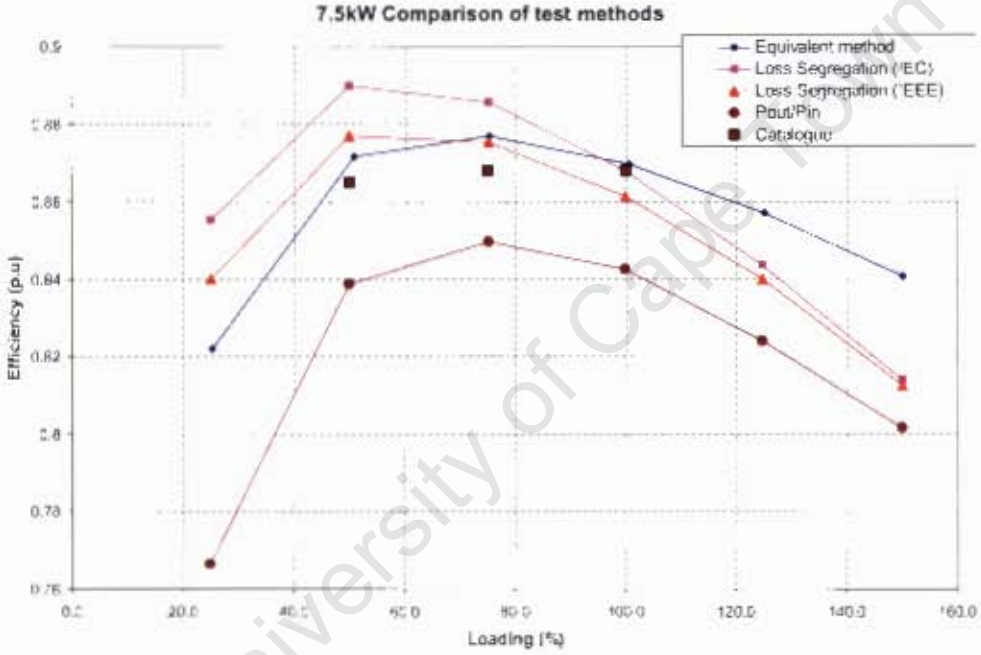

Figure 4-13: 7.5kW test comparison

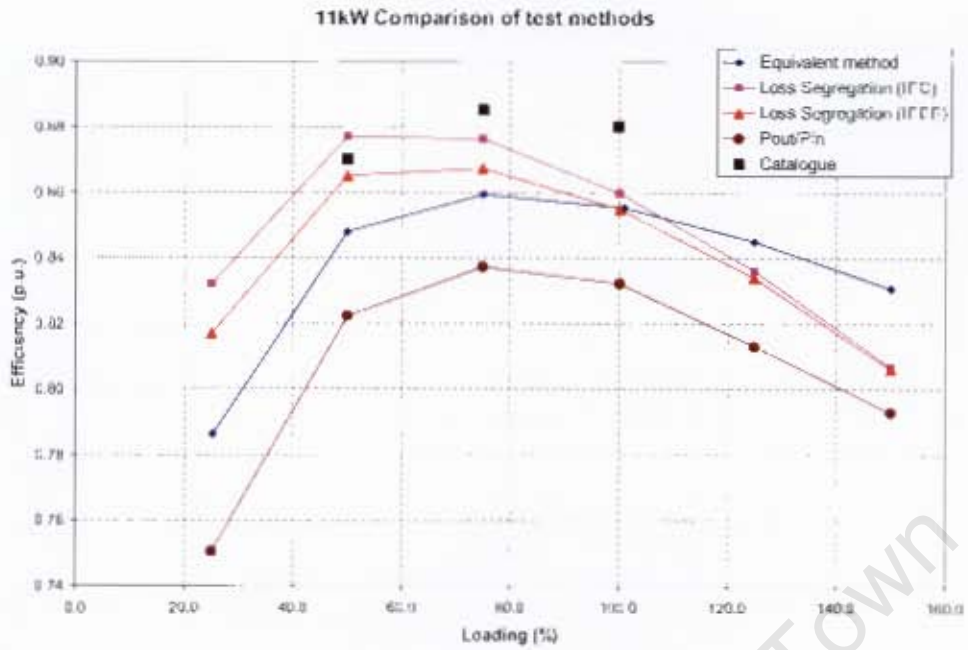

Figure 4-14: 11kW test comparison

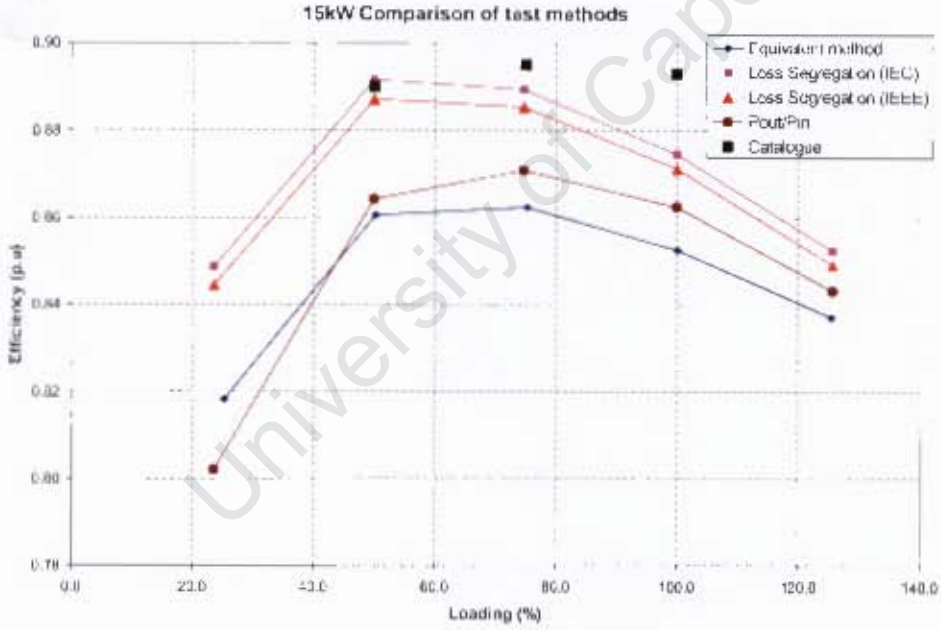

Figure 4-15: 15kW test comparison

Motor efficiency vary according to both the standard and methods used. This has been clearly shown in sections 4.3.1 and 4.3.2.

4.5. Concluding remarks

The determination of efficiency is definitely a debatable issue that is still continuing. A need clearly exists for a single universal standard for induction motor efficiency determination. The chapter has shown that the IEC and IEEE standards' method 2 and B respectively, are the most accurate and repeatable standards. Although South Africa has its own testing standard SANS 34-2, is has been shown to be outdated and unsupported.

The IEEE (2004) and IEC (2007) standard will therefore be used in the motor rewind testing presented in the next chapter.

Chapter 5: REPAIR AND REWIND OF INDUCTION MOTORS

5.1. Overview

This chapter presents a thorough literature review on the impact of repair and rewind on induction motors and the techniques used in the repair and rewind of induction motors.

Findings from a case study of the different rewind techniques followed by two local rewinding companies are also presented.

5.2. Motor Failure

Despite the versatility and ruggedness of Squirrel cage induction motors, they are subjected to the same failure modes as other electrical machines. A survey conducted by the Institute of Electrical and Electronics Engineers (IEEE) [51] and Electrical Apparatus Service Association (EASA)[32], identified the distribution of failures in induction motors. The results are shown in Table 5-1

Table 5-1: Distribution of failures in Induction Motors [32]

Motor component	Percentage failure
Bearings	51.07%
Rotor Bars/End Rings	4.70%
Shaft or Couplings	2.44%
External Device	15.58%
Stator Winding	15.76%
Not Specific	10.45%

The cause for motor failures is a result of stresses on one or a number of the different components of the motor i.e. stator, rotor, shaft and bearings [51].

In an interview with the marketing director of a large electric motor rewind company in South Afric,) it was mentioned that the reason for the increase in motor failure in South Africa was due to:

- The extra pressure on all equipment, in particular motors, due to infrastructure upgrades for the 2010 World Cup and
- power supply upgrading [52].

This has resulted in more downtime caused by motor failure.

5.2.1. Motor Stresses

There are several stresses that can lead to the failure of motors' windings, rotors, bearings and shafts. These motor stresses can be grouped as follows [51] [53]:

- **Bearing stresses**: Thermal, dynamic and static loading, vibration and shock, environmental, mechanical, electrical

- **Stator stresses**: Thermal, electrical, mechanical, and environmental

- **Rotor stresses**: Thermal, dynamic, mechanical, environmental, magnetic, residual, and miscellaneous

- **Shaft stresses**: Dynamic, mechanical, environmental, thermal, residual, and electromagnetic

When these stresses are controlled, the probability of premature failure of any motor component can be reduced] [51].

5.3. Motor repair procedures

Motors are repaired according to certain international standards. The two most referenced standards are:

- IEEE 1068: *Recommended practice for the repair and rewinding of motors for the petroleum and Chemical Industry*,

- EASA: *Guide to good motor repair and replacement*

In South Africa, the South African Bureau of Standards (SABS) published the SABS 0242-1: *The rewinding and refurbishing of rotating electrical machines.*

These standards outline repair methods that are commonly used to repair electric motors [54] [55] [56]. The following review will concentrate on motor rewinding.

5.3.1. Inspection, dismantling and testing

On arrival, a motor is inspected for electrical and mechanical failure. The motor is then dismantled and the following tests are performed: voltage insulation test, high-voltage withstand test, rotor-bar test, interturn test and phase resistance or line resistance comparison test.

5.3.2. Winding removal and core processing

Winding removal and core processing is the most important part of the motor repair as this has the highest potential for affecting the motor's efficiency [57].

5.3.2.1. Winding removal

Rewinding a damaged motor requires the removal of the old windings. According to EASA and SABS, a record of the winding details must be done first (i.e. the number of poles; the number of slots; the number of turns per coil; the number of wires in parallel per coil; the size of wire; the number of coils per phase group; the number of phase groups; the coil pitch; etc). The winding details need to be checked against the motor manufacturer's original design data [56] [57].Once that is done the removal process begins by the removal of one coil end.

There are a number of methods used for winding removal. These include:

Oven Burnout: The stator is placed into a burnout oven that is set at a recommended temperature. The SABS recommends temperature control not exceeding 380 °C [56]. The EASA recommends applying an oven temperature of 343 ℃, and not overheating the stator core above 360 ℃ for organic and 400 ℃ for inorganic cores [57]. Experimental studies have found that temperatures according to EASA are low but

just high enough to burnout the winding coils [58]. This results in further difficulty in removing the old windings, which could increase the potential for damage to the stator laminations [58].

Mechanical removal: There are a number of mechanical removal methods available. These are very rarely used in rewind shops.

- ***Water Blasting***: A high-pressure stream of water is used to blast the coils out of the stator slots.
- ***Hot vapor process chemical stripping:*** The stator is submerged in a bath of non-chlorinated petroleum for a short time and then the windings are removed.
- ***Hydraulic removal:*** The coils and insulation are removed slowly using a steady hydraulic pull.

Direct Flame: A flame from a torch or other source is directed into the core of the motor and applied until the insulation is reduced to ash, and the windings removed. The temperature is not controlled and can cause severe damage to the core [59]. The uncontrollably high temperature from the flame causes warping and hot spots on the stator core.

After the windings are removed, the stator is cleaned.

5.3.2.2. Core processing

Once the core has been cleaned, the integrity of the stator core is tested according to the loop or core test (as per SABS, EASA and IEEE guidelines). The condition of the core is the most difficult to control through the rewind process [57]. Damage to the cores integrity of the core can occur from

- Baking: Elevated, uncontrolled temperatures can lead to the fusing of lamentations [57].
- Mechanical damage: Filing the core, mechanical stripping, etc.

The core test has been proven to be the most effective test to detect short circuited laminations in the core iron.

Loop/ Core test: The test requires a current carrying cable to be looped through the stator bore and around the frame as shown in Figure 5-1. This technique uses the stator core dimensions and an assumed value of magnetic flux density in the back iron to calculate the magnetizing volt-amperes needed to produce that density. The condition of the core is then determined from the core temperature or/and input power [58].

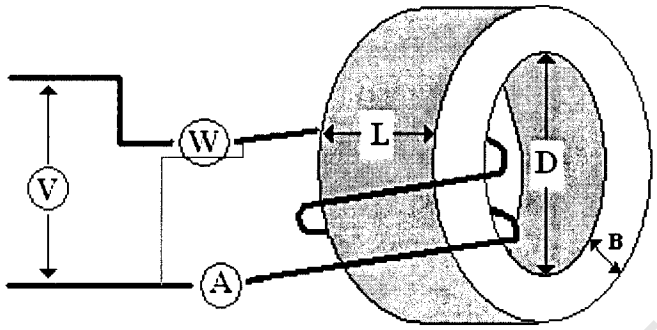

Figure 5-1: Loop test wiring diagram

Core test from input power: Core testing through input power is done in the following two steps. This is defined in the EASA guidelines [58].

Step 1: The number of loop turns and the current magnitude to produce the required level of magnetic flux density is calculated using Equations 5.1, 5.2 and 5.3. The suggested magnetic flux for running motors is 1.2 Tesla [57].

$$LT = \frac{V}{f \times L \times D \times B_C \times \gamma \times 4.44} \quad \textbf{(5.1)}$$

Where, LT = loop turns

V = supply voltage

L = Axial Length [m]

f = Test frequency (Hz)

D = Back iron depth [m]

B_C = *Back iron flux (1.2T)*

γ =*Stacking factor (generally 0.95)*

$$mmf = H \times l$$

$$where \ \ H = \frac{B}{\mu} \tag{5.2}$$

Where, mmf = magnetomotive force

H =Field intensity

l = length of the flux path

μ = the permeability or characteristics of the medium

$$A = \frac{mmf}{LT} \tag{5.3}$$

Where, A =Estimated current

Step 2: Losses in the back iron are then calculated using Equation 5.4.

$$W / kg = \frac{Input \ \ Power}{Core \ \ Weight} \tag{5.4}$$

Where, W/kg =losses in the core back iron

Core losses in the range of 2.5 - 4 W/kg were measured from testing cores of new motors [57]. Commercial core loss testers are available that compute the W/kg loss automatically [57]. These have the advantage of simple operation and convenient printouts for documenting test results.

Core test from core temperature: Core testing by observing the temperature is the simplest method. The temperature of the core is observed by means of temperature sensors, while inducing flux in the back iron of the core. Equation 5.5, a rearrangement of Equations 5.1 to 5.4, can be used to calculate the required voltage to supply the flux. This method is available option in the SABS rewind guideline [56].

$$V = \frac{B_C \times L \times B}{Core \ \ Weight} \tag{5.5}$$

Where, W/kg =losses in the core back iron

5.3.3. Winding and varnishing

When the core has passed the core test, the replacement of the winding can be done. This process is done with extreme care to replace the original cross sectional area of a turn, the same number of turns per coil, and the indentified span and connection of the coils [54] [55] [56]. Higher insulation class of the winding or change in winding configuration can be done at this point, if required. Winding can be done in the following ways:

Hand Winding: The coils are wound using a '*tower-type*' coil winding machine with a mechanical counter. The mean-length per turn (MLT) and tension are dependant on the artisan. This method has a high potential for poor layering, which makes the insertion into the stator slot difficult and causes wire crossing. An increase in the MLT occurs and this results in an increase in the stator resistance [59] [62].

Machine Winding with either Automatic Coil or Computerized Coil: Automatic coil winding has the advantage of maintaining constant tension and proper count of the coils. The method is however still manual and requires observation by the artisan. The computerized coil winding is fully automated. Proper tension, correct layering, and turn counts are performed accurately.

Once the coils have been wound and inserted into the stator slots, the motor's windings are insulated with varnish. There are several varnish methods:

Dip and Bake: The wound core is dipped into a varnish, usually epoxy, for about 20 hours and then baked in a temperature controlled oven. A good dip and bake would involve two dips and bakes without any shortcuts. This is an inexpensive system and is therefore the most commonly used method by rewind shops [59]. Partial discharge occurs where voids, mainly caused by air bubbles are trapped within the insulation. The discharge in the voids reduces the insulation life and could result in another motor failure [59].

Vacuum Pressure Impregnation (VPI): VPI is a very expensive process due to the equipment required. The rewound stator is dipped into a vacuum pressured tank with

varnish. The pressurized tank ensures that there are no voids, caused bubbles, by creating a vacuum. Varnish is forced everywhere through the high pressure. Capacitance between the stator core and windings is used to determine when penetration is complete. Pressure is then returned to atmospheric conditions and excess resin drained from the core. The core is then baked. The method works very well for Medium Voltage motors which have taped windings that holds the varnish [59]. The dip and bake is also the preferred method for low voltage induction motors.

Trickle Varnishing: Trickle varnishing with epoxy or polyester is quite inexpensive and has been found to fall somewhere between the dip and bake and VPI methods. The resin is poured from the front end of a vertically positioned stator core. Curing occurs simultaneously from heat produced by a controlled electric current. The voids are removed due to gravity and capillary action. The final result is an equivalent of 3 dips and bakes, without voids. [59].

5.3.4. Assembling of motor

Generally, before reassembly, the rotor is balanced. This is done by mounting the rotor on pedestals and spun at multiple speeds. The vibration of the rotor is checked. Excessive vibration in an electric motor can reduce bearing life and can damage the motor structure [59]. Bearings, fans and end plates are replaced in the reverse order of the dismantling process. The motor is then lubricated, and finally painted.

5.3.5. Final testing

Before shipment, a number of tests are done on the motor. These final tests could include:

- High-voltage test,
- Current balance at no-load,
- Vibration (horizontal foot-mounted motors only),
- Input power at no-load, Bearing temperature
- Noise,
- Temperature rise

5.3.6. Impact of poor repair procedures on induction motor loss

Poor repairing procedures can increase motor losses. Table 5-2 highlights some of the problems that can increase losses during motor repair [37] [32].

Table 5-2: Impact of rewind and repair procedures on induction motor loss

Motor loss	Affected by
Stator core losses	Overheating core steel during stripping Damaging core insulation during winding removal Excessive abrasion and grinding during core cleaning
Friction and Windage losses	Bearings and cooling fan not replaced to original conditions Incorrect bearing fits Incorrect bearing preload Under/over lubrication
Stator Winding Losses (I^2R losses)	Reducing conductor cross-sectional area Changing number of turns Using wrong winding configuration Machining rotor
Rotor losses (I^2R losses)	Altering rotor bars and end rings Changing cage design
Stray load losses	Change in air gap symmetry and air gap unconventional behaviour Bent motor shaft or damaged end shields

5.4. Motor rewind procedures and practices in South Africa - Case Study

The variation in motor rewinding techniques used by South African motor repairers is not known. The rewinding techniques/procedures currently used by two motor rewinding companies situated in Cape Town are presented in this case study. These companies were chosen because they represent the lower and upper range of

The single loop of wire (in yellow in Figure 5-5) is inserted into the stator core and a 50Hz supply is used create a flux (see Section 5.3.2.2). The back iron of the core is fluxed and the power input is measured to calculate the loss per kg. Damage to the core or "hot spots" are determined from comparing the core tester's output (W/kg) to Table 5-4. Commercial core tester readings for the rewound motors are shown in Appendix G.

Table 5-4: Decision based in core testing results

W/kg	Decision	Action
up to 5	Good	N/A
5 to 8	Acceptable	do further tests
8 to 12	Acceptable	Check for mechanical damage
Above 12	Bad	Reject

5.6.1.4. Rewinding

Utilizing the recorded data from the old windings and the manufacturer's data, the stator is rewound by hand using as a '*tower-type*' coil winding machine with a mechanical counter. Figure 5-6 shows the winding area at Company A. The coils are inserted by hand with the tension and layering determined by the technician.

Figure 5-6: Company A's winding area

5.6.1.5. Insulating Varnish

Company A can perform the varnish insulation using the VPI or the Dip and Bake method.

VPI: The rewound stator is inserted into a VPI Tank. The vacuum is set to 0.1 millibar and the varnish is pressurized to 5 Bar to force the resin into all voids. The measured capacitance between the stator core and windings is used to determine when penetration is complete. The excess varnish is then drained and the core is baked.

Dip and Bake: Figure 5-7 is the Company A dip tank. The stator core is dipped into the tank and then sealed. The core remains in the tank until the air bubbles disappear. This takes up to 6 hours. The excess varnish is then drained and the core is baked.

Figure 5-7: Company A's dipping tank

5.6.1.6. Baking and Curing

The rewound stator is then placed into a dedicated curing oven to enable the resin to set and attain the desired mechanical strength. Figure 5-8 is the Company A curing oven.

Figure 5-8: Curing oven

5.6.1.7. Reassembly and final testing

The motor is then reassembled (see Figure 5-9) and tested as specified in the SABS standard. Tests include a high potential and no-load test. The motor is then painted and returned to the customer.

Figure 5-9: Reassembled motor 55kW awaiting final tests and painting

5.6.2. Company B

Company B has no official rewind procedure standard. The rewind process is based on *'experience'*.

5.6.2.1. Dismantling and Inspection

Motors entering Company B's shop are dismantled and inspected visually for any signs of damage. During the 3kW motor repair associated with this study, no tests such as continuity, insulation resistance, high potential and surge comparison tests were performed.

5.6.2.2. Winding Removal

If the motor is to be rewound, the old windings are removed. The front-end windings are cut by means of an angle grinder and the windings are burnt out using direct flame from a blow torch. This is shown in Figure 5-10. Removing varnish by gas torch is allowed by SABS 0242-1 standard.

Figure 5-10: Coil removal using blow torch

The removed windings are then used to record the winding details (wire size, coil pitch, length, number of turns, etc). Burnout windings of the 3kW motor are shown in Figure 5.11.

Figure 5-11: Old removed windings

5.6.2.3. Core Test

Core testing facilities with variable voltage supplies are available as shown in Figure 5-12. However, core testing is only done upon customer's request. When core testing is done, a single loop of wire is inserted through the stator and current is passed through it. No prior calculations are done to determine current levels, loop turns, etc (see Section 5.3.2.2). The stator is then '*felt*' by hand to locate "hot spots" which would indicate short-circuiting of laminations. The damaged area would then be grinded away in order to remove hot spots.

Figure 5-12: Core testing facilities

5.6.2.4. Rewinding

The recorded data from the old winding is used for rewinding the motor. The coils are produced by hand using a '*tower-type*' coil winding machine with a counter (see Figure 5-13).

Figure 5-13: Hand winding with counter

The windings are inserted by hand into the stator slots, whilst the artisan tries to maintain the correct tension and layering. Figure 5-14 shows the insertion of the windings of the 3kW motor.

Figure 5-14: Insertion of the windings on the 3kW motor.

5.6.2.5. Insulating Varnish

The rewound stator is then impregnated with insulation vanish. The stator is dipped into the varnish tank as shown in Figure 5-15. The rewound motor core is left over night to allow the air between the windings to '*bubble out*'. The stator is then removed and hung to allow the excess varnish to drip off.

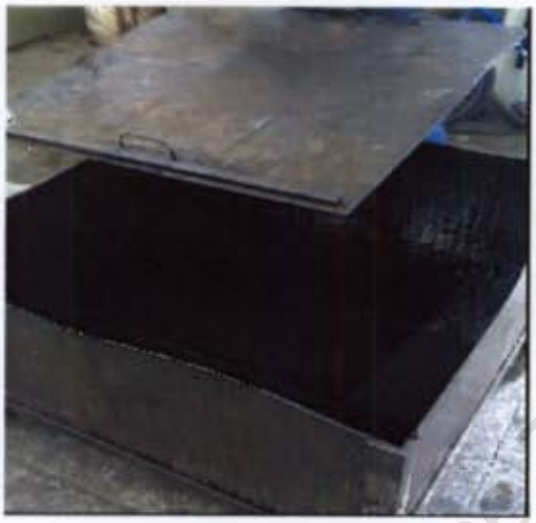

Figure 5-15: Company B's varnish dip tank

5.6.2.6. Baking and Curing

The rewound stator is then placed into a curing oven for a duration of time. This curing process takes more than 6 hours and in some cases overnight at a temperature of 200°C. The oven was constructed on site using heating elements from stoves, heaters, a timer and insulation material.

Figure 5-16: Company B's curing oven

5.6.2.7. Reassembly and final testing

The motor is then reassembled, painted and final testing is done. The final test compromises of a single no-load test. The motor is connected to a variable voltage supply and set to 40, 60, 80, and 100% of rated voltage (see Figure 5-17). The rms current in each phase is measured and if the current is not too high, the motor is classified as a good rewind.

Figure 5-17: Company B's variable voltage supply control panel

5.7. Concluding remarks

Rewind and repair procedures are well documented in international and local standards. Detailed discussions were presented on the rewinding procedures used by two South African motor repairers.

Chapter 6: IMPACT OF REWINDING ON MOTOR EFFICIENCY: TEST RESULTS

6.1. Overview

This chapter presents a detailed discussion of the results from the rewind study.

Sections 6.3 to 6.10 present the impact of rewinding on each of the eight motors. The focus is on the results at 100%, 75% and 50% loading points. These part-loads are the most common motor loading points in industry.

Section 6.11 addresses the trend in each motor losses and the efficiency change observed in the eight motors.

Finally, section 6.12, presents and discusses the impact of rewind techniques on two 3kW motors at rated load.

The efficiency vs load and loss vs load curves of other load points are found in Appendix H.

6.2. Test Methodology

Eight brand new motors underwent a single full rewind process. The motors were subjected to five full test cycles at each load point, before and after rewind according to IEC and IEEE standards. The five tests were then averaged. The averaged efficiency value was used in the final discussion.

The 3kW motor was tested on the 3kW test bed, the 7.5, 11 and 15kW motors were tested on the 15kW test bed, and the 22, 37, 45 and 55kW were tested on the 250kW test bed.

6.3. 3kW motor results

The impact of rewinding on the efficiency of the 3kW motor is shown in Figure 6-1. A drop in efficiency ranging from 0.97% to 2% was observed between 100% and 50% load points.

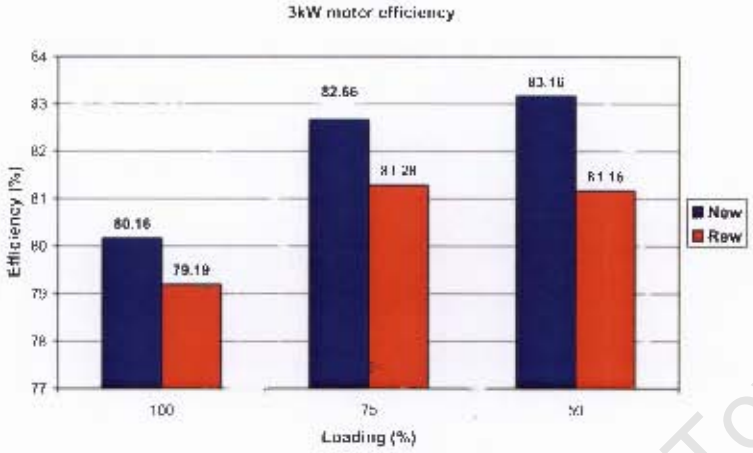

Figure 6-1: 3kW motor efficiency change

The drop in efficiency of the 3kW motor is a result of increase in losses. The loss distribution is shown in Figure 6-2. The largest increase is the core and friction and windage losses followed by the SLLs then, stator and rotor winding losses.

The increase in core loss and SLL is the result of core damage. The winding removal, after oven burn out, damaged the stator teeth and laminations during extraction. Core test results from the were unavailable for this motor.

The increase in stator winding losses correlates with higher stator currents (see Table 6.1). Higher currents were recorded although a lower stator resistance was measured (see Table 6.1). The increase in current and winding/copper losses is the due to the increase in motor torque and drop in speed. This occurs to allow the motor to produce the same kW.

The fan was unaltered and the bearings greased during reassembly. Over greasing, which is thought to reduce the friction, can in fact lead to an increase in the friction loss (see discussion in section 6.11). The over greasing of the 3kW motor's bearings and fan is the cause for the increase in friction and windage losses.

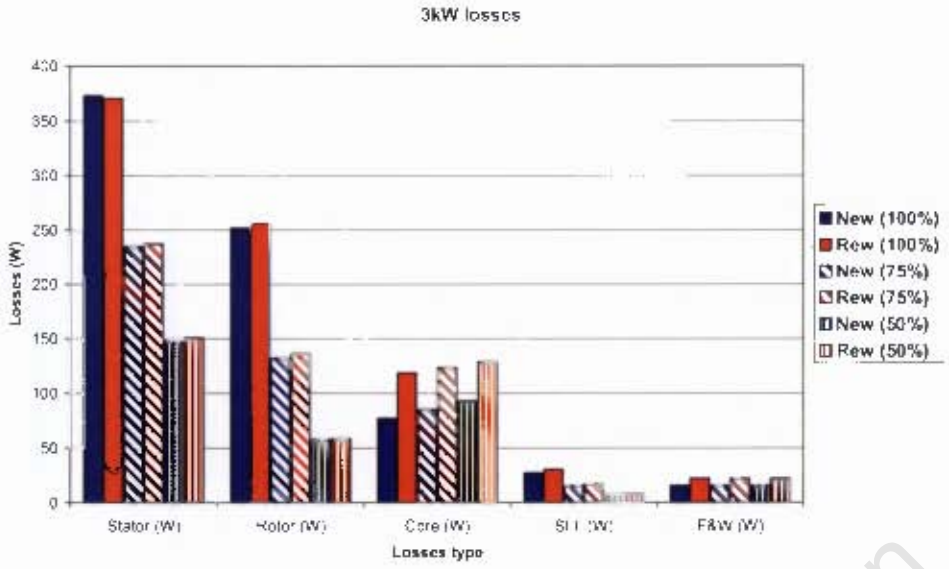

Figure 6-2: Change in losses of the 3kW motor

Other recorded changes such as stator currents, operating speed, stator resistance and temperature rise before and after rewind on the 3kW are shown in Table 6-1. The rewound 3kW motor draws larger stator currents, runs at a lower speed and at higher operating temperatures. The temperature corrected winding resistance is shown in table.

Table 6-1: Other changes due to motor rewind

Loading (%)	Load current (A)		Speed (rpm)		Corr Res (O)		Temp Rise °C	
	New	Rew	New	Rew	New	Rew	New	Rew
100	6.65	6.95	1388.67	1386.1	2.47	2.34	97.5	98
75	5.32	5.62	1421.67	1419.4				
50	4.27	4.55	1450	1449				

The increase in friction and windage losses causes an increase in shaft torque. This increase in torque forces the motor to run slower in order to produce the required output power (see Appendix H).

The higher operating temperature is due to a decrease in heat removal caused by a slower running fan and the higher dissipated losses in the form of heat..

The lower stator resistance may be explained by the use of better raw material (considering the original wire gauge was used). Tighter wound coils which have smaller mean length per turn (MLT) could also have lead to the drop in resistance.

6.4. 7.5kW motor results

The impact of rewinding on the efficiency of the 7.5kW motor is shown in Figure 6-3. A small drop in efficiency ranging from 0.1 to 0.7% was observed at the three loading points. The efficiency drop at 100 % is negligible as it is within the repeatability tolerance. Therefore, only the drop in efficiency at 75 and 50% will be discussed.

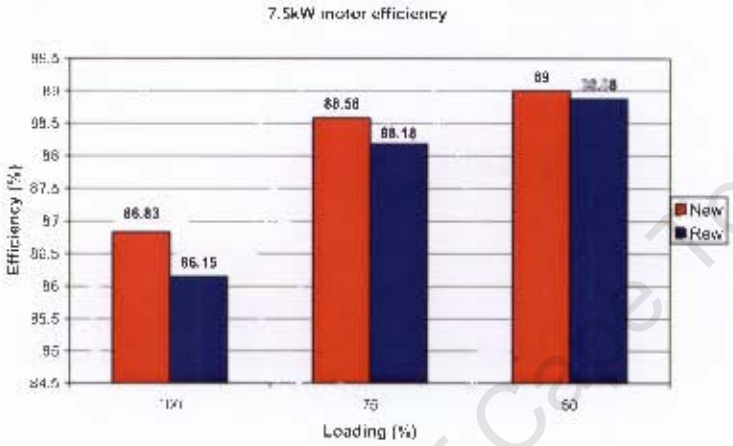

Figure 6-3: 7.5kW motor efficiency change

Figure 6.4 shows the loss distribution of the 7.5kW motor. The largest increase is the stator winding loss followed by the SLL, then the rotor bar losses and finally the core and friction and windage losses.

The increase in stator winding losses is the result of an increase in the stator winding resistance and stator currents (see Table 6-4). The increase in core loss and SLL, like in the 3kW motor, is an indication of core damage. Core testing of the 3kW core, after winding removal, required 'further core testing' (see Section 6.11). This damage occurred during the winding removal and oven burnout. The rotor was left unaltered yet an increase in rotor winding losses was recorded at 75% and 100% loading points. This increase is due a change in the rewound motor's slip, speed and torque characteristics (see discussion in Section 6.11).

rewinding companies in South Africa. This investigation into the companies will show the vast differences between rewinding shops in South Africa.

5.5. Rewind Company Profiles

The two rewind companies that were investigated were:

- Company A – Large rewind company and
- Company B Small rewind company

The presented information was obtained from the companies' website, site visit and interviews conducted by the author.

5.5.1. Company A

Company A was established in 1913. Since its establishment, the company has grown into the most comprehensive and leading electrical machine repairer in Southern Africa. Company A has the capability to rewind both small and large machines (including unorthodox designs such as Schrage and Lorence-Scott machines). Cage Induction motors up to 14MW have been rewound and test-run in their large machines workshop. Figure 5-2 shows Company A's workshop.

Figure 5-2: Company A's workshop

the accuracy of the observed information against the manufacturer's design specifications.

Figure 5-4: Company A's Controlled-temperature oven

5.6.1.3. Core Testing

The core is cleaned of dirt through water blasting. All dried motor cores are then core tested using a commercial core tester (see Figure 5-5).

Figure 5-5: Commercial core tester from Heary du Preez & Associates

The friction and windage losses are the only losses that have dropped. Correct application of bearing greasing during motor reassembly has resulted in the lower friction and windage losses.

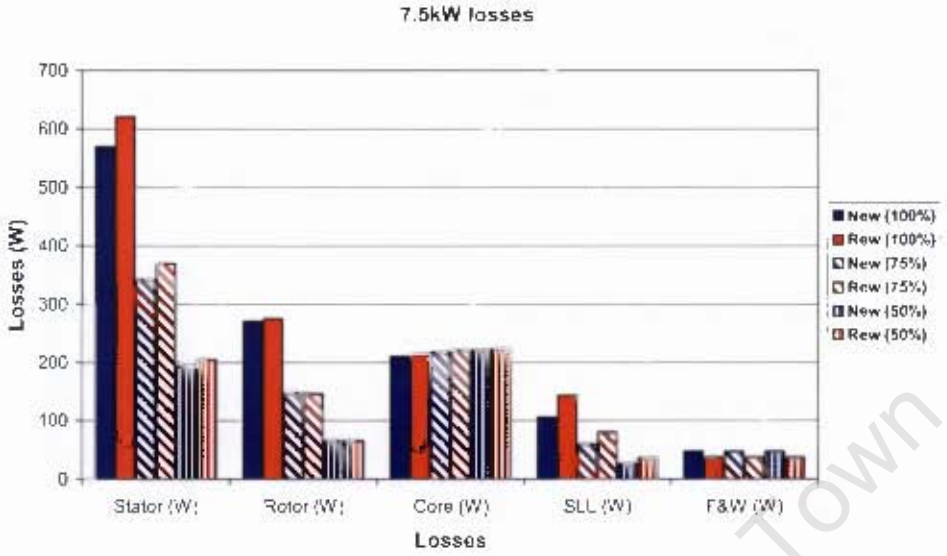

Figure 6-4: Change in losses of the 7.5kW motor

Other recorded changes such as stator currents, operating speed, stator resistance and temperature rise before and after rewind on the 7.5kW are shown in Table 6-2. The rewound 7.5kW motor draws larger stator currents and runs at higher speeds and operating temperatures.

Table 6-2: Other changes due to motor rewind

Loading (%)	Load current (A)		Speed (rpm)		Corr Res (Ω)		Temp Rise °C	
	New	Rew	New	Rew	New	Rew	New	Rew
100	15.35	15.49	1453.00	1449.53	2.43	2.57	92.03	93.76
75	11.91	12.09	1466.80	1464.53				
50	9.00	9.26	1479.50	1477.95				

The higher currents are caused by the increase in stator resistance. The higher resistance can be explained by the use of larger MLT in the winding coils. The higher operating temperature of the rewound motor is the result of the higher dissipated losses in the machine.

6.5. 11kW motor results

The impact of rewinding on the efficiency of the 11kW motor is shown in Figure 6-5. Large drops in efficiency, ranging from 1.59 to 2.83% have been observed at the three loading points. The drop in efficiency of the 11kW is a result of increase in motor losses as shown in Figure 6-6.

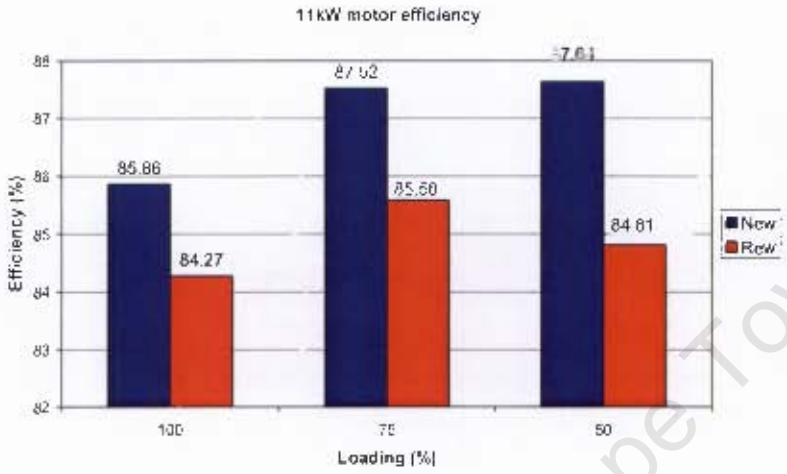

Figure 6-5: 11kW motor efficiency change

The largest increase in losses was the core loss and SLL. This was followed by the stator winding and rotor bar losses.

The large increase in the core loss and SLL is again the result of damage to the core during the core processing. Core test results (see Section 6.11), showed that the core failed the test. This means that the damage to the core was significant. In normal circumstances, the core would have been rejected and on request from the customer, restacked. To avoid inconsistency in the project, the motor was rewound with the damaged core. The result of the damage is clearly seen in the large increase in core losses.

The friction and windage losses on the other hand have dropped. This is the result of correct greasing on the motor bearings and the reduced operating speed of the rwound motor.

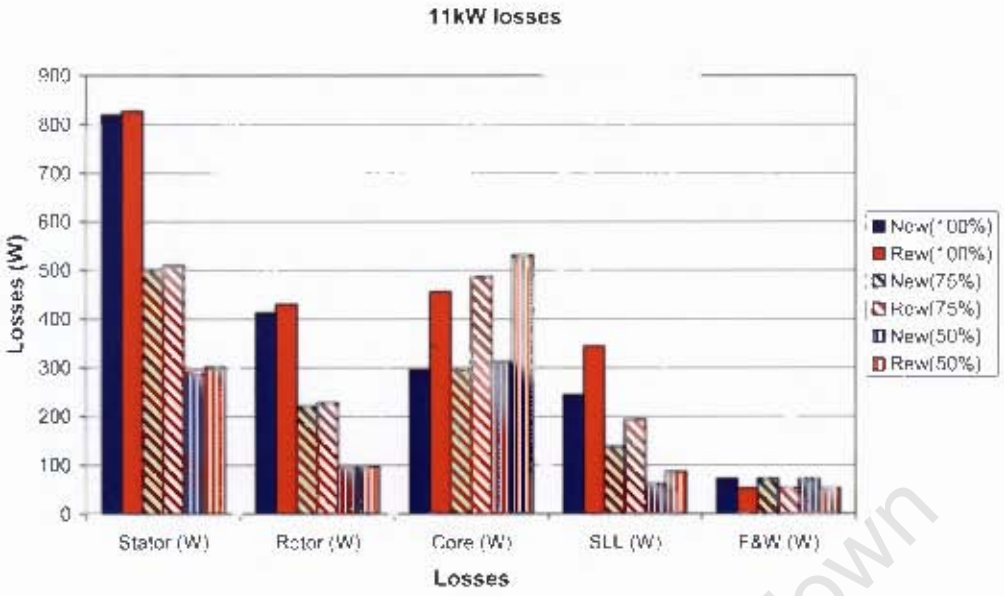

Figure 6-6: Change in losses of the 11kW motor

Other recorded changes such as stator currents, operating speed, stator resistance and temperature rise before and after rewind on the 11kW are shown in Table 6-3 below. The rewound 11kW motor draws larger stator currents and runs at lower speeds and much higher operating temperatures. The stator resistance of the rewound motor is also higher.

Table 6-3: Other changes due to motor rewind

Loading (%)	Load current (A)		Speed (rpm)		Corr Res (Ω)		Temp Rise °C	
	New	Rew	New	Rew	New	Rew	New	Rew
100	23.91	24.38	1449.46	1449.18	1.37	1.41	98.78	104.71
75	18.82	19.22	1464.56	1465.43				
50	14.51	14.85	1477.52	1478.92				

The higher stator resistance is due to an increase in coils' MLT. The increase in motor temperature is caused by the higher dissipated losses and higher stator currents. Poor heat removal from the slower running fan also adds to this.

6.6. 15kW motor results

The impact of rewinding on the efficiency of the 15kW motor is shown in Figure 6-7. Large drops in efficiency, ranging between 1.86 to 2.5% have been observed at the three loading points. The drop in efficiency of the 15kW is a result of increase in motor losses as shown in Figure 6-8.

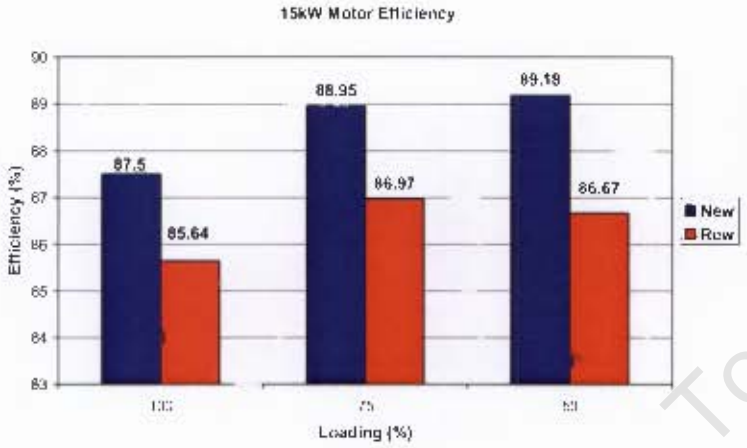

Figure 6-7: 15kW motor efficiency change

The largest change in the losses is the core loss and SLL followed by the friction and windage, stator winding and rotor bar losses.

The large increase in the core loss and SLL, like in the 11kW motor, is an indication of damage to the core during the core processing. Core test results from core tests, done after winding removal, are very high and close to rejection (see section 6.11). The rotor loss has increased significantly even though the rotor is unchanged during the rewind process. This again is due to a change in the motors slip, speed and torque characteristics.

The friction and windage losses on the other hand has dropped. This is the result of correct greasing on the motor bearings and the reduced operating speed of the rewound motor.

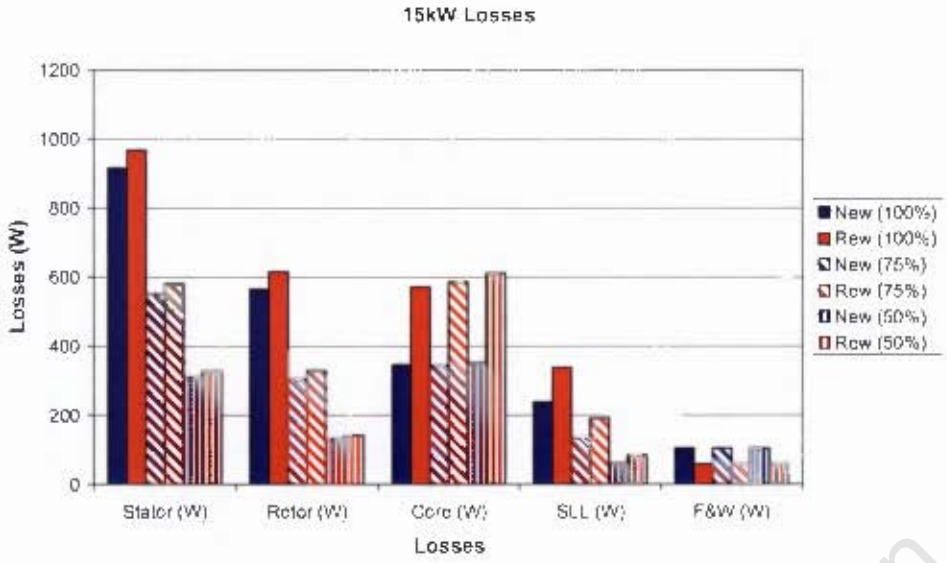

Figure 6-8: Change in losses of the 15kW motor

Other recorded changes such as stator currents, operating speed, stator resistance and temperature rise before and after rewind on the 15kW are shown in Table 6-4 below. The rewound 15kW motor draws larger stator currents and runs at lower speeds and at much higher operating temperatures. The stator resistance of the rewound motor is also higher.

Table 6-4: Other changes due to motor rewind

Loading (%)	Load current (A)		Speed (rpm)		Corr Res (O)		Temp Rise °C	
	New	Rew	New	Rew	New	Rew	New	Rew
100	31.09	31.77	1450.70	1444.25	0.88	1.01	98.37	123.21
75	24.18	24.78	1466.30	1461.39				
50	18.23	18.73	1479.90	1476.48				

The higher stator resistance and operating temperature can be explained in the same way as the 11kW motor.

6.7. 22kW motor results

The impact of rewinding on the efficiency of the 22kW motor is shown in Figure 6-9. Efficiency drops between 0.48 to 0.59% have been observed at the three loading points. The drop in efficiency of the 22kW is a result of change in motor loss. This is shown in Figure 6-10.

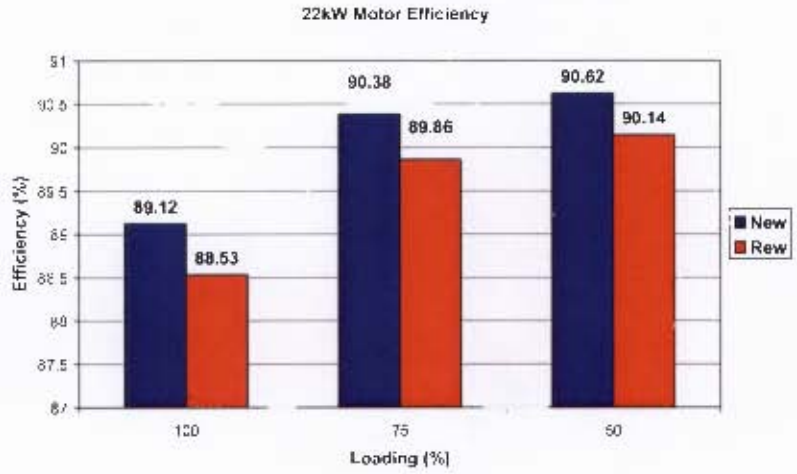

Figure 6-9: 22kW motor efficiency change

The largest change in the losses is the core, stator and rotor winding losses followed by the SLL and friction and windage losses.

The increase in the core loss and SLL again indicate damage to the core during the core processing. Core test results from core tests, done after winding removal, were unavailable from the rewinding company A.

The stator winding losses is due to a higher stator currents and resistance (see Table 6-5).

The rotor bar losses have increased significantly. Due to the large increase, a change in the motors slip, speed and torque characteristics are not the only reason for the increase. Some damage to the rotor cage could have occurred. This is just an assumption as the author could not inspect rotor after the motor assembly.

The friction and windage loss has dropped. This is the result of correct greasing on the motor bearings and the lower operating speed of the motor.

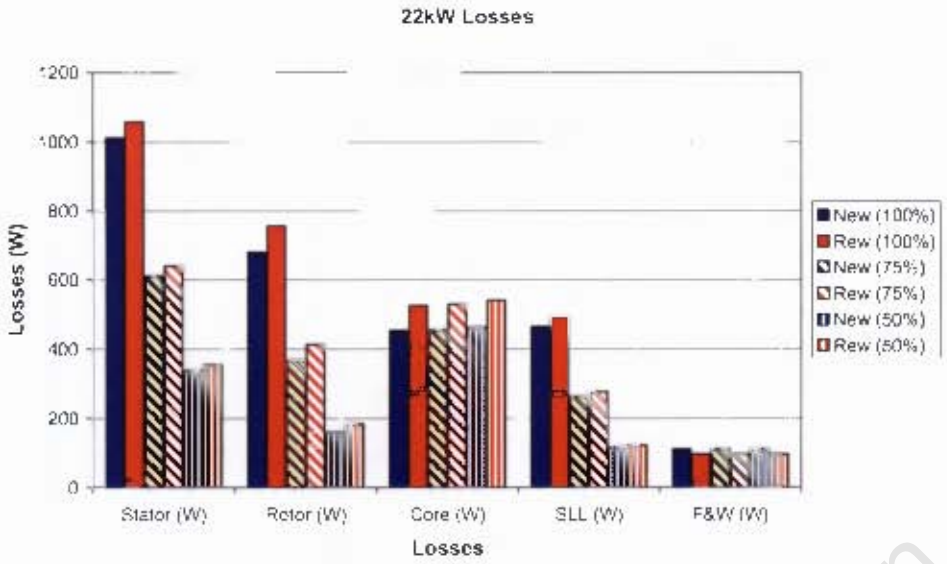

Figure 6-10: Change in losses of the 22kW motor

Other recorded changes such as stator currents, operating speed, stator resistance and temperature rise before and after rewind on the 22kW are shown in Table 6-5. The rewound 22kW motor draws larger stator currents and runs at lower speeds and higher operating temperatures. The stator resistance of the rewound motor is also higher.

Table 6-5: Other changes due to motor rewind

Loading (%)	Load current (A)		Speed (rpm)		Corr Res (Ω)		Temp Rise °C	
	New	Rew	New	Rew	New	Rew	New	Rew
100	44.63	45.72	1457.50	1453.33	0.52	0.53	107.5	111.43
75	34.52	35.61	1469.90	1466.44				
50	25.79	26.55	1480.80	1478.37				

The slow running fan affects heat removal and the higher losses, dissipated in the form of heat, increase operating temperatures.

6.8. 37kW motor results

The impact of rewinding on the efficiency of the 37kW motor is shown in Figure 6-11. Small drops in efficiency, between 0.05 to 0.36%, have occurred at all the three

loading points. With a repeatability accuracy of 0.1%, the most significant change in efficiency is at the 50% loading point. The change in efficiency of the 37kW is a result of change in losses as shown in Figure 6.12.

Figure 6-11: 37kW motor efficiency change

The largest change in the losses is the decrease in F&W losses and increase in core losses. The stator winding and rotor bar losses have increased slightly.

The decrease in F&W losses is the result of correct greasing. Core test results done on the core indicate mechanical damage (see section 6.11). The damage has caused an increase in core losses.

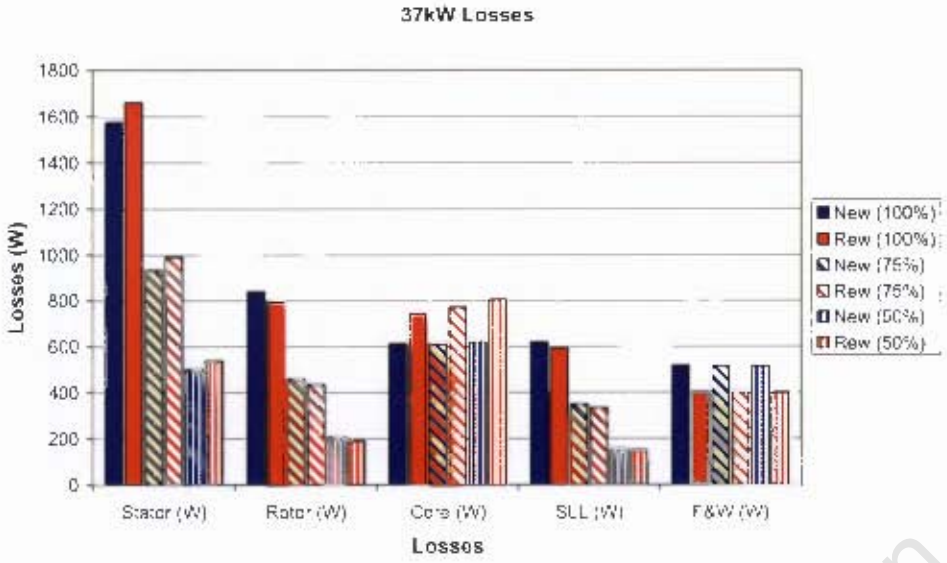

Figure 6-12: Change in losses of the 37kW motor

Other recorded changes such as stator currents, operating speed, stator resistance and temperature rise before and after rewind on the 37kW are shown in Table 6-6. The 37kW rewound motor draws larger stator currents, runs slightly faster and operates at lower temperatures. The stator resistance has increased.

Table 6-6: Other changes due to motor rewind

Loading (%)	Load current (A)		Speed (rpm)		Corr Res (Ω)		Temp Rise °C	
	New	Rew	New	Rew	New	Rew	New	Rew
100	72.41	72.61	1469	1470.7	0.29	0.3	100.23	96.8
75	55.71	56.53	1478	1479.4				
50	40.91	41.70	1485	1486.8				

The higher stator resistance is the result of larger MLT's. This increase in resistance leads to the increase in stator currents.

The shaft speed is faster due a drop in shaft torque. The higher speed increases motor cooling from the fan therefore allowing the motor to run cooler.

6.9. 45kW motor results

The impact of rewinding on the efficiency of the 45kW motor is shown in Figure 6-13. A drop in efficiency between 0.21 to 0.43% has occurred at the three loading points. The change in efficiency of the 45kW is a result of change in losses. These are shown in Figure 6.14.

Figure 6-13: 45kW motor efficiency change

The stator winding, rotor bar and core losses have increased while the SLL and F&W losses have decreased.

The SLL has had the largest change. The increase in the core loss and SLL is an indication of damage on the motor's stator teeth and slots during winding removal. The stator losses have increased due to the increase in stator resistance (see Table 6-7). The rotor bar losses have increased due to the change in the motors slip, speed and torque characteristics. The increase in core losses indicate damage to the core and this is also seen from results core testing which are high (see section 6.11).

The decrease in SLLs is the result of a change in motor temperature and rotor losses. This is discussed in section 6.11.

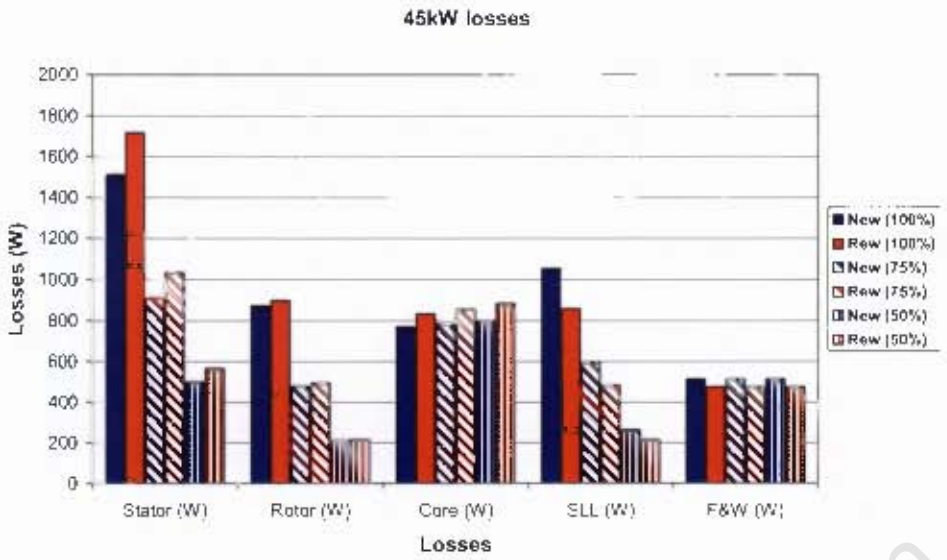

Figure 6-14: Change in losses of the 45kW motor

Other recorded changes such as stator currents, operating speed, stator resistance and temperature rise before and after rewind on the 45kW are shown in Table 6-7. The rewound 45kW motor draws larger stator currents, runs slower and operates at a higher temperature.

Table 6-7: Other changes due to motor rewind

Loading (%)	Load current (A)		Speed (rpm)		Core Res (O)		Temp Rise °C	
	New	Rew	New	Rew	New	Rew	New	Rew
100	85.213	87.231	1481	1472.7	0.21	0.22	102.5	109.8
75	67.147	67.876	1488	1480.9				
50	49.438	50.26	1495	1488.7				

The shaft speed is slower and the operating temperature higher. The slower running fan, on the shaft, causes poorer heat removal. The motor's higher losses dissipated as heat also increases heating.

6.10. 55kW motor results

The impact of rewinding on the efficiency of the 55kW motor is shown in Figure 6-15. The 55kW motor is the only motor to show efficiency improvement. This occurred at the 50% loading points. The change at 75% is within the repeatability accuracy of the test and therefore can be ignored. The change in efficiency is a result of change in losses shown in Figure 6.16.

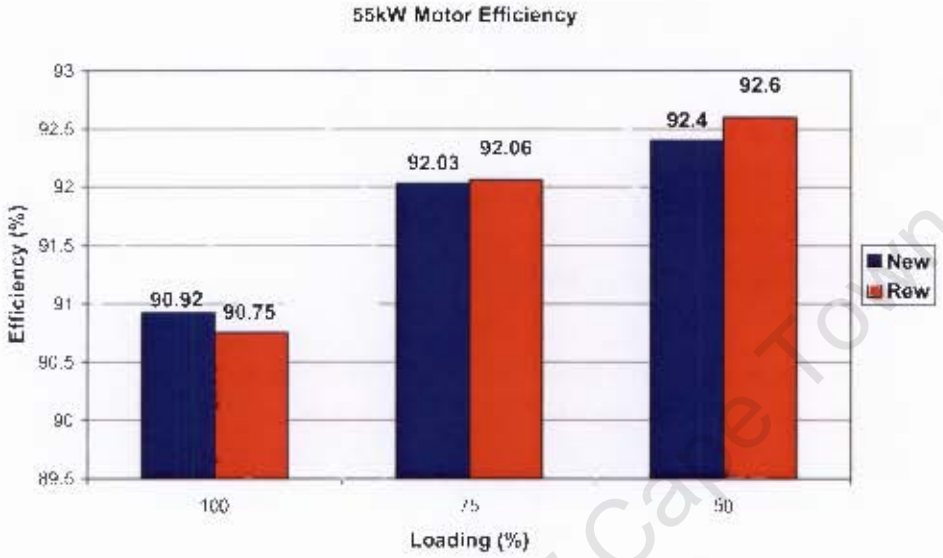

Figure 6-15: 55kW motor efficiency change

Loss reduction has been observed in the core, SLL and F&W losses.

The decrease in SLLs is the result of a change in motor temperature and rotor bar losses. This is discussed in section 6.11. The F&W losses decrease is the result of correct greasing of the bearings and the lower operating speed of the rewound motor.

The small drop in core losses is the result of little to no damage on the core during the core processing. Core tests done on the 55kW core were the only result to have been found as good (see section 6.11).

The stator losses have increased due to higher stator currents and resistance (see Table 6-8). Changes in the speed, slip and torque, like in previous motors, have resulted in the increase in rotor bar losses.

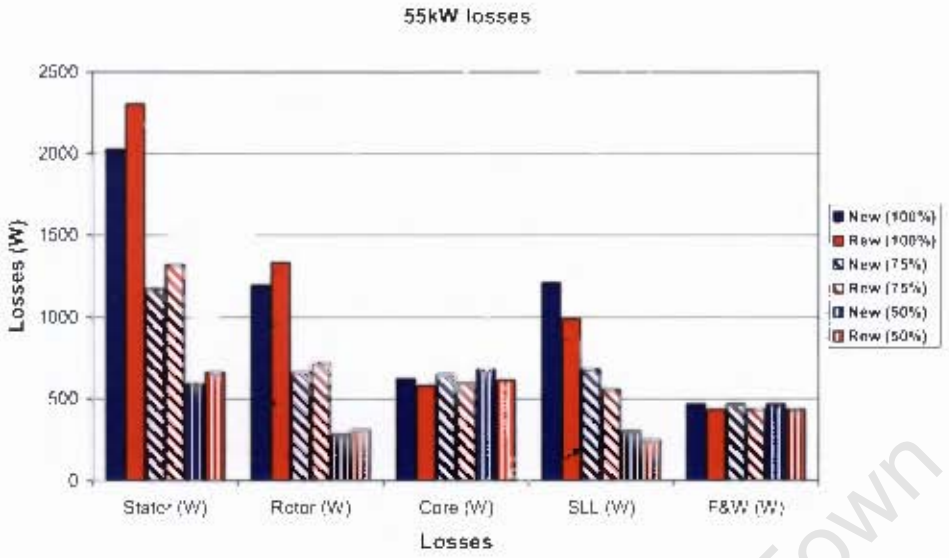

Figure 6-16: Change in losses of the 55kW motor

Other recorded changes such as stator currents, operating speed, stator resistance and temperature rise before and after rewind on the 55kW are shown in Table 6-8. The rewound 55kW motor draws larger stator currents, runs slower and operates at a higher temperature.

Table 6-8: Other changes due to motor rewind

Loading (%)	Load current (A)		Speed (rpm)		Corr Res (O)		Temp Rise °C	
	New	Rew	New	Rew	New	Rew	New	Rew
100	103.04	103.54	1469.8	1468.3	0.2	0.22	106	114.17
75	78.533	78.28	1478.3	1478				
50	56.038	55.473	1486.4	1487.3				

The slower running fan, on the shaft, causes poorer cooling. The motor's higher losses dissipated as heat also result in increasing temperature rise.

6.11. Motor loss and efficiency discussion

Discussions of the changes in motor efficiency and losses are presented in this section.

6.11.1. Motor loss discussion

Stator copper losses

Figure 6-17 shows the stator copper losses trend of all the motors. The stator losses showed the biggest contribution to the overall losses in all eight motors. It also accounts for up 45% of total losses. The losses increased from between 1 to 15 % after rewind. The cause of this is due to the increase in the stator currents and winding resistance as discussed in each motor. The winding resistance is directly affected by the wire gauge used, and the tightness of the wound coils.

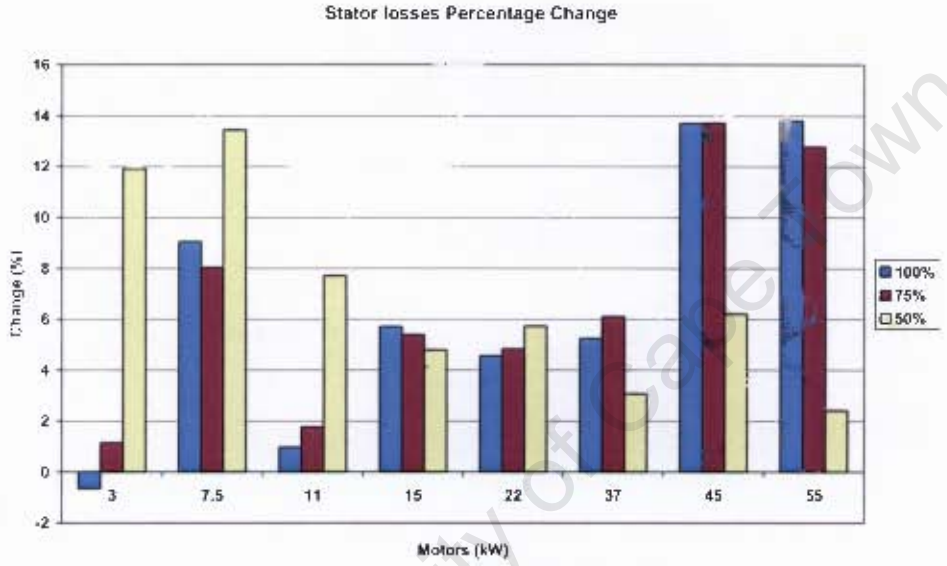

Figure 6-17: Stator Copper losses percentage change

Controlled, tighter hand wound coils and larger winding diameters have been found to lead to drop of 5.3% in the stator loss [37].

Rotor copper losses

Figure 6-18 shows the rotor copper losses trend for all the motors. The rotor losses were found to account for 30% of motor total losses. With the motors just going through the rewinding process, no changes on rotor losses were expected after rewind. However, changes in rotor losses were found in all eight motors with two of the eight showing significant changes of over 10%.

Figure 6-18: Rotor Copper losses percentage change

The increase in rotor losses was consistent with an increase in temperature and torque and a decrease in speed. These changes affect the operating characteristics of the motor. Figure 6.19 is an illustration of this. The new and rewound motor are compared on their power delivery.

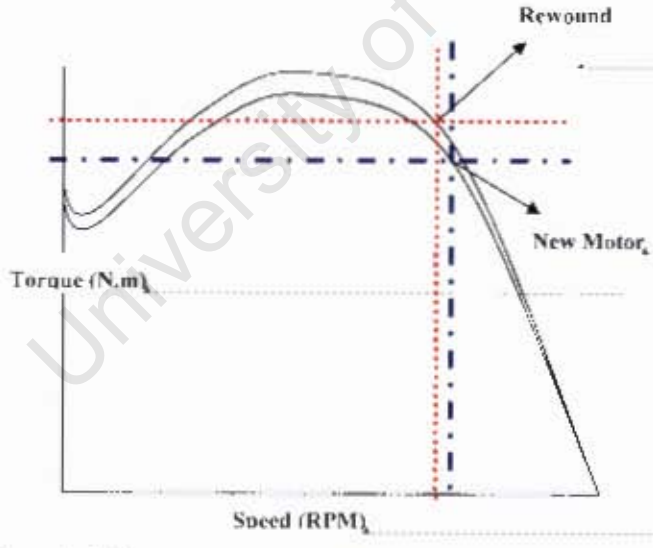

Figure 6-19: Change in motor characteristics due to motor rewinding

The rewound motors were found to run slower and at higher torques (see Appendix H). The decrease in speed, which affects heat removal, causes higher operating slip that lead to higher rotor losses (see equation 4.12 in Chapter 4). The 37kW motor was the only motor to have lower rotor losses and this correlated with the higher speeds and cooler temperatures.

Core losses

Figure 6-20 shows the core losses trend of all the motors. Seven out of the eight motors show an increase in core losses. Core losses were found to account for up 20% of total losses. This is especially evident in the 11kW and 15kW motors where the core losses have almost doubled. Prior to rewinding (after burnout of old windings at Company A) the 11kW motor failed the core test. The 15kW motor was very close to the rejection range as shown in Table 6-9. Additional core loss may have been incurred during the removal process. This is an indication that the damage is possible even in a controlled environment, by a SABS approved company. The 11kW motor was rewound with the failed core. Core loss increase is unavoidable due to the impact of the mechanical winding removal. This causes a deterioration and damage of the steel laminations.

Table 6-9: Core tester results

Motor (kW)	W/kg	Core decision
7.5	6.20	further tests
11	13.57	Reject
15	11.85	Check for mechanical damage
22	N/A	N/A
37	8.15	Check for mechanical damage
45	7.94	further tests
55	3.48	Good

The 55kW motor is the only motor to have a drop in core loss. The burnout process, if done according to a standards such as the SABS, has been found to alleviate residual stresses between laminations and hence reduce core losses. This is according to

reports from reputable rewinding companies. There have been no documented results or/and research to date but this result supports these comments.

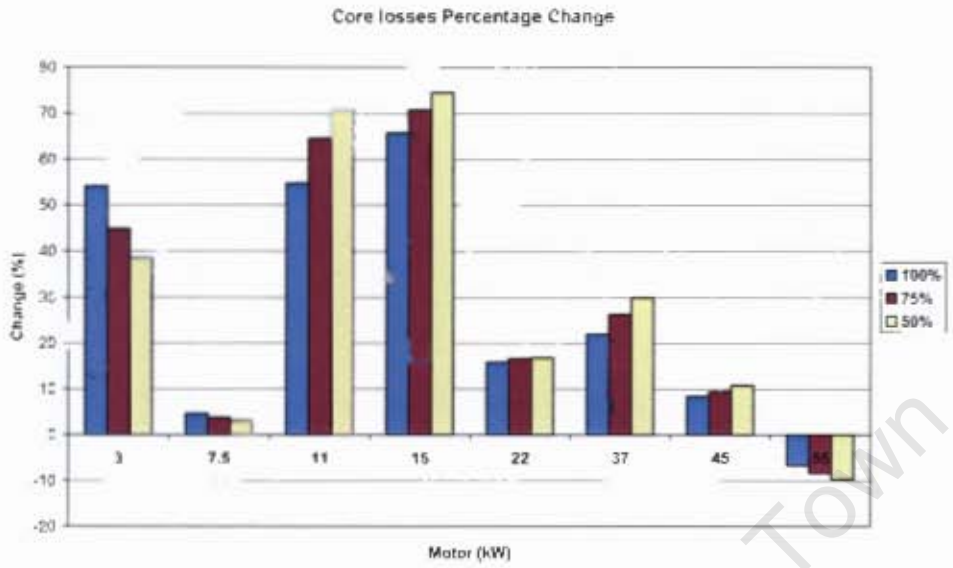

Figure 6-20: Core losses percentage change

Stray load losses (SLL)

Figure 6-21 shows the SLLs trend of all the motors. The change is equal at each loading point due to the linearization of the SLL (see Chapter 4). Five of the tested motors show an increase in SLL and three show a decrease after rewinding.

The increase in SLL is generally the result of slot and tooth damage, which are more vulnerable to the smaller motors. The damage occurs during the rotor and winding removal. The damaged slots and teeth cause an increase in the leakage flux and therefore an increase in the SLL.

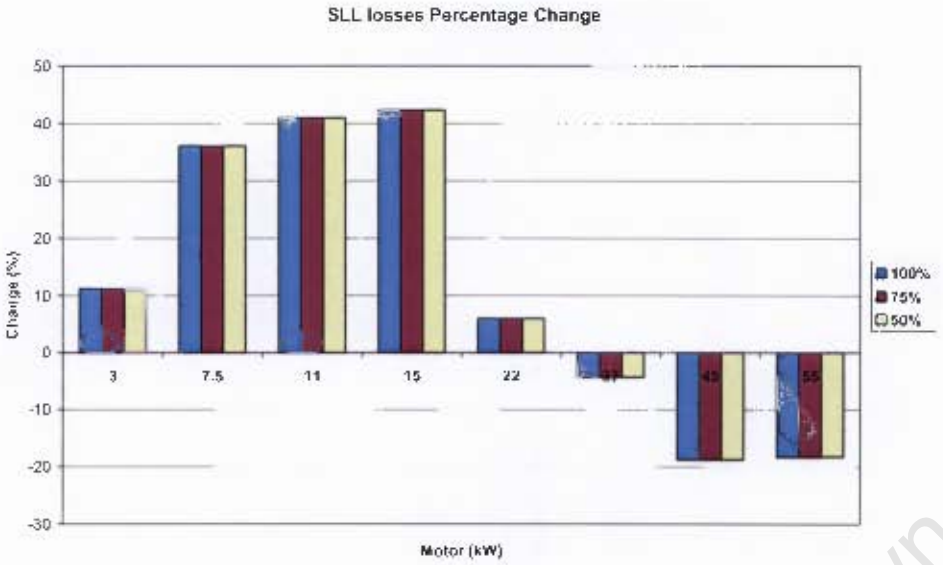

Figure 6-21: Stray Load losses percentage change

The drop in SLL according to documented research has a high correlation between temperature rise and rotor losses. According to Cao [37], the drop in SLL after rewind correlates with a drop in temperature rise and rotor losses. The impact of the lower rotor losses, will result in the leakage currents in harmonic equivalent circuits to be diverted into the magnetizing branch. The result of this would be less drag torque and therefore less stray load loss. This was found to occur on the 37kW where the temperature rise and rotor loss dropped with a drop in the SLL.

Friction & Windage losses

Figure 6-22 shows the SLLs trend of all the motors. The change is constant on all loading point. The friction and windage losses on all the motors reduced except for the 3kW. This decrease in F&W losses, as discussed for each motor, is a result of correct greasing of bearings and refitting of bearings and fans on the all motors. Changes in these losses are generally due to the quality of workmanship. Over greasing, which is expected to reduce friction, has the opposite effect at higher temperatures [37]. Over greasing is evident in the 3kW motor.

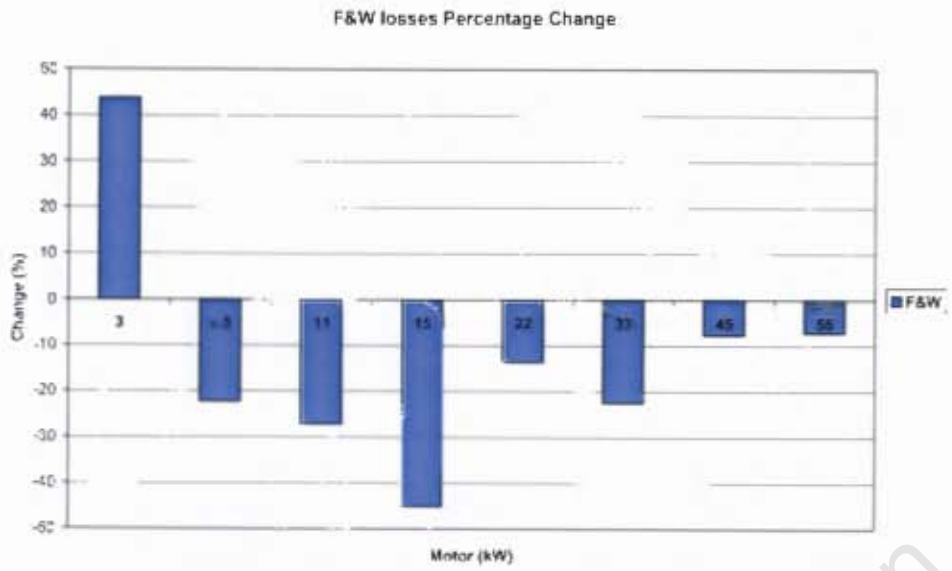

Figure 6-22: F&W loss percentage change

6.11.2. Efficiency discussion

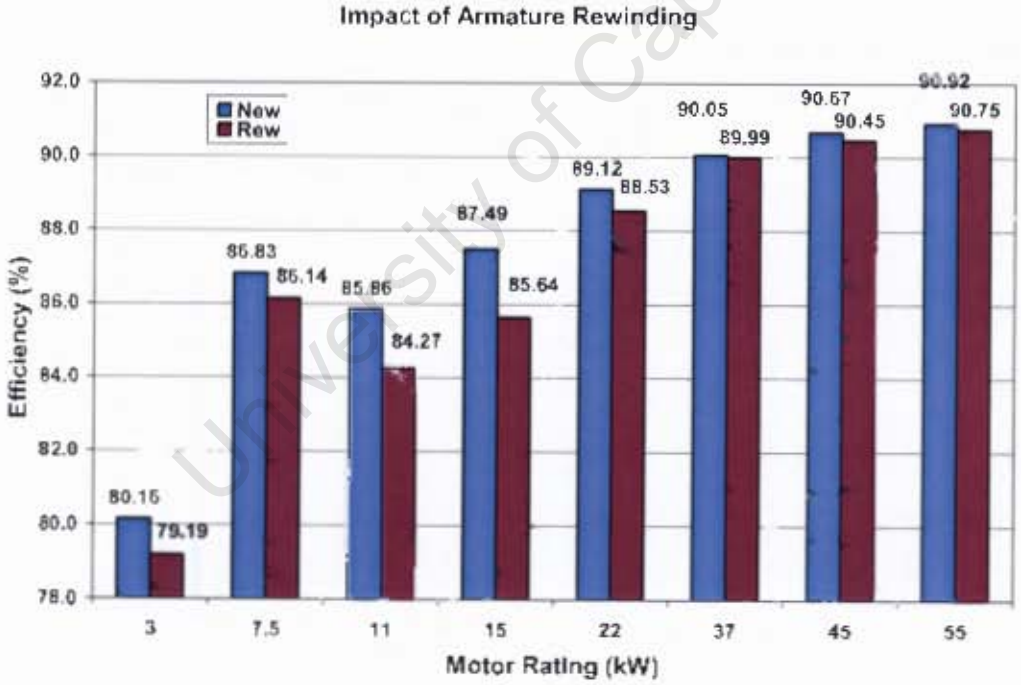

Figure 6-23: Impact of Armature rewinding

Figure 6-23, showing change in efficiency at rated load, and the results presented in sections 4.8.1 to 4.8.3 clearly show that motor rewinding on all eight motor caused a drop in motor efficiency. The smaller motors (3-15kW), which generally have lower efficiencies, show large efficiency drops of up to 3% compared to larger motors (22-55kW). This is a result of the large percentage increase in motor losses after rewinding. With a repeatability accuracy of 0.1% taken in to account, the efficiency drops at rated load for the 37kW and 55kW motors are very small (ranging from 0 to 0.07%). Large efficiency drops are observed at higher loading points of the motors (100 - 150%).

Efficiency improvement was observed on the lower loading point of the 55kW. This is the result of a change in the efficiency profile and the improvement in core losses after rewind.

Figure 6-24 below, shows the efficiency profile of the 55kW motor before and after rewind. The profile has improved at part loads below rated and has dropped at part loads above rated.

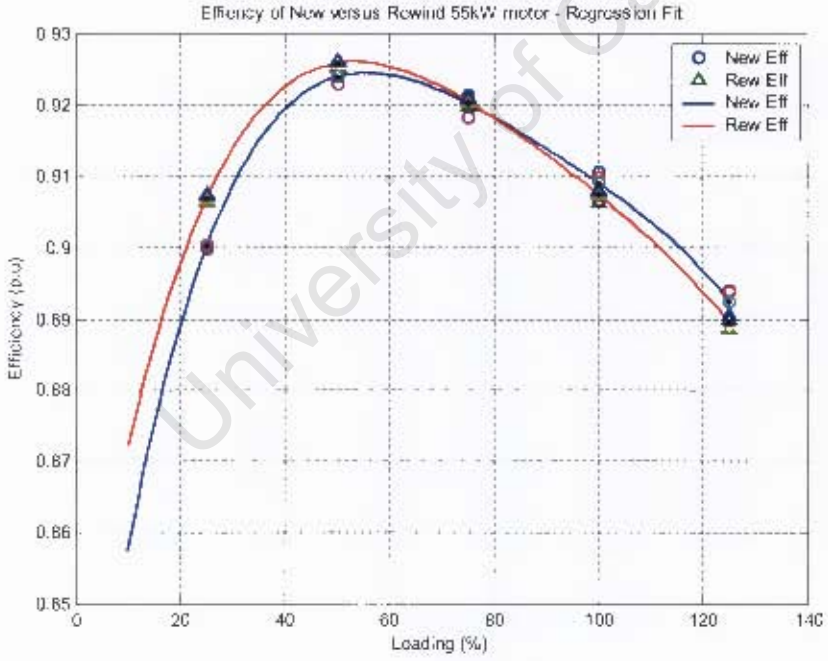

Figure 6-24: Shift in peak

The shift in the peaks is the result of a change in the load-dependant and load-independent losses. Figure 6-25 shows the load-dependant and load-independent losses. The peak as discussed in Chapter 3 occurs at the point where the load-dependant and load-independent losses equal. The Loss vs Load curves in Appendix H of the 55kW motor shows that the biggest contribution to this change in profile is the large drop in core losses at the lower loading points.

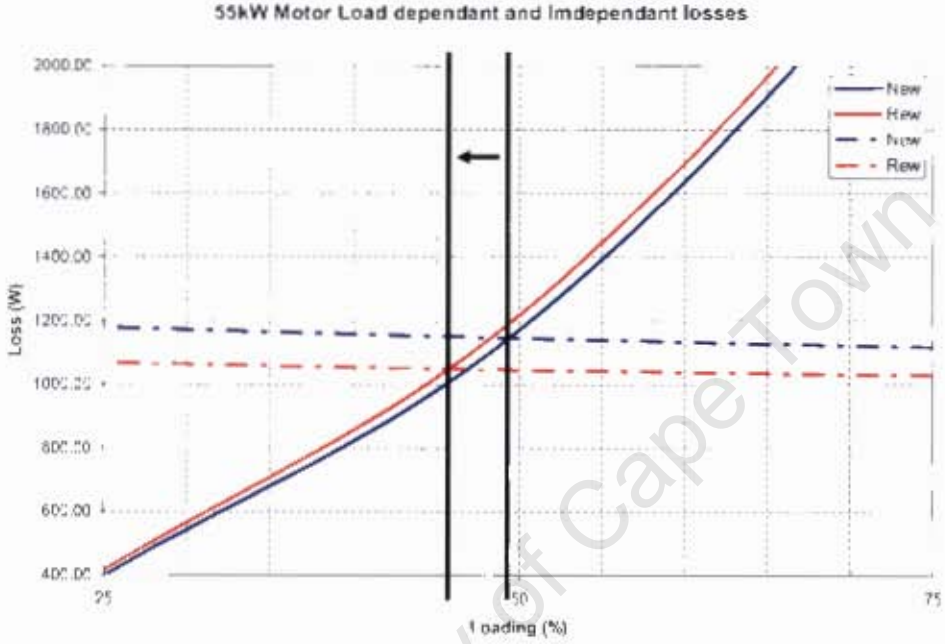

Figure 6-25: Load-dependent and load-independent losses

6.12. Comparison of rewind procedures

The comparison of the impact of rewinding procedures on motor losses and efficiency will be discussed.

Two 3kW motors were sent to the two different rewinding companies, Company A and Company B, discussed in Chapter 5. The two motors went through the entire rewind process as discussed in Chapter 5 at each rewind company.

The motors were tested before and after rewinding according to the IEEE and IEC standards on the 3kW test bed.

6.12.1. Company A loss results

Figure 6-26 shows the change in losses of the 3kW rewound at Company A at rated load. Appendix H has more results on the other loading points.

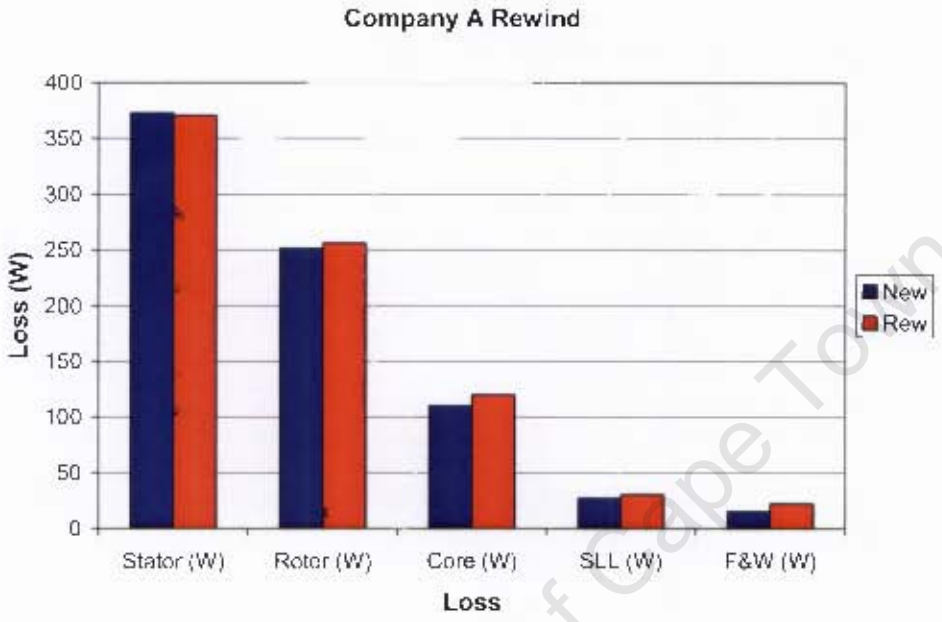

Figure 6-26: Impact of winding at Company A

The increase in F&W losses is the biggest contributor of the efficiency change in the motor rewound by Company A. This is illustrated by the trend in Figure 6-27 below.

The 40% increase in the F&W loss, is the result of over greasing during the motor reassemble. Damage to the core during winding removal has again caused the increase in SLLs and core losses. This has been consistent with the other eight motors, which were also rewound by Company A. The rotor losses have increased slightly while the stator losses have dropped. The lower stator losses are the result of a good mean length per turn (MLT) in the coils and could also be due to windings' raw material. It has been found that although the same wire gauge is used the resistance of a winding are affected by type of raw material [37].

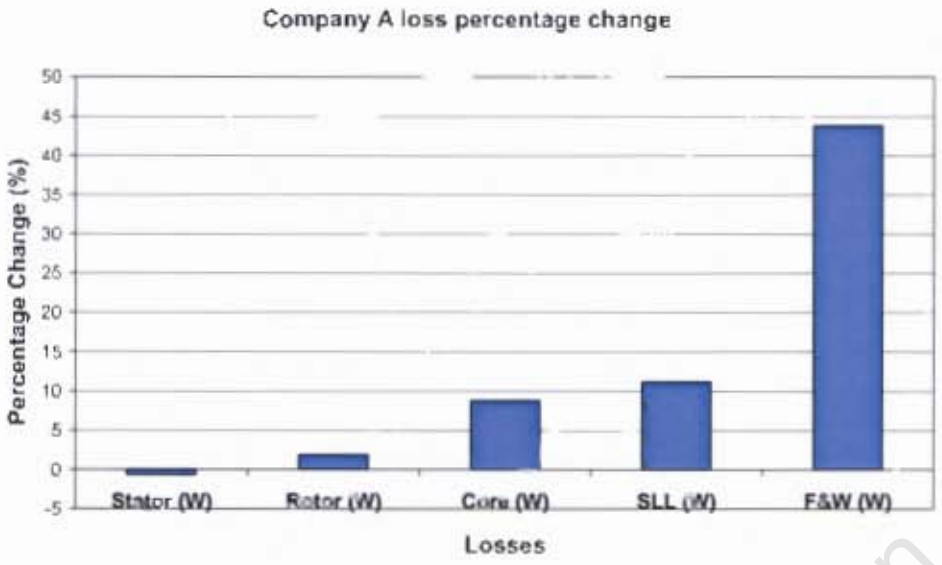

Figure 6-27: Percentage loss change of the 3kW rewound in Company A

6.12.2. Company B loss results

Figure 6-28 shows the change in losses of the 3kW rewound at Company B at rated load. Appendix H has more results on other loads.

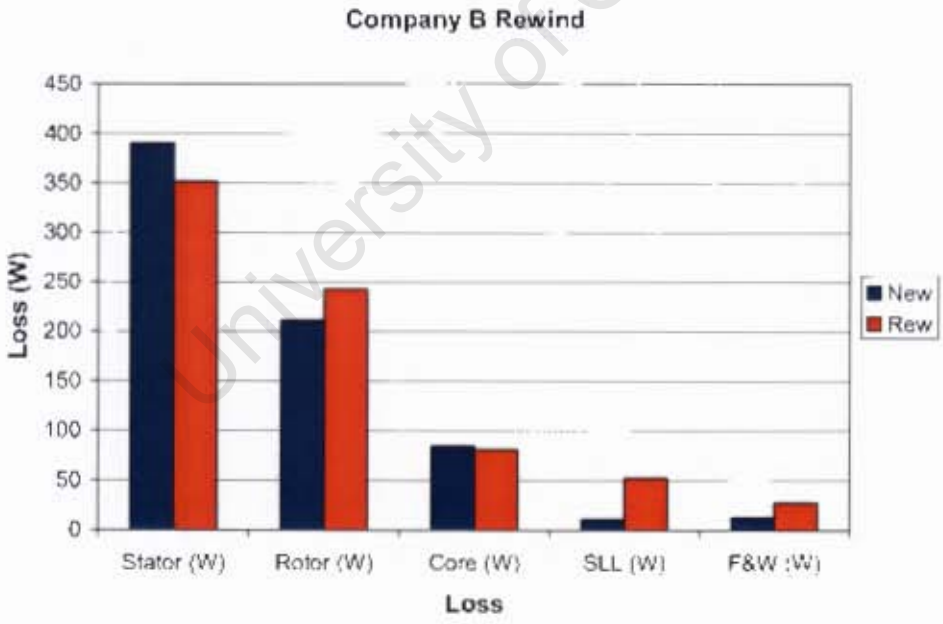

Figure 6-28: Percentage change due to Company B Rewind

The largest increase in the rewound motor, by Company B, is the SLL by more 300%. Figure 6-29 shows the percentage change in loss at rated load.

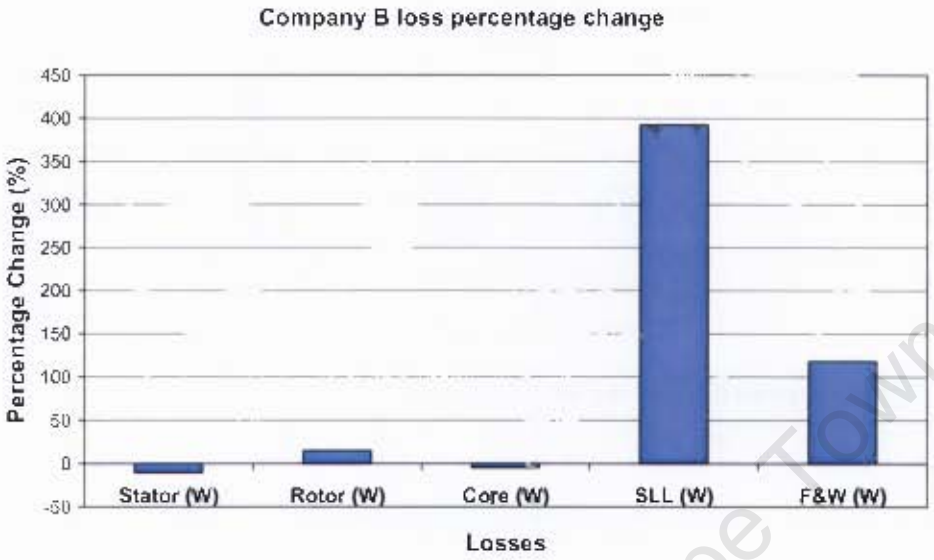

Figure 6-29: Percentage loss change of the 3kW rewound in Company A

The increase in SLL was found to be caused by damage to the stator teeth (see Figure 6-30) during winding removal. The burnout system used by Company B does not allow for easy removal. This is because the vanish on the windings are not burnt off adequately. The exposed teeth lead to increased leakage flux and in turn increase SLL. Unexpectedly, the core losses have decreased slightly. This core, like that of the 55kW, has had its lamination stresses released during burnout. The stator winding losses have also decreased. This is due to a lower resistance that can be explained by the type wire used and tighter wound coils.

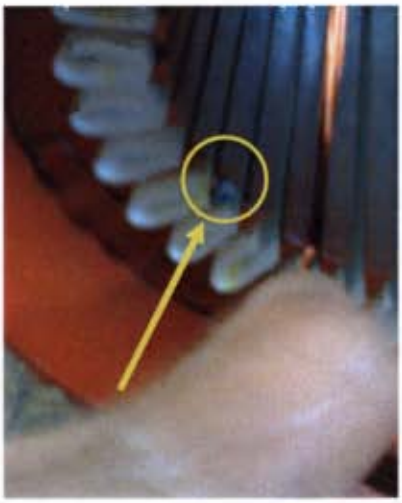

Figure 6-30: Damage to the slot teeth due to winding extraction

6.12.3. Efficiency comparison of rewound motors

Table 6-10 shows the comparison of efficiency change at the rated load for the motors rewound at Company A and Company B. A drop in the motor efficiency has occurred on both the rewound motors. The Company A motor has a smaller efficiency drop than that of Company B motor. This is a direct consequence of the procedures used.

Table 6-10: Efficiency comparison of Company A and Company B

Rewinder	New	Rew	Change (%)
	Eff (%)		
Company A	80.16	79.19	-0.9
Company B	81.14	80.05	-1.09

6.13. Concluding remarks

The impact of rewinding several motors was shown to have a negative impact on induction motor efficiency in general. Furthermore, the procedures of different repairers affect motor efficiency differently. It was found that the procedures, which do not conform to national standards have a greater impact on motor efficiency.

Chapter 7: MOTOR REPAIR VERSUS REPLACEMENT ECONOMICS

7.1. Overview

This chapter investigates the economics of whether to repair or replace a failed motor. In industry, there are four economic are presented to illustrate the advantages and disadvantage of each model.

7.2. Options available when motors fail

When motors fail, industries and manufacturers have the choice to either repair or replace the failed motor. Figure 7-1, taken from [32], shows a flowchart of available options that can be followed to restore production after a motor failed.

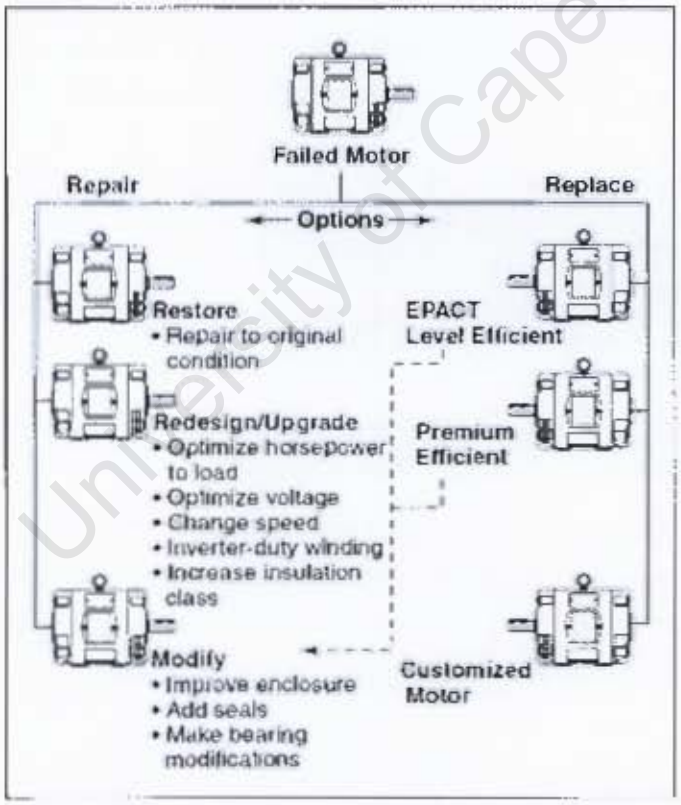

Figure 7-1: Replace-Repair decision model [EASA]

The damaged motor can be repaired to its original condition, upgraded to operate efficiently at the operating loading or modified to prevent similar damage to it. Replacing the motor can be done with either a similar rated motor or a more efficiency motor.

7.2.1. Repair versus Replace Decision

With the ongoing power crisis and the increase in electricity prices in South Africa, electricity costs have become a large contributor to the cost of any business. Electric motors are linked to the majority, if not all, manufacturing processes and therefore any costs related to the purchasing, maintenance and consumed energy represent a significant cost. The expenditure related to the repair or replacement of failed motors is therefore very important [71]. There are four economic models that were found to assist with making the decision to repair or replace failed motors [72-76]. These are:

- Initial purchase costs
- Annual cost of operation,
- Pay back period or
- Life cycle cost.

7.2.1.1. Initial Purchase Costs

The cost of repairing versus replacing failed motors is still the major determining point around the world and especially in developing countries [77]. Figure 7-2 shows the recent prices between repairing and replacing motors. The difference between the prices increases as the motor rating increases.

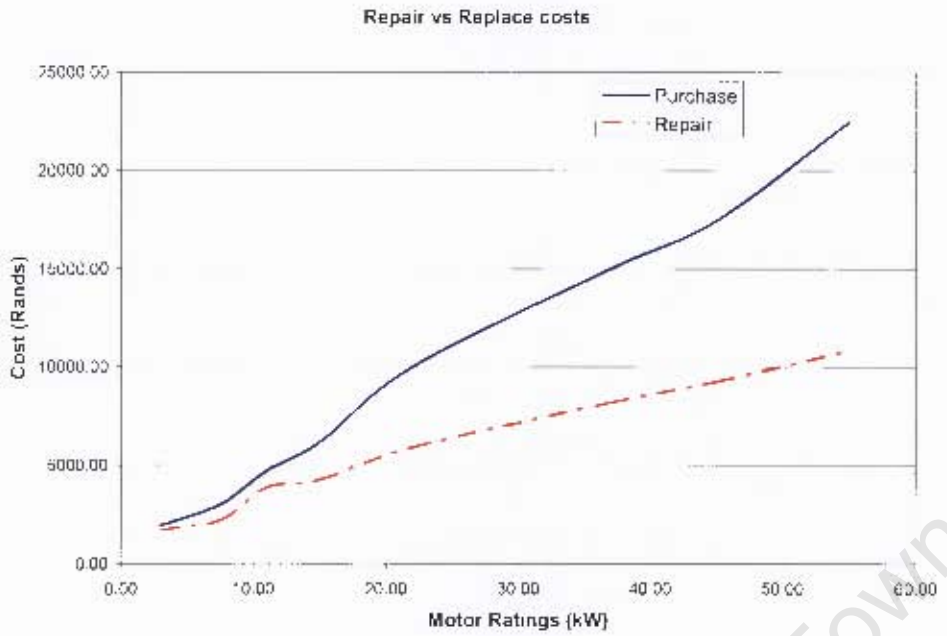

Figure 7-2: Initial costing of rewind and replace

The most commonly used practise in industry is to repair the motor if repair cost is less that 60% of the cost of a new motor [71]. In other words, if the cost to purchase a new motor is R5000.00, the user would be willing to pay up to R3000.00 to have the failed motor repaired.

Initial purchase costing alone as a decision-making tool is not ideal. The gap between the repair and rewind prices is getting smaller due to utility initiatives like discounts. This encourages the replacement of motor due to the impact of rewinding on motors.

7.2.1.2. Annual Cost of Operation (ACO)

The annual operating cost considers the cost associated with operating a motor annually. In general, motor-related costs represents one of the top three operating costs for the average industrial user as compared to payroll, building and inventory expenses [71]. The ACO is based on the motor's operating load point, the energy usage and demand charges, the operating hours, the motor size and the efficiency of the evaluated motor. The relationship between these parameters is shown in equation 7.1 [72-75],

$$Cost = Load \times D \times C \times kW_{motor} \times \frac{100}{\eta} \quad (7.1)$$

Where Cost = the annual cost in Rands

D = operating hours in a year

C = cost of energy (kWh)

kW = motor power ratings

η = motor efficiency (at operating load point)

The energy cost savings differential relating to a rewind versus replacement decision can be calculated as followed.

$$Savings = Load \times D \times C \times kW_{motor} \times \left(\frac{100}{\eta_{rewind}} - \frac{100}{\eta_{replace}} \right) \quad (7.2)$$

Where Savings = the annual cost savings in Rands

η_{rewind} and *$\eta_{replace}$* *= full load motor efficiency of old and new motor*

Motor efficiencies vary as the load change or even due to the rewind process. This was seen and discussed in Chapters 4 and 6. The annual cost of operation economic model (Equations 7.1 and 7.2) evaluates costing over a motor's full load efficiency which is assumed to be constant at that point. This is an inherent weakness in the annual cost of operations.

7.2.1.3. Simple payback period (SPP)

The simple pay back method gives the number of years required to recover the differential between the cost of replacing versus repairing motors (see section 7.2.1.1). The SPP has been known to be simplest economic model in making economic decisions [72], Equation 5.3 [72-74]], is used in simple payback analysis. The denominator of the equation is the annual cost savings of two motor options.

$$SPP - \frac{X_{replace} - X_{rewind}}{Load \times D \times C \times kW_{motor} \times \left(\frac{100}{\eta_{rewind}} - \frac{100}{\eta_{replace}} \right)} \quad (7.3)$$

Where $X_{replace} - X_{rewind}$ = *the cost of new motor minus cost of repair in Rands*

A decision would be made depending on the SPP being less or more than the companies' acceptable SPP. In many cases, a two-year SPP is the maximum before performing a motor replacement [75].

The use of the load eff (?)

7.2.1.4. Life Cycle Cost (LCC)

The life cycle cost of any piece of equipment (motors in this case) is the total 'lifetime' operational cost. LCC analysis, using Equation 7.4 [76], is made up of the purchase costs, installation and commission costs, operation costs, repair and maintenance costs, energy costs, operation and downtime costs, environmental and disposal costs.

$$LCC = C_{IC} + C_{IN} + C_E + C_O + C_M + C_S + C_{ENV} + C_D \quad (7.4)$$

Where C_{IC} = *Initial costs (purchase price of entire motor system)*

C_{IN} = *Installation and commissioning costs (can include training)*

C_E = *Energy costs (entire motor system)*

C_O = *Operating costs (labor cost)*

C_M = *Maintenance and Repair costs*

C_S = *Down Time costs*

C_{ENV} = *Environmental costs (contamination cost)*

C_D = *Decommissioning and Disposal costs*

The LCC model is more complex than the SPP and AOC and is regarded as a good comparison tool between possible repair versus replacement alternatives [76].

Present Worth Life Cycle Analysis

For greater precision, the present worth life cycle costing (PWLCC) may be used. The PWLCC method considers both, the time value of money and energy cost inflation [73]. The PWLCC evaluation is done using equations 7.5 and 7.6.

Equation 7.5 is first used to calculate the effective interest rate. The effective interest is then used in Equation 7.6 to calculate the present worth (PW). The PW value is then multiplied by the LCC to obtain the PWLCC.

$$i = \frac{100 + R2}{100 + R1} - 1 \qquad (7.5)$$

Where, i = Effective interest rate

R1 = inflation rate

R2 = annual rate of return

$$PW = \frac{(1+i)^n - 1}{i(1+i)^n} \qquad (7.6)$$

Where, PW = Present Worth

i = Effective interest rate

n = number of years

Impact of change in variables on LCC model

The LCC economic model has many variables dependent on the business/facility i.e. cost of electricity, operation costs, and operating hours. It also contains parameters of the motor, i.e. initial motor purchase or repair costs, motor efficiency, loading point, motor life. These variables affect the LCC and in turn the repair versus replacement decision. To assess the impact of these variables on the LCC, a simple sensitivity analysis is presented.

Equation 7.7 is a simplified LCC equation used in the simple sensitivity analysis.

$$LCC - D\left(Load \times C \times kW_{motor} \times \frac{100}{Eff} \right) + IC + k \qquad (7.7)$$

The equation relates the important variables such as the initial cost (IC), operating hours (D), loading point (Load), electricity price (C), and motor efficiency (*Eff*). The constant k is a lumped parameter, representing the maintenance, operating, installation, downtime and environmental costs. Figure 7-3 below shows the effects of varying these important variables.

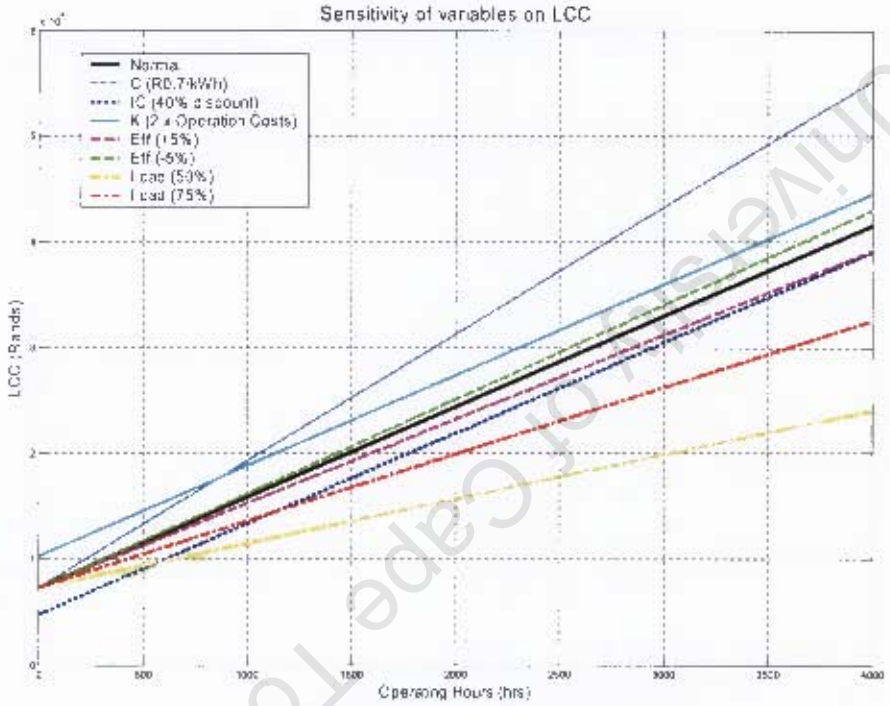

Figure 7-3: Effects of varying variables.

The most significant effect on the LCC can easily be seen as the cost of electricity. The cost of electricity is an uncontrollable factor in industry. Eskom over the last two years have increase electricity prices by as much as 50%. This has resulted in huge profit losses. The motor loading point, the initial purchase cost and the cost of operation. Interestingly, the loss in efficiency (of up to 5%) has a smaller effect on the LCC than was expected but is still significant.

7.3. Motor Systems

Motors operate in electrical systems that are integrated with several devices and subsystem. These systems convert electricity into mechanical power for applications such as motion of fluids (in pumps, fans, compressors), materials processing (mills, mixers), etc [79]. Figure 7-4 shows a typical industrial motor system which consists of a variable speed drive, motor and a pump. The overall system efficiency is made up the efficiency of each component.

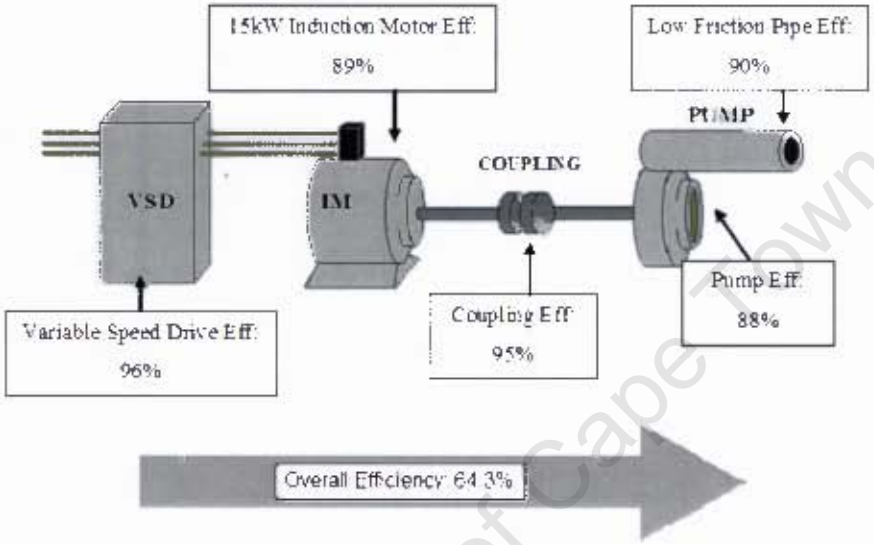

Figure 7-4: Typical motor system

When motors fail in motor-driven systems, a feasible solution is needed to restore production in the shortest time possible. This will ensure the lowest cost incurred due to the downtime. Motor repair is an intuitive solution to failures. However, this may not always be feasible. Several case studies are considered in the next section to illustrate this.

7.4. Case Examples

The motor system shown in Figure 7-4, in the previous section, will be considered in simple scenarios that will investigate the economic models discussed in the previous sections.

The following assumptions will be used in the analysis:

Duty: 4000 hrs

Energy Cost: 50c/kWh

7.4.1. Scenario 1 – Initial purchase costs

As discussed in Section 7.2.1.1, the most commonly used practice in industry is to repair a failed motor if its repair cost is less that 60% of the cost of a new motor. Table 7-1 shows recent purchase and repair prices for motors used in the project. The percentage of the repair costs to the purchase costs is shown. The repair versus replace decision based on this common practice is evident in the table.

It can be seen that the failed 15kW motor in Figure 7.4 would be replaced rather than repaired.

Table 7-1: Repair/Replace Decision table

Motor Ratings (kW)	New Motor	Repair Cost	% of New	Decision
7.5	R 2,992.00	R 2,190.00	73.20	Replace
11	R 4,717.00	R 3,850.00	81.62	Replace
15	R 6,167.00	R 4,250.00	68.92	Replace
22	R 9,992.00	R 5,890.00	58.95	Replace
37	R 15,009.00	R 8,180.00	54.50	Repair
45	R 17,465.00	R 9,259.00	53.01	Repair
55	R 22,480.00	R 10,850.00	48.27	Repair

7.4.2. Scenario 2 – ACO

The ACO for the 15kW motor operating at 100%, 75% and 50% loading are shown in Table 7-2. The increase in losses after rewinding has resulted in lower efficiencies (see section 6.7 in Chapter 6) and therefore higher ACO (3% increase).

Table 7-2: ACO of 15kW motor

Loading (%)	Efficiency (New %)	Efficiency Change after Rewind (%)	ACO (New)	ACO (after Rewind)
100%	87.55	-1.86	R 34,266.13	R 35,009.92
75%	89.00	-1.98	R 25,280.90	R 25,854.94
50%	89.21	-2.51	R 16,814.26	R 17,301.44

It can be seen that replacing the damaged motor with a brand new motor will result in lower annual operating costs compared to the repaired motor.

7.4.3. Scenario 3 – SPP

The payback period to recover the difference between buying a new motor versus replacing it is discussed here. The SPP for the 15kW motor operating at 100%, 75% and 50% loading is shown in Table 7-3. The payback period ranges from 2.6 to 4 years depending on the load of the motor.

If a typical minimum payback period of 2 years is required, the preferred option would clearly be to rewind the 15kW motor.

Table 7-3: SPP for the 15kW at 50 - 100% loading

Loading (%)	Eff (new)	Eff (rewind)	Payback Period (yrs)
100	87.55	85.69	2.6
75	89.00	87.02	3.3
50	89.21	86.70	3.9

7.4.4. Scenario 4 – LCC

The LCC analyses of a 15kW rewound/new motor is shown in Table 7-4. The motor has been analyzed over a 20-year life span of the motor. The motor is assumed to fail after ten years. Electric motors are repaired 2-3 times over their lifetime [80].This is the result of an increase in motor temperature rise due to the higher losses results in a loss of motor life.

Motor temperature rise has a negative influence on a motor's life. Motor insulation life halves for every 10 degrees temperature rise according to [60]. The increase in operating temperature of the rewound 15kW motor of more than 10 degrees (see Chapter 6) will result in a 50% reduction in its insulation life. The motor will therefore potentially fail within ten years. This result therefore supports the assumption made in this scenario

Other assumptions made to this LCC analysis are:

- An annual drop in efficiency of 1%, due to wear and tear, every five years,
- An increase in energy costs of 20% every year,
- Constant interest rate, Inflation rate and return in investment over twenty years
- The cost of repair after 10 years is a future rewind cost

Error! Not a valid link.

The LCC analysis of the scenario shows that the option to rewind a failed motor will cost about 3% more than replacing the motor in the 20 year lifetime. With industries such as the Sasol having more that 1200 motors installed of which 8% are rewound annually, the cost of rewinding could lead to significant profit or losses.

7.5. Concluding remarks

When comparing the results based on the scenarios from the different models, LCC, SPP and Energy costs, the decision to replace the damaged motor rather than rewinding is the most economical option. The results also, although simple, can accumulate to losses in the millions of Rands when larger motor systems are evaluated.

Chapter 8: CONCLUSIONS AND RECOMMENDATIONS

8.1. Conclusions

This thesis investigates the impact of armature rewinding on induction motor efficiency in South Africa. The research was conducted in the Electrical Machines Laboratory at the University of Cape Town (UCT), where three induction motor test-beds were constructed. An in depth study was first conducted to compare international motor testing standards.

Efficiency tests were conducted on the following range of squirrel-cage induction motors: 3kW, 7.5kW, 11kW, 15kW, 22kW, 37kW, 45kW and 55kW. The tests were performed according to the IEC 34-2, JEC 2137 and IEEE 112 standards, and the results were compared. The results showed that the JEC 2137 standard estimates higher efficiencies due to the omission of the stray-load loss (SLL) in the determination of motor efficiency. Futhermore, it was shown that the IEC 34-2 (2007) and IEEE 112 standards produced similar results. The IEC efficiency results were approximately 0.5% higher than those of the IEEE 112 standard.

A second study was conducted to determine the impact of armature rewinding on induction motor efficiency. New squirrel-cage induction motors ranging from 3kW to 55kW were purchased for testing. The IEC (2007) and IEEE 112 standards, loss segregation method, were used to test the motors. Several tests were performed on each motor to assess the accuracy and repeatability of test results. Statistical analyses were performed on the test results for each motor to obtain a representative average efficiency performance curve for each motor. The motors were then sent for complete armature rewinding and retested according to the afore-mentioned procedure.

The impact of rewinding was shown to be significant with efficiency drops ranging from 0.1 to 1.86% at rated loading. The changes in the core and stator losses were

found to have the biggest influence on the efficiency changes. The increase in core losses were due to damage on the core during the winding removal process. The stator winding losses, on the other hand, were the result of the increase in winding resistance and torque. Increase in the inserted coil's mean length per turn and the difference in the raw material used in the wire are the cause of the increase stator resistance. A change in the efficiency profile was also evident as a result of the changes in the constant and load dependant losses.

In addition to the above tests, two new 3kW motors were rewound by a large and small rewind companies. The results showed a decrease in efficiency of 0.9% (large rewind shop) and 1.09% (small rewind shop) at full load. This indicates that the techniques and procedures used at different companies affect the losses and therefore efficiency.

When motors fail, industries and manufacturers have the choice to either repair or replace the failed motor. Four economic models, Initial Purchase Costs, Annual Cost of operation (ACO), Simple payback period (SPP) and Life cycle costing were discussed and used on scenario of a failed 15kW in a motor system. It was concluded from the four economic models that the replacement of the failed motor was more cost effective than having it rewound. This was due to the negative impact on efficiency due to rewinding. The LCC economic model was found to be the best model to use as it incorporated all the associated costs with running a motor over its 20yr life span.

8.2. Recommendations for Future Work

The following recommendations are made for future work:

- Inline torque measurements should be adopted on all test beds as to improve accuracy.
- A separate test motor should be used on the beds before any test to assess repeatability of the test beds. This will ensure that the test beds do not change between tests.

- The spread in efficiency results of the same motors should be tested on a round-robin basis in laboratories around South Africa.
- The impact of core burnout on the stresses between core-stacked laminations and the consequence of this on core losses should be investigated.
- The impact of core damage and core restacking should be investigated with induced motor failures prior to repair.
- Assess the impact of multiple rewinds on the efficiency of induction motors
- Assess the impacts on motor efficiency of rewinds conducted by repairers in other regions around South Africa.
- The impact of operational factors that are detrimental to motor efficiency should be investigated. These factors could include: aging of winding insulation, corrosion, duty-cycle of the motor, exposure to power quality problems, damage due to failures, effects of repairs, thermal stress due to overloading, mechanical stresses due to misalignment, eccentricities, etc.

REFERENCES

[1]. 'Eskom Holdings Limited Annual report 2008', [Online] Available: http://www.eskom.co.za/annreport08/ar_2008/downloads/eskom_ar2008.pdf, Accessed: 28/04/09

[2]. T. L. Mthombeni, 'Energy Efficient Motor Systems for Eskom Demand Side Management', Industrial and Commercial Use of Energy Proceedings, 29-30 May 2007

[3]. Department Of Minerals And Energy Of The Republic Of South Africa White Paper On Renewable Energy 2003, [Online] Available: www.dme.gov.za/pdfs/energy/renewable/white_paper_renewable_energy.pdf, Accessed: 27/01/09

[4]. C. Swarz, A. B. Sebitosi, L. Mthombeni, 'Energy efficiency measurement methods for motors in industry in South Africa', University of Cape Town, 2006

[5]. University of Cape Town Energy Research Center

[6]. A. H. Bonnett, 'Root Cause AC Motor Failure Analysis with a Focus on Shaft Failures', IEEE Transactions On Industry Applications, Vol. 36, No. 5, September/October 2000

[7]. A. H. Bonnett, and T. Albers, 'Squirrel-Cage Rotor Options for AC Induction Motors', IEEE Transactions On Industry Applications, Vol. 37, No. 4, July/August 2001

[8]. S. O'Donnell, 'Repair company builds capacity to meet demand', Cramer Media's Engineering News Online, 25th May 2007 , [Online] Available: http://www.engineeringnews.co.za/article/repair-company-builds-capacity-to-meet-demand-2007-05-25 , Accessed: 27/06/08

[9]. A. K Wallace and T. E Rollman, 'High Efficiency Testing Laboratory for motors, drives and generators', *Power Electronics and Variable Speed Drives*, (Conf. Publ. No. 429) 1996.

[10]. 'Standard Test Procedure for Polyphase Induction Motors and Generators', IEEE Std 112, 2004.

[11]. 'Methods for Determining Losses and Efficiency of Rotating Electrical Machinery from Tests', IEC 60034-2, 2007.

[12]. H. M. Mzungu, A. B. Sebitosi, M. A. Khan, *'Comparison of Standards for Determining Losses and Efficiency of Three-Phase Induction Motors'* , *Vector Journal*, July 2007

[13]. S. Kusumba, 'Dynamometer Proportional Load Control' , Master of Science in Electrical Engineering, Cleveland State University, December, 2004

[14]. J. Song and Q. Chen, 'A study of Dynamic Electric Dynamometer Based on Seaprate-excited DC Generator, *Journal of Asian Electric Vehicles,* Volume 3 Number 1, June 2005

[15]. P. C. Sen, 'Principals of Electric Machines and Power Electronics' *,John Wiley & Sons, 2nd Edition*, Published 1996

[16]. R. Schicker, G. Wegener, 'Measuring Torque Coorectly', Hottinger Baldwin Messtenchnik GmbH, 2002

[17]. *R. L.* Nailen, 'Designing an a-c motor test center (Part 1)' *,Electrical Apparatus,* Sep 1999

[18]. Gates synchronous belts; [Online] Available: http://www.gates.com/europe/file_display_common.cfm?thispath=Europe%2Fdocuments%5Fmodule&file=20069%5FE2%5FINDUSTRIAL%5FBELT%5FBROCHURE%2Epdf, Accessed: 22/06/08

[19]. 'PT_PowerGrip_05', [Online] Available: http://www.gates.com/europe/file_display_common.cfm?thispath=Europe%2Fdocuments%5Fmodule&file=20054%5FE2%5FINDUSTRIAL%5FBELT%5FCATALOGUE%2Epdf, Accessed: 21/06/08

[20]. Fenner lock type couplings manuals

[21]. HRF ball bearing manuals

[22]. A. Boglietti, A. Cavagnino, M. Lazzari, and M. Pastorelli, 'International Standards for the Induction Motor Efficiency Evaluation: A Critical Analysis of the Stray-Load Loss Determination Aldo IEEE Standard Test Procedure for Polyphase Induction Motors and Generators, IEEE STD 112-B, 1996', IEEE transactions on industry applications, vol. 40, no. 5, September/October 2004

[23]. *R. L.* Nailen, 'Designing an a-c motor test center (Part 2)' *,Electrical Apparatus,* Oct 1999

[24]. Load cell manuals

[25]. HMB T1 torque transducer manuals

[26]. HMB carrier frequency module manual

[27]. Yokogawa Analyzer manual

[28]. DT -2336 Tachometer manual

[29]. Yokogawa galvanometer manual

[30]. Pico Technology, 'Thermocouple Application note' [Online] Available: http://www.picotech.com/applications/thermocouple.html, Accessed: 29/04/09

[31]. H. M. Mzungu, 'Cost of Voltage Dips and Interruptions in Industry', *University of Cape Town Undergraduate thesis*, 2006

[32]. EASA. 'A guide to motor repair and replacement'. [Online] Available: http://www.easa.com/indus/ac_gd199.pdf

[33]. B. Renier, K. Hameyer, and R. Belmans, 'Comparison of standards for determining efficiency of three phase induction motors', *IEEE Transactions on Energy Conversion*, Vol. 14, No. 3, September 1999

[34]. A. T. de Almeida, F. J. T. E. Ferreira, J. F. Busch, and P. Angers, 'Comparative Analysis of IEEE 112-B and IEC 34-2 Efficiency Testing Standards Using Stray Load Losses in Low-Voltage Three-Phase, Cage Induction Motors', *IEEE Transactions On Industry Applications*, vol. 38, no. 2, March/April 2002

[35]. H. Köfler, 'Stray Load Losses in Induction Machines: A Review of experimental measuring Methods and a critical Performance Evaluation', [Online] Available: www.icrepq.com/pdfs/KOFLER375.pdf , Accessed: 27/01/09

[36]. E.l B. Agamloh, 'The Partial Load Efficiency of Induction Motors', *IEEE Advanced Energy Corporation,* 2007

[37]. W. Cao, and K. J. Bradley, 'Assessing the Impacts of Rewind and Repeated Rewinds on Induction Motors: Is an Opportunity for Re-Designing the Machine Being Wasted?', *IEEE Transactions On Industry Applications*, Vol. 42, No. 4, July/August 2006

[38]. B. Slaets, P. Van Roy, R. Belmans, 'Determining the Efficiency of Induction Machines, Converters and Softstarters', [Online] Available: http://www.esat.kuleuven.ac.be/electa/publications/fulltexts/pub_164.pdf Accessed: 14/09/08

[39]. P. Kelly-Detwiler, G. A. Soares, 'Harmonization of Induction Motor Efficiency Standards in Latin America', Electric Machines and Drives Conference Record, 1997. IEEE International

[40]. A. H. Bonnet, 'An Overview of How AC Induction Motor Performance Has Been Affected by the October 24, 1997 Implementation of the Energy Policy Act

of 1992', IEEE Transactions On Industry Applications, Vol. 36, No. 1, January/February 2000

[41]. A. Boglietti, A. Cavagnino, M. Lazzari, and M. Pastorelli, 'International Standards for the Induction Motor Efficiency Evaluation: A Critical Analysis of the Stray-Load Loss Determination Aldo IEEE Standard Test Procedure for Polyphase Induction Motors and Generators, IEEE STD 112-B, 1996', *IEEE transactions on industry applications*, vol. 40, no. 5, September/October 2004

[42]. 'Methods for determining losses and efficiency of rotating electrical machinery from tests (excluding machines for traction vehicles)', SANS 34-2 1972

[43]. 'Energy Efficiency Test Methods for Three-Phase Induction Motors', CSA C390- 1993, 1998

[44]. 'Rotating Electric Machines – Methods For Determining Losses & Efficiency' Australian Standard AS/NZS1359.102

[45]. R. L. Nailen, 'New horses in the motor efficiency derby', Electrical Apparatus, Sep 2007

[46]. A Nagornyy, A. K. Wallace, and A. von Jouanne, 'Stray Load Loss efficiency connections', IEEE Industry Applications Magazine, May/June 2004, WWW.IEEE.Org/Ias

[47]. M. Aoulkadi, A. Binder, 'Comparison of different evaluation methods to determine stray load losses in induction machines with eh-star method', IEEE Transactions on Industry Applications, Volume 44, Issue 6, Nov-Dec 2008

[48]. 'Understanding IEEE 112 Method B (or CSA C390)', EPACT and Motor Testing, June 1997, [Online] Available: http://www.iprocessmart.com/leeson/leeson_epact_motor_testing.htm, Accessed: 27/01/09

[49]. G. G. Gray, W. J. Martiny, 'Efficiency testing of medium induction motors-a comment on IEEE Std112-1991', IEEE transactions on Energy conversion, Volume 11, Issue 3, Sep 1996 Page(s):495 - 499

[50]. EASA, "Understanding Energy Efficient Motors", [Online] Available: https://smtp.cpuaid.com/easa/resources/cgis/displayitem.cgi?category=2&name=Promotional+Materials&item=5, Accessed: 27/01/09

[51]. A. Bonnett and C. Young , 'Explaining Motor Failure', Oct 1, 2004 , EASA [Online] Available: http://ecmweb.com/mag/electric_explaining_motor_failure/

[52]. S. O'Donnell, 'Repair company builds capacity to meet demand', *Engineering News*, 25 May 07 [3]

[53]. A. H. Bonnett 'Root Cause AC Motor Failure Analysis with a Focus on Shaft Failures',„ *IEEE Transactions On Industry Applications*, Vol. 36, No. 5, September/October 2000

[54]. IEEE 1068: *Recommended practice for the repair and rewinding of motors for the petroleum and Chemical Industry*,

[55]. EASA: *Guide to good motor repair and replacement*

[56]. SABS 0242-1: *The rewinding and refurbishing of rotating electrical*

[57]. H. du Preez, 'Core Testing: The Heart of Quality and Successful Repair of Induction Motors and Armatures', ***Henry du Preez & Associates.***

[58]. P. Christensen, Stator Core testing, ***EASA Engineering Committee.***

[59]. H. W. Penrose, 'Repair Specification For Low Voltage Polyphase Induction Motors Intended For PWM Inverter Application', ***Final Project Presented to the Kennedy-Western University***

[60]. 'Loss of Life in Induction Machines Operating With Unbalanced Supplies', P. Pillay, and M. Manyage, December 14, 2004. Paper no. TEC-00058-2002.

[61]. H. du Preez, 'Efficiency and the Repair of motors', Henry du Preez and Associates, LH Marthinusen Rotating Machines Conference, 2007

[62]. J. C. Hirzel, "Impact of rewinding on motor efficiency," in *Conf. Rec. Annu. Pulp and Paper Ind. Tech. Conf.*, Jun. 20–24, 1994, pp. 104–107.

[63]. E. D. Bortoni, J. Haddad, A. H. M. Santos, E. M. de Azevedo, and R. A. Yamachita, 'Analysis of Repairs on Three-Phase Squirrel-Cage Induction Motors Performance', *IEEE Transactions On Energy Conversion*, Vol. 22, No. 2, June 2007

[64]. G. Bergh, D. Willemse and A. Maritz, 'Sasol's experience with Electric Motor Management Strategies', Sasol, LH Marthinusen Rotating Machines Conference, 2007

[65]. J. A. Rice , "Mathematical Statistics, Second Edition" by. Duxbury Press (An imprint of Wadsworth Publishing company). copyright '95

[66]. D. B. Pengra and L. T. Dillman, 'Notes on Data Analysis and Experimental Uncertainty', Ohio Wesleyan University, University of Washington,

[67]. Repeatability Definition

[68]. L. Underhill and D. Bradfield, "Introstat", Department of Statistical Sciences, University of Cape Town. Jan '07

[69]. W. Cao, K. J. Bradley, H. Zhang and I. French, 'Experimental Uncertainty in Estimation of the Losses and Efficiency of Induction Motors', 2006 IEEE

[70]. B. Lu, T. G. Habetler and W. Cao, 'Error Analysis of Motor-Efficiency Estimation and Measurement', 2007 IEEE

[71]. T. Clayton, 'Practical Perspectives On Motor Management' Kaman Industrial Technologies

[72]. N. M. Kaufman, 'A 100 Motor Study: Investigating Pre-Epact Motors As A Subset Of The Industrial Motor Population With Regards To The Economics Of Motor Repair/Replace Decisions', *MSc Thesis, North Carolina State University*, 2005

[73]. 'Energy Management Guide For Selection and Use of Fixed Frequency Medium AC Squirrel-Cage Polyphase Induction Motors, *NEMA Standards Publication,* MG 10-2001

[74]. 'Achieving More with Less: Efficiency and Economics of Motor Decision Tools', *Advanced Energy*, March 2006

[75]. H. W. Penrose, 'Electric Motor Energy and Reliability Analysis Using the US Department of Energy's MotorMaster+', [Online] Available: www.reliabilityweb.com/excerpts/excerpts/MM+%20Analysis.pdf Accessed: 16/10/08

[76]. 'Pump Life Cycle Costs: A guide analysis for pumping systems', [Online] Available: www.pumps.org/estore/stdi/LCC_TOC.pdf Accessed: 16/10/08

[77]. 'Selecting the best motor and equipment', [Online] Available: http://www.electricmotors.com/rightmotor.html, Accessed: 07/10/08

[78]. 'A new approach to the efficiency in South African industry.', C. D. Pitis, J. F van Rensburg, M Kleingeld, E. H. Mathews, North West University, [Online] Available: http://www.erc.uct.ac.za/jesa/volume18/18-1jesa-pitis.pdf

[79]. A. de Almeida, 'Definition: What Is A Motor System?', University of Coimbra, [Online] Available: www.iea.org/Textbase/work/2006/motor/De%20ALMEIDA%20IEA-Motor-Part-I-15-May-06-Final.pdf Accessed: 16/10/08

[80]. A. T. de Almeida and F. J.T.E. Ferreira, 'Actions to promote energy-efficient electric motor repair', International Journal of Energy Technology and Policy, Volume 1, Number 3 / 2003, Pages: 302 - 314

[81]. [Online] Available: http://www.mathworks.com/

APPENDIX A

	UCT	Nr.:
		Date: 10/03/2008

DATA SHEET
Three-phase Induction Motor - Squirrel Cage

Customer	:
Product line	: Low Voltage Electric Motors - IEC - General Purpose - IP55 - Cast Iron Frame - Standard Efficiency - Multivoltage

Frame	: 100L
Output	: 3 kW
Frequency	: 50 Hz
Poles	: 4
Rated speed	: 1390
Slip	: 7.33
Rated voltage	: 220/380 V
Rated current	: 11.4/6.63 A
L. R. Amperes	: 68.7/39.8 A
Il/In	: 6.0
No load current	: 5.70/3.30 A
Rated torque	: 20.62 Nm
Locked rotor torque	: 240 %
Breakdown torque	: 250 %
Design	: N
Insulation class	: F
Locked rotor time	: 8 s (hot)
Service factor	: 1.00
Duty cycle	: S1
Ambient temperature	: 40
Altitude	: 1000 m.a.s.l
Enclosure	: IP55
Aprox. weight	: 32.0 kg
Moment of inertia	: 0.00842 kgm²
Sound Pressure Level	: 53 db(A)

	Front	Rear
Bearing	6206 ZZ	6205 ZZ
Regreasing int.	---	---
Grease amount	---	---

Load	Power factor	Efficiency (%)
100%	0.84	81.9
75%	0.77	82.0
50%	0.64	81.5

Notes:

*The values shown are subject to change without prior notice. Noise level with tolerance of +3 dB(A).

Performed:	Checked:
LEON CHRISTIANS	

Version 6.0

	UCT	Nr.:
		Date: 10/03/2008

DATA SHEET
Three-phase Induction Motor - Squirrel Cage

Customer	:
Product line	: Low Voltage Electric Motors - IEC - General Purpose - IP55 - Cast Iron Frame - Standard Efficiency - Multivoltage

Frame	: 132M
Output	: 7.5 kW
Frequency	: 50 Hz
Poles	: 4
Rated speed	: 1450
Slip	: 3.33
Rated voltage	: 380/660 V
Rated current	: 15.1/8.69 A
L. R. Amperes	: 101/58.2 A
Il/In	: 6.7
No load current	: 6.65/3.83 A
Rated torque	: 49.42 Nm
Locked rotor torque	: 180 %
Breakdown torque	: 250 %
Design	: N
Insulation class	: F
Locked rotor time	: 8 s (hot)
Service factor	: 1.00
Duty cycle	: S1
Ambient temperature	: 40
Altitude	: 1000 m.a.s.l
Enclosure	: IP55
Aprox. weight	: 68.4 kg
Moment of inertia	: 0.04652 kgm²
Sound Pressure Level	: 60 db(A)

	Front	Rear
Bearing	6308 ZZ	6207 ZZ
Regreasing int.	---	---
Grease amount	---	---

Load	Power factor	Efficiency (%)
100%	0.87	86.8
75%	0.82	86.8
50%	0.71	86.5

Notes:

*The values shown are subject to change without prior notice. Noise level with tolerance of +3 dB(A).

Performed:	Checked:
LEON CHRISTIANS	

Version 6.0

UCT

Nr.:

Date: 10/03/2008

DATA SHEET

Three-phase Induction Motor - Squirrel Cage

Customer	:
Product line	: Low Voltage Electric Motors - IEC - General Purpose - IP55 - Cast Iron Frame - Standard Efficiency - Multivoltage

Frame	: 160M
Output	: 11 kW
Frequency	: 50 Hz
Poles	: 4
Rated speed	: 1455
Slip	: 3.00
Rated voltage	: 380/660 V
Rated current	: 22.9/13.2 A
L. R. Amperes	: 137/79.1 A
Il/In	: 6.0
No load current	: 10.0/5.76 A
Rated torque	: 72.24 Nm
Locked rotor torque	: 200 %
Breakdown torque	: 230 %
Design	: N
Insulation class	: F
Locked rotor time	: 12 s (hot)
Service factor	: 1.00
Duty cycle	: S1
Ambient temperature	: 40
Altitude	: 1000 m.a.s.l
Enclosure	: IP55
Aprox. weight	: 105 kg
Moment of inertia	: 0.07528 kgm²
Sound Pressure Level	: 67 db(A)

	Front	Rear
Bearing	6309 C3	6209 Z-C3
Regreasing int.	20000 h	20000 h
Grease amount	13 g	9 g

Load	Power factor	Efficiency (%)
100%	0.83	88.0
75%	0.79	88.5
50%	0.68	87.0

Notes:

*The values shown are subject to change without prior notice. Noise level with tolerance of +3 dB(A).

Performed:	Checked:
LEON CHRISTIANS	

	UCT	Nr.:
		Date: 10/03/2008

DATA SHEET
Three-phase Induction Motor - Squirrel Cage

Customer	:	
Product line	:	Low Voltage Electric Motors - IEC - General Purpose - IP55 - Cast Iron Frame - Standard Efficiency - Multivoltage

Frame	:	160L
Output	:	15 kW
Frequency	:	50 Hz
Poles	:	4
Rated speed	:	1455
Slip	:	3.00
Rated voltage	:	380/660 V
Rated current	:	30.0/17.3 A
L. R. Amperes	:	174/100 A
Il/In	:	5.8
No load current	:	12.0/6.91 A
Rated torque	:	98.50 Nm
Locked rotor torque	:	200 %
Breakdown torque	:	220 %
Design	:	N
Insulation class	:	F
Locked rotor time	:	12 s (hot)
Service factor	:	1.00
Duty cycle	:	S1
Ambient temperature	:	40
Altitude	:	1000 m.a.s.l
Enclosure	:	IP55
Aprox. weight	:	122 kg
Moment of inertia	:	0.10539 kgm²
Sound Pressure Level	:	67 db(A)

	Front	Rear
Bearing	6309 C3	6209 Z-C3
Regreasing int.	20000 h	20000 h
Grease amount	13 g	9 g

Load	Power factor	Efficiency (%)
100%	0.85	89.3
75%	0.82	89.5
50%	0.72	89.0

Notes:

*The values shown are subject to change without prior notice. Noise level with tolerance of +3 dB(A).

Performed:	Checked:
LEON CHRISTIANS	

Version 6.0

WEG Test Electric Motors and Drives Cape Town

Nr.:

Date: 24-AUG-2007

DATA SHEET
Three-phase Induction Motor - Squirrel Cage

Customer	: UCT
Motor line	: Standard

Frame	: 180L
Rated Output	: 22.0 kW
Frequency	: 50 Hz
Poles	: 4 poles
Full load speed	: 1465 rpm
Slip	: 2.33 %
Voltage	: 380/660 V
Full load current	: 42.6/24.5 A
Locked rotor amps	: 298/172 A
Locked rotor current (Il/In)	: 7.00
No load current	: 16.0/9.21 A
Full load torque	: 143 Nm
Locked rotor torque	: 280 %
Breakdown torque	: 280 %
Design	: N
Insulation class	: F
Temperature rise	: 80 K
Locked rotor time	: 14 s

Service factor	: 1.00
Duty cycle	: S1
Ambient temperature	: 40 °C
Altitude	: 1000 m.a.s.l
Degree of protection	: IP55
Aprox. weight	: 183 kg
Moment of inertia	: 0.1973 kgm²
Noise level	: 64 dB(A)

	D.E.	N.D.E.
Bearings	6311-C3	6211-Z-C3
Regreasing int.	20000 h	20000 h
Grease amount	18 g	11 g

Performance under load

Load	cos ø	Efficiency(%)
100%	0.85	92.3
75%	0.81	92.4
50%	0.72	91.5

Note:

DRAWING AND DIMENSIONS

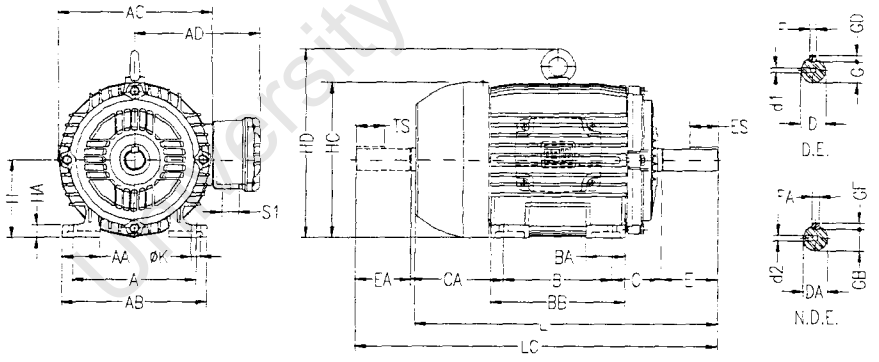

A 279	AA 80	AB 350	AC 358	AD 270	B 279	BA 75	BB 332
C 121	CA 200	D 48k6	E 110	ES 80	F 14	G 42.5	GD 9
DA 48k6	EA 110	TS 80	FA 14	GB 42.5	GF 9	H 180	HA 28
HC 360	HD 413	K 14.5	L 702	LC 820	S1 2xM32x1.5	d1 DM16	d2 DM16

Performed: Jolene Hall	Checked:

*The values shown are subject to change without prior notice.

Version 4.06

Weg Test Electric Motors and Drives Cape Town

Nr.:

Date: 24-AUG-2007

DATA SHEET
Three-phase Induction Motor - Squirrel Cage

Customer	: UCT
Motor line	: Standard

Frame	: 225S/M	Service factor	: 1.00
Rated Output	: 37.0 kW	Duty cycle	: S1
Frequency	: 50 Hz	Ambient temperature	: 40 °C
Poles	: 4 poles	Altitude	: 1000 m.a.s.l
Full load speed	: 1480 rpm	Degree of protection	: IP55
Slip	: 1.33 %	Aprox. weight	: 350 kg
Voltage	: 380/660 V	Moment of inertia	: 0.6299 kgm²
Full load current	: 69.1/39.8 A	Noise level	: 70 dB(A)
Locked rotor amps	: 498/286 A		
Locked rotor current (Il/In)	: 7.20		
No load current	: 24.0/13.8 A		
Full load torque	: 239 Nm		
Locked rotor torque	: 230 %		
Breakdown torque	: 270 %		
Design	: N		
Insulation class	: F		
Temperature rise	: 80 K		
Locked rotor time	: 20 s		

	D.E.	N.D.E.
Bearings	6314-C3	6314-C3
Regreasing int.	11638 h	11638 h
Grease amount	27 g	27 g

Performance under load

Load	cos ø	Efficiency(%)
100%	0.88	92.5
75%	0.85	92.0
50%	0.76	89.5

Note:

DRAWING AND DIMENSIONS

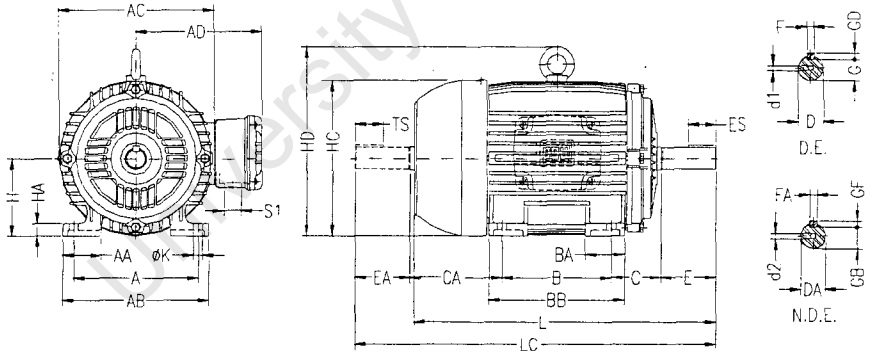

A	AA	AB	AC	AD	B	BA	BB
356	80	436	476	368	286/311	105	391
C	CA	D	E	ES	F	G	GD
149	280/255	60m6	140	125	18	53	11
DA	EA	TS	FA	GB	GF	H	HA
60m6	140	125	18	53	11	225	34
HC	HD	K	L	LC	S1	d1	d2
466	537	18.5	847	995	2xM32x1.5	M20	M20

Performed: Jolene Hall	Checked:

*The values shown are subject to change without prior notice.

Version 4.06

WEG Cest Electric Motors and Drives Cape Town

Nr.:

Date: 27-AUG-2007

DATA SHEET
Three-phase Induction Motor - Squirrel Cage

Customer	: UCT
Motor line	: Standard

Frame	: 225S/M	Service factor	: 1.00
Rated Output	: 45.0 kW	Duty cycle	: S1
Frequency	: 50 Hz	Ambient temperature	: 40 °C
Poles	: 4 poles	Altitude	: 1000 m.a.s.l
Full load speed	: 1475 rpm	Degree of protection	: IP55
Slip	: 1.67 %	Aprox. weight	: 382 kg
Voltage	: 380/660 V	Moment of inertia	: 0.7699 kgm²
Full load current	: 83.2/47.9 A	Noise level	: 70 dB(A)
Locked rotor amps	: 582/335 A		
Locked rotor current (Il/In)	: 7.00		
No load current	: 28.0/16.1 A		
Full load torque	: 292 Nm		
Locked rotor torque	: 230 %		
Breakdown torque	: 270 %		
Design	: N		
Insulation class	: F		
Temperature rise	: 80 K		
Locked rotor time	: 16 s		

	D.E.	N.D.E.
Bearings	6314-C3	6314-C3
Regreasing int.	11638 h	11638 h
Grease amount	27 g	27 g

Performance under load

Load	cos ø	Efficiency(%)
100%	0.88	93.4
75%	0.85	92.5
50%	0.76	91.0

Note:

DRAWING AND DIMENSIONS

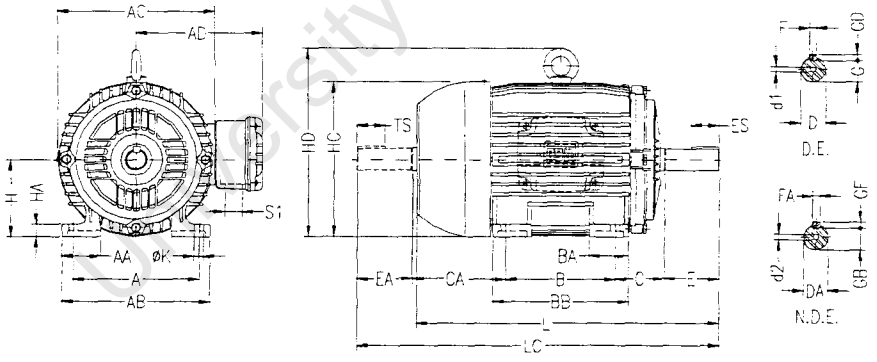

A	AA	AB	AC	AD	B	BA	BB
356	80	436	476	368	286/311	105	391
C	CA	D	E	ES	F	G	GD
149	280/255	60m6	140	125	18	53	11
DA	EA	TS	FA	GB	GF	H	HA
60m6	140	125	18	53	11	225	34
HC	HD	K	L	LC	S1	d1	d2
466	537	18.5	847	995	2xM32x1.5	M20	M20

Performed: Jolene Hall	Checked:

*The values shown are subject to change without prior notice.

Version 4.06

Weg Electric Motors and Drives Cape Town

Nr.:

Date: 24-AUG-2007

DATA SHEET
Three-phase Induction Motor - Squirrel Cage

Customer	: UCT
Motor line	: Standard

Frame	: 250S/M
Rated Output	: 55.0 kW
Frequency	: 50 Hz
Poles	: 4 poles
Full load speed	: 1475 rpm
Slip	: 1.67 %
Voltage	: 380/660 V
Full load current	: 99.4/57.2 A
Locked rotor amps	: 646/372 A
Locked rotor current (Il/In)	: 6.50
No load current	: 30.0/17.3 A
Full load torque	: 356 Nm
Locked rotor torque	: 230 %
Breakdown torque	: 260 %
Design	: N
Insulation class	: F
Temperature rise	: 80 K
Locked rotor time	: 16 s

Service factor	: 1.00
Duty cycle	: S1
Ambient temperature	: 40 °C
Altitude	: 1000 m.a.s.l
Degree of protection	: IP55
Aprox. weight	: 460 kg
Moment of inertia	: 0.9798 kgm²
Noise level	: 70 dB(A)

	D.E.	N.D.E.
Bearings	6316-C3	6314-C3
Regreasing int.	10420 h	11638 h
Grease amount	34 g	27 g

Performance under load

Load	cos ø	Efficiency(%)
100%	0.90	93.4
75%	0.87	93.1
50%	0.80	92.7

Note:

DRAWING AND DIMENSIONS

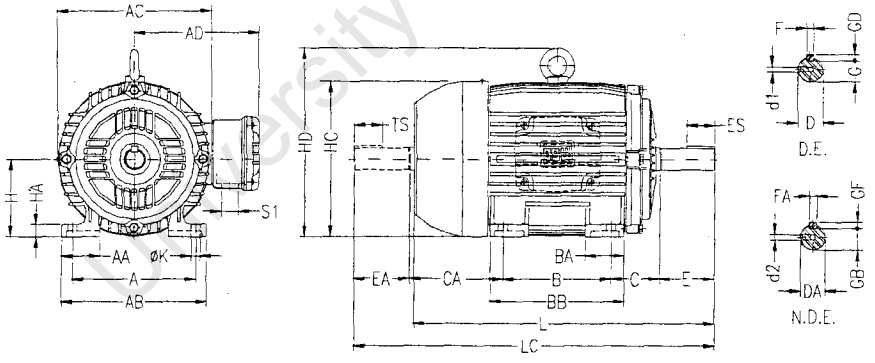

A	AA	AB	AC	AD	B	BA	BB
406	100	506	476	368	311/349	138	449
C	CA	D	E	ES	F	G	GD
168	312/274	70m6	140	125	20	62.5	12
DA	EA	TS	FA	GB	GF	H	HA
60m6	140	125	18	53	11	250	42
HC	HD	K	L	LC	S1	d1	d2
491	562	24	923	1071	2xM40x1.5	M20	M20

Performed: Jolene Hall	Checked:

*The values shown are subject to change without prior notice.

Version 4.06

APPENDIX B

Torque calculation through DC dynamometer losses

Test Setup

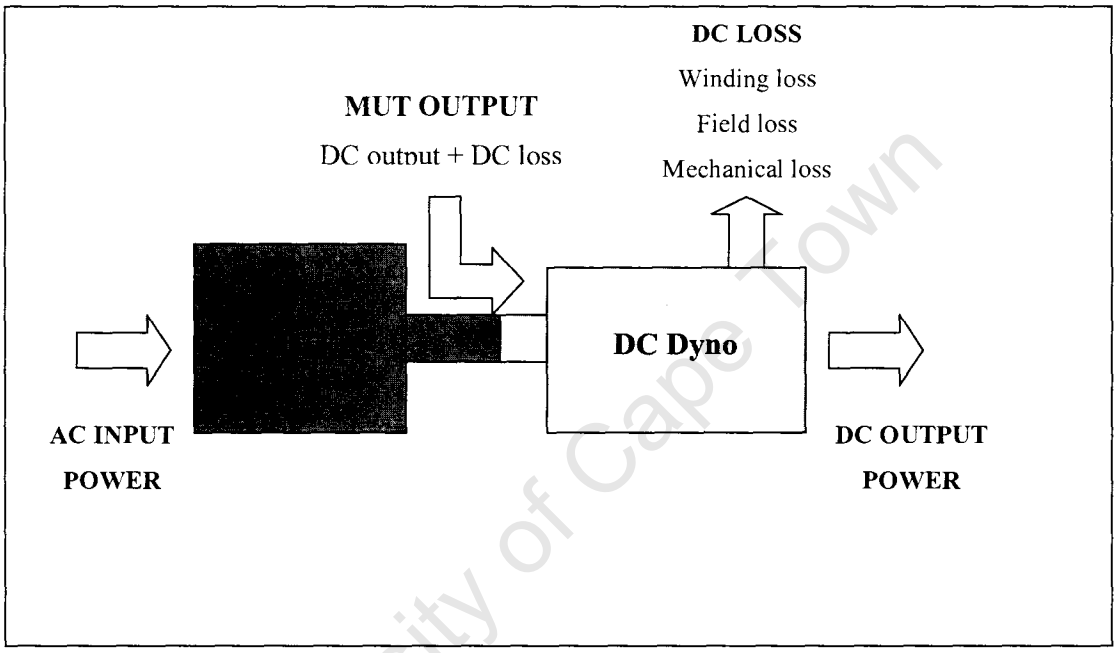

Motor under test (MUT): 3kW Weg Induction Motor

DC dyno: 3.5kW DC Motor

Calculations

$$P_{AC\text{-}shaft} = P_{output\text{-}DC} + (P_{field\text{-}DC} + P_{mech\text{-}DC} + P_{wind\text{-}DC}) \qquad \textbf{(B1.1)}$$

Where:

$P_{AC\text{-}shaft}$ is the output power of the motor under test

$P_{output\text{-}DC}$ is the output power of the DC motor dynamometer

$P_{field\text{-}DC}$ is the DC motor dynamometer field losses

$P_{mech\text{-}DC}$ is the DC motor dynamometer mechanical losses

$P_{wind\text{-}DC}$ is the DC motor dynamometer winding losses

$$T_{shaft} = \frac{P_{AC-shaft}}{W_{shaft}} \qquad \textbf{(B1.2)}$$

T_{shaft} is the MUT output shaft torque

$P_{AC\text{-}shaft}$ is the output power of the motor under test (Equation B1.1)

W_{shaft} is the MUT shaft speed

Results

Torque calculation through DC dynamometer losses

Table B 1: Data and results

MUT			DC Dyno						
Speed (RPM)	**w (rad/s)**	**Input power (W)**	**Armature Current (A)**	**Armature Voltage (V)**	**Winding losses (W)**	**Field losses (W)**	**Mech losses (W)**	**Output power (W)**	**Torque (N.m)**
1423	149.02	2903.49	15.7	160	246.49	85	60	2512	**19.48**
1442	151.01	2199.18	11.5	167	132.25	86.43	60	1920.5	**14.56**
1464	153.31	1085.04	5.2	175	27.04	88	60	910	**7.08**
1481	155.09	364.52	1.15	183	1.32	92.75	60	210.45	**2.35**

Torque comparison with Torque Transducer

Table B 2: Torque comparison with Torque Transducer

Loading (%)	Torque (N.m)	Torque Transducer (N.m)	Error (%)
100	**19.48**	**20.07**	**2.92**
75	**14.56**	**15**	**2.91**
50	**7.08**	**10**	**29.23**
25	**2.35**	**5**	**52.99**

OPERATING MANUAL

Torque transducers

T1 and T2

244.00-4.3-2.1 e

2. Construction and Method of Operation

2.1 Mechanical Construction

Torque transducers T1 and T2 consist of a cast aluminium housing (stator) and a measuring unit (rotor) to which the strain gauges are applied. The rotor is supported in the housing by means of two ball bearings. The measuring shaft can be connected to the rotating parts of the object to be measured via the two shaft ends.

Supply voltage and measuring signal transmission is via five hard silver slip rings with silver graphite carbon brushes. The two sets of brushes are arranged in such a way that two diametrically opposed brushes are spring loaded on each slip ring. This ensures reliable contact even under conditions of vibration.

The slip-ring brushes can be lifted by means of a knob on the outside of the housing, even while the unit is running. Brush abrasion and wear can thus be avoided during the periods between measurements. A impeller on the rotor cools the bearings and slip rings and blows any brush dust from the slip-ring bodies.

Fig. 2.1: Construction

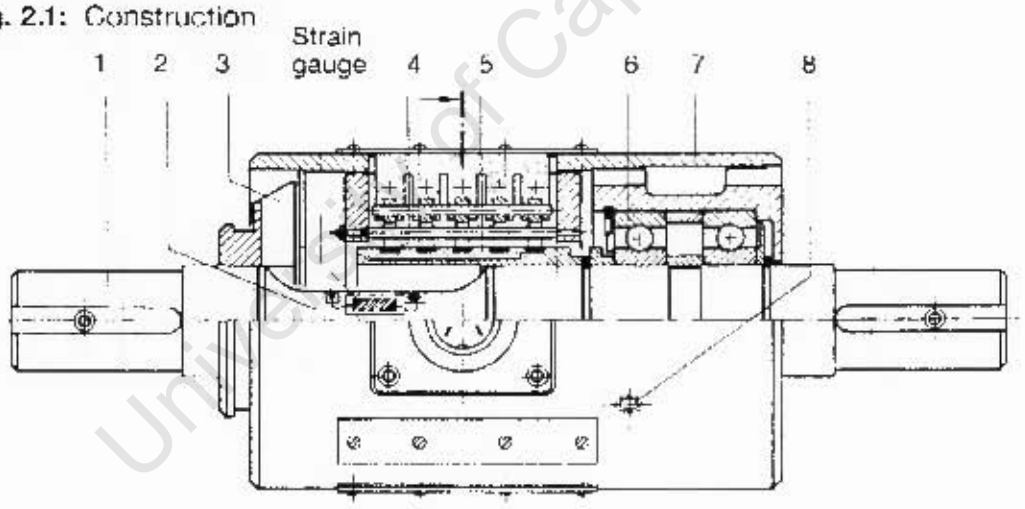

1 = Shaft end; **2** = Measuring unit (Rotor); **3** = Impeller; **4** = Hard silver slip rings; **5** – Slip-ring body; **6** = Ball bearing; **7** – Housing; **8** = Tapped hole;

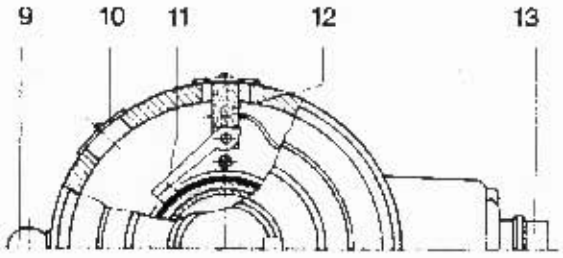

9 = Adjusting knob; **10** = Cover; **11** = Silver graphite carbon brushes; **12** = Brush set; **13** = Tuchel Flange plug T 3085

2.2 Electrical Construction

Series T1 and T2 transducers have the same structure.

The strain gauges R1 . . . R4 applied to the unit under test are applied in the direction of main strain and are connected together to form a Wheatstone bridge. They are arranged in such a way that only torques de-tune the bridge and thus change the bridge output voltage. Any flexural moments and longitudinal force have no effect within the indicated limits. The effects of temperatures over a wide range are compensated by means of an additional component.

The effective torque elastically deforms the item being measured and thus the strain gauges. The strain gauges change their resistance in proportion to their change in length; this de-tunes the Wheatstone bridge.

A clear measurement of bridge de-tuning is the ratio U_A/U_B, which is given in mV/V. This is the output signal of the torque transducer, and changes linearly with torque. In the case of torque transducers T1 and T2, the output signal is 1.5 mV/V for the rated torque in each case.

Fig. 3.2: Torque Measuring System

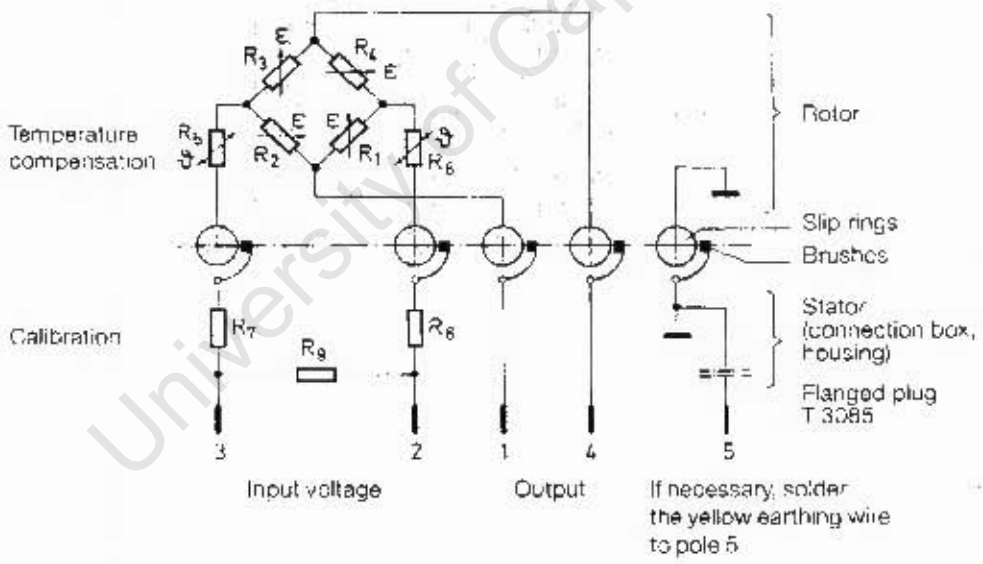

5. Measurements

Torque transducers T1 and T2 can be connected to both DC and carrier frequency amplifiers for evaluation and processing of the torque proportional signals.

5.1 Measuring Characteristics

Transducers T1 and T2:

- Strain gauge measuring system (full bridge)
- Sensitivity 1.5 mV/V
- Rated supply voltage 0.5 . . . 12 V
- Input resistance 350 Ohms.

5.2 Connection of Amplifier

Torque transducers T1 and T2 should be connected by Tuchel plug T 3085 in accordance with the amplifier connection diagram. The cables listed in section 4.2 are suitable as leads.

5.2.1 Adjusting the Amplifier

The amplifier should be adjusted in accordance with the operating manual after the torque transducer has been installed. This procedure is based on the following points:

- Select the "strain gauge full bridge" mode;
- Bridge supply voltage 0.5 . . . 12 V;
- Balance the bridge zero point without load on the torque transducer;
- Select the measuring range in accordance with the expected torque level;
- Calibrate.

5.3 Bridge Zero Balance of the Measuring System

For exact reproducibility of the torque applied, it is necessary to balance the zero signal of the measuring system, that is, the "measuring zero point" must be determined by balancing the bridge circuit.

For zero balance, calibration and measurement it is recommended that the torque transducer should first be allowed to run at the envisaged speed until constant temperature distribution is obtained.

The torque transducer must be stationary and relieved of all additional torques for the zero balance and calibration. Any residual torques caused by friction can be compensated out at the zero balance stage providing that they are constant and small.

The bridge zero balance is carried out using the measuring amplifier controls as indicated in the operating instructions.

5.4 Calibration

When calibrating the measuring system to determine the torque, the numerical value of the torque detected is expected to coincide with the measuring signal output by the amplifier, or the relationship is expected to be expressed by a fixed proportionality factor. This relationship between the numerical value of the quantity to be measured and the measured value produced by the measuring instrument is obtained by calibration.

In principle, there are several ways of calibrating the measuring system built up with torque transducers T1 or T2 and a DC voltage or carrier frequency amplifier.

The most important calibration methods are listed and explained below.
The selection of any particular method is based upon the accuracy of measurement required and the instrument technology concerned.

8. Dimensions in mm

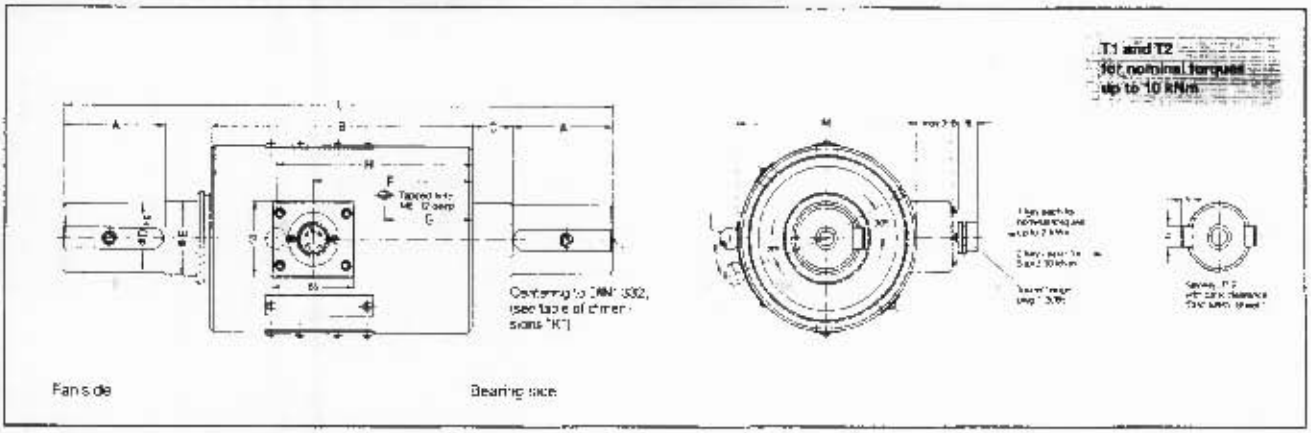

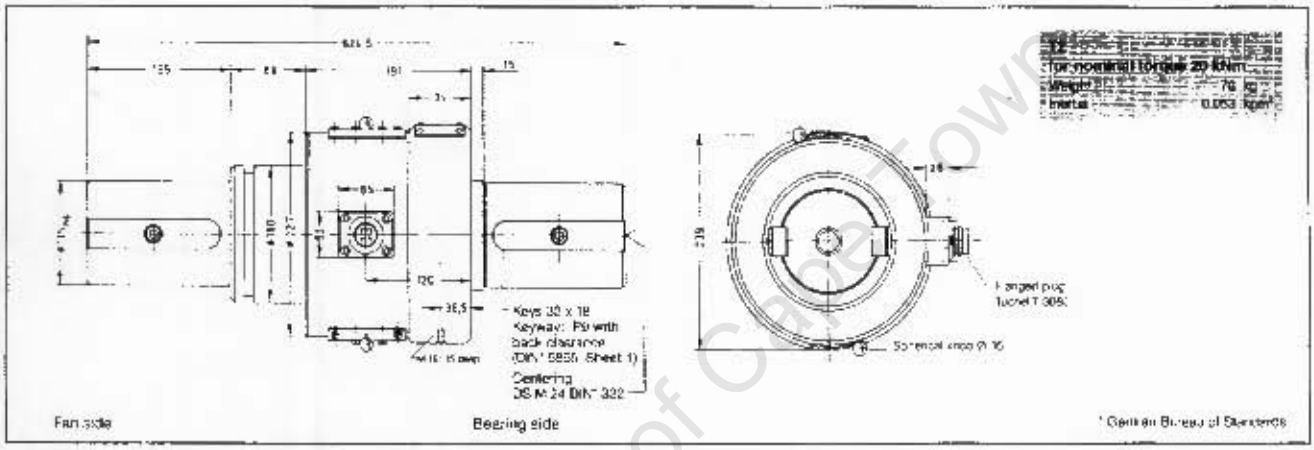

Table of dimensions - T1 and T2 for nominal torques up to 10 kNm

Nominal Torque	Weight (kg)	Dimensions (mm)											
		L	M	A	B	C	ØD	ØE	F	G	H	K	Key
10, 20, 50, 100 Nm	4.8	320	120	60	184	12	20	25	115	60	144	M 5	6 x 6
200, 500 Nm	6.2	345	120	60	184	17	30	40	115	60	144	M 12	10 x 8
1 kNm	8.2	370	120	70	184	24	48	50	115	60	144	M 16	14 x 9
2 kNm	11.5	438	140	80	208	32	62	55	125	67	155	M 20	16 x 10
5 kNm	27.3	535	190	100	278	22	75	80	166	84	182	M 20	20 x 12
10 kNm	37.5	675	190	120	278	23	92	96	166	84	182	M 20	25 x 12

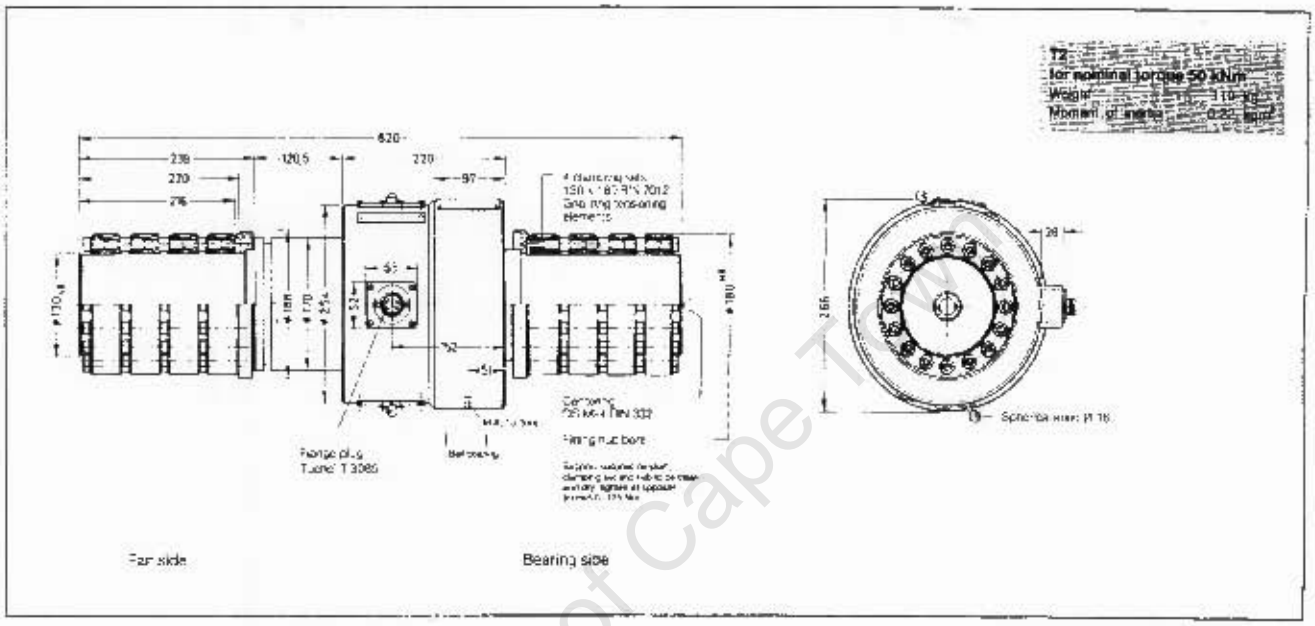

APPENDIX C

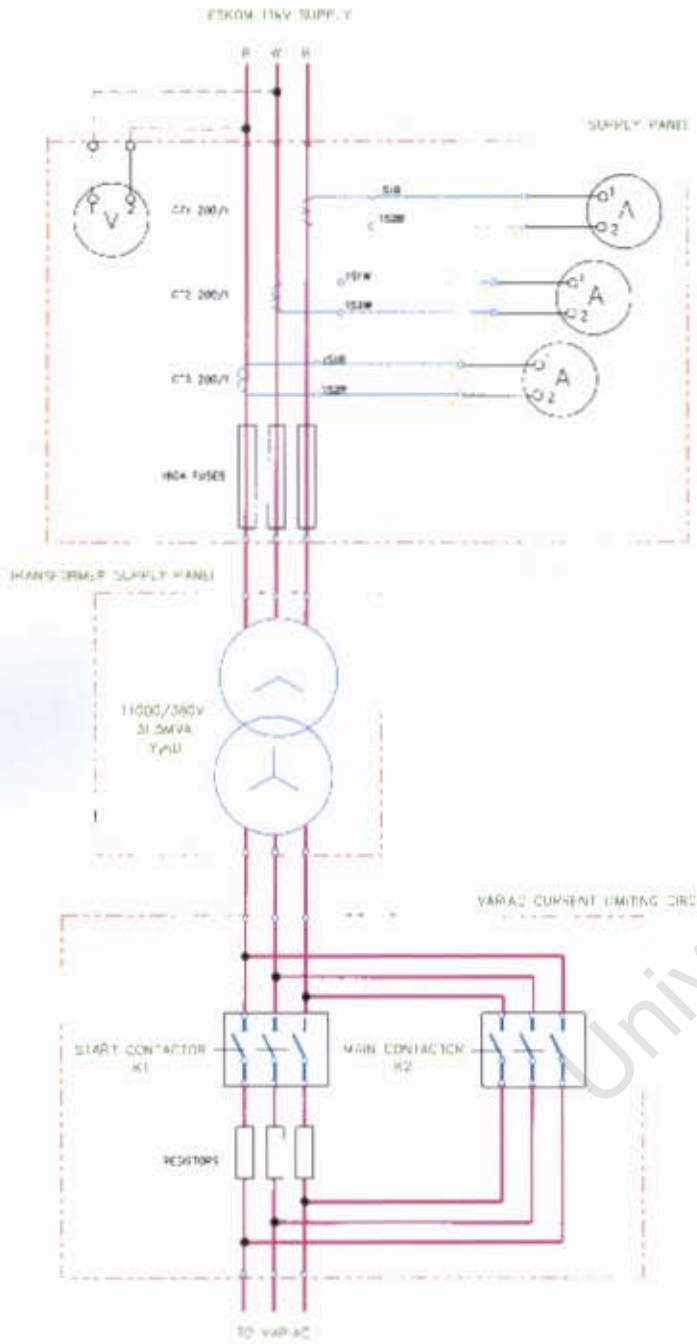

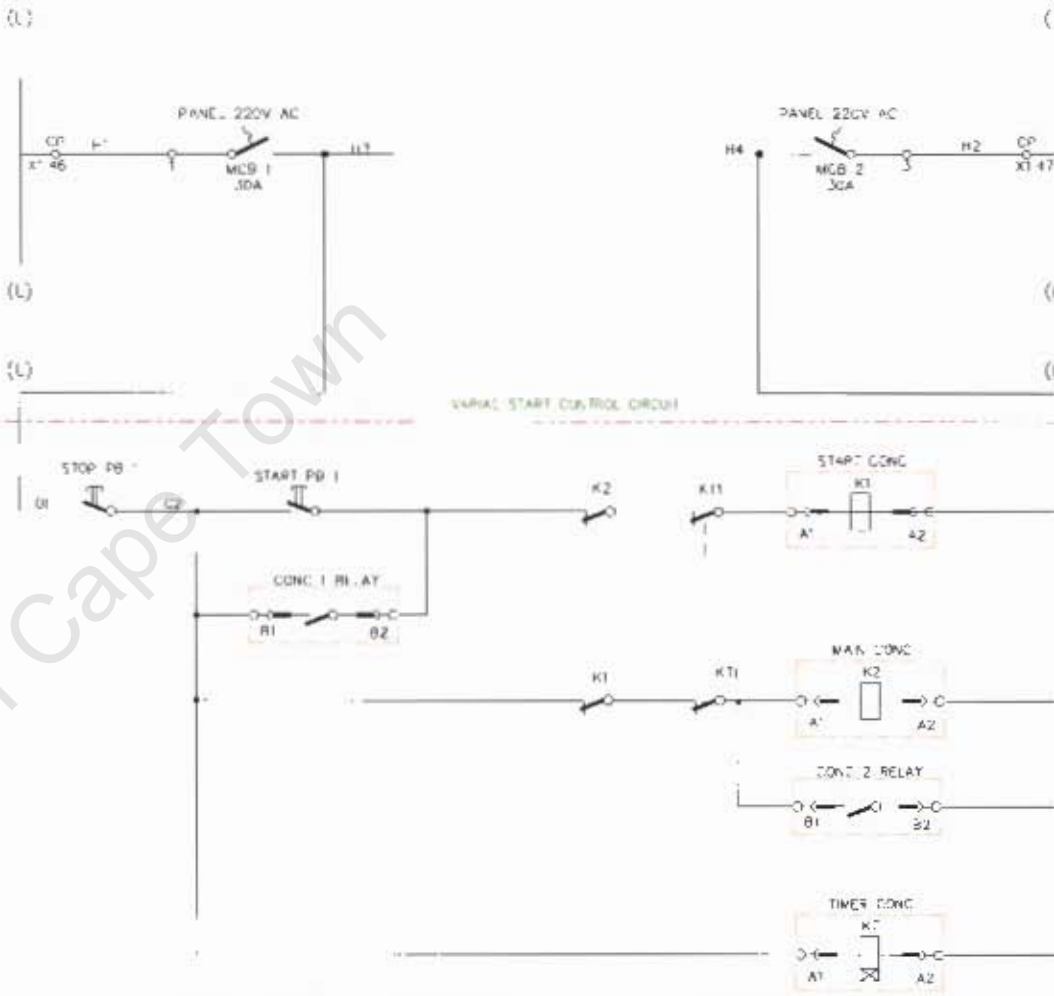

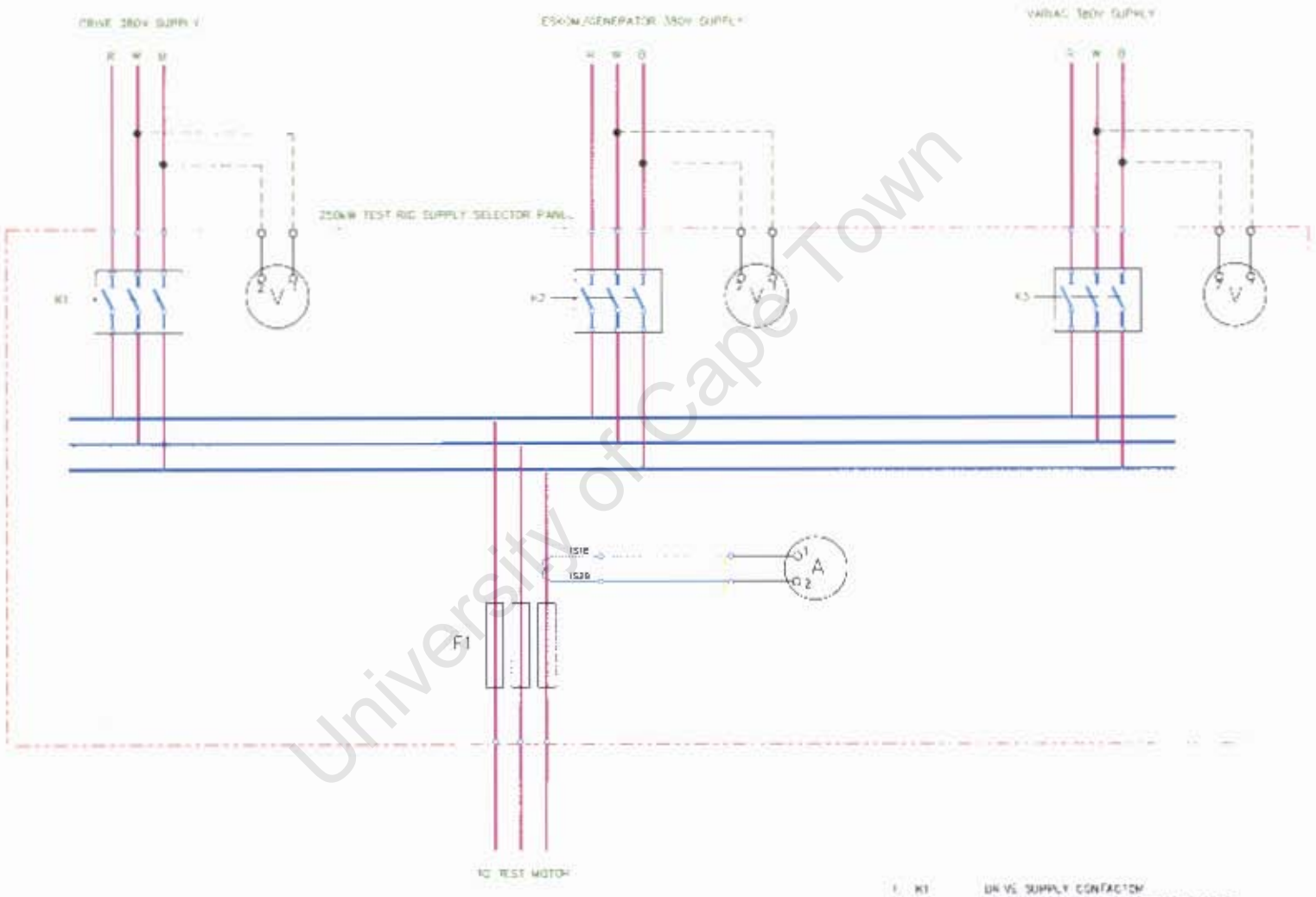

1	K1	DRIVE SUPPLY CONTACTOR
2	K2	ESKOM/ GENERATOR SUPPLY CONTACTOR
3	K3	VARIAC SUPPLY CONTACTOR
4	F1	PROTECTION FUSES
5	V	VOLTMETER
6	A	AMMMETER

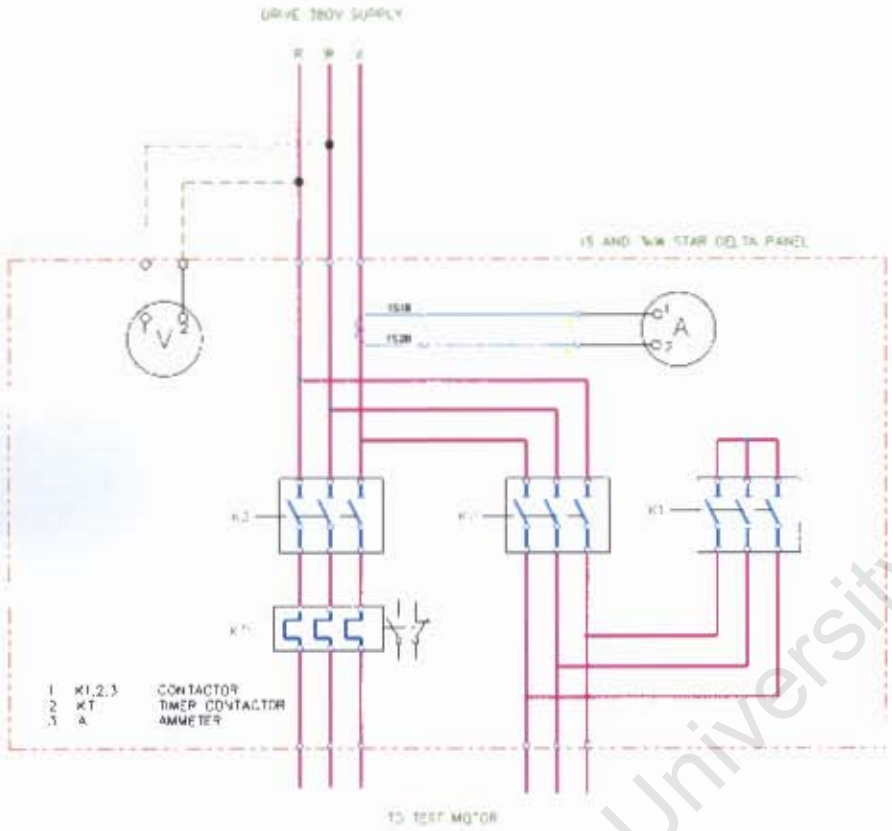

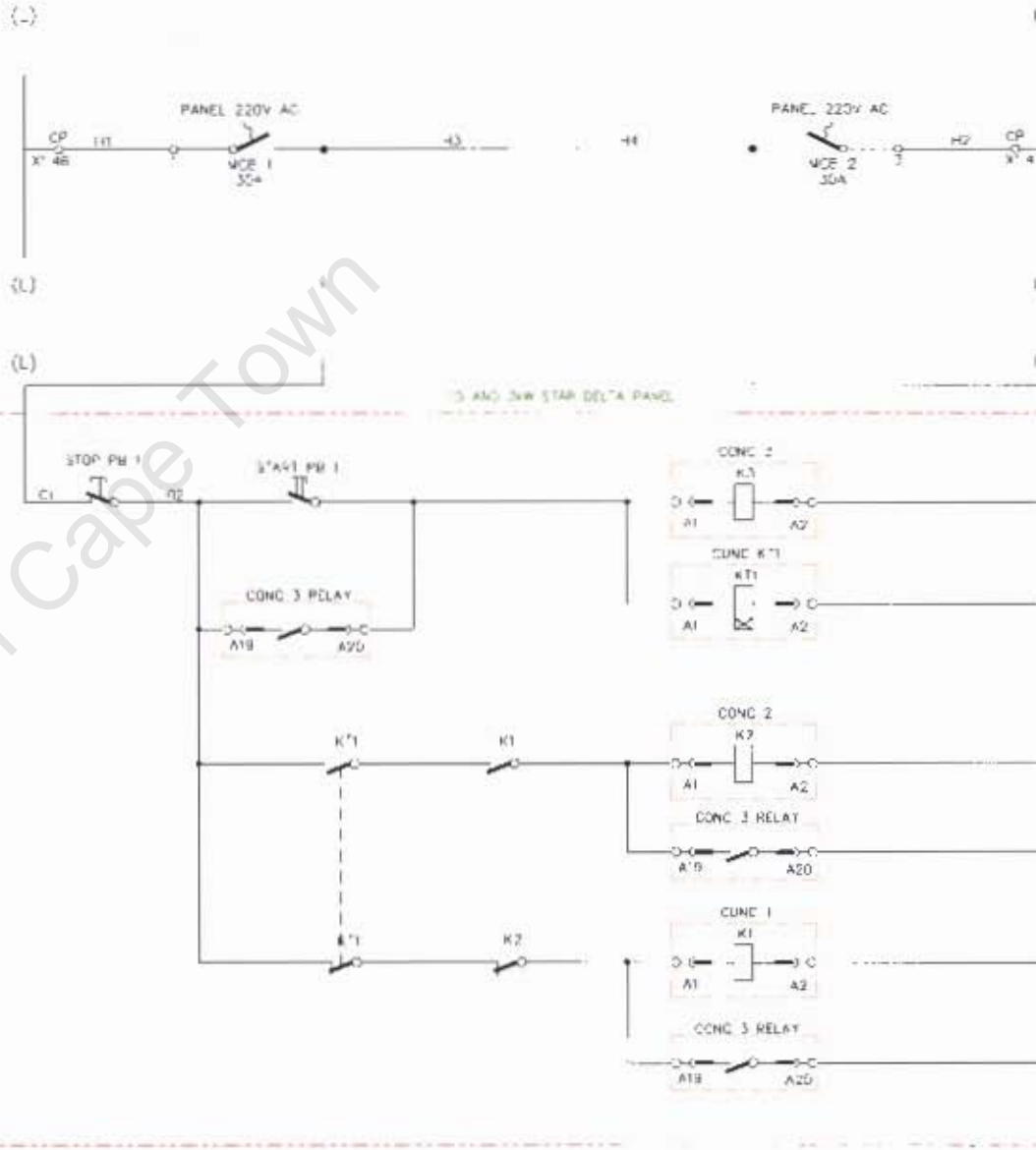

220AC SUPPLY BOARD

(L)

(N)

220V AC SUPPLY BUS

PANEL 220V AC

MCB 1 32A

PANEL SUPPLY

PANEL 220V AC

MCB 2 30A

(L)

(N)

250kW SUPPLY SELECTOR PANEL

220V AC SUPPLY

STOP PB 1

START PB 1

START PB 2

START PB 3

CONC 1

CONC 1 RELAY

CONC 2

CONC 2 RELAY

CONC 3

CONC 3 RELAY

DRIVE SUPPLY ON

DRIVE SUPPLY OFF

ESKOM/GENERATOR SUPPLY ON

ESKOM/GENERATOR SUPPLY OFF

VARIAC SUPPLY ON

VARIAC SUPPLY OFF

GREEN

RED

ORANGE

RED

ORANGE

RED

PROCEDURE FOR RUNNING THE GENERATOR SET

- Check to see that the variac is in the minimum position and then TURN ON 3Φ 380V power to the variac on the panel. This supplies current to the field of synchronous machine

- TURN ON the supply board [**500kW Synchronous Motor Output**] for the stepped down voltage (*from the synchronous generator through the transformer*)

- Check that all bolts and couplings on the machines are tight

Use either **75kW induction motor** or **250kW DC motor** as prime mover and **follow the appropriate instructions**

75kW INDUCTION MOTOR

NOTE: ONLY USE IF MACHINE CABLING IS CONNECTED TO DRIVE

- TURN ON 3Φ 380V supply [**Main Motor Supply**] for the induction motor drive
- Check induction motor drive is set to 100%
- START the induction motor drive

250kW DC MOTOR

- Check that voltage and current are at zero
- Turn on supply contactor to main drive **(GEN SET DRIVE)**
- Turn on drive and enable thyristors
- Set current direction to controlled speed up
- Apply current (**POSITION 1**)
- Apply voltage till required speed is achieved

- START the stepped down supply board

- Adjust the variac and monitor the synchronous field current to acquire the desired output voltage

- To STOP the generator set, follow the instructions in REVERSE! **NOTE:** ***For DC motor, set the current position to controlled speed down first***

PROCEDURE FOR RUNNING TEST MOTORS

- Ensure that access gate to test area is closed
- Clear the test area of any tools and loose equipment
- Ensure that the protection cage is over the pulley and torque transducer

- Choose test motor supply and follow accordingly

DRIVE SUPPLY	GENERATOR SUPPLY
➢ Turn on supply to drive and to test rig supply box (orange supply box) ➢ Check induction motor drive is set to 100% ➢ *SELECT DRIVE SUPPLY* on the supply box ➢ START the induction motor drive **VARIAC SUPPLY** ➢ Check that there is supply to the variac and that the variac is at minimum ➢ *SELECT VARIAC SUPPLY* on supply box and turn up voltage to motor	➢ Check that voltage and current are at zero on DC drive ➢ Turn on supply contactor to main drive **(GEN SET DRIVE)** ➢ Turn on drive and enable thyristors ➢ Set current direction to controlled speed up ➢ Apply current (**POSITION 1**) ➢ Apply voltage till required speed is achieved ➢ **SELECT RIG** to using the selector switch ➢ START the stepped down supply board ➢ *SELECT GEN SUPPLY* on the supply box ➢ Adjust the variac and monitor the synchronous field current to acquire the desired output voltage

- To STOP the motor, follow the instructions in REVERSE! **NOTE:** ***For DC GENERATOR SUPPLY, set the current position to controlled speed down first before slowing machine down***

- **NOTE:** ***Before testing check to see that the direction of the drive supply is the same as the direction for the generator supply***

PROCEDURE FOR RUNNING THE 250kW TEST RIG

- Ensure that access gate to test area is closed
- Clear the test area of any tools and loose equipment
- Ensure that the protection cage is over the pulley and torque transducer

- Check the rotation of the Induction motor (facing the induction motor shaft)

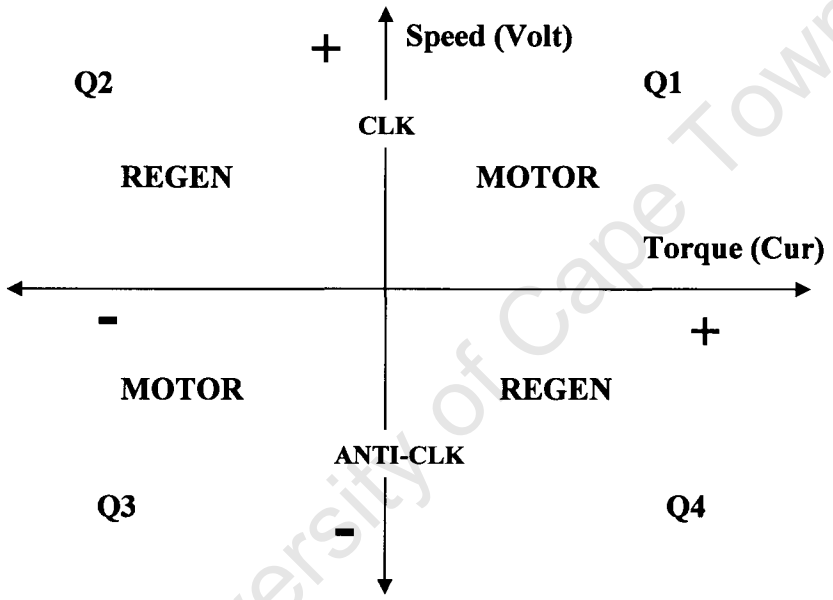

- If the rotation is Clockwise (the DC drive in Q1), switch current* direction to speed down (or **CONTROL I**)
- If the rotation is Anti-clockwise (the DC drive in Q3), switch current direction to speed UP (or **CONTROL II**)
- Start induction motor (**from either drive, supply or variac**) from **orange start box**

- Ensure current and voltage is at zero on TEST RIG DRIVE and turn on supply contactor to main drive **(GEN SET DRIVE)**
- Turn on drive and enable thyristors
- Apply current to load Induction motor

APPENDIX D

EFFICIENCY AND LOSS CALCULATION PROGRAM FLOW CHART

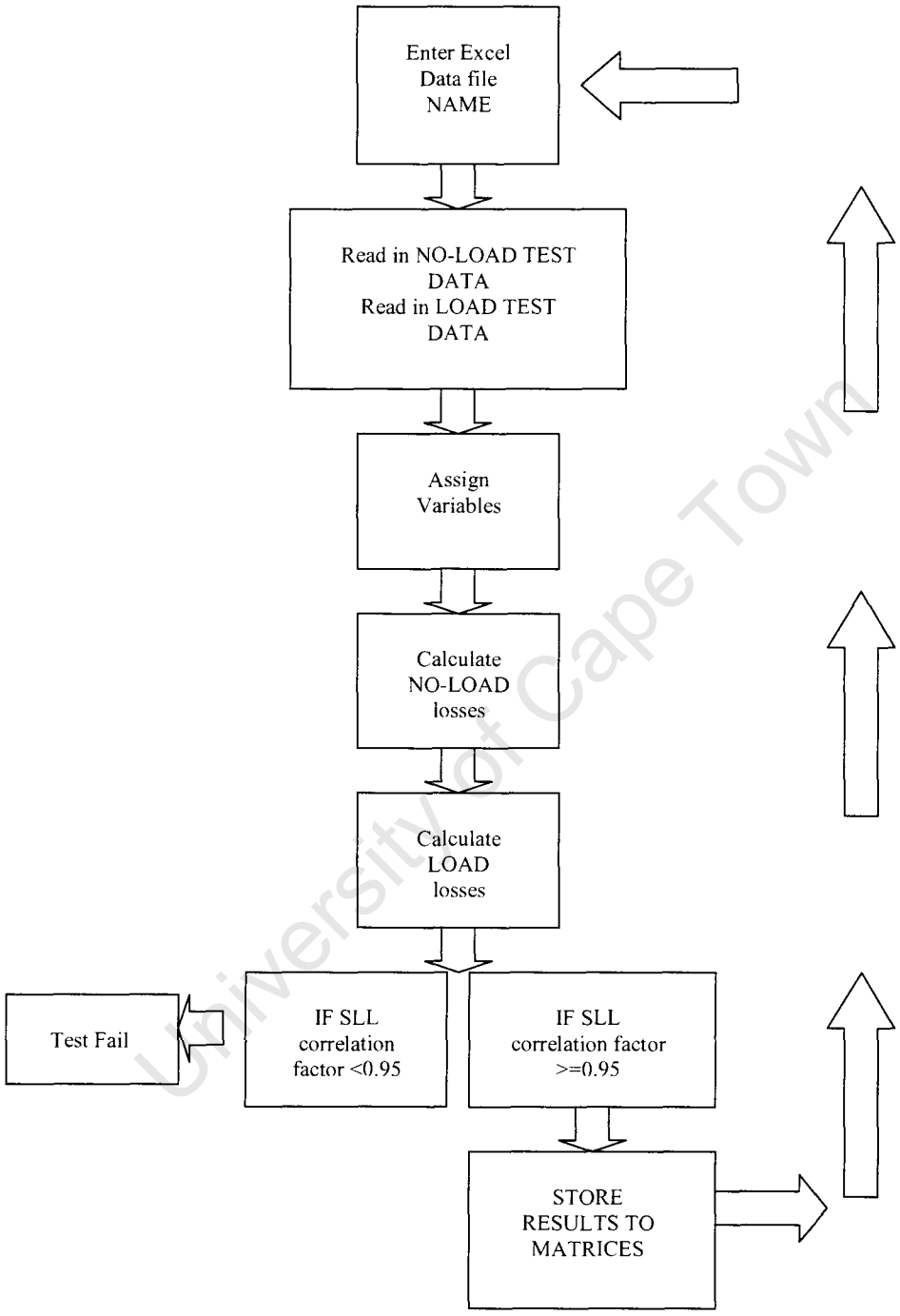

EFFICIENCY AND LOSS CALCULATION PROGRAM CODE

```
function [loss] = Fif(x)
clc

v=x;
heskin = [0];
%.....
%                Section 1                .
%.....
NoData1 = xlsread('15kv 1-set1-nlb.xls', 'Sheet1');
NoData2 = xlsread('15kv 1-Ash-nl2.xls', 'Sheet1');
NoData3 = xlsread('15kv 1-Ash-nl1.xls', 'Sheet1');
```

```
%-------------------------------------------------------
U1 = NoData1 (23:29,3);
NO_I1 = NoData1 (23:29,4);
Pin1 = NoData1 (23:29,5);
R1_nl1 = NoData1 (23:29,7);
I1 = NO_I1/sqrt(3);
U_sqrd1= U1.^2;
NO_Temp1 = NoData1 (23:29,3);
%-------------------------------------------------------
U2 = NoData2 (23:29,3);
NO_I2 = NoData2 (23:29,4);
Pin2 = NoData2 (23:29,5);
R1_nl2 = NoData2(23:29,7);
I2 = NO_I2/sqrt(3);
U_sqrd2= U2.^2;
NO_Temp2 = NoData2 (23:29,3);
% %-------------------------------------------------------
U3 = NoData3 (23:29,3);
NO_I3 = NoData3 (23:29,4);
Pin3 = NoData3 (23:29,5);
R1_nl3 = NoData3 (23:29,7);
I3 = NO_I3/sqrt(3);
U_sqrd3= U3.^2;
NO_Temp3 = NoData3 (23:29,3);
%-------------------------------
R_rated = NoData1 (16,14);
R_after = NoData1 (19,14);
%-------------------------------------------------------
%       Calculating Stator Copper losses
%-------------------------------------------------------
P_Cu1_nl1=3*I1.^2.*R1_nl1;            %Stator copper losses [W]
P_Cu1_nl2=3*I2.^2.*R1_nl2;
P_Cu1_nl3=3*I3.^2.*R1_nl3;
%-------------------------------------------------------
%           Calculating Constant Losses
%-------------------------------------------------------
Pk1 = Pin1 - P_Cu1_nl1 ;                    %Constant Losses [W]
Pk2 = Pin2 - P_Cu1_nl2 ;
Pk3 = Pin3 - P_Cu1_nl3 ;
%-------------------------------------------------------
%    Averaging the no-load test data
%-------------------------------------------------------

U = (U1+U2+U3)/3;
NO_I = (NO_I1+NO_I2+NO_I3)/3;
Pin = (Pin1+Pin2+Pin3)/3;
R1_nl = (R1_nl1 +R1_nl2 +R1_nl3 )/3;
I_AVE = NO_I./sqrt(3);
U_sqrd= U.^2;
NO_Temp = (NO_Temp1+NO_Temp2+NO_Temp2)/3;
P_Cu1_nl=3*I_AVE.^2.*R1_nl;
Pk = Pin - P_Cu1_nl;
%-------------------------------------------------------
%    Determining the friction and windage losses
%-------------------------------------------------------
%creating linear constant losses from constant losses data
X_U_sqrd= [ U_sqrd(4:7), ones(size(U_sqrd(4:7)))];
% X_U_sqrd2= [ U_sqrd2(4:7), ones(size(U_sqrd2(4:7)))];
% X_U_sqrd3= [ U_sqrd3(4:7), ones(size(U_sqrd3(4:7)))];
%Determine coefficients of the best fit straight line by matrix psuedo-
%inversion for experimental data. Best fit line for noload Pk vs U^2 data:
Coeff_Pk = X_U_sqrd \ Pk(4:7);
% Coeff_Pk2 = X_U_sqrd2 \ Pk2(4:7);
% Coeff_Pk3 = X_U_sqrd3 \ Pk3(4:7);

% fprintf('The friction and windage losses for 15kW Zest Motor in [W] is:\n');
% disp(Coeff_Pk(2));

%Define an arbitrary U^2 vector to generate Pk points using the resulting
%linear fit to experimental data:
U_sqrd_fit = [0: 190000]';

%Generate Pk points using the resulting polynomial fits to exp data:
Pk_poly_fit = polyval(Coeff_Pk,U_sqrd_fit);
% Pk_poly_fit2 = polyval(Coeff_Pk2,U_sqrd_fit);
% Pk_poly_fit3 = polyval(Coeff_Pk3,U_sqrd_fit);

%-------------------------------------------------------
%           Calculating Iron core Losses
```

```
%-------------------------------------------------
P_Fric =Coeff_Pk(2);

P_fe2 = Pk(1:3) - P_Fric;

%Creates a cubic matrix for the best fit of iron losses vs line voltage:
%Y_Mat=[ U1.^3 U1.^2 U1 ones(size(U1))];
X_U2=[ U(1:3).^3, U(1:3).^2, U(1:3), ones(size(U(1:3)))];
%Y_U3=[ U3.^3 U3.^2 U3 ones(size(U3))];

%Determine coeffs of the best fit cubic polyn by matrix pseudo-inversion
%for experimental data. Best fit polynomial for Induction machine no-load
%iron losses:
%Coeff_P_fe1 = X_U1 \ P_fe1;
Coeff_P_fe2 = X_U2 \ P_fe2;
%Coeff_P_fe3 = X_U3 \ P_fe3;
%Define an arbitrary line voltage to generate Iron losses's points
%using the resulting polynomial fits to the experimental data:
U_fit = [300:700]';

%Generate P_fe points using the resulting polynomial fits to exp data:
%P_fe_poly_fit1 = polyval(Coeff_P_fe1,U_fit);
P_fe_poly_fit2 = polyval(Coeff_P_fe2,U_fit);
%P_fe_poly_fit3 = polyval(Coeff_P_fe3,U_fit);

% figure(1);
% subplot(2,2,1),
% p1 = plot(U_sqrd(4:7),Pk(4:7),'^', U_sqrd_fit,Pk_poly_fit,'r');
% xlabel('U^2 [V^2]'), ylabel('Constant Losses [W]')
%      title('No-load Constant losses vs voltage^2')
%      grid on;
%-----------------------------------------------------------------
%           Assigning variables to the data values
%-----------------------------------------------------------------
 switch (v)

    case (1)
        PData = xlsread('15kw 3-set1-Ash.xls', 'Sheet1');
        case (2)
        PData = xlsread('15kw 3-Ash.xls', 'Sheet1');

         case (3)
        PData = xlsread('15kw 1-Ash-nll.xls', 'Sheet1');
    case (4)
        PData = xlsread('15kw 3-Ash.xls', 'Sheet1');
end

%PData = xlsread('15kw 1-set1-nll.xls', 'Sheet1');

Nr2 = PData (15:19,2);
Tshaft = PData (15:19,8);
U2 = PData (15:19,4);
Pin2 = PData (15:19,6);
L_I2 = PData (15:19,5);
I2 = L_I2/sqrt(3);
f2 = PData (15:19,7);
T2 = PData (15:19,8);
R1 = PData (15:19,14);
L_percent=PData(36:40,19);
%-----------------------------------------------------------------
%Calculating Pshaft
%-----------------------------------------------------------------
wm = Nr2*(2*pi)/60;              %Shaft speed [rad/sec]
Pshaft = Tshaft.*wm;             %Shaft power [W]
%-----------------------------------------------------------------
%Calculating Efficiency from Direct Torque and rotor angular speed
%-----------------------------------------------------------------
Eff_dir=Pshaft./Pin2;            %direct method efficiency
%-----------------------------------------------------------------
%   Calculating percentage loading of the induction machine
%-----------------------------------------------------------------
%creating cubic efficiency regression line from the efficiency data
X_L_percent2 = [ L_percent.^5, L_percent.^4, L_percent.^3, L_percent.^2,...
                 L_percent, ones(size(L_percent))];

%Determine coefficients of the best fit straight line by matrix pseudo-
%inversion for experimental data.
Coeff_Eff_dir = X_L_percent2 \ Eff_dir;
```

```
%Define an arbitrary L_percent vector to generate P_Cu1 points using
%the resulting linear fit to experimental data:
L_percent_fit = [10:150]';

%Generate P_Cu1 points using the resulting polynomial fits to exp data:
Eff_dir_poly_fit = polyval(Coeff_Eff_dir,L_percent_fit);

%-------------------------------------------------------------
%   Calculating Armature resistance at each loading point IEC
%-------------------------------------------------------------
r = linspace(R_rated,R_after,4); %linear resistance during loading conditions
R1_IEC = [R_rated, r]';    %Armature resistance at each loading point

%-------------------------------------------------------------
%Calculating Stator copper losses of the standard induction machine
%-------------------------------------------------------------
P_Cu1 = 3*(I2.^2).*R1;      %Copper losses of the primary windings [W]
P_Cu1_IEC = 3*(I2.^2).*R1_IEC ;

%creating cubic stator losses regression line from stator copper loss data
X_L_percent = [ L_percent.^2, L_percent, ones(size(L_percent))];

%Determine coefficients of the best fit straight line by matrix psuedo-
%inversion for experimental data.
H_Coeff_P_Cu1 = X_L_percent \ P_Cu1;

%Generate P_Cu1 points using the resulting polynomial fits to exp data:
P_Cu1_poly_fit = polyval(H_Coeff_P_Cu1,L_percent_fit);

%-------------------------------------------------------------
%Calculating Corrected Stator coppers losses at each loading point
%-------------------------------------------------------------
Temp = PData (4,5);
amb = PData(5,5);

k_theta=(235-amb+25+Temp)./(235+Temp); %temp. correction factor for windings

P_Cu1_corr_IEC = P_Cu1_IEC.*k_theta; %corrected stator losses

P_Cu1_corr = PData (36:40,10);

%-------------------------------------------------------------
%Calculating Line voltages to estimate iron losses for each loading point
%from the no-load iron losses already determined
%-------------------------------------------------------------
R1_heatrun = PData (3,5);
cos_alpha=Pin2./(sqrt(3).*U2.*I2);    %determining cos_alpha from the data
sin_alpha=sqrt(1-cos_alpha.^2);       %determining sin_alpha from cos_alpha

Ur_LL2=sqrt((U2-sqrt(3).*I2.*R1_heatrun.*cos_alpha).^2+...
(sqrt(3)*I2.*R1_heatrun.*sin_alpha).^2);    %determines the required line voltage for
each loading point

%-------------------------------------------------------------
%Calculating Iron losses at each load point:
P_iron1 = polyval(Coeff_P_fe2,U2);     %determining the each load's fe

P_iron_IEC = polyval(Coeff_P_fe2,Ur_LL2); %loss from the no load fe losses

%-------------------------------------------------------------
%   Calculating the Rotor copper losses at each load point:
%-------------------------------------------------------------
s=((120/4*f2)-Nr2)./(120/4*f2);     %slip at each load point

P_Cu2=(Pin2-P_Cu1-P_iron1).*s;
P_Cu_IEC=(Pin2-P_Cu1-P_iron_IEC).*s;%Copper losses on the rotor windings

%Determine coefficients of the best fit straight line by matrix psuedo-
%inversion for experimental data.
Coeff_P_Cu2 = X_L_percent \ P_Cu2;

%Generate P_Cu1 points using the resulting polynomial fits to exp data:
P_Cu2_poly_fit = polyval(Coeff_P_Cu2,L_percent_fit);

%-------------------------------------------------------------
%Corrected Rotor losses at each point are given by:
P_Cu2_corr_IEC=(Pin2-P_Cu1_corr_IEC-P_iron_IEC).*s.*k_theta;
```

```
P_Cu2_corr=PData (36:40,13);

%-------------------------------------------------------------
%      Calculating the Residual Losses at each load point (SANS IEC
%-------------------------------------------------------------
Rated_Curr = I2(2);

P_SANS = 0.005*Pin2(2); %0.5% of load

P_Lr_SANS = P_SANS*(I2./Rated_Curr);
%-------------------------------------------------------------
%      Calculating the Residual Losses at each load point
%-------------------------------------------------------------
P_Lr=Pin2-Pshaft-P_Cu1-P_Cu2-P_iron1-Coeff_Pk(2);
P_Lr_IEC=Pin2-Pshaft-P_Cu1_IEC-P_Cu_IEC-P_iron_IEC-Coeff_Pk(2);

%creating linear regression line from the Residual loss data
X_Tshaft_sqrd = [ Tshaft.^2, ones(size(Tshaft.^2))];

%Determine coefficients of the best fit straight line by matrix pseudo-
%inversion for experimental data.
Coeff_P_Lr = X_Tshaft_sqrd \ P_Lr;

%Define an arbitrary L_percent vector to generate P_Cul points using
%the resulting linear fit to experimental data:
Tshaft_sqrd_fit = [0:16000]';

%Generate P_Cul points using the resulting polynomial fits to exp data:
P_Lr_poly_fit = polyval(Coeff_P_Lr,Tshaft_sqrd_fit);

%-------------------------------------------------------------
%Smoothing the Residual Losses data to estimate Additional load losses
%It should also be noted that there are seven data points for this machine
%and linearised to the form P_Lr = A*Tshaft.^2+B

%IEEE 112-B
A=((5*sum(P_Lr.*(Tshaft.^2))-sum(P_Lr)*sum(Tshaft.^2)))...
    /(5*sum(Tshaft.^4)-(sum(Tshaft.^2))^2); %gradient of the regression

B=sum(P_Lr)/5-A*sum(Tshaft.^2)/5;          %intercept of the regression

%The correlation factor for the experimental data points from the
%regression line is calculated as follows:
gamma=(5*sum(P_Lr.*(Tshaft.^2))-sum(P_Lr)*sum(Tshaft.^2))...
    /sqrt((5*sum(Tshaft.^4)-(sum(Tshaft.^2)^2))...
    *(5*sum(P_Lr.^2)-(sum(P_Lr))^2)); %data correlation factor
%-------------------------------------------------------------
n=0;
x=1;
G =[0];
B =[0];
for n=0:1:4

    if gamma >=0.9
        A1=A;
        gamma1 = gamma;
        break
    end

    T = Tshaft;
    P = P_Lr;

    T(x,:)= [];
    P(x,:)= [];

    gamma1=(4*sum(P.*(T.^2))-sum(P)*sum(T.^2))...
    /sqrt((4*sum(T.^4)-(sum(T.^2)^2))...
    *(4*sum(P.^2)-(sum(P))^2)) ;

    Q=((4*sum(P.*(T.^2))-sum(P)*sum(T.^2)))...
    /(4*sum(T.^4)-(sum(T.^2))^2);

    G(x,1)=gamma1;
    B(x,1)= Q;

     if gamma1 >=0.9
        A1=Q;
        break
```

```
    end
 x=x+1;
end

if gamma1<0.9
        [gamma1,x] = max(G);
        A1=B(x);
  end
%-----------------------------------------------------------------
%Smoothing the Residual Losses data to estimate Additional load losses
%it should also be noted that there are seven data points for this machine
%and linearised to the form P_Lr = A*Tshaft.^2+E

%IEC

A_IEC=((5*sum(P_Lr_IEC.*(Tshaft.^2))-sum(P_Lr_IEC)*sum(Tshaft.^2)))...
    /(5*sum(Tshaft.^4)-(sum(Tshaft.^2))^2);  %gradient of the regression

B_IEC=sum(P_Lr_IEC)/5-A*sum(Tshaft.^2)/5;            %intercept of the regression

gamma_IEC=(5*sum(P_Lr_IEC.*(Tshaft.^2))-sum(P_Lr_IEC)*sum(Tshaft.^2))...
    /sqrt((5*sum(Tshaft.^4)-(sum(Tshaft.^2)^2))...
    *(5*sum(P_Lr_IEC.^2)-(sum(P_Lr_IEC))^2)); %data correlation factor

%-----------------------------------------------------------------

p=0;
g=1;
I =[0];
E =[0];
for p=0:1:4

    if gamma_IEC >=0.95
        A1_IEC=A_IEC;
        gamma1_IEC = gamma_IEC;
        break
    end

    T = Tshaft;
    P = P_Lr_IEC;

    T(g,:)= [];
    P(g,:)= [];

    gamma1_IEC=(4*sum(P.*(T.^2))-sum(P)*sum(T.^2))...
    /sqrt((4*sum(T.^4)-(sum(T.^2)^2))...
    *(4*sum(P.^2)-(sum(P))^2)) ;

    Q=((4*sum(P.*(T.^2))-sum(P)*sum(T.^2)))...
    /(4*sum(T.^4)-(sum(T.^2))^2);

    I(g,1)=gamma1_IEC;
    E(g,1)= Q;

     if gamma1_IEC >=0.95
        A1_IEC=Q;
        break

    end
 g=g+1;
end

if gamma1_IEC<0.95
        [gamma1,g] = max(I);
        A1_IEC=E(g);
  end
%-----------------------------------------------------------------
%           Calculating the Additional Load losses
%-----------------------------------------------------------------
%IEEE
Tsh = PData (15:19,8);
P_LL=A1*(Tsh.^2)  ;         %Additional losses

%-----------------------------------------------------------------
%IEC
Tsh = PData (15:19,8);
P_LL_IEC=A1_IEC*(Tsh.^2)  ;         %Additional losses
```

```
%-------------------------------------------------------------
%Calculating the Total Losses of the machine at each load point
%-------------------------------------------------------------

P_iron = P_iron1;

P_total=P_iron+P_Cu2_corr+P_Cu1_corr+P_LL+P_Fric;

P_total_IEC =P_iron_IEC+P_Cu2_corr_IEC+P_Cu1_corr_IEC+P_LL_IEC+P_Fric;

P_total_JEC =P_iron_IEC+P_Cu2_corr_IEC+P_Cu1_corr_IEC+P_Fric;

P_total_SANS=P_iron+P_Cu2_corr+P_Cu1_corr+P_Lr_SANS+P_Fric;
% ------------------------------------------------------------
%     Equivalent Circuit Method
%-------------------------------------------------------------


%-------------------------------------------------------------
%Calculating Efficiency from the electric input power and the
%total losses of the standard induction machine i.e indirect method
%-------------------------------------------------------------
Eff_indir=(Pin2-P_total)./Pin2;     %indirect method estimating the
                                    %machine efficiency at each load point

Eff_indir_IEC=(Pin2-P_total_IEC)./Pin2;

Eff_indir_JEC=(Pin2-P_total_JEC)./Pin2;

Eff_indir_SANS=(Pin2-P_total_SANS)./Pin2;


% Eff_indir_SANS=(Pin2-P_total_SANS)./Pin2;


% Eff_indir_SANS=(Pin2-P_total_SANS)./Pin2;
%Determine coefficients of the best fit straight line by matrix pseudo-
\inversion for experimental data.
Coeff_Eff_indir = X_L_percent2 \ Eff_indir;


%Generate F_Cu1 points using the resulting polynomial fits to exp data:
Eff_indir_poly_fit = polyval(Coeff_Eff_indir,L_percent_fit);
Pout =Pin2-P_total;

% ------------------------------------------------------------

Inf = [Eff_indir Eff_dir];

inf = [L_percent];


heskin (1,:)  = P_Fric;
heskin (2,:)  = A;
heskin (3,:)  =A1;
heskin (4,:)  =I_AVE(2);
heskin (5,:)  =gamma1;


mzungu (1,:)  = P_Fric;
mzungu (2,:)  = A_IEC;
mzungu (3,:)  =A1_IEC;
mzungu (4,:)  =I_AVE(2);
mzungu (5,:)  =gamma1_IEC;

Inf2 = [P_Fric, A, A1 gamma1];

loss = [L_percent Eff_indir P_Cu1_corr P_Cu2_corr P_LL  P_iron heskin I_AVE(1:5) Eff_dir
P_Cu1_corr_IEC P_Cu2_corr_IEC P_iron_IEC...
        P_LL_IEC mzungu Eff_indir_IEC Eff_indir_JEC Eff_indir_SANS Nr2 L_I2 Tsh Pout
Pin2];

% other_EFF = [Eff_indir_SANS Eff_indir_JEC Eff_EC Eff_indir ];
%
% T LL Pin2
%
%            r     blue          .     point              -     solid
%            g     green         o     circle             :     dotted
%            r     red           x     x-mark             -.    dashdot
```

```
%            c      cyan           +      plus                 --     dashed
%            m      magenta        *      star               (none)   no line
%            y      yellow         s      square
%            k      black          d      diamond
%                                  v      triangle (down)
%                                  ^      triangle (up)
%                                  <      triangle (left)
%                                  >      triangle (right)
%                                  p      pentagram
%                                  h      hexagram
```

COMPARISON PROGRAM FLOW CHART

32

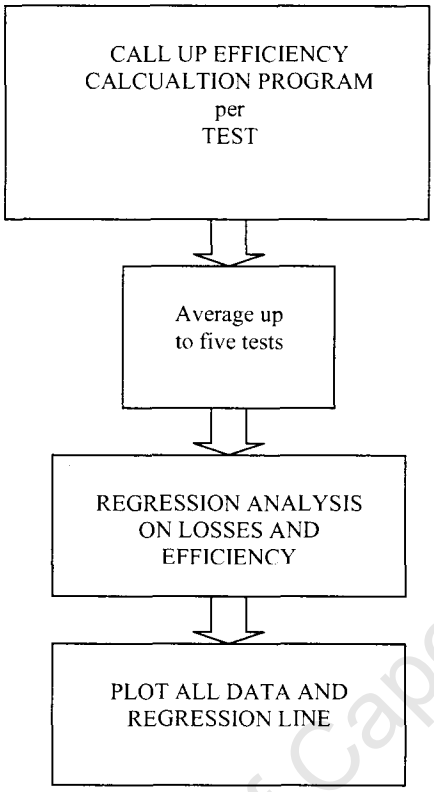

COMPARISON PROGRAM CODE

```
clc;
clear;
L_percent_fit = [10:130]';
% ..............................................................................
% Rewound Motor
% ..............................................................................
Test_1 = Fif(1)

RStator_loss_1 = Test_1(1:5,3);
RRotor_loss_1 = Test_1(1:5,4);
RCore_loss_1 = Test_1(1:5,6);
RSLL_loss_1 = Test_1(1:5,5);
RCorr_Fr_A_1= Test_1(1:5,7);
REff_1 = Test_1(1:5,2);
RLoad_1 = Test_1(1:5,1);
RFr_loss_1 = RCorr_Fr_A_1(1,1);
RI_1 = Test_1(1:5,8);

R_L_percent_1 = [RLoad_1.^4, RLoad_1.^3, RLoad_1.^2,...
                 RLoad_1, ones(size(RLoad_1))];

R_Eff_dir_1= R_L_percent_1 \ REff_1;

Eff_1 = Test_1(1:5,9);


R_Poly_fit_1 = polyval(R_Eff_dir_1,L_percent_fit);


Test_2 = Fif(2);

RStator_loss_2 = Test_2(1:5,3);
RRotor_loss_2 = Test_2(1:5,4);
RCore_loss_2 = Test_2(1:5,5);
```

```
RSLL_loss_2 = Test_2(1:5,6);
RCorr_Fr_A_2= Test_2(1:5,7);
REff_2 = Test_2(1:5,2);
RLoad_2 = Test_2(1:5,1);
RFr_loss_2 = RCorr_Fr_A_2(1,1);
RI_2 = Test_1(1:5,8);
R_L_percent_2 = [ RLoad_2.^4, RLoad_2.^3, RLoad_2.^2,...
                  RLoad_2, ones(size(RLoad_2))];

R_Eff_dir_2= R_L_percent_2 \ REff_2;



R_Poly_fit_2 = polyval(R_Eff_dir_2,L_percent_fit);
Eff_2 = Test_1(1:5,9);

Test_3 = Fif(3);

RStator_loss_3 = Test_3(1:5,3);
RRotor_loss_3 = Test_3(1:5,4);
RCore_loss_3 = Test_3(1:5,6);
RSLL_loss_3 = Test_3(1:5,5);
RCorr_Fr_A_3= Test_3(1:5,7);
REff_3 = Test_3(1:5,2);
RLoad_3 = Test_3(1:5,1);
RFr_loss_3 = RCorr_Fr_A_3(1,1);
RI_3 = Test_1(1:5,8);
R_L_percent_3 = [ RLoad_3.^4, RLoad_3.^3, RLoad_3.^2,...
                  RLoad_3, ones(size(RLoad_3))];

R_Eff_dir_3= R_L_percent_3 \ REff_3;



R_Poly_fit_3 = polyval(R_Eff_dir_3,L_percent_fit);

Test_4 = Fif(4);

RStator_loss_4 = Test_4(1:5,3);
RRotor_loss_4 = Test_4(1:5,4);
RCore_loss_4 = Test_4(1:5,6);
RSLL_loss_4 = Test_4(1:5,5);
RCorr_Fr_A_4= Test_4(1:5,7);
REff_4 = Test_4(1:5,2);
RLoad_4 = Test_4(1:5,1);
RFr_loss_4 = RCorr_Fr_A_4(1,1);
RI_4 = Test_1(1:5,8);
R_L_percent_4 = [ RLoad_4.^4, RLoad_4.^3, RLoad_4.^2,...
                  RLoad_4, ones(size(RLoad_4))];

R_Eff_dir_4= R_L_percent_4 \ REff_4;
R_Poly_fit_4 = polyval(R_Eff_dir_4,L_percent_fit);

Test_5 = Fiff(1);

RStator_loss_5 = Test_5(1:5,3);
RRotor_loss_5 = Test_5(1:5,4);
RCore_loss_5 = Test_5(1:5,6);
RSLL_loss_5 = Test_5(1:5,5);
RCorr_Fr_A_5= Test_5(1:5,7);
REff_5 = Test_5(1:5,2);
RLoad_5 = Test_5(1:5,1);
RFr_loss_5 = RCorr_Fr_A_5(1,1);
RI_5 = Test_1(1:5,8);
R_L_percent_5 = [RLoad_5.^4, RLoad_5.^3, RLoad_5.^2,...
                  RLoad_5, ones(size(RLoad_5))];

R_Eff_dir_5= R_L_percent_5 \ REff_5;



R_Poly_fit_5 = polyval(R_Eff_dir_5,L_percent_fit);

Test_6 = Fiff(2);

RStator_loss_6 = Test_6(1:5,3);
RRotor_loss_6 = Test_6(1:5,4);
RCore_loss_6 = Test_6(1:5,6);
RSLL_loss_6 = Test_6(1:5,5);
```

```
RCorr_Fr_A_6= Test_6(1:5,7);
REff_6 = Test_6(1:5,2);
RLoad_6 = Test_6(1:5,1);
RFr_loss_6 = RCorr_Fr_A_6(1,1);
RI_6 = Test_1(1:5,8);
R_L_percent_6 = [RLoad_6.^4, RLoad_6.^3, RLoad_6.^2,...
                 RLoad_6, ones(size(RLoad_6))];

R_Eff_dir_6= R_L_percent_6 \ REff_6;



R_Poly_fit_6 = polyval(R_Eff_dir_6,L_percent_fit);

Test_7 = Fiff(3);

RStator_loss_7 = Test_7(1:5,3);
RRotor_loss_7 = Test_7(1:5,4);
RCore_loss_7 = Test_7(1:5,6);
RSLL_loss_7 = Test_7(1:5,5);
RCorr_Fr_A_7= Test_7(1:5,7);
REff_7 = Test_7(1:5,2);
RLoad_7 = Test_7(1:5,1);
RFr_loss_7 = RCorr_Fr_A_7(1,1);
RI_7 = Test_1(1:5,8);
R_L_percent_7 = [RLoad_7.^4, RLoad_7.^3, RLoad_7.^2,...
                 RLoad_7, ones(size(RLoad_7))];

R_Eff_dir_7= R_L_percent_7 \ REff_7;



R_Poly_fit_7 = polyval(R_Eff_dir_7,L_percent_fit);

Test_8 = Fiff(4);

RStator_loss_8 = Test_8(1:5,3);
RRotor_loss_8 = Test_8(1:5,4);
RCore_loss_8 = Test_8(1:5,6);
RSLL_loss_8 = Test_8(1:5,5);
RCorr_Fr_A_8= Test_8(1:5,7);
REff_8 = Test_8(1:5,2);
RLoad_8 = Test_8(1:5,1);
RFr_loss_8 = RCorr_Fr_A_8(1,1);
RI_8 = Test_1(1:5,8);
R_L_percent_8 = [RLoad_8.^4, RLoad_8.^3, RLoad_8.^2,...
                 RLoad_8, ones(size(RLoad_8))];

R_Eff_dir_8= R_L_percent_8 \ REff_8;



R_Poly_fit_8 = polyval(R_Eff_dir_8,L_percent_fit);



figure (1)

p1 = plot(L_percent_fit,R_Poly_fit_1, 'b',...
    L_percent_fit,R_Poly_fit_2, 'b',...
    L_percent_fit,R_Poly_fit_3, 'b',...
    L_percent_fit,R_Poly_fit_4, 'r',...
    L_percent_fit,R_Poly_fit_5, 'b',...
    L_percent_fit,R_Poly_fit_6, 'b',...
    L_percent_fit,R_Poly_fit_7, 'b',...
    L_percent_fit,R_Poly_fit_8, 'r',...
    RLoad_1, REff_1, 'r*',...
    RLoad_2, REff_2, 'g*',...
    RLoad_3, REff_3, 'b*',...
    RLoad_5, REff_5, 'b*',...
    RLoad_6, REff_6, 'm*',...
    RLoad_7, REff_7, 'm*',...
    RLoad_8, REff_8, 'mo',...
    RLoad_4, REff_4, 'g*');
    set(p1, 'linewidth',2),...
    xlabel('Loading (%)'), ylabel('Efficiency (p.u)')
    title('Effiency for 15kW motor')
    grid on;
```

```
Eff_IEC_1 = Test_1(1:5,15);
Eff_dir_1_IEC= R_L_percent_1 \ Eff_IEC_1;
R_Poly_fit_1_IEC = polyval(Eff_dir_1_IEC,L_percent_fit);

Eff_IEC_2 = Test_2(1:5,15);
Eff_dir_2_IEC= R_L_percent_2 \ Eff_IEC_2;
R_Poly_fit_2_IEC = polyval(Eff_dir_2_IEC,L_percent_fit);

Eff_IEC_3 = Test_3(1:5,15);
Eff_dir_3_IEC= R_L_percent_3 \ Eff_IEC_3;
R_Poly_fit_3_IEC = polyval(Eff_dir_3_IEC,L_percent_fit);

Eff_IEC_4 = Test_4(1:5,15);
Eff_dir_4_IEC= R_L_percent_4 \ Eff_IEC_4;
R_Poly_fit_4_IEC = polyval(Eff_dir_4_IEC,L_percent_fit);

Eff_IEC_5 = Test_5(1:5,15);
Eff_dir_5_IEC= R_L_percent_5 \ Eff_IEC_5;
R_Poly_fit_5_IEC = polyval(Eff_dir_5_IEC,L_percent_fit);

Eff_IEC_6 = Test_6(1:5,15);
Eff_dir_6_IEC= R_L_percent_6 \ Eff_IEC_6;
R_Poly_fit_6_IEC = polyval(Eff_dir_6_IEC,L_percent_fit);

Eff_IEC_7 = Test_7(1:5,15);
Eff_dir_7_IEC= R_L_percent_7 \ Eff_IEC_7;
R_Poly_fit_7_IEC = polyval(Eff_dir_7_IEC,L_percent_fit);

Eff_IEC_8 = Test_8(1:5,15);
Eff_dir_8_IEC= R_L_percent_8 \ Eff_IEC_8;
R_Poly_fit_8_IEC = polyval(Eff_dir_8_IEC,L_percent_fit);

  figure (3)
p1 = plot(L_percent_fit,R_Poly_fit_1_IEC, 'b',...
    L_percent_fit,R_Poly_fit_2_IEC, 'b',...
    L_percent_fit,R_Poly_fit_3_IEC, 'b',...
    L_percent_fit,R_Poly_fit_4_IEC, 'r',...
    L_percent_fit,R_Poly_fit_5_IEC, 'b',...
    L_percent_fit,R_Poly_fit_6_IEC, 'b',...
    L_percent_fit,R_Poly_fit_7_IEC, 'b',...
    L_percent_fit,R_Poly_fit_8_IEC, 'b',...
    RLoad_1, Eff_IEC_1, 'r^',...
    RLoad_2, Eff_IEC_2, 'g^',...
    RLoad_3, Eff_IEC_3, 'k^',...
    RLoad_5, Eff_IEC_5, 'b^',...
    RLoad_6, Eff_IEC_6, 'y^',...
    RLoad_7, Eff_IEC_7, 'm^',...
    RLoad_8, Eff_IEC_8, 'm^',...
    RLoad_4, Eff_IEC_4, 'c^');
    set(p1,'linewidth',2),...
    xlabel('Loading (%)'), ylabel('Efficiency (p.u)')
    title('Effiency for 15kW motor')
    grid on;

     figure (4)

p1 = plot(L_percent_fit,R_Poly_fit_1_IEC, 'b',...
    L_percent_fit,R_Poly_fit_2_IEC, 'b',...
    L_percent_fit,R_Poly_fit_3_IEC, 'b',...
    L_percent_fit,R_Poly_fit_4_IEC, 'r',...
    L_percent_fit,R_Poly_fit_8_IEC, 'b',...
    RLoad_1, Eff_IEC_1, 'r^',...
    RLoad_2, Eff_IEC_2, 'g^',...
    RLoad_3, Eff_IEC_3, 'k^',...
    RLoad_8, Eff_IEC_8, 'm^',...
    RLoad_4, Eff_IEC_4, 'c^');
    set(p1,'linewidth',2),...
    xlabel('Loading (%)'), ylabel('Efficiency (p.u)')
    title('Effiency for 15kW motor')
    grid on;


    figure (2)

p1 = plot(L_percent_fit,R_Poly_fit_3, 'b',...
    L_percent_fit,R_Poly_fit_4, 'b',...
    L_percent_fit,R_Poly_fit_8, 'b',...
```

```
    L_percent_fit,R_Poly_fit_1, 'k',...
    L_percent_fit,R_Poly_fit_2, 'k',...
    RLoad_3, REff_3, 'bo',...
    RLoad_1, REff_1, 'bo',...
    RLoad_2, REff_2, 'r^',...
    RLoad_4, REff_4, 'r^',...
    RLoad_8, REff_8, 'r^');
    set(pl,'LineWidth',2),...
    xlabel('Loading (%)'), ylabel('Efficiency (p.u)' )
    title('Efficiency for 15kW motor')
    grid on;

% f_LL full

%
%              k      Blue           .      point              -      solid
%              g      green          o      circle             :      dotted
%              r      red            x      x-mark             -.     dashdot
%              c      cyan           +      plus               --     dashed
%              m      magenta        *      star             (none)   no line
%              y      yellow         s      square
%              k      black          d      diamond
%                                    v      triangle (down)
%                                    ^      triangle (up)
%                                    <      triangle (left)
%                                    >      triangle (right)
%                                    p      pentagram
%                                    h      hexagram
```

APPENDIX E

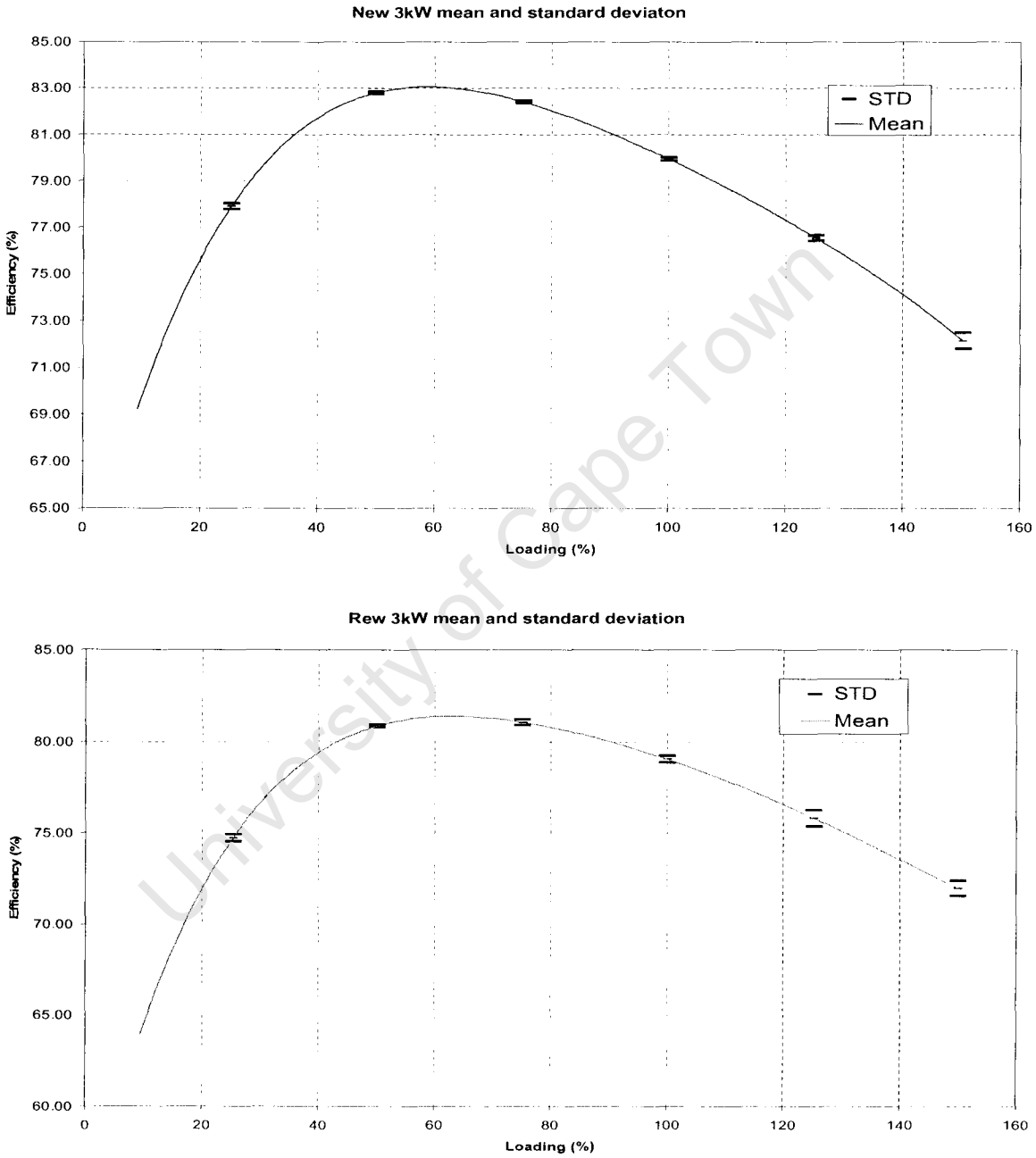

Figure H 1: Variation or Standard deviation of repeated test before and after rewind of 3kW motor

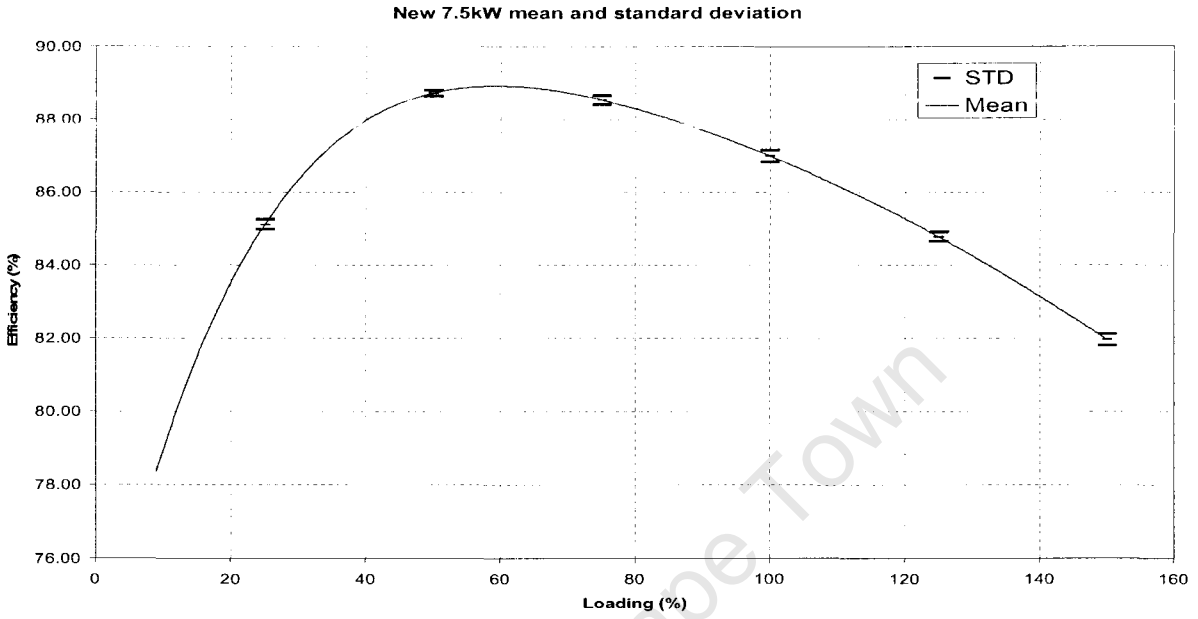

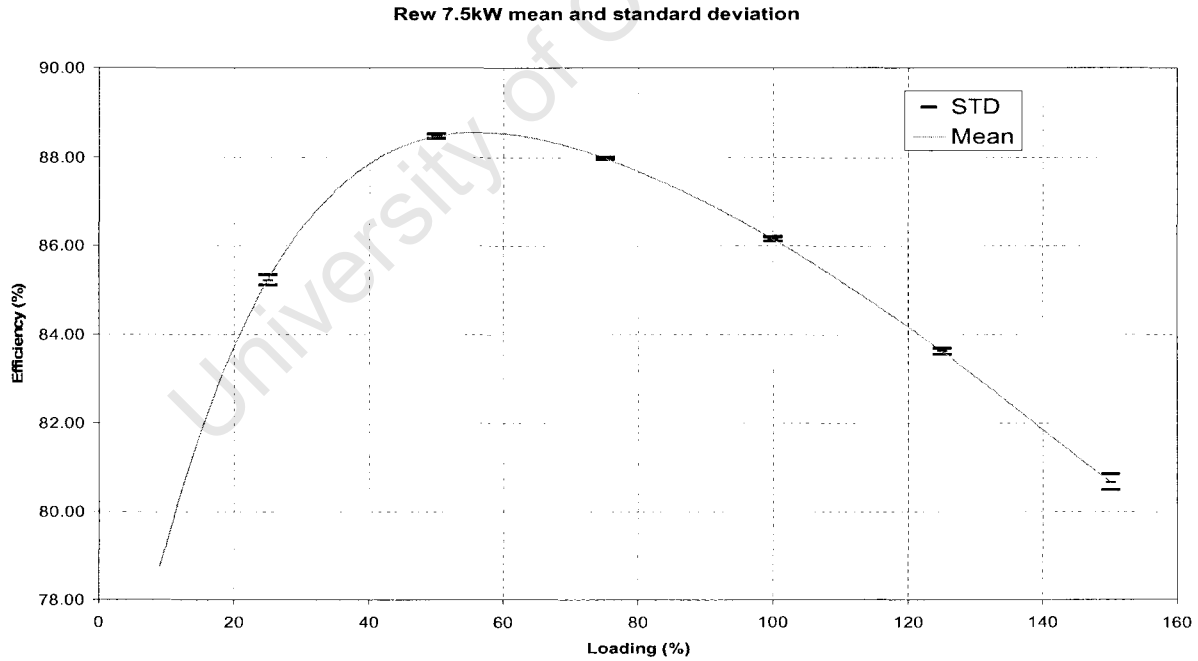

Figure H 2: Variation or Standard deviation of repeated test before and after rewind of 7.5kW motor

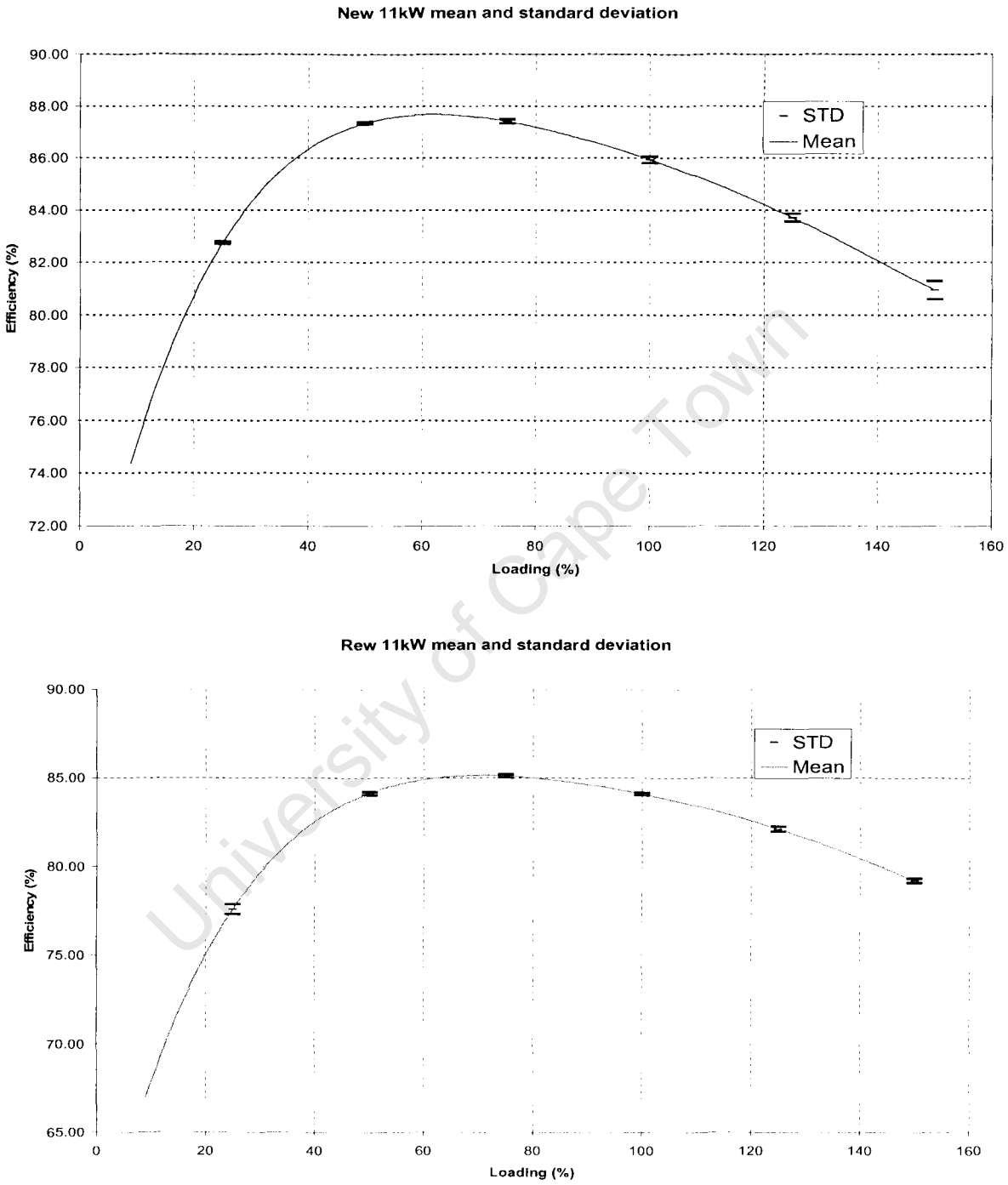

Figure H 3: Variation or Standard deviation of repeated test before and after rewind of 11kW motor

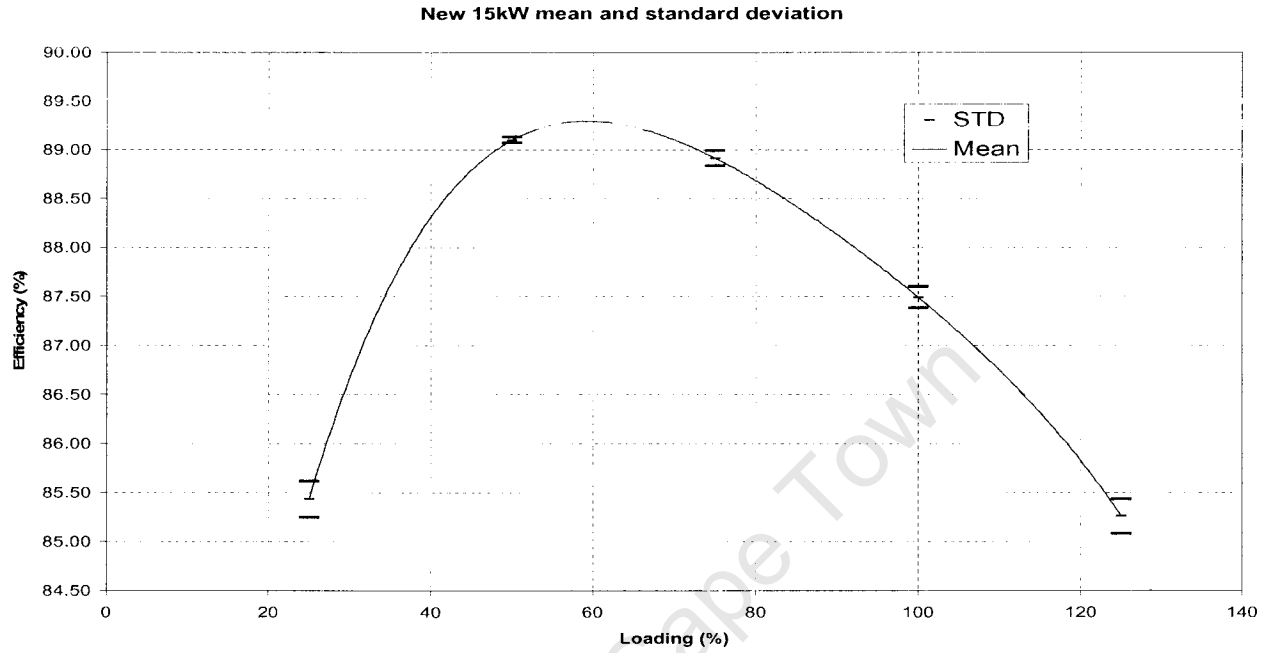

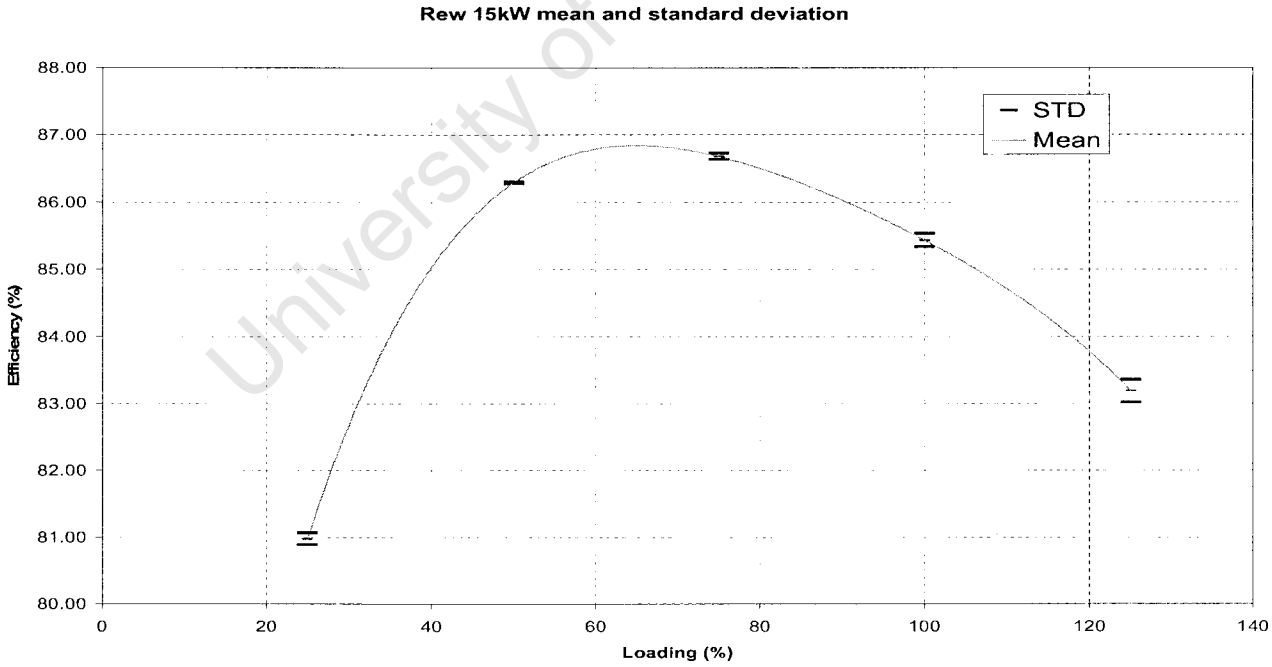

Figure H 4: Variation or Standard deviation of repeated test before and after rewind of 15kW motor

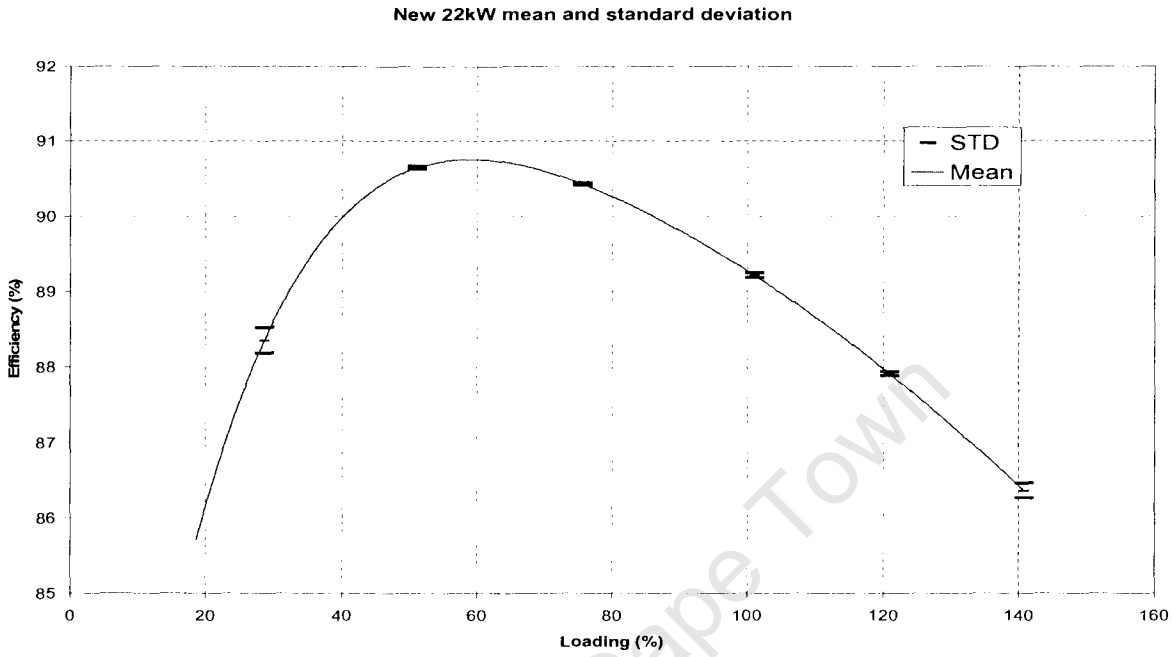

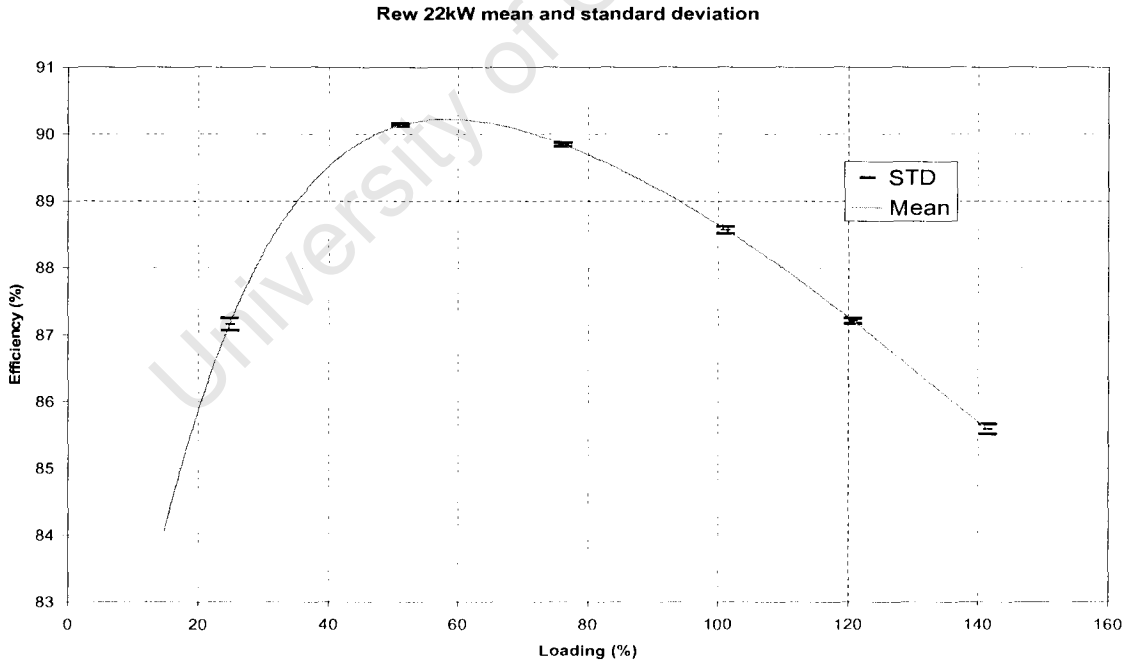

Figure H 5: Variation or Standard deviation of repeated test before and after rewind of 22kW motor

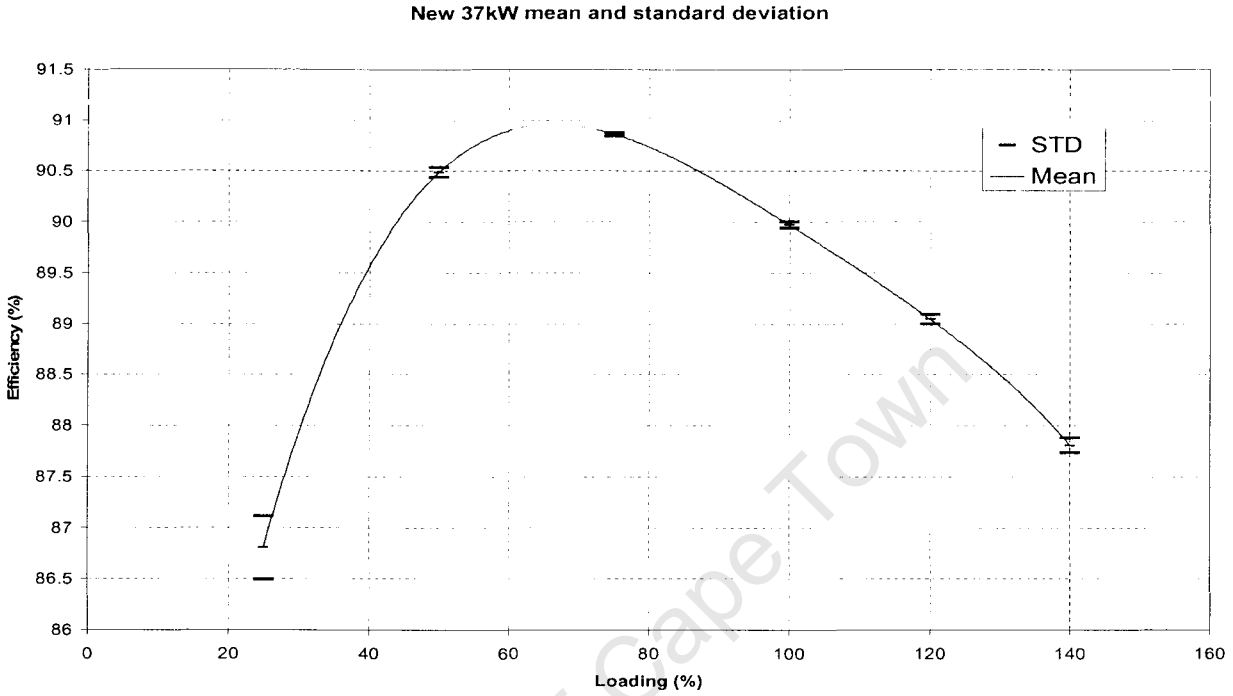

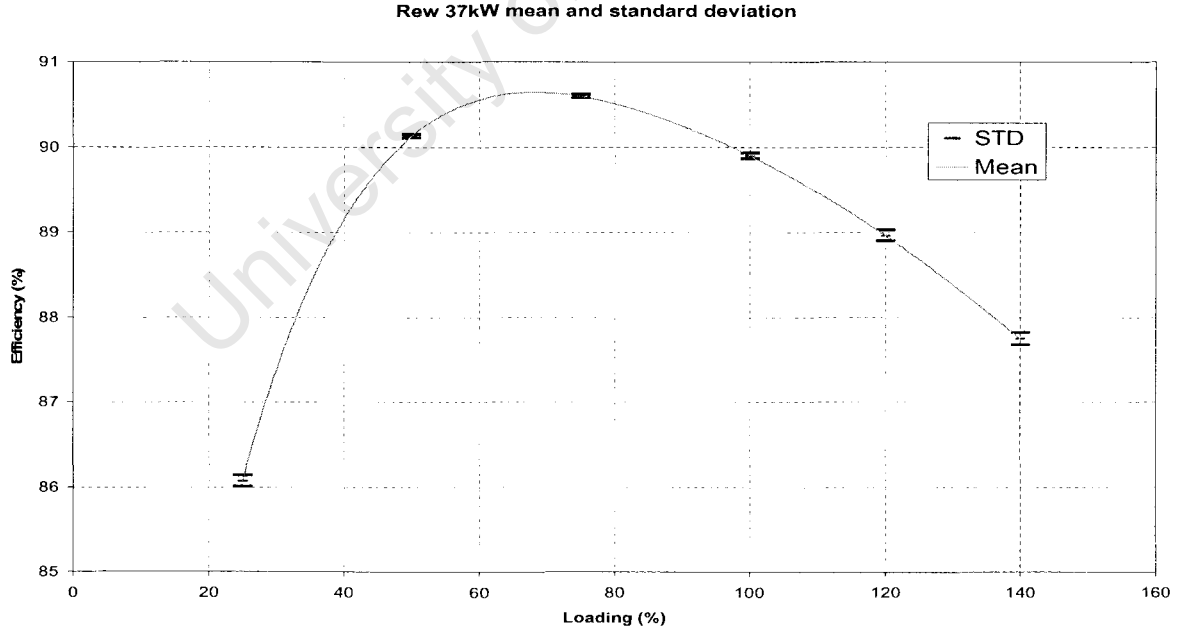

Figure H 6: Variation or Standard deviation of repeated test before and after rewind of 37kW motor

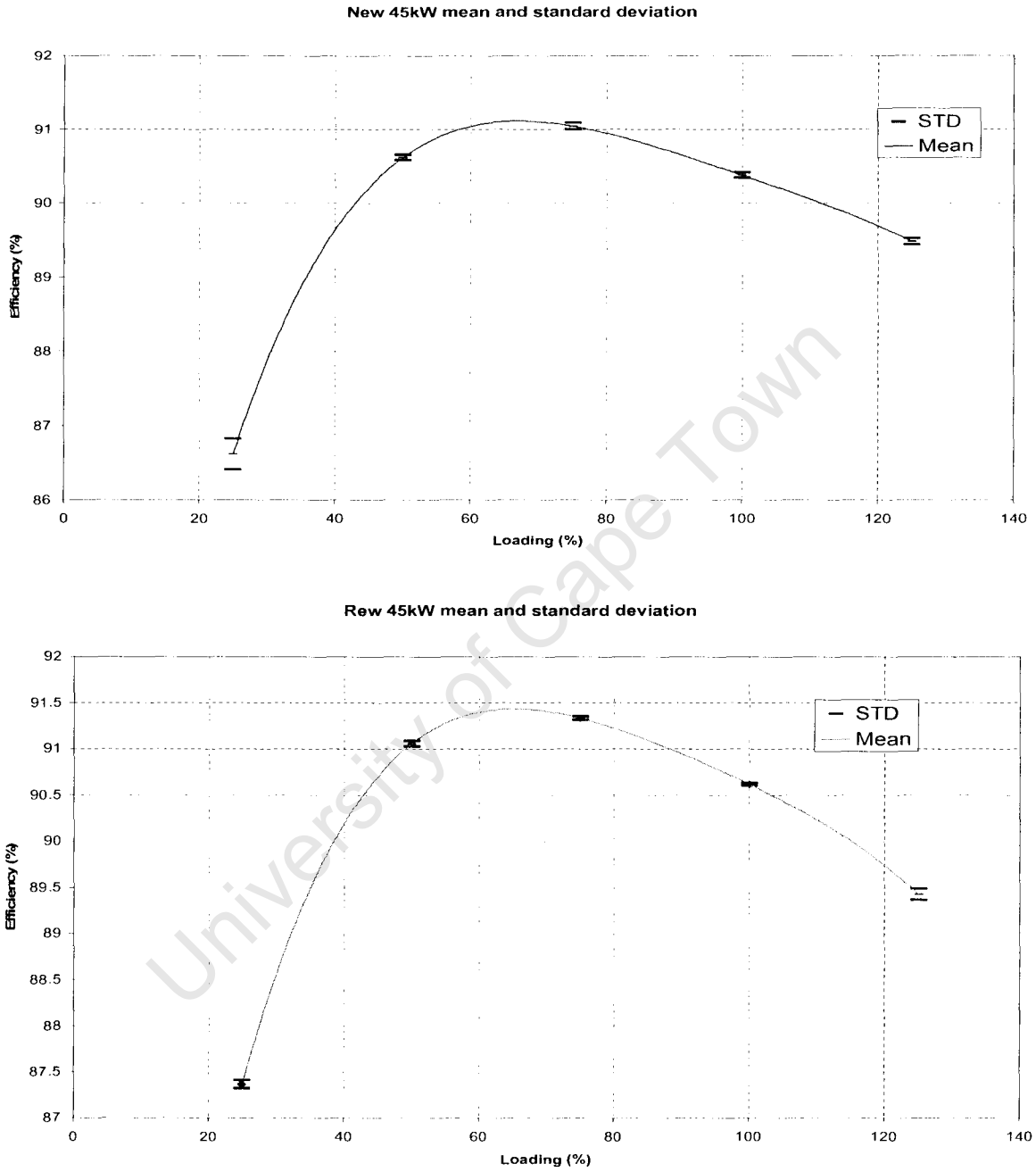

Figure H 7: Variation or Standard deviation of repeated test before and after rewind of 45kW motor

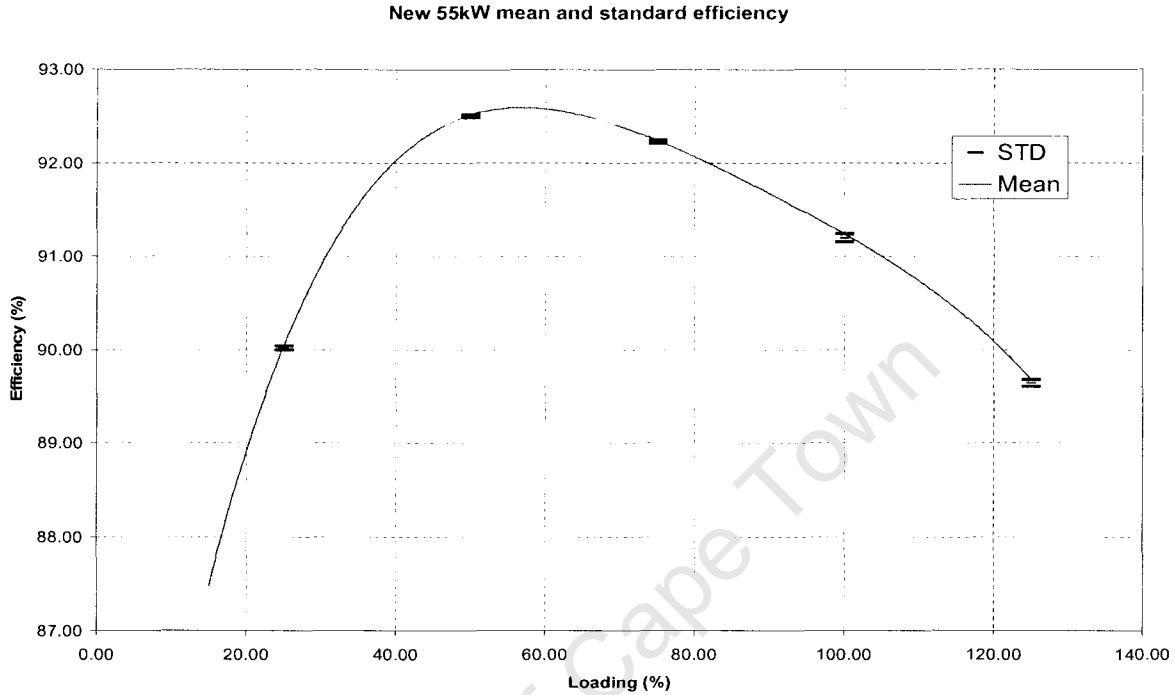

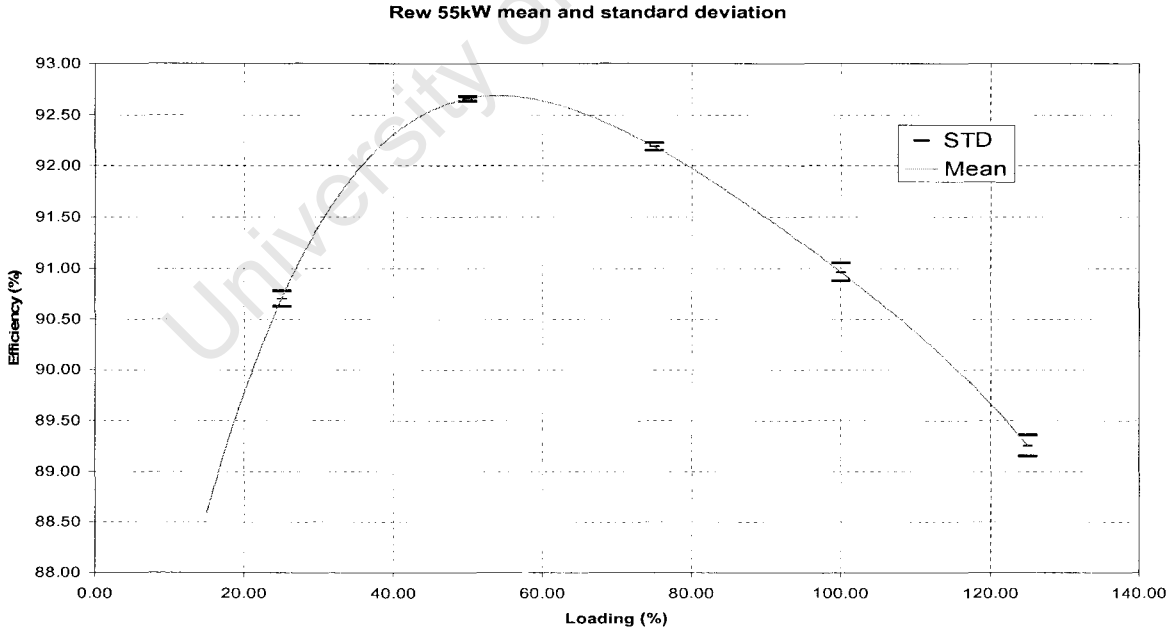

Figure H 8: Variation or Standard deviation of repeated test before and after rewind of 55kW motor

APPENDIX F

Motor parameters

The equivalent circuit parameters of three motors (7.5, 11 and 15kW) before and after rewinding.

Figure F1 shows the equivalent circuit used.

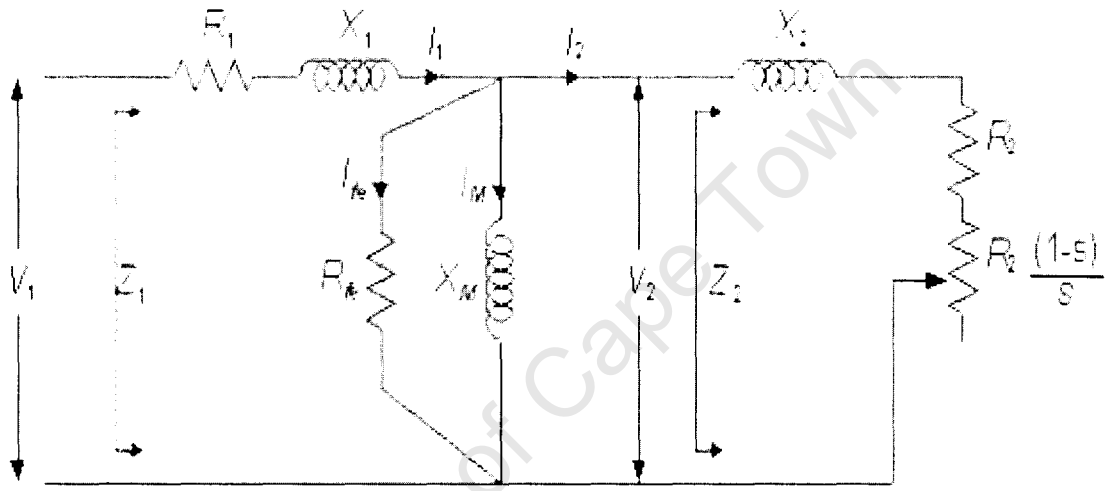

Figure F1: Equivalent circuit

The parameters were calculated from no-load and blocked rotor tests on each motor. The changes in motor parameters due to rewinding are shown in Table F1.

Table F1: Change and percentage change of motor parameters

Motor Parameter	Motor rating								
	7.5kW			11kW			15kW		
	Before	After	% Change	Before	After	% Change	Before	After	% Change
Xm	120.38	117.32	**-2.54**	66.37	62.71	**-5.52**	54.07	53.78	**-0.53**
Rfe	2027.9	1956.1	**-3.54**	1066.7	625.13	**-41.40**	1079.9	585	**-45.83**
X1	4.1812	4.2159	**0.83**	3.0107	3.2032	**6.39**	2.3704	2.3763	**0.25**
R1	2.407	2.515	**4.49**	1.2899	1.3536	**4.94**	0.875	0.935	**6.86**
X2	4.1821	4.2109	**0.69**	3.0065	3.1993	**6.41**	2.3704	2.3715	**0.05**
R2	1.8666	1.6505	**-11.58**	1.68	1.8116	**7.83**	1.5309	1.3959	**-8.82**

Loss comparison of Loss Segregation vs Equivalent Circuit methods

Table F2: 7.5kW

Loading (%)	Loss Seg	Equiv	Loss Seg	Equiv	Loss Seg	Equiv	Loss Seg	Equiv	Loss Seg	Equiv
	Stator (W)		Rotor (W)		Core (W)		SLL (W)		F&W (W)	
150	1311.98	1005.44	681.44	659.54	230.07	200.13	236.94	168.59	47.5	**49.442**
125	884.57	707.13	446.22	445.55	191.68	204.58	164.54	138.57		
100	569.06	477.45	270.44	281.25	168.68	209.05	105.31	110.09		
75	341.81	298.941	146.45	154.08	160.34	213.78	59.24	81.49		
50	192.33	179.01	64.87	69.29	164.84	218.44	26.33	54.64		
25	106	103.97	17.57	17.12	181.32	223.43	6.58	27.16		

Table F2: 11kW

Loading (%)	Loss Seg	Equiv	Loss Seg	Equiv	Loss Seg	Equiv	Loss Seg	Equiv	Loss Seg	Equiv
	Stator (W)		Rotor (W)		Core (W)		SLL (W)		F&W (W)	
150	1896.38	1186.09	1101.25	1215.28	337.98	402.38	548.12	353.80	71.44	71.906
125	1274.58	854.74	717.52	825.67	309.62	408.65	380.64	291.63		
100	818.79	602.43	428.9	530.05	294.57	414.92	243.61	233.66		
75	499.79	394.08	230.72	287.29	295.54	422.03	137.03	172.02		
50	291.47	254.53	100.89	126.34	311.03	429.11	60.9	114.08		
25	172.49	171.13	26.66	32.30	342.37	436.40	15.23	57.68		

Table F2: 15kW

Loading (%)	Loss Seg	Equiv	Loss Seg	Equiv	Loss Seg	Equiv	Loss Seg	Equiv	Loss Seg	Equiv
	Stator (W)		Rotor (W)		Core (W)		SLL (W)		F&W (W)	
125	1433.8	1426.92	939.98	1051.23	355.46	406.13	370.81	547.66	104.42	81.65
100	914.32	891.49	564.35	713.64	344.95	411.85	237.32	432.88		
75	550.32	495.82	303.64	463.16	343.12	417.79	133.49	322.83		
50	309.24	217.72	130.65	285.84	350.13	424.13	59.33	213.93		
25	170.61	55.35	33.4	180.62	365.97	430.73	14.83	107.86		

APPENDIX G

Cape Town

Cape Town.
021 555 8660

Henry du Preez & Associates
P.O. Box 552050
Benmore
2010, South Africa
Phone: 27-11-783 9762
Fax: 27-11-783 9762

Type: 800 A Core Tester.

Core Tests.

Job No.	803128				
Make:	WEG				
Rate kW:	7.5	kW.		h.p.	10.1
Rated Voltage:	380	Volts.			
Rated Speed:	1450	r.p.m.		No. Poles	4.137931
Rated Current:	15.1	Amps.			
Frequency:	50	Hz			
Serial No.	07FEV08				

MOTOR DIMENSIONS:

Core Length:	120	mm.	**Stacking Factor:**	0.95	0.95
No. of Air Ducts:			**If no Stacking Factor is entered then computer will**		
Air duct Length:		mm.	**default to 0.95 as a value.**		
Internal Diameter:	150	mm.			
External Diameter:	220	mm.	**Back Iron Flux Density:**	1.2	1.2
			If no density is stated a density of 1.2 Tesla		
Depth of Slots:	15.0	mm.	**will be used as a default value.**		

Remarks:

Core Area: (Back Iron.) 2280 Sq. mm.

Using the core dimensions and assumed back iron core flux density.

Volts per turn: 0.607392 Volts.

0
20

Core Mass: (Yoke only).

Yoke **"H"** 20 **Iron Length:** 628.3 mm
(Circumferential)

Mass: (Yoke) 10.396948 kg.

Power: **Watts.** 84 **(as read on the core tester Watt meter).**

Current: 116 **amps** **Iron Loss** 64.4888 **Watts**

Loss per kg. 6.2026663 **w /kg.**

W/kg.		
upto 5	Good	do further tests
5 to 8	Acceptable	Check for mechanical damage
8 to 12	further tests	Acceptable
Above 12	Reject.	

Result: *do further tests*

Optional: **Watts per kg/Current vs Flux.**

Volts/turn.	Watts	Current	Flux -Tesla.	Watts/kg.	Current Amps
0.6	84	116	1.18539592	7.04391314	116
			0	0	0
			0	0	0
			0	0	0
			0	0	0
			0	0	0

Watts in Iron
73.2352
0
0
0
0
0

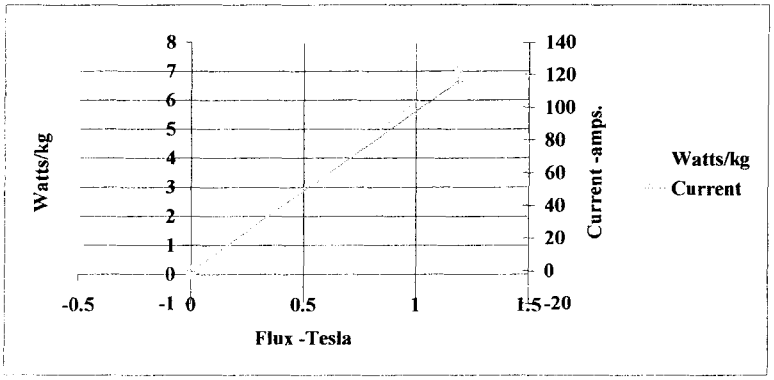

Cape Town

Cape Town.
021 555 8660

Henry du Preez & Associates
P.O. Box 652060 CC.
Benmore
2010 South Africa
Phone: 27-11-783 9762
Fax: 27-11-783 9762

Type: 800 A Core Tester.

Core Tests.

Job No.	8031333				
Make:	WEG				
Rate kW:	11.0	kW.		h.p.	14.7
Rated Voltage:	380	Volts.			
Rated Speed:	1455	r.p.m.		No. Poles	4.1237113
Rated Current:	22.9	Amps.			
Frequency:	50	Hz			
Serial No.	16MA108				

MOTOR DIMENSIONS:

Core Length:	155	mm.	**Stacking Factor:**	0.95	0.95
No. of Air Ducts:			**If no Stacking Factor is entered then computer will**		
Air duct Length:		mm.	**default to 0.95 as a value.**		
Internal Diameter:	158	mm.			
External Diameter:	242	mm.	**Back Iron Flux Density:**	1.2	1.2
			If no density is stated a density of 1.2 Tesla		
Depth of Slots:	17.0	mm.	**will be used as a default value.**		

Remarks:

Core Area: (Back Iron.) 3681.25 **Sq. mm.**

Using the core dimensions and assumed back iron core flux density.

Volts per turn: 0.980685 **Volts.** 0

25

Core Mass: (Yoke only).

Yoke **"H"** 25 **Iron Length:** 681.706 mm
(Circumferential)

Mass: (Yoke) 18.147826 **kg.**

Power: **Watts.** 345 **(as read on the core tester Watt meter).**

Current: 261 **amps** **Iron Loss** 246.22455 **Watts**

Loss per kg. 13.567716 **w /kg.**

W/kg.		
upto 5	Good	do further tests
5 to 8	Acceptable	Check for mechanical damage
8 to 12	further tests	Acceptable
Above 12	Reject.	

Result: *Reject*

Optional: **Watts per kg/Current vs Flux.**

Volts/turn.	Watts	Current	Flux -Tesla.	Watts/kg.	Current Amps
0.98	345	261	1.19916181	16.0076031	261
			0	0	0
			0	0	0
			0	0	0
			0	0	0
			0	0	0

Watts in Iron
290.5032
0
0
0
0
0

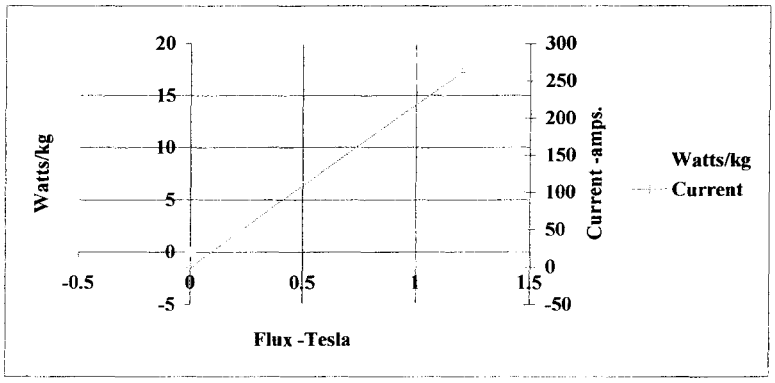

Cape Town

Cape Town.
021 555 8660

Henry du Preez & Associates
P.O. Box 652050,
Benmore
2010, South Africa
Phone: 27-11-783 5792
Fax: 27-11-783 5762

Type: 800 A Core Tester.

Core Tests.

Job No.	8031326				
Make:	WEG				
Rate kW:	15.0	kW.		h.p.	20.1
Rated Voltage:	380	Volts.			
Rated Speed:	1455	r.p.m.		No. Poles	4.1237113
Rated Current:	30.0	Amps.			
Frequency:	50	Hz			
Serial No.	4754/6862				

MOTOR DIMENSIONS:

Core Length:	212	mm.	**Stacking Factor:**	0.95	0.95
No. of Air Ducts:			**If no Stacking Factor is entered then computer will**		
Air duct Length:		mm.	**default to 0.95 as a value.**		
Internal Diameter:	160	mm.			
External Diameter:	240	mm.	**Back Iron Flux Density:**	1.2	1.2
			If no density is stated a density of 1.2 Tesla		
Depth of Slots:	20.0	mm.	**will be used as a default value.**		

Remarks:

Core Area: (Back Iron.) 4028 **Sq. mm.**

Using the core dimensions and assumed back iron core flux density.

Volts per turn: 1.0730592 **Volts.** 0

20

Core Mass: (Yoke only).

Yoke **"H"** 20 **Iron Length:** 691.13 **mm**
(Circumferential)

Mass: (Yoke) 19.857234 **kg.**

Power: **Watts.** 314 **(as read on the core tester Watt meter).**

Current: 233 **amps** **Iron Loss** 235.28095 **Watts**

Loss per kg. 11.848626 **w /kg.**

W/kg.		
upto 5	Good	
5 to 8	Acceptable	Check for mechanical damage
8 to 12	further tests	Acceptable
Above 12	Reject.	

do further tests

Result: *do further tests*

Optional: **Watts per kg/Current vs Flux.**

Volts/turn.	Watts	Current	Flux -Tesla.	Watts/kg.	Current Amps
1.07	314	233	1.1965789	13.6257041	233
			0	0	0
			0	0	0
			0	0	0
			0	0	0
			0	0	0

Watts in Iron
270.5688
0
0
0
0
0

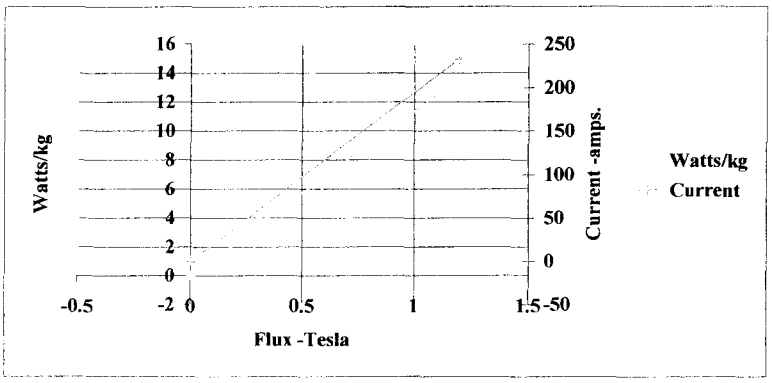

Cape Town

Cape Town.
021 555 8660

Henry du Preez & Associates
P.O. Box 852359
Bramley
2019 South Africa
Phone 27-11-783-9762
Fax 27-11-783-9762

Type: 800 A Core Tester.

Core Tests.

Job No.	8031399				
Make:	WEG				
Rate kW:	37.0	kW.		h.p.	49.6
Rated Voltage:	380	Volts.			
Rated Speed:	1470	r.p.m.		No. Poles	4.0816327
Rated Current:	40.4	Amps.			
Frequency:	50	Hz			
Serial No.	1.002E+09				

MOTOR DIMENSIONS:

Core Length:	160	mm.	**Stacking Factor:**	0.95	0.95
No. of Air Ducts:			**If no Stacking Factor is entered then computer will**		
Air duct Length:		mm.	**default to 0.95 as a value.**		
Internal Diameter:	260	mm.			
External Diameter:	360	mm.	**Back Iron Flux Density:**	1.2	1.2
			If no density is stated a density of 1.2 Tesla		
Depth of Slots:	20.0	mm.	**will be used as a default value.**		

Remarks:

Core Area: (Back Iron.) 4560 **Sq. mm.**

Using the core dimensions and assumed back iron core flux density.

Volts per turn: 1.214784 **Volts.** 0

30

Core Mass: (Yoke only).

Yoke **"H"** 30 **Iron Length:** 1036.7 **mm**
(Circumferential)

Mass: (Yoke) 34.843826 **kg.**

Power: **Watts.** 358 **(as read on the core tester Watt meter).**

Current: 226 **amps** **Iron Loss** 283.9398 **Watts**

Loss per kg. 8.1489271 **w /kg.**

W/kg.		
upto 5	Good	
5 to 8	Acceptable	Check for mechanical damage
8 to 12	further tests	Acceptable
Above 12	Reject.	

do further tests

Result: *do further tests*

Optional: **Watts per kg/Current vs Flux.**

Volts/turn.	Watts	Current	Flux -Tesla.	Watts/kg.	Current Amps
1.21	358	226	1.19527422	9.10173287	226
			0	0	0
			0	0	0
			0	0	0
			0	0	0
			0	0	0

Watts in Iron
317.1392
0
0
0
0
0

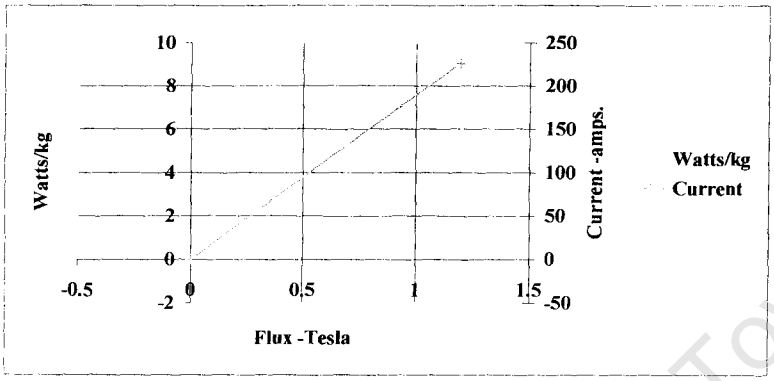

Cape Town

Cape Town.
021 555 8660

Henry du Preez & Associates
P.O. Box 652050
Benmore
2010, South Africa
Phone: 27-11-783 9762
Fax: 27-11-783 9762

Type: 800 A Core Tester.

Core Tests.

Job No.	8031327				
Make:	WEG				
Rate kW:	45.0	kW.		h.p.	60.3
Rated Voltage:	380	Volts.			
Rated Speed:	1475	r.p.m.		No. Poles	4.0677966
Rated Current:	81.5	Amps.			
Frequency:	50	Hz			
Serial No.	03SET07				

MOTOR DIMENSIONS:

Core Length:	195	mm.	**Stacking Factor:**	0.95	0.95
No. of Air Ducts:			**If no Stacking Factor is entered then computer will**		
Air duct Length:		mm.	**default to 0.95 as a value.**		
Internal Diameter:	260	mm.			
External Diameter:	375	mm.	**Back Iron Flux Density:**	1.2	1.2
			If no density is stated a density of 1.2 Tesla		
Depth of Slots:	20.0	mm.	**will be used as a default value.**		

Remarks:

Core Area: (Back Iron.) 6946.875 **Sq. mm.**

Using the core dimensions and assumed back iron core flux density.

Volts per turn: 1.8506475 **Volts.**

0
37.5

Core Mass: (Yoke only).

Yoke **"H"** 37.5 **Iron Length:** 1060.26 **mm**
(Circumferential)

Mass: (Yoke) 54.366643 **kg.**

Power: **Watts.** 540 **(as read on the core tester Watt meter).**

Current: 273 **amps** **Iron Loss** 431.93295 **Watts**

Loss per kg. 7.9448155 **w /kg.**

W/kg.		
upto 5	Good	
5 to 8	Acceptable	Check for mechanical damage
8 to 12	further tests	Acceptable
Above 12	Reject.	

do further tests

Result: *do further tests*

Optional: **Watts per kg/Current vs Flux.**

Volts/turn.	Watts	Current	Flux -Tesla.	Watts/kg.	Current Amps
1.8	540	273	1.16715906	8.83587383	273
			0	0	0
			0	0	0
			0	0	0
			0	0	0
			0	0	0

Watts in Iron
480.3768
0
0
0
0
0

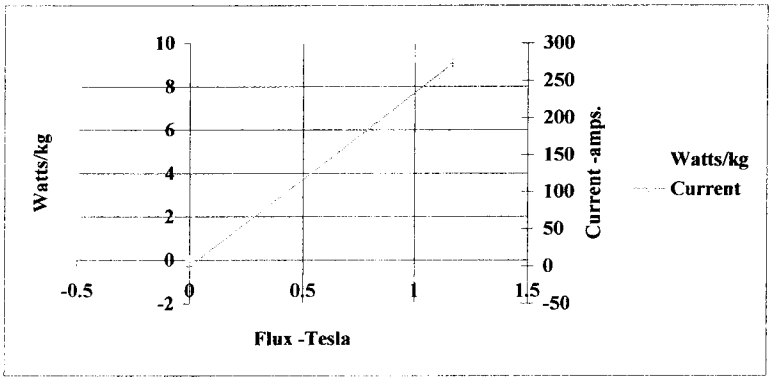

Cape Town

Cape Town.
021 555 8660

Henry du Preez & Associates
P.O. Box 552950
Benmore
2010 South Africa
Phone: 27-11-783 9762
Fax: 27-11-783 9762

Type: 800 A Core Tester.

Core Tests.

Job No.	8031332				
Make:	WEG				
Rate kW:	55.0	kW.		h.p.	73.7
Rated Voltage:	380	Volts.			
Rated Speed:	1470	r.p.m.		No. Poles	4.0816327
Rated Current:	99.6	Amps.			
Frequency:	50	Hz			
Serial No.	27AG007				

MOTOR DIMENSIONS:

Core Length:	255	mm.	**Stacking Factor:**	0.95	0.95
No. of Air Ducts:			**If no Stacking Factor is entered then computer will**		
Air duct Length:		mm.	**default to 0.95 as a value.**		
Internal Diameter:	260	mm.			
External Diameter:	375	mm.	**Back Iron Flux Density:**	1.2	1.2
			If no density is stated a density of 1.2 Tesla		
Depth of Slots:	20.0	mm.	**will be used as a default value.**		

Remarks:

Core Area: (Back Iron.) 9084.375 **Sq. mm.**

Using the core dimensions and assumed back iron core flux density.

Volts per turn: 2.4200775 **Volts.**

0
37.5

Core Mass: (Yoke only).

Yoke **"H"** 37.5 **Iron Length:** 1060.26 **mm**
(Circumferential)

Mass: (Yoke) 71.094841 **kg.**

Power: **Watts.** 292 **(as read on the core tester Watt meter).**

Current: 175 **amps** **Iron Loss** 247.59375 **Watts**

Loss per kg. 3.4825839 **w /kg.**

W/kg.		
upto 5	Good	Good Core
5 to 8	Acceptable	Check for mechanical damage
8 to 12	further tests	Acceptable
Above 12	Reject.	

Result: *Good Core*

Optional: **Watts per kg/Current vs Flux.**

Volts/turn.	Watts	Current	Flux -Tesla.	Watts/kg.	Current Amps
2.4	292	175	1.19004453	3.76257962	175
			0	0	0
			0	0	0
			0	0	0
			0	0	0
			0	0	0

Watts in Iron
267.5
0
0
0
0
0

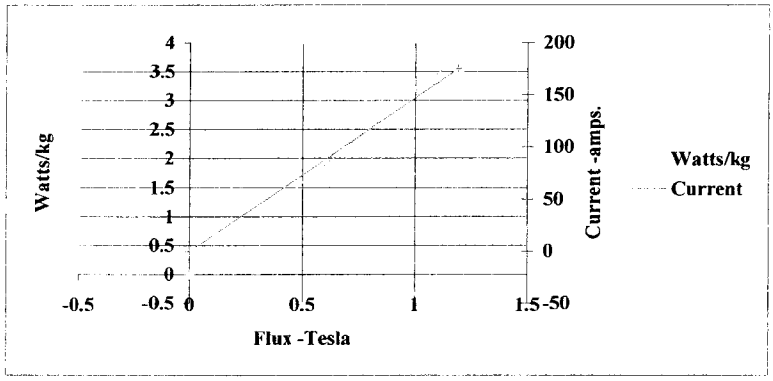

APPENDIX H

3kW motor-LHM

Efficiency

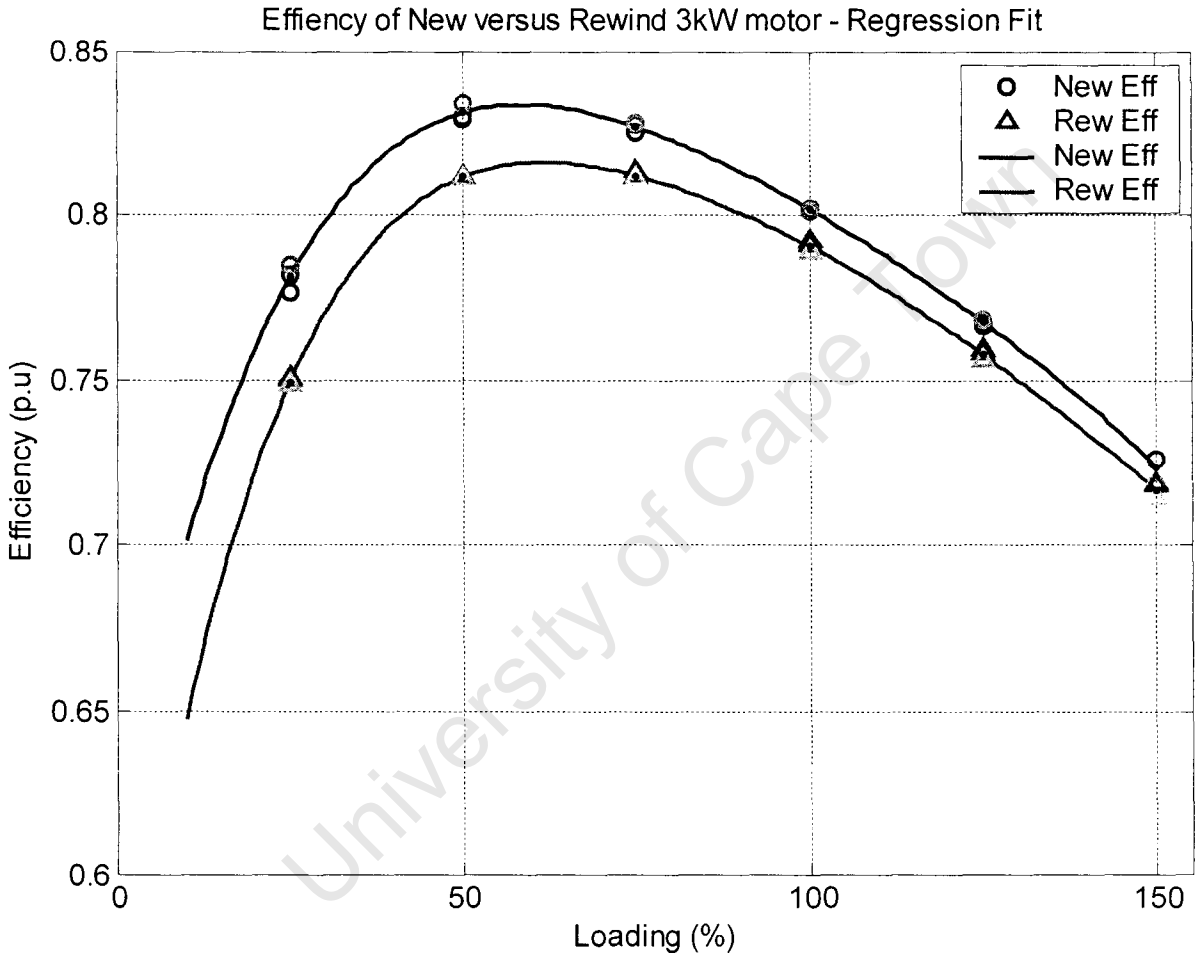

Motor loss

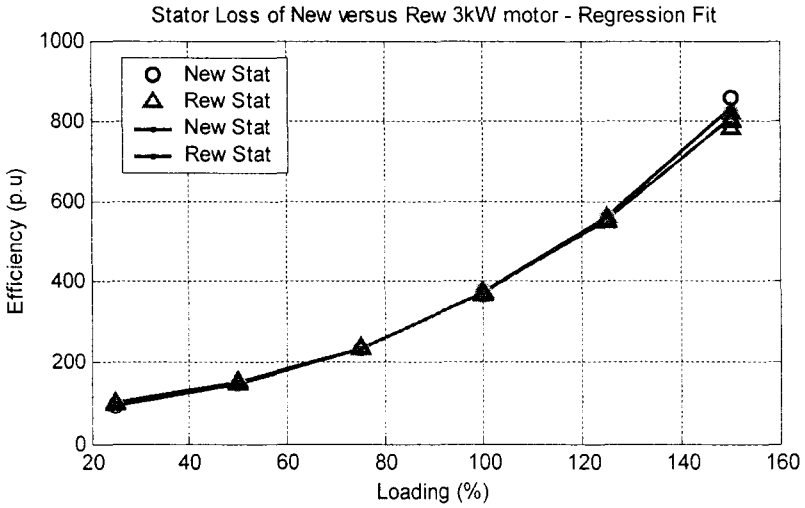

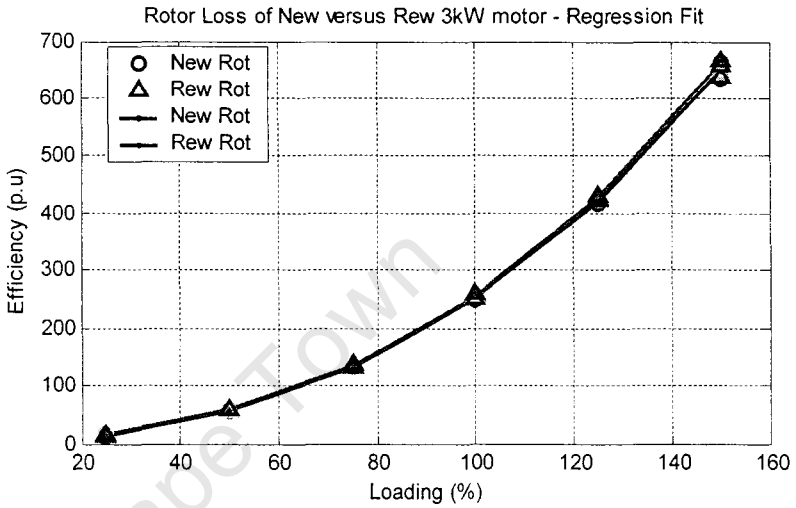

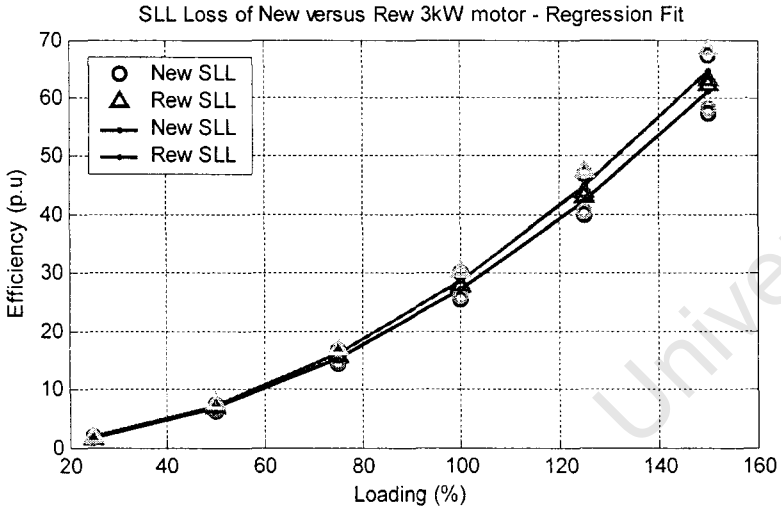

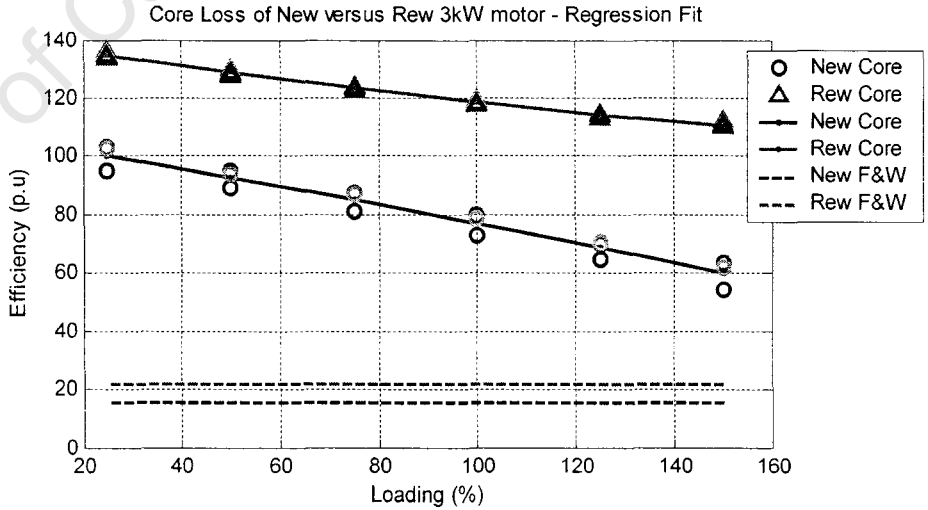

Efficiency

Loading (%)	New	Rew	Change (%)
	Eff (%)		
150	72.24	71.89	-0.35
125	76.80	75.95	-0.85
100	80.16	79.19	-0.97
75	82.66	81.28	-1.38
50	83.16	81.16	-2.00
25	78.08	75.10	-2.98

Motor loss

Loading (%)	New	Rew	New	Rew	New	Rew	New	Rew	New	Rew
	Stator (W)		Rotor (W)		Core (W)		SLL (W)		F&W (W)	
150	831.05	805.42	648.91	663.18	59.95	110.52	61.03	67.81	15.30	22.00
125	560.85	553.68	418.73	429.04	68.56	114.07	42.38	47.09		
100	372.80	370.41	251.48	256.12	76.96	118.56	27.12	30.14		
75	234.27	236.93	131.95	135.81	85.01	123.11	15.26	16.95		
50	147.26	150.81	57.26	58.29	92.78	128.50	6.78	7.53		
25	95.13	100.92	14.42	15.21	100.21	134.26	1.70	1.88		

Speed		Torque		Stator Current	
New	Rew	New	Rew	New	Rew
1313	1303	29.65	30.9	9.82	10.15
1356	1347	24.66	25.8	8.07	8.51
1391	1387	19.77	20.6	6.65	6.95
1424	1421	14.88	15.5	5.32	5.62
1451	1449	9.79	10.3	4.27	4.55
1478	1473	4.99	5.2	3.47	3.76

	New	Rew
Actual Res (Ω)	1.85	1.78
Corr Res (Ω)	2.47	2.32

New	Rew
No load current (A)	
3.22	3.31
Temp Rise °C	
97.50	98.00

3kW motor-Steenberg

Efficiency

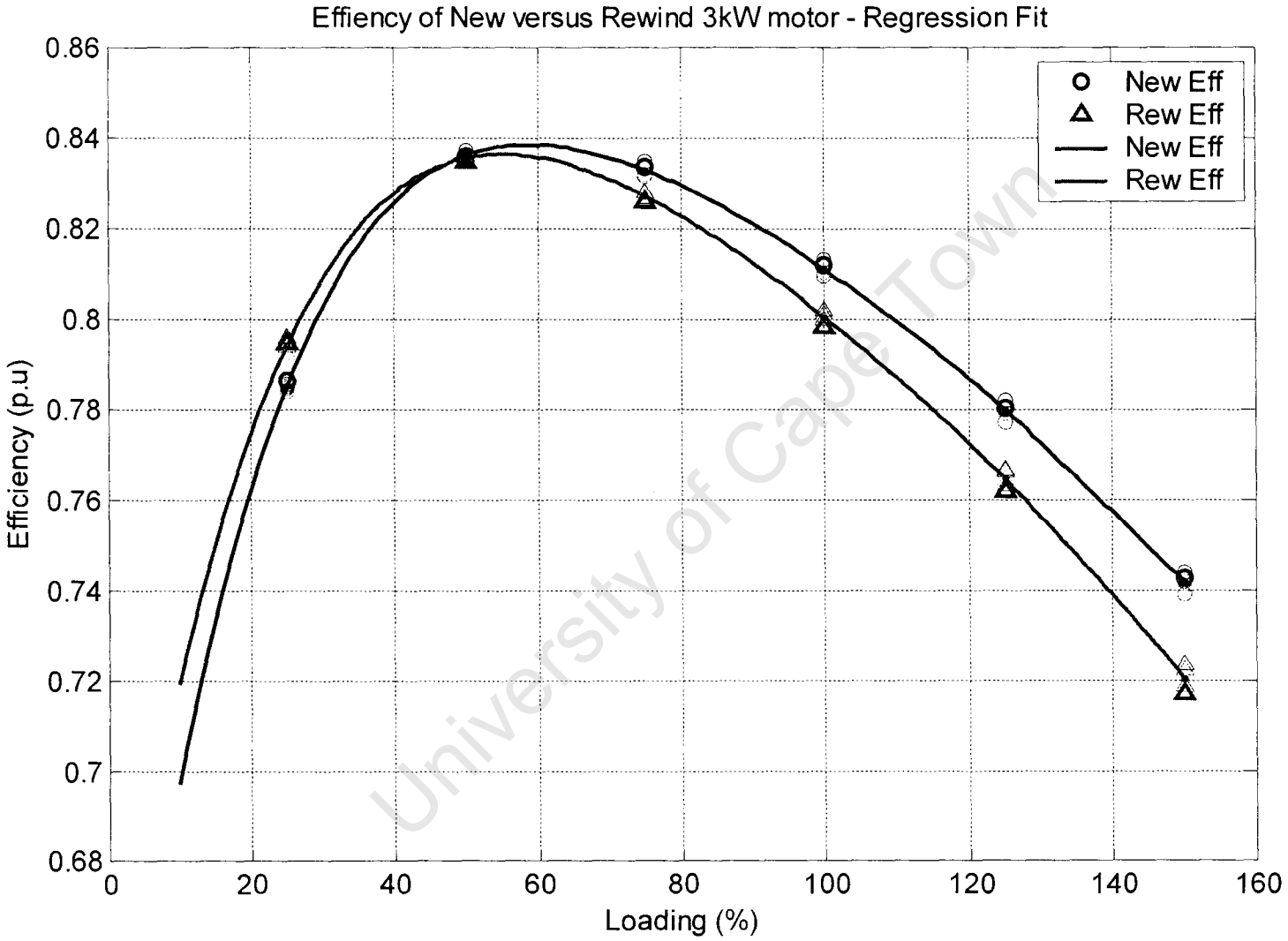

Motor loss

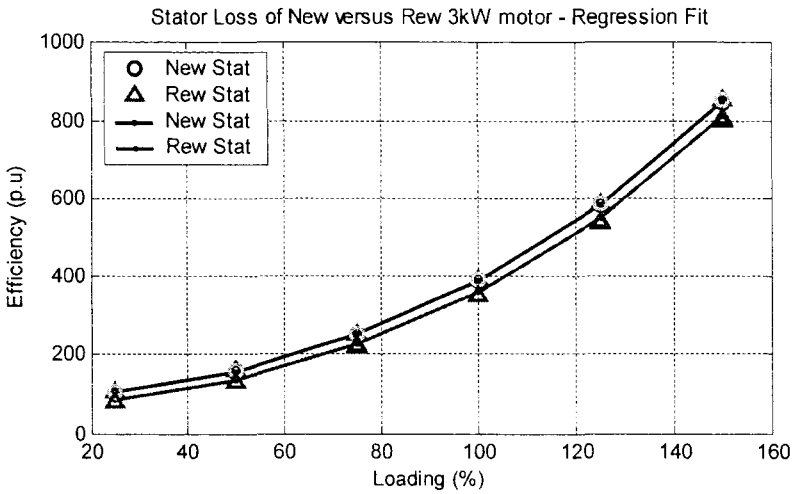

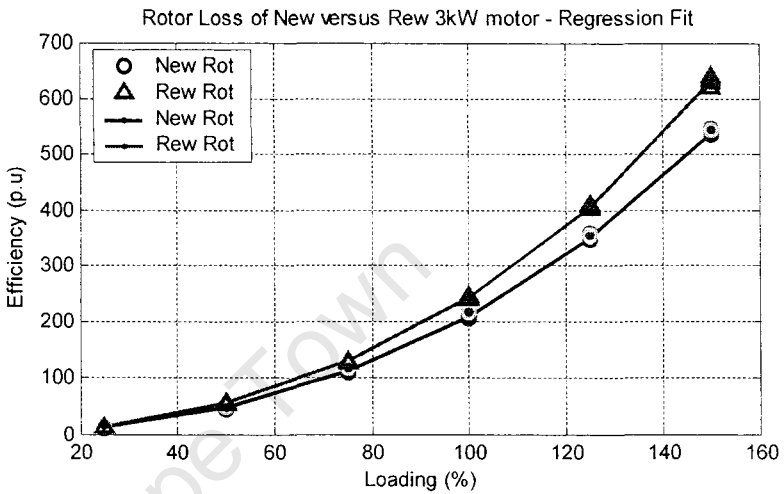

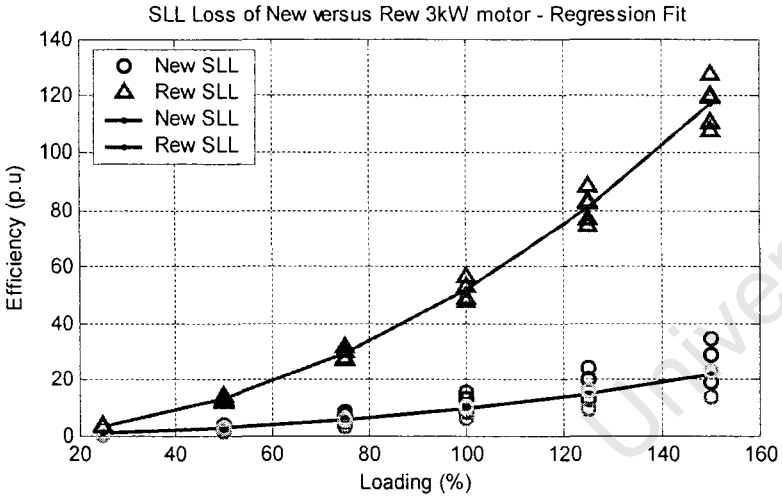

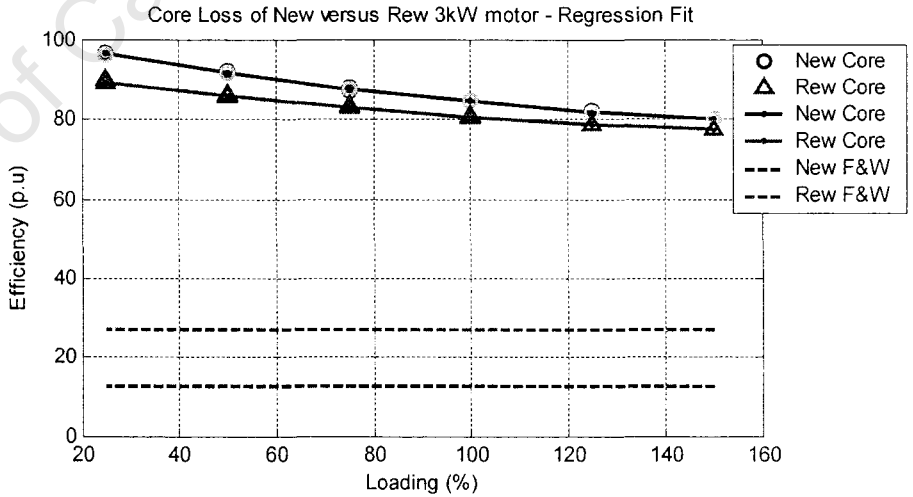

Efficiency change due to Steenberg Rewind

	New	Rew	

Loading (%)	New	Rew	Change (%)
	Eff (%)		
150	74.18	72.05	-2.13
125	78.00	76.46	-1.54
100	81.14	80.05	-1.09
75	83.33	82.73	-0.60
50	83.64	83.57	-0.07
25	78.52	79.43	0.90

Loss comparison

Loading (%)	New	Rew	New	Rew	New	Rew	New	Rew	New	Rew
	Stator (W)		Rotor (W)		Core (W)		SLL (W)		F&W (W)	
150	848.33	802.39	541.80	630.89	79.83	77.44	23.78	117.04	12.53	27.28
125	585.73	540.05	353.12	405.88	81.61	78.62	16.51	81.28		
100	390.18	351.26	210.88	242.55	84.29	80.47	10.57	52.02		
75	250.81	218.67	112.75	128.53	87.48	82.94	5.94	29.26		
50	157.44	130.74	48.30	55.41	91.65	85.73	2.64	13.01		
25	103.85	80.97	11.99	14.05	96.35	89.13	0.66	3.25		

Speed		Torque		Stator Current	
New	Rew	New	Rew	New	Rew
1337	1315	30.9	30.9	10.086	10.315
1372	1358	25.8	25.8	8.3679	8.4523
1404	1394	20.6	20.6	6.8232	6.8104
1432	1426	15.5	15.5	5.5115	5.3889
1457	1453	10.3	10.3	4.3889	4.1716
1478	1478	5.3	5.2	3.5945	3.3027

	New	Rew
Actual Res (Ω)	1.89	1.79
Corr Res (Ω)	2.50	2.52

New	Rew
No load current (A)	
3.21	2.96

7.5kW motor

Efficiency

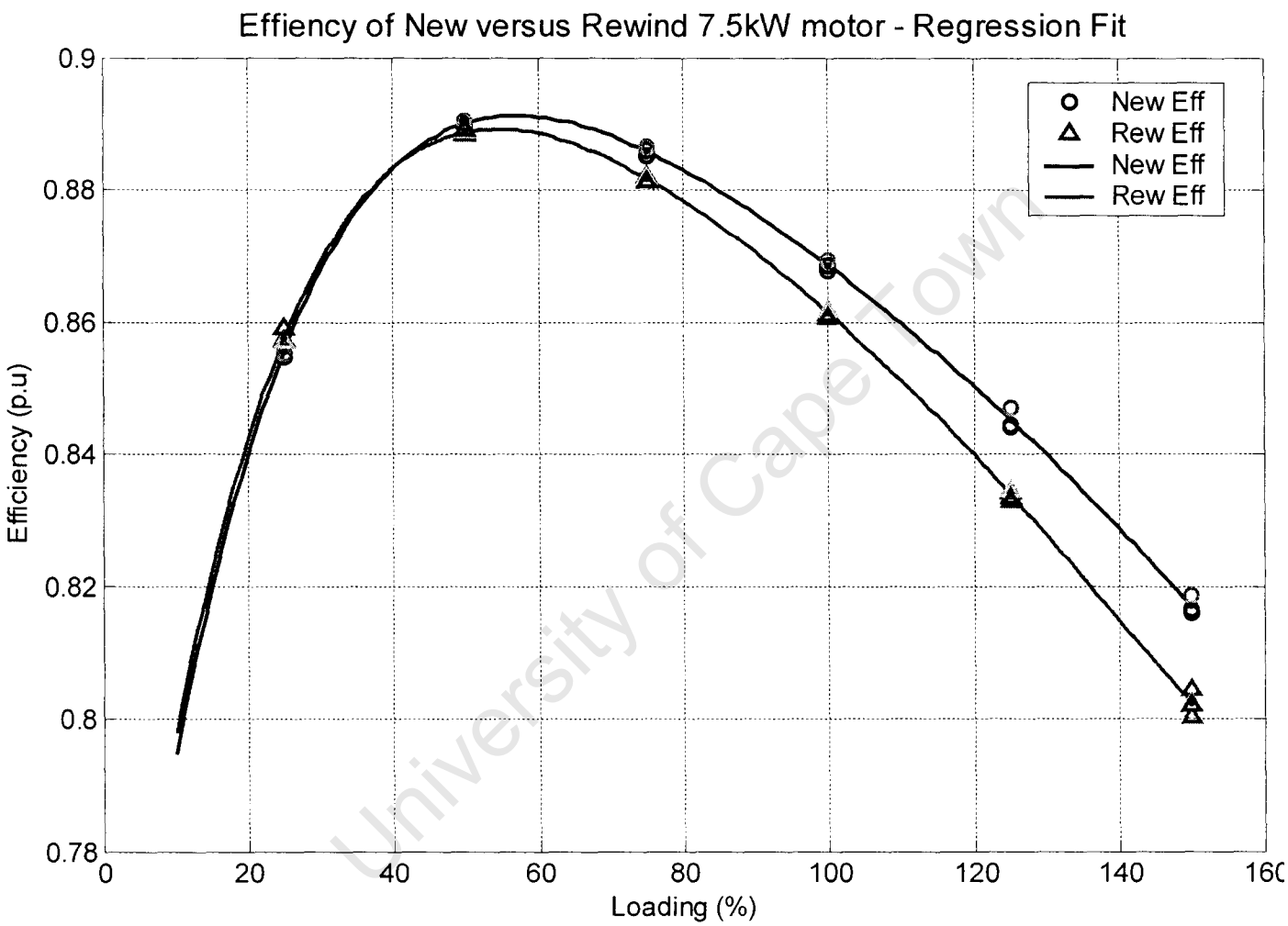

Motor loss

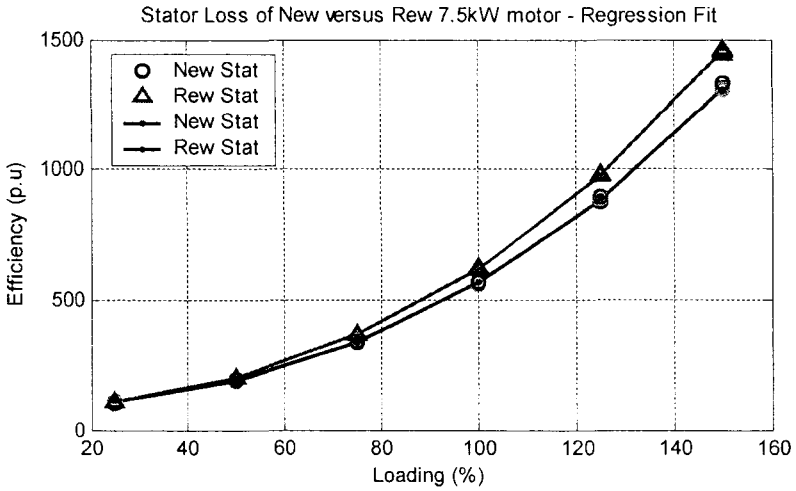

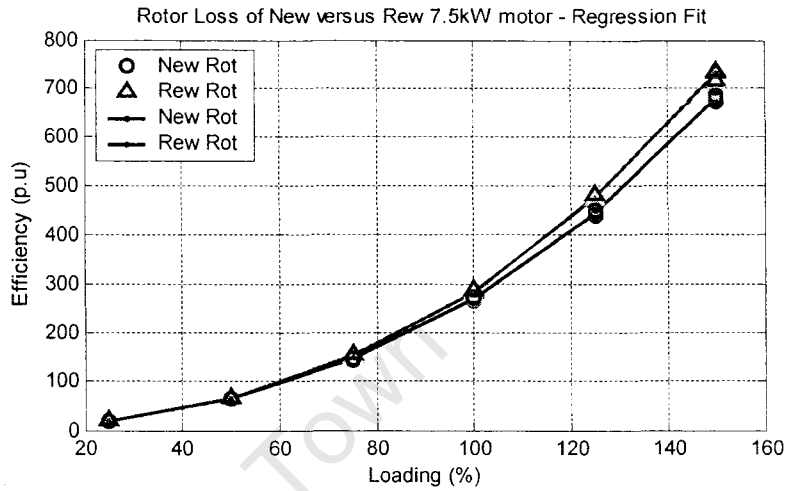

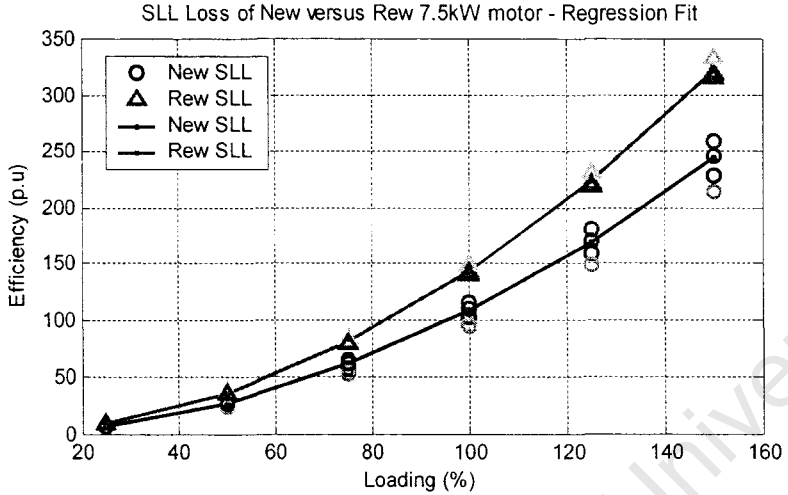

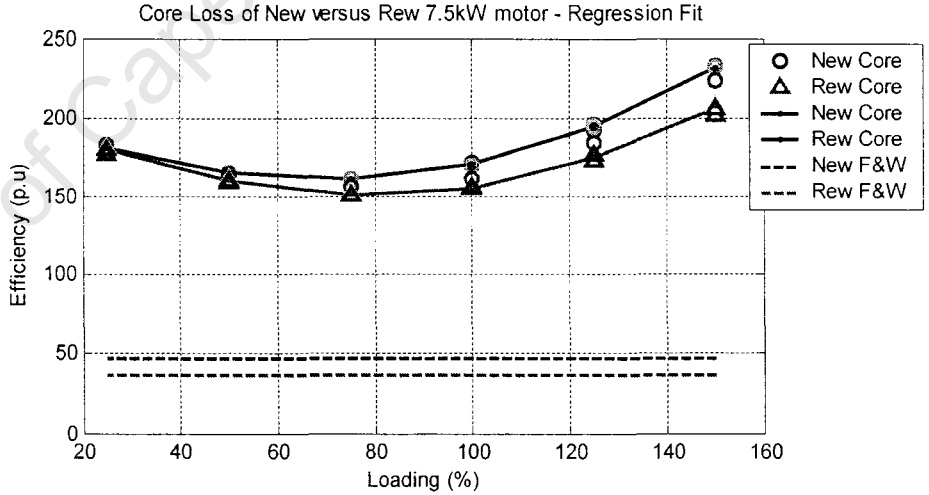

Efficiency

Loading (%)	New	Rew	Change (%)
	Eff		
150	81.51	80.22	-1.29
125	84.42	83.39	-1.03
100	86.83	86.15	-0.68
75	88.58	88.18	-0.40
50	89.00	88.88	-0.12
25	85.54	85.77	0.22

Motor loss

Loading (%)	New	Rew	New	Rew	New	Rew	New	Rew	New	Rew
	Stator (W)		Rotor (W)		Core (W)		SLL (W)		F&W (W)	
150	1311.98	1454.18	681.44	728.59	180.41	210.53	236.94	322.36	47.50	36.90
125	884.57	976.25	446.22	475.00	192.29	203.81	164.54	223.86		
100	569.06	620.56	270.44	284.60	202.21	211.49	105.31	143.27		
75	341.81	369.32	146.45	153.42	210.58	218.42	59.24	80.59		
50	192.33	204.27	64.87	66.10	215.27	221.75	26.33	35.82		
25	106.00	111.76	17.57	19.10	218.46	222.39	6.58	8.95		

Speed		Torque		Stator Current	
New	Rew	New	Rew	New	Rew
1416.50	1412.81	74.12	74.23	23.108	23.584
1436.50	1431.93	61.30	61.76	19.038	19.176
1453.00	1449.53	49.20	49.36	15.25	15.49
1466.80	1464.53	37.07	37.02	11.91	12.09
1479.50	1477.95	24.55	25.00	9.00	9.26
1490.50	1487.65	12.30	12.31	6.7	6.6568

	New	Rew
Actual Res (Ω)	1.90	1.95
Corr Res (Ω)	2.43	2.57

New	Rew
No load current (A)	
3.12	3.18
Temp Rise °C	
92.03	93.76

11kW motor

Efficiency

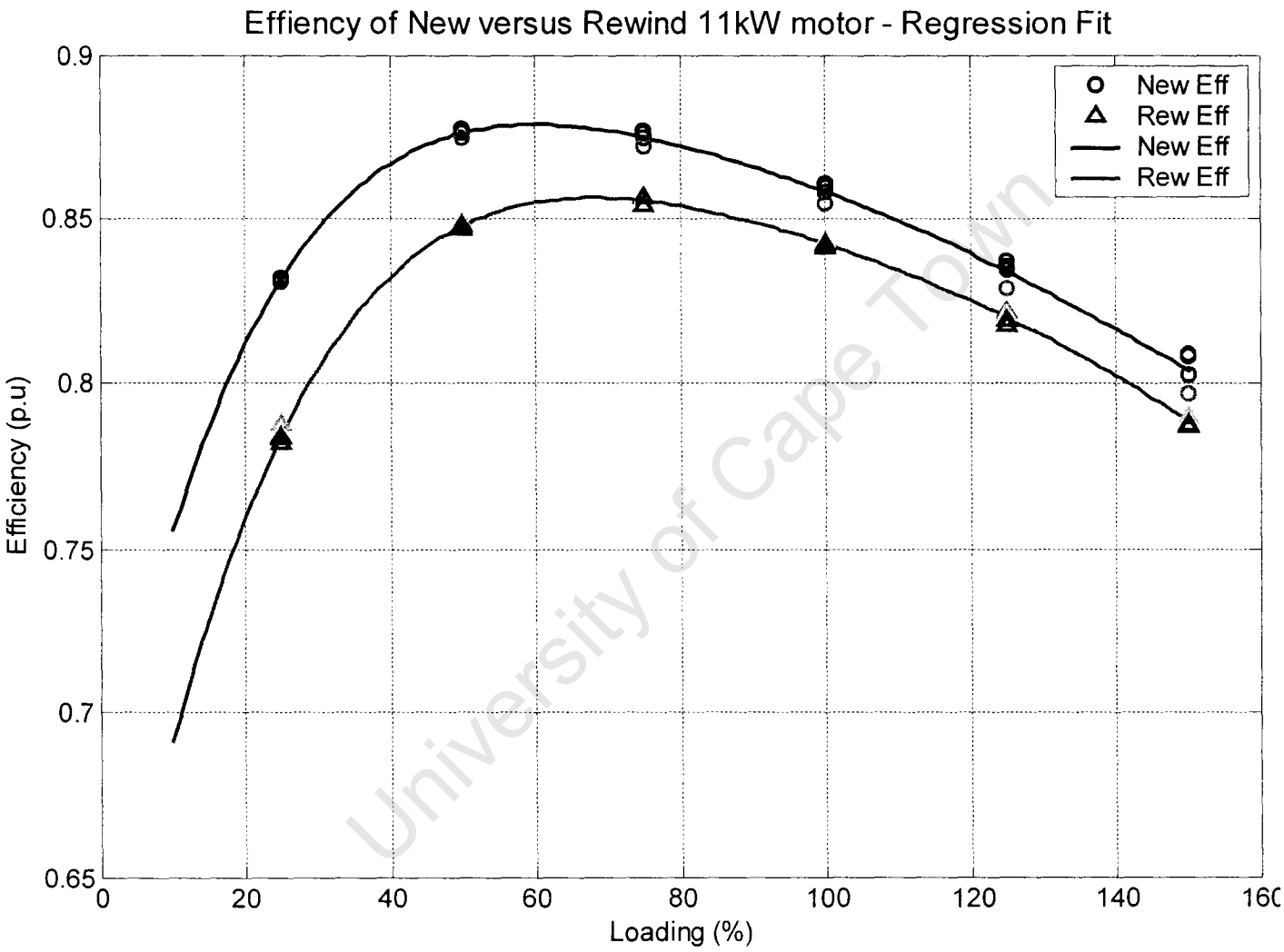

Motor loss

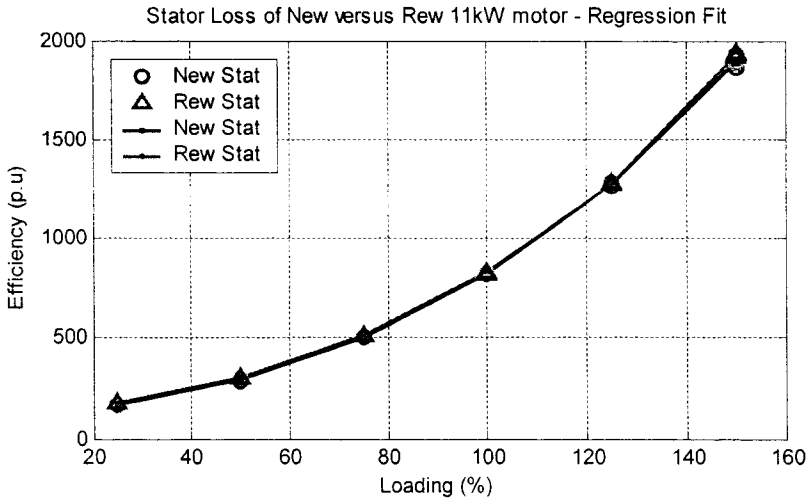

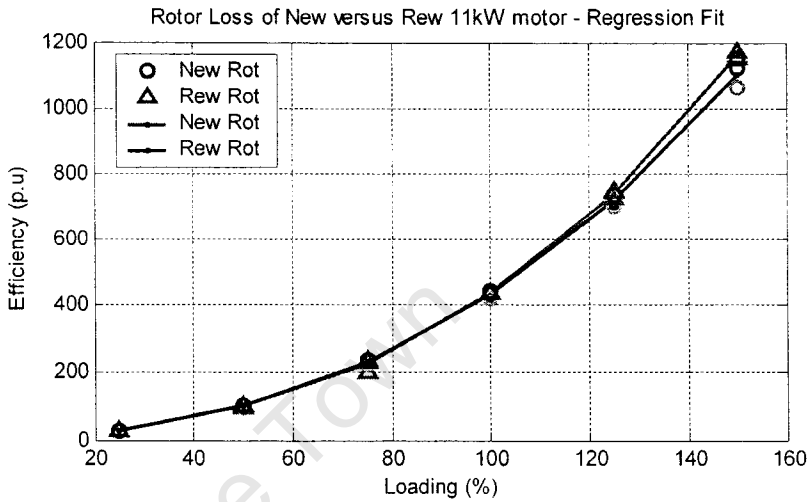

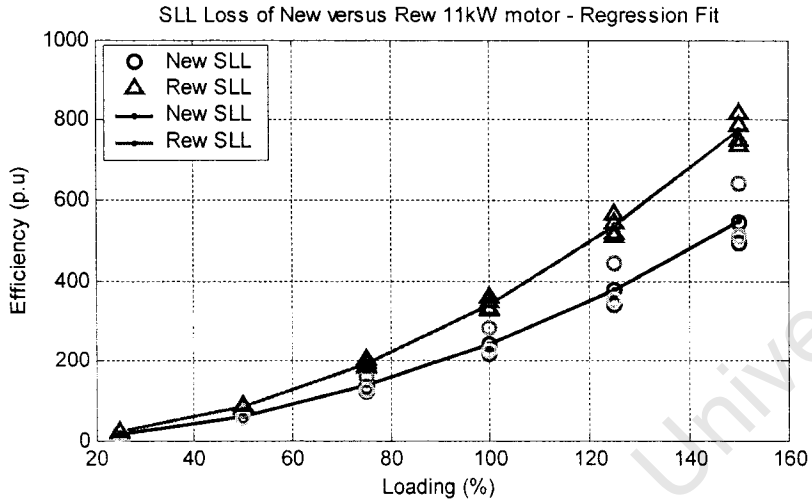

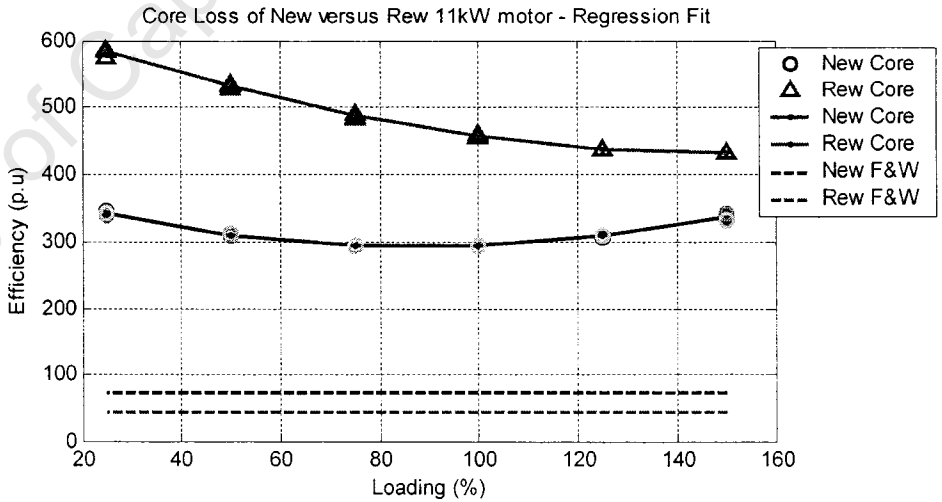

11kW motor

Efficiency

Loading (%)	New	Rew	Change (%)
	Eff (%)		
150	80.44	78.89	-1.55
125	83.43	82.01	-1.41
100	85.86	84.27	-1.59
75	87.52	85.58	-1.93
50	87.64	84.81	-2.83
25	83.17	78.44	-4.73

Motor loss

Loading (%)	New	Rew	New	Rew	New	Rew	New	Rew	New	Rew
	Stator (W)		Rotor (W)		Core (W)		SLL (W)		F&W (W)	
150	1896.38	1929.05	1101.25	1164.95	337.98	431.28	548.12	772.60	71.44	52.10
125	1274.58	1276.10	717.52	738.53	309.62	437.20	380.64	536.53		
100	818.79	826.68	428.90	436.86	294.57	455.90	243.61	343.38		
75	499.79	508.58	230.72	226.24	295.54	486.20	137.03	193.15		
50	291.47	300.41	100.89	99.63	311.03	530.79	60.90	85.84		
25	172.49	179.88	26.66	27.29	342.37	583.16	15.23	21.46		

Speed		Torque		Stator Current	
New	Rew	New	Rew	New	Rew
1412.92	1407.17	108.41	108.23	36.27	37.18
1432.00	1431.15	90.27	90.30	29.75	30.28
1449.46	1449.18	72.22	72.23	23.91	24.40
1464.56	1465.43	54.13	54.21	18.82	19.20
1477.52	1478.92	36.10	36.08	14.51	14.81
1489.24	1490.85	18.08	18.10	11.25	11.45

	New	Rew
Actual Res (Ω)	0.99	1.02
Corr Res (Ω)	1.37	1.41

New	Rew
No load current (A)	
5.50	5.79
Temp Rise °C	
98.78	104.71

15kW motor

Efficiency

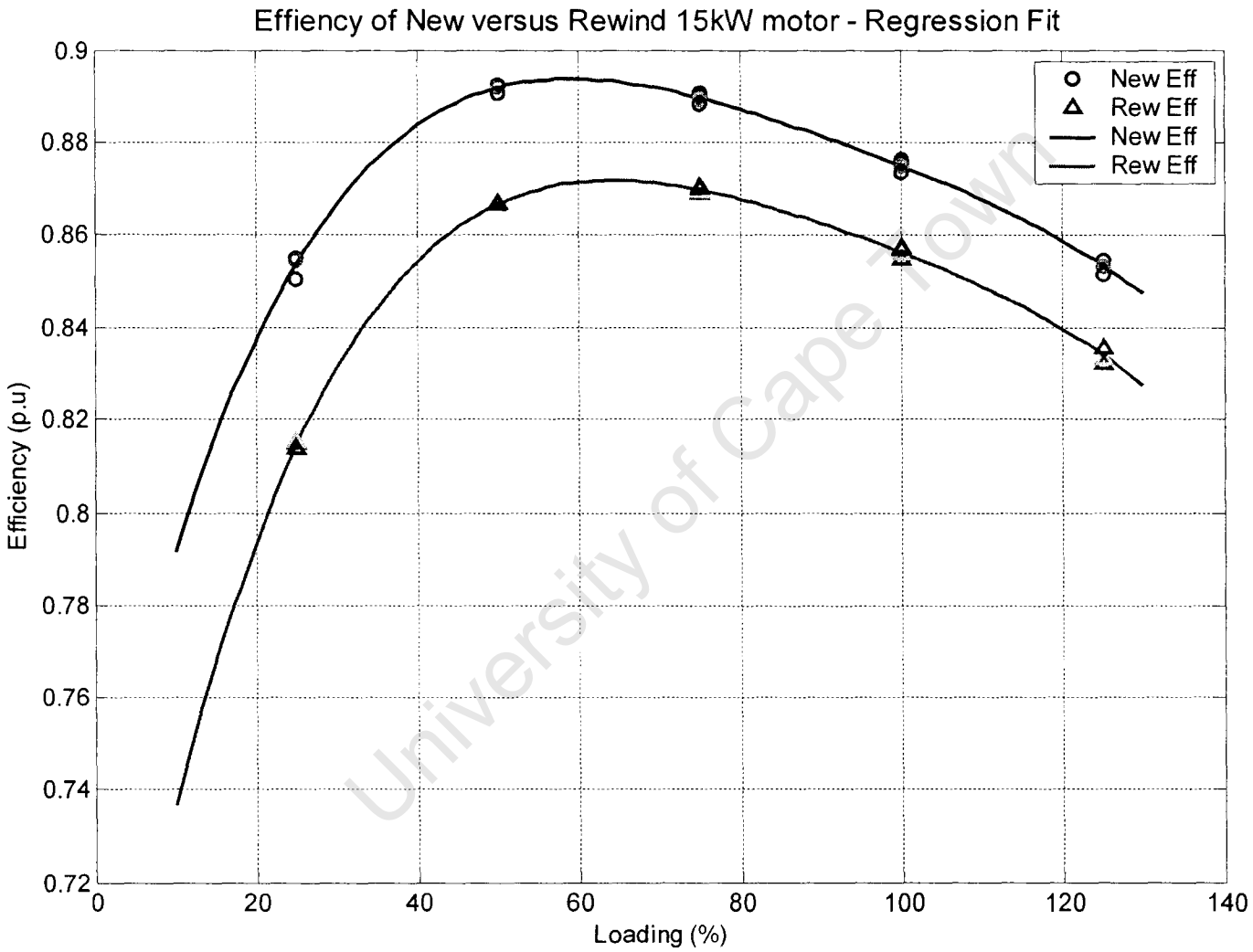

Motor loss

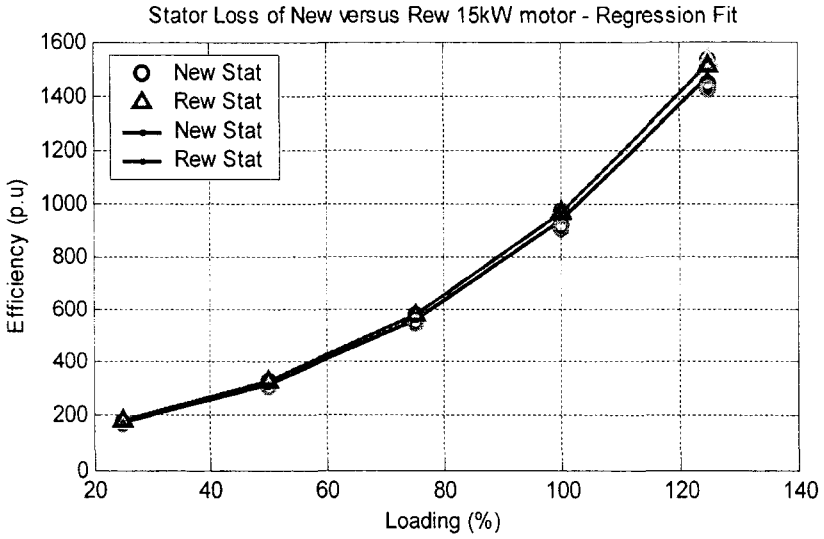

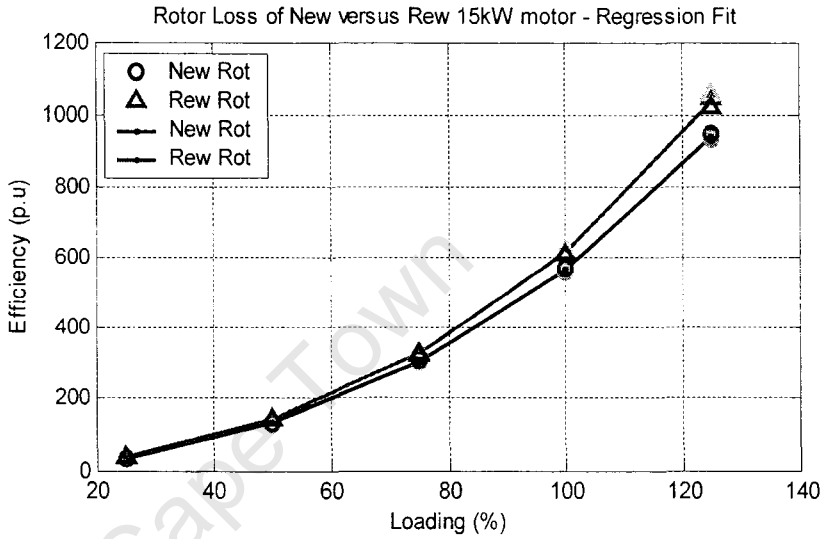

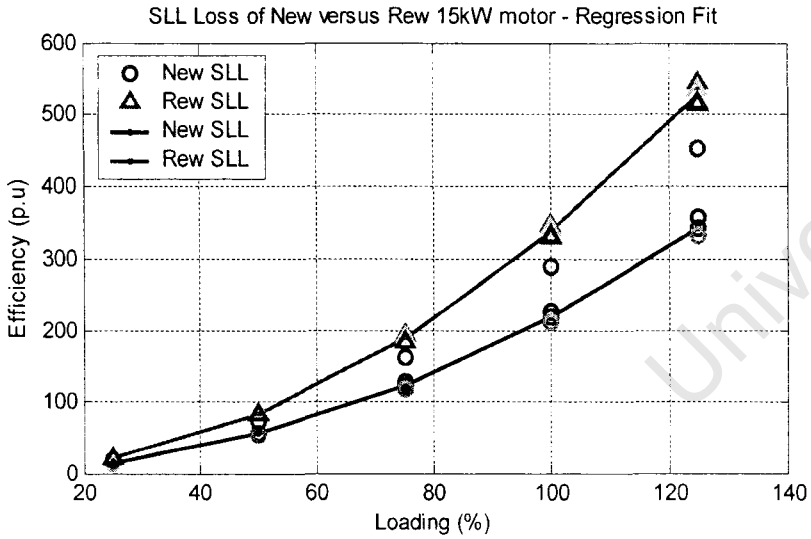

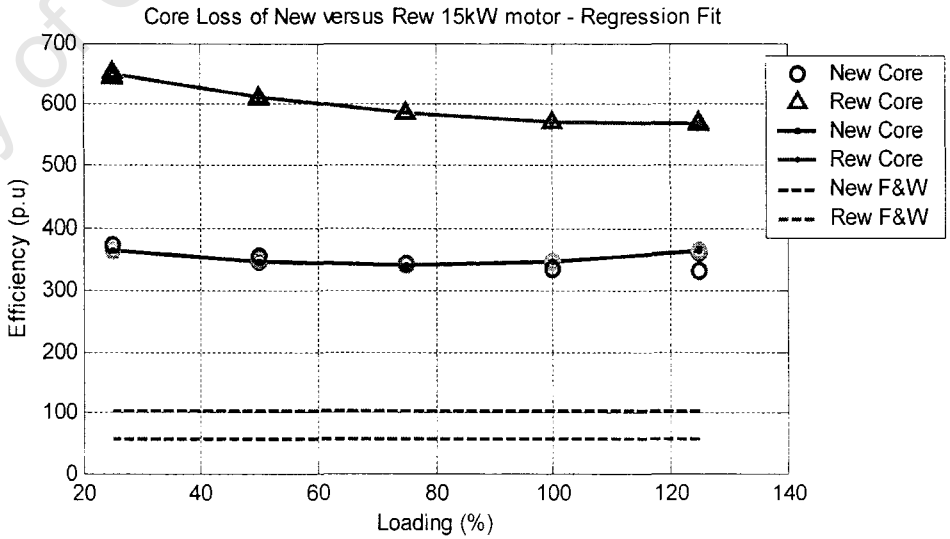

15kW motor

Efficiency

Loading (%)	New Eff (%)	Rew Eff (%)	Change (%)
125	85.36	83.40	-1.96
100	87.50	85.64	-1.86
75	88.95	86.97	-1.98
50	89.18	86.67	-2.50
25	85.38	81.46	-3.92

Motor loss

Loading (%)	New Stator (W)	Rew Stator (W)	New Rotor (W)	Rew Rotor (W)	New Core (W)	Rew Core (W)	New SLL (W)	Rew SLL (W)	New F&W (W)	Rew F&W (W)
125	1433.80	1520.15	939.98	1038.00	355.46	569.21	370.81	527.74	104.42	57.54
100	914.32	966.59	564.35	614.91	344.95	571.39	237.32	337.75		
75	550.32	579.99	303.64	328.06	343.12	585.72	133.49	189.99		
50	309.24	326.94	130.65	141.79	350.13	610.81	59.33	84.44		
25	170.61	180.05	33.40	36.33	365.97	649.29	14.83	21.11		

	New	Rew
Actual Res (Ω)	0.67	0.69
Corr Res (Ω)	0.88	1.01

Speed New	Speed Rew	Torque New	Torque Rew	Stator Current New	Stator Current Rew
1432.70	1423.66	123.60	123.10	38.99	39.76
1450.70	1444.25	98.30	98.43	31.09	31.77
1466.30	1461.39	73.80	73.94	24.18	24.78
1479.90	1476.48	49.10	49.31	18.23	18.73
1493.40	1489.87	21.20	24.67	13.15	14.05

New	Rew
No load current (A)	
6.62	6.81
Temp Rise °C	
98.37	123.21

22kW motor

Efficiency

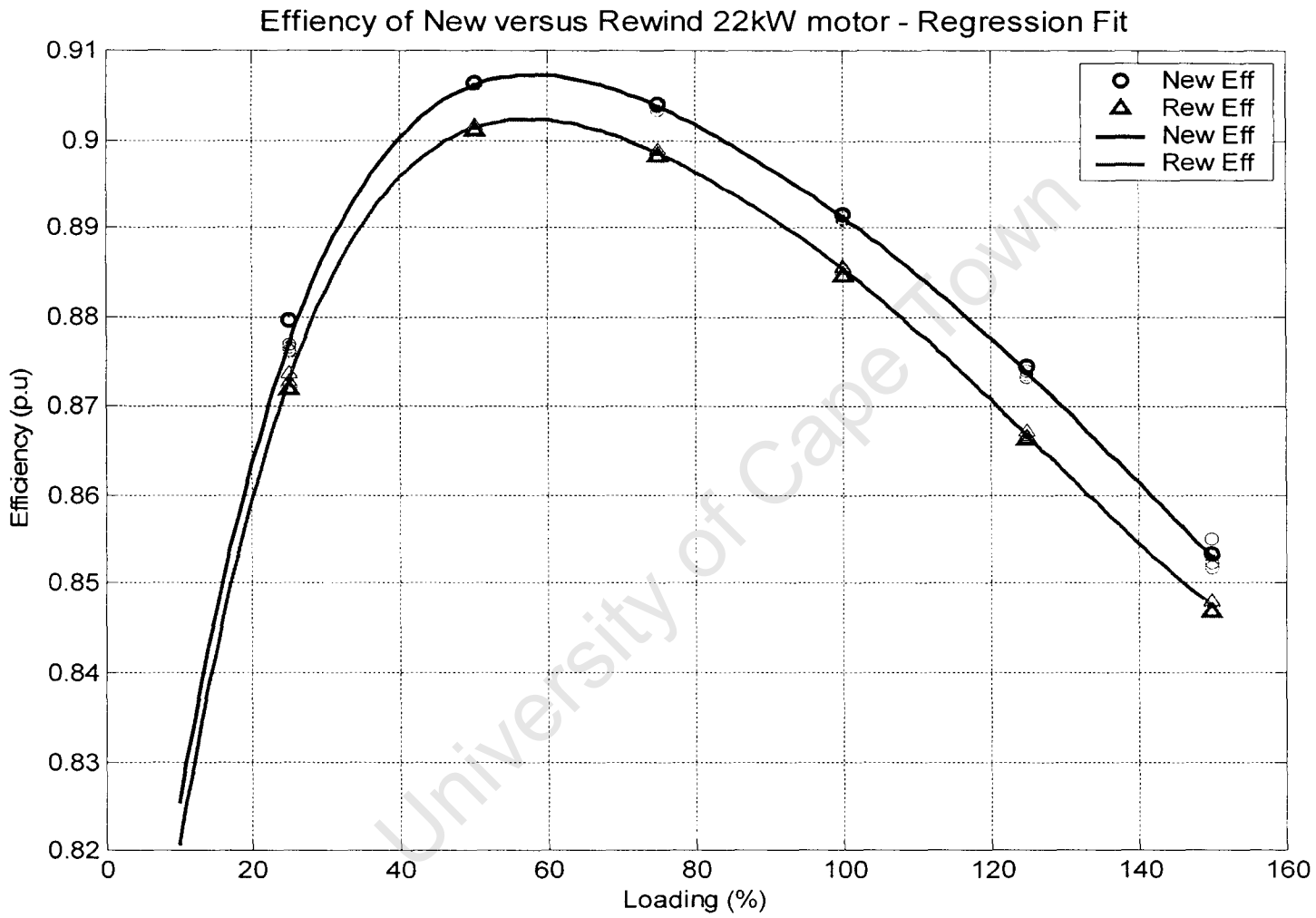

Motor loss

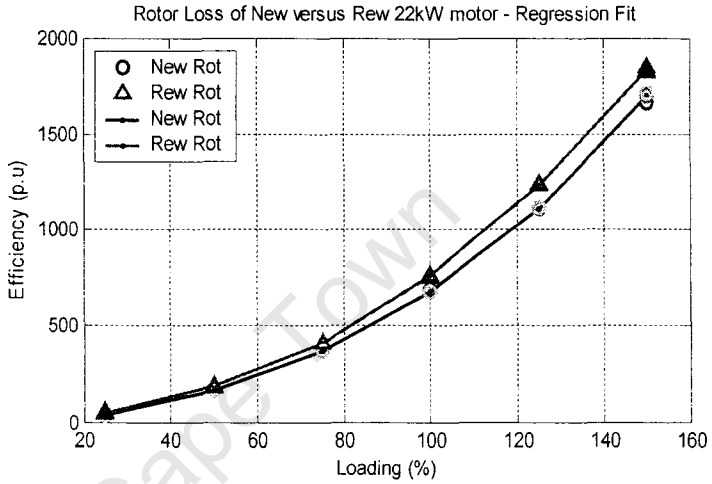

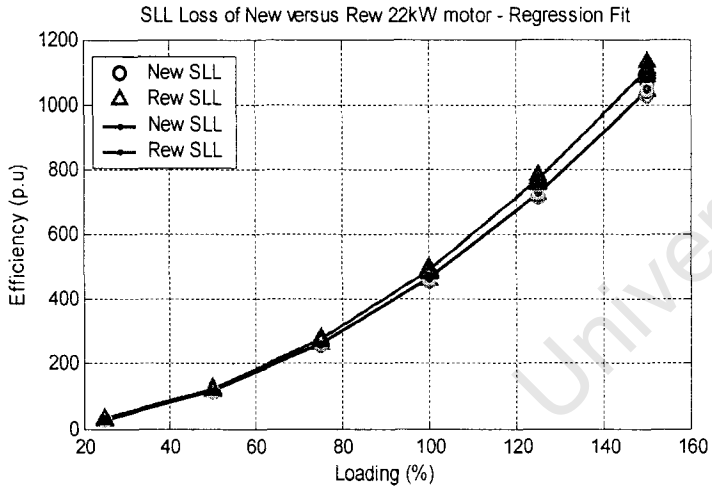

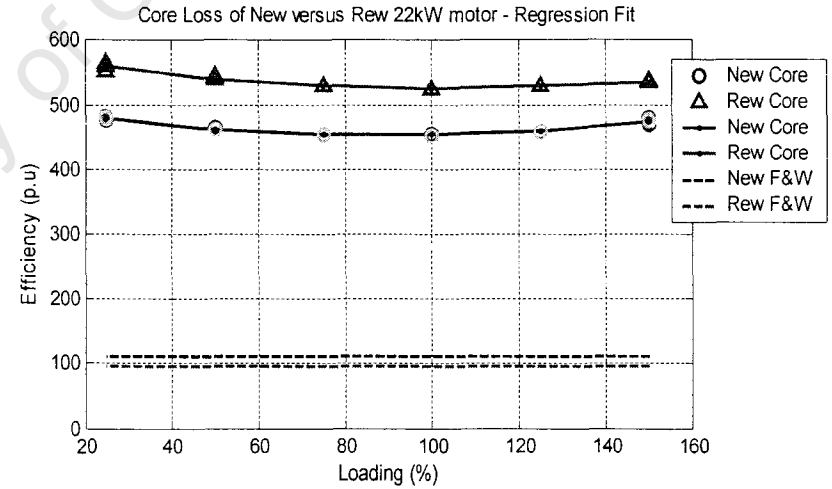

22kW motor

Efficiency

Loading (%)	New	Rew	Change (%)
	Eff		
150	85.30	84.75	-0.55
125	87.38	86.68	-0.70
100	89.12	88.53	-0.59
75	90.38	89.86	-0.52
50	90.62	90.14	-0.48
25	87.71	87.30	-0.41

Motor loss

Loading (%)	New	Rew	New	Rew	New	Rew	New	Rew	New	Rew
	Stator (W)		Rotor (W)		Core (W)		SLL (W)		F&W (W)	
150	2311.16	2377.30	1697.80	1830.82	474.83	534.44	1044.90	1106.72	111.03	96.15
125	1561.34	1633.42	1111.64	1233.70	459.47	528.06	725.61	768.56		
100	1011.42	1057.56	679.61	755.31	453.22	524.76	464.39	491.87		
75	609.17	638.58	367.23	412.80	454.10	529.10	261.22	276.68		
50	338.11	354.28	159.65	183.23	462.60	540.16	116.10	122.97		
25	177.37	184.02	38.61	49.58	479.23	558.01	29.02	30.74		

	New	Rew
Actual Res (Ω)	0.38	0.39
Corr Res (Ω)	0.52	0.53

Speed		Torque		Stator Current	
New	Rew	New	Rew	New	Rew
1438.70	1430.00	196.30	203.47	59.89	63.42
1444.97	1442.21	179.21	174.09	54.69	54.12
1457.50	1453.33	145.52	146.35	44.63	45.72
1469.90	1466.44	108.79	109.81	34.52	35.61
1480.80	1478.37	72.85	73.54	25.79	26.55
1487.27	1489.99	49.09	35.54	20.90	18.88

New	Rew
No load current (A)	
8.96	8.99
Temp Rise °C	
107.50	111.43

37kW motor

Efficiency

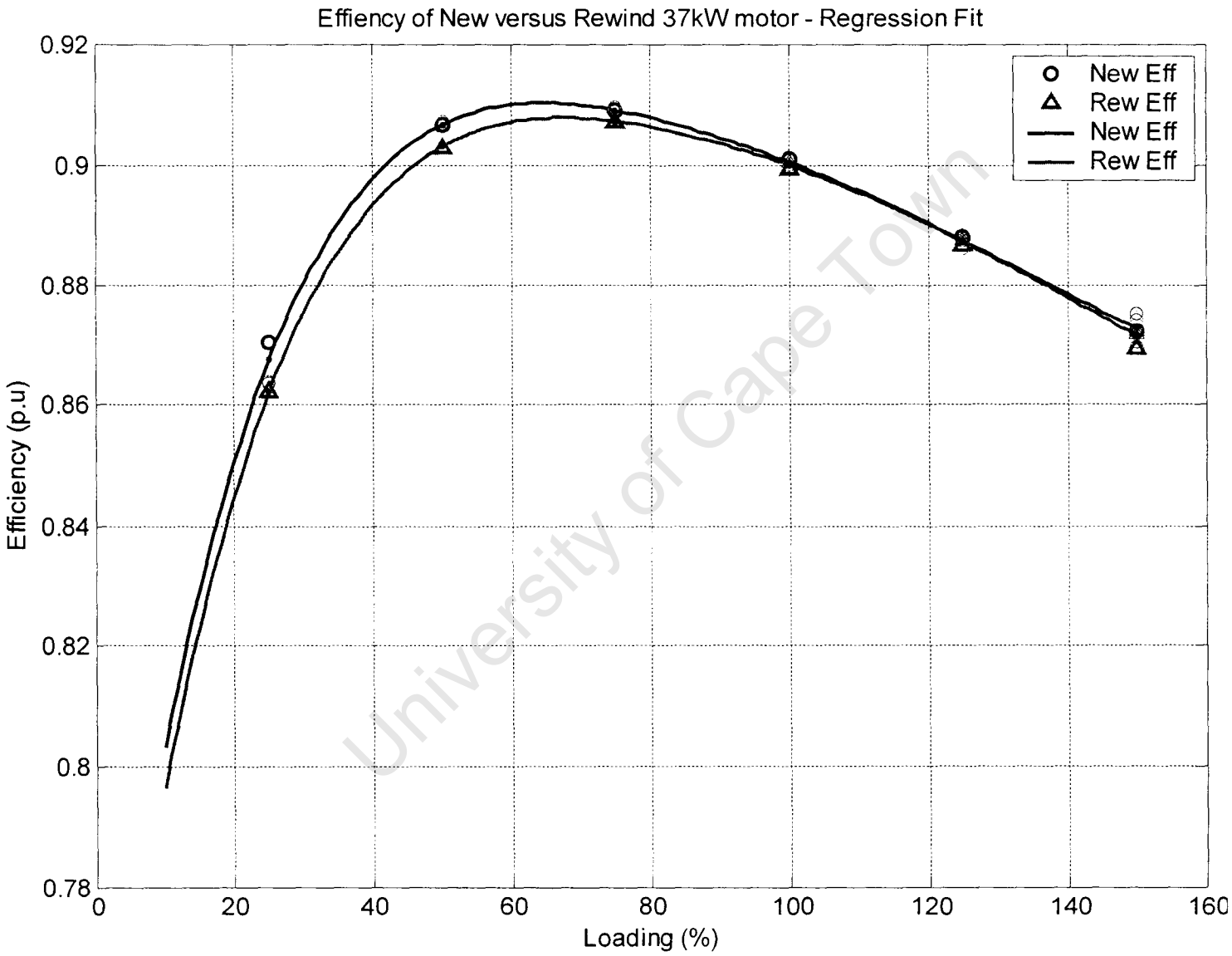

Motor loss

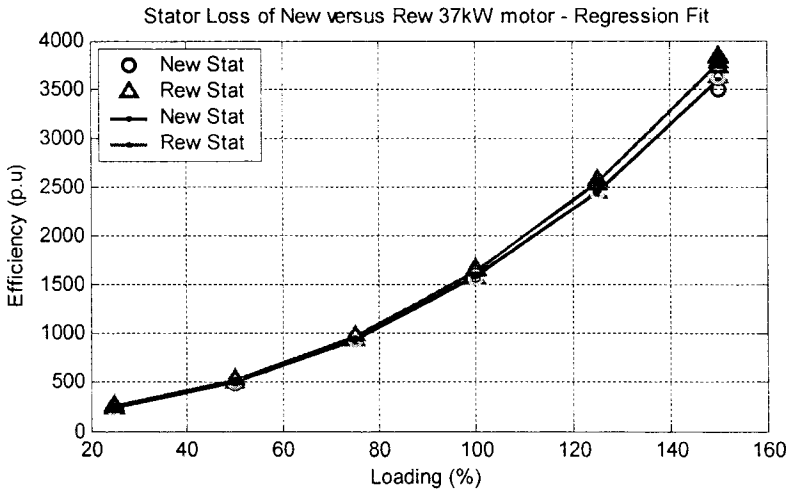

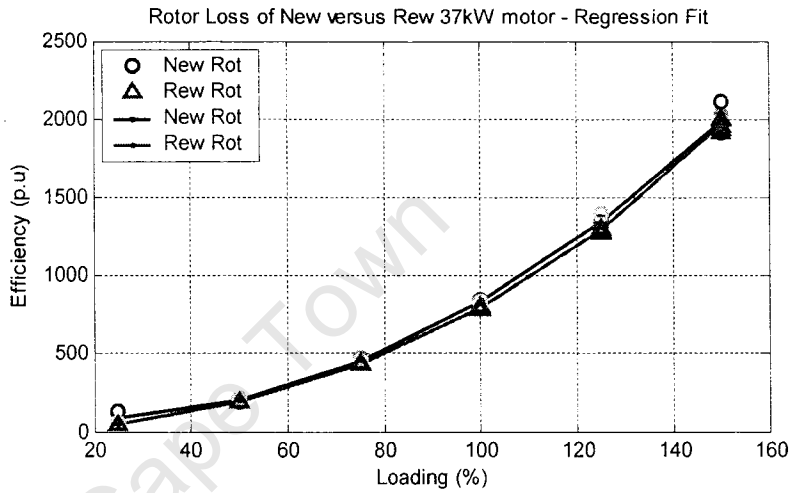

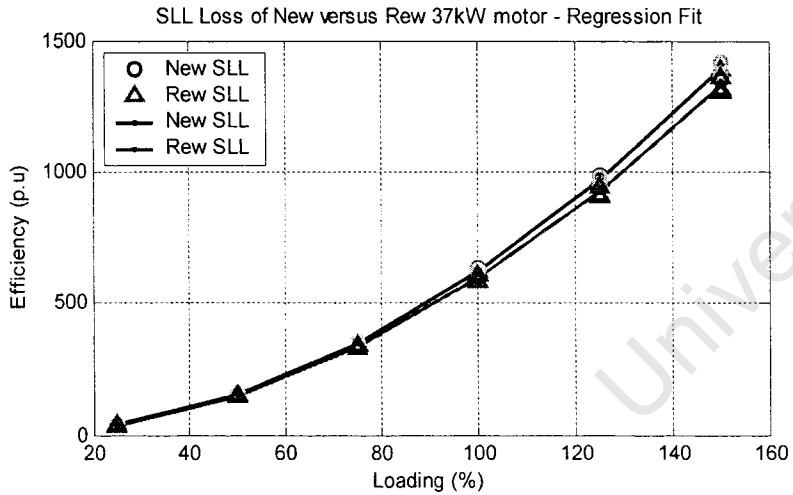

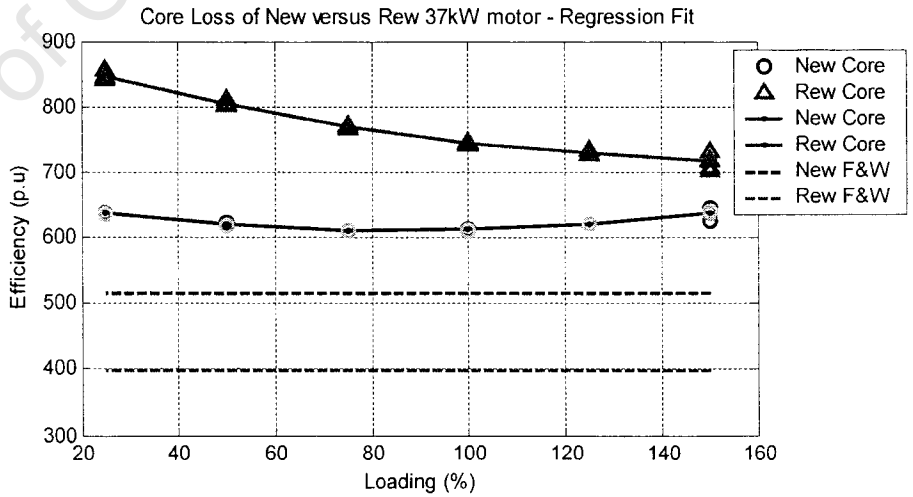

Efficiency

Loading (%)	New	Rew	Change (%)
	Eff (%)		
150	87.28	87.16	-0.12
125	88.76	88.74	-0.02
100	90.05	89.99	-0.05
75	90.90	90.72	-0.18
50	90.66	90.31	-0.36
25	86.75	86.20	-0.55

Motor loss

Loading (%)	New	Rew	New	Rew	New	Rew	New	Rew	New	Rew
	Stator (W)		Rotor (W)		Core (W)		SLL (W)		F&W (W)	
150	3595.58	3808.56	1989.54	1961.08	637.59	715.85	1390.14	1330.56	514.85	398.97
125	2446.58	2568.56	1342.60	1290.42	620.74	729.19	965.39	924.00		
100	1576.92	1659.58	837.97	794.70	611.23	744.93	617.85	591.36		
75	932.73	989.62	456.09	433.03	610.14	770.54	347.54	332.64		
50	498.50	536.96	204.70	189.62	619.62	805.01	154.46	147.84		
25	241.28	268.09	86.68	49.29	636.18	846.29	38.62	36.96		

Speed		Torque		Load Current	
New	Rew	New	Rew	New	Rew
1454	1455.1	336.40	336.68	100.08	101.45
1461	1463.4	289.77	288.69	86.42	86.72
1469	1470.7	241.76	241.33	72.41	72.61
1478	1479.4	181.53	182.14	55.71	56.53
1485	1486.8	121.52	121.81	40.91	41.70
1493	1494	61.11	61.89	28.57	29.73

	New	Rew
Actual Res (Ω)	0.22	0.23
Corr Res (Ω)	0.29	0.30

New	Rew
No load current (A)	
12.56	12.88
Temp Rise °C	
100.23	96.80

45kW motor

Efficiency

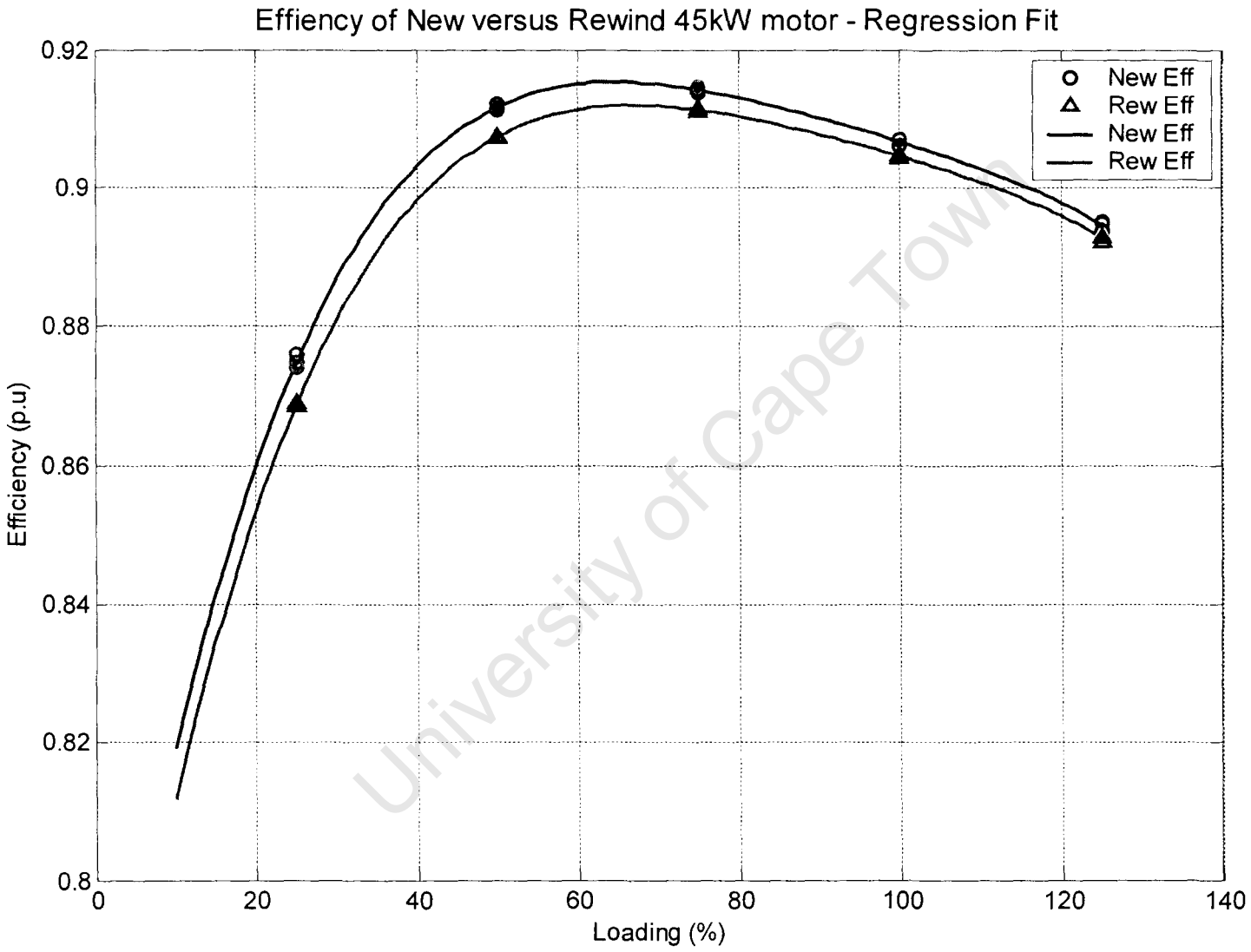

Motor loss

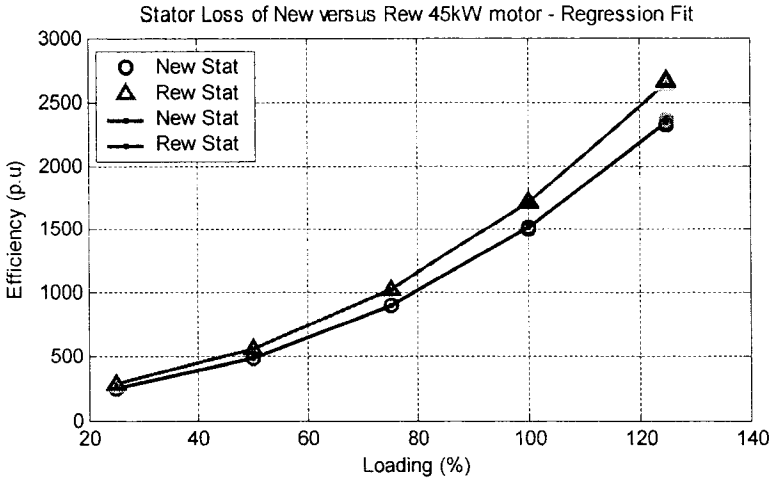

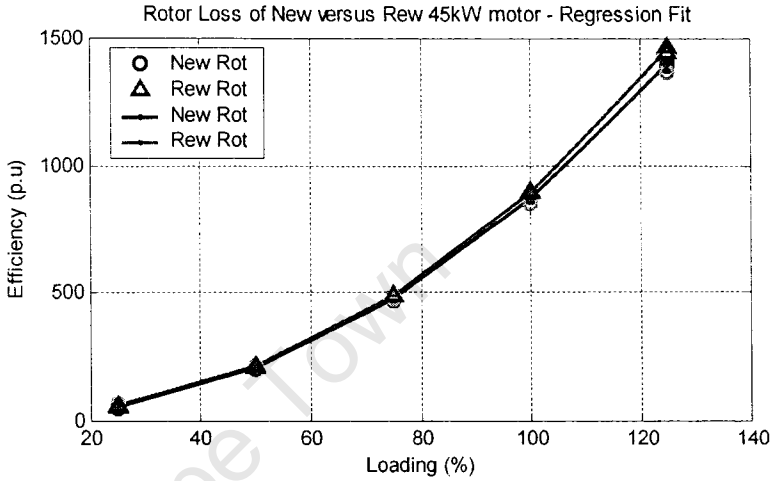

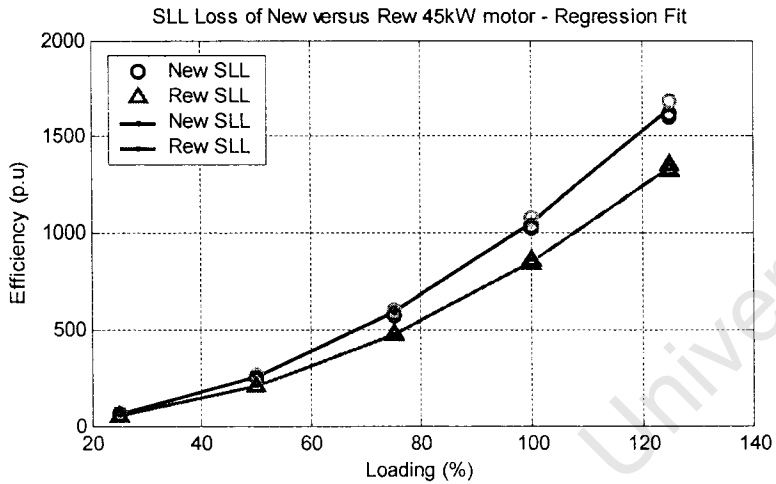

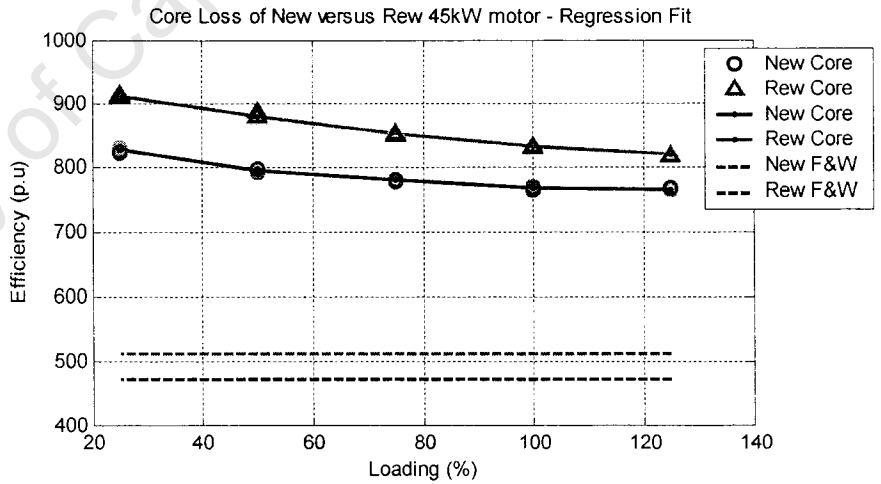

Efficiency

Loading (%)	New	Rew	Change (%)
	Eff (%)		
125	89.46	89.28	-0.18
100	90.67	90.45	-0.21
75	91.42	91.13	-0.29
50	91.17	90.74	-0.43
25	87.48	86.87	-0.62

Motor loss

Loading (%)	New	Rew	New	Rew	New	Rew	New	Rew	New	Rew
	Stator (W)		Rotor (W)		Core (W)		SLL (W)		F&W (W)	
125	2345.53	2650.85	1395.18	1455.63	765.96	818.50	1642.85	1335.33	512.11	472.84
100	1508.63	1715.23	870.07	896.22	766.78	831.08	1051.43	854.62		
75	906.76	1031.05	475.80	490.91	778.60	851.69	591.43	480.72		
50	496.79	563.54	209.79	214.75	794.40	880.29	262.86	213.65		
25	254.89	286.55	53.99	56.55	826.32	911.54	65.71	53.41		

	New	Rew
Actual Res (Ω)	0.149	0.159
Corr Res (Ω)	0.214	0.218

Speed		Torque		Stator Current	
New	Rew	New	Rew	New	Rew
1473	1463.3	357.14	366.28	106.84	109.29
1481	1472.7	291.24	292.54	85.213	87.231
1488	1480.9	218.71	220.10	67.147	67.876
1495	1488.7	147.22	146.83	49.438	50.26
1464	1495.6	72.81	75.23	35.959	36.139

New	Rew
No load current (A)	
28.81	29.17
Temp Rise °C	
102.50	109.80

55kW motor

Efficiency

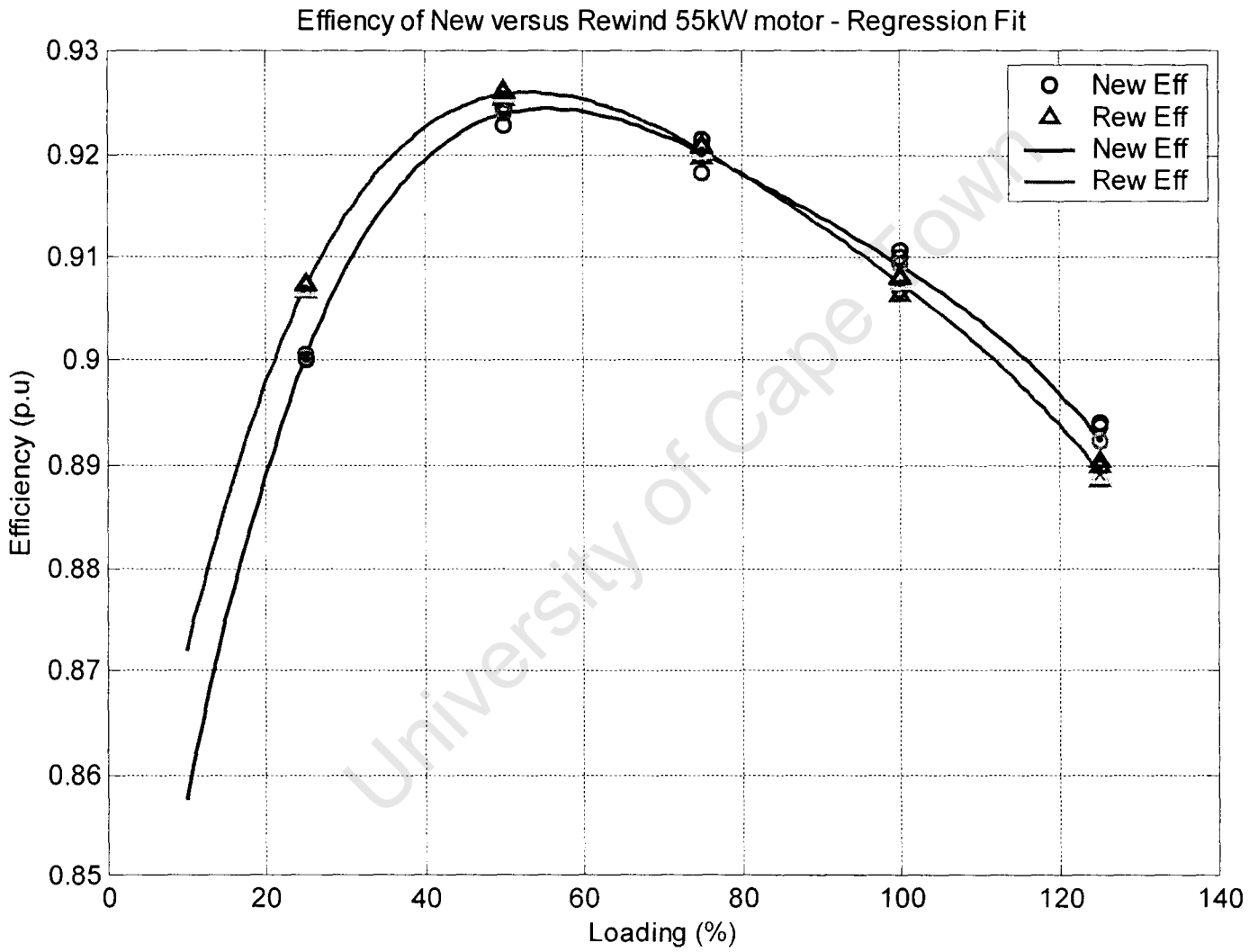

Motor loss

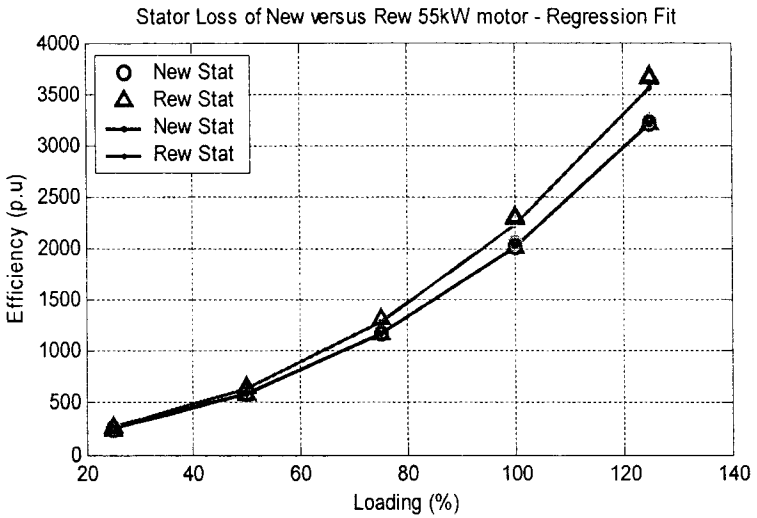

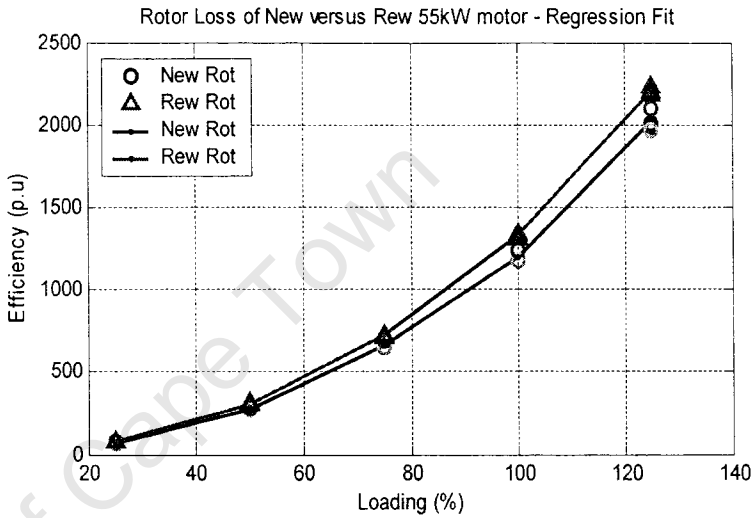

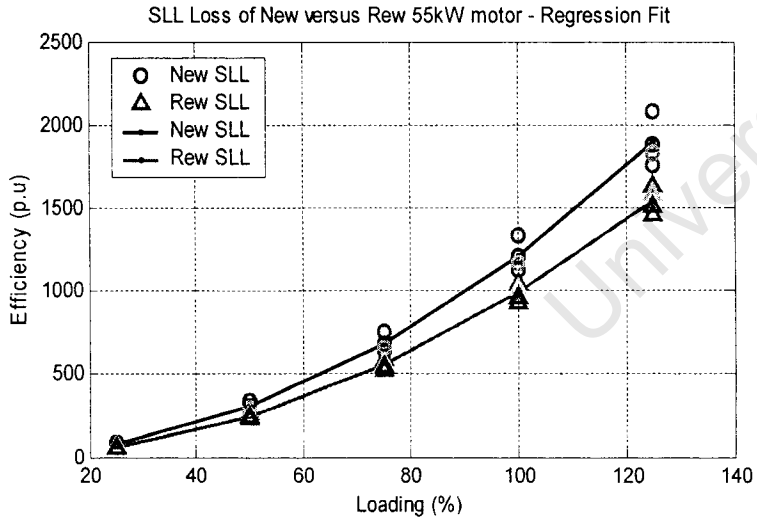

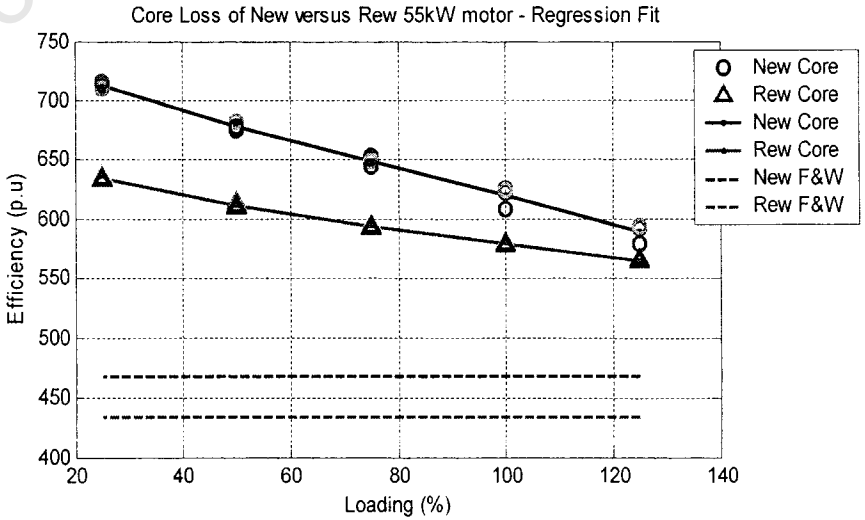

Efficiency

Loading (%)	New	Rew	Change (%)
	Eff (%)		
125	89.25	88.95	-0.30
100	90.92	90.75	-0.17
75	92.03	92.06	0.03
50	92.40	92.60	0.19
25	90.03	90.71	68

Motor loss

Loading (%)	New	Rew	New	Rew	New	Rew	New	Rew	New	Rew
	Stator (W)		Rotor (W)		Core (W)		SLL (W)		F&W (W)	
125	3216.75	3680.48	2014.35	2206.90	589.51	565.48	1888.50	1543.60	467.34	433.80
100	2022.85	2301.98	1193.40	1330.68	620.53	578.74	1208.65	987.89		
75	1168.90	1318.23	659.10	717.21	648.85	594.26	679.86	555.69		
50	588.90	659.07	278.30	310.83	677.60	611.62	302.16	246.98		
25	249.54	274.39	71.44	77.61	712.79	634.21	75.54	61.74		

	New	Rew
Actual Res (Ω)	0.15	0.16
Corr Res (Ω)	0.20	0.22

Speed		Torque		Stator Current	
New	Rew	New	Rew	New	Rew
1453.3	1449.4	432.1	430.59	144.06	146.91
1461.9	1459.1	358.1	356.73	123.67	125.96
1469.8	1468.3	268.5	267.64	103.04	103.54
1478.3	1478	178.0	179.09	78.533	78.28
1486.4	1487.3	89.5	89.30	56.031	55.473
1494	1495.4	432.1	430.59	36.057	35.79

New	Rew
No load current (A)	
14.94	14.94
Temp Rise °C	
106.00	106.00